Universidade do Porto

Faculdade de Engenharia

FEUP

Production of TAME and n-Propyl Propionate by Reactive Distillation

Dissertation presented to the
Faculty of Engineering of the University of Porto
for the degree of Doctor in Chemical Engineering

by

Carlos Filipe Moreira Duarte

Supervisor
Professor Doutor José Miguel Loureiro

Laboratory of Reaction and Separation Engineering
Department of Chemical Engineering
Faculty of Engineering of the Univerisity of Porto
Porto, Portugal

June 2006

ABSTRACT

In this work, the production of Tertiary-Amyl Methyl Ether (TAME) and n-Propyl Propionate via Reactive Distillation (RD) was studied. Since it is necessary to possess accurate data related to the kinetics of the reactions that take place in each one of the systems and since no such data existed for n-Propyl Propionate synthesis, heterogeneously catalysed batch reactor experiments were performed, using 1-Propanol and Propionic Acid as reactants and Amberlyst 46 as catalyst. From these experiments, it was found that the system, using this catalyst, behaved in accordance to a Pseudo-Homogeneous model for which the Kinetic and Equilibrium constants equations were regressed from the experimental data. These expressions showed good agreement when reconciliation simulations were run. The equation for the Non-Catalytic Kinetic constant was also determined and found to be inferior to the Catalytic constant by 3 orders of magnitude under the expected operating conditions and, as such, was not considered further on when the reaction rate was calculated.

This step was followed by the calculation of Reactive Residue Curve Maps (RRCMs), using, in the case of TAME synthesis, a Modified (Dortmund) UNIFAC model for activity and Vapour-Liquid Equilibrium (VLE) calculations. Since the TAME system is composed by four chemical species, a simplification consisting of summing ("lumping") the two isoamylenes - 2-Methyl 1-Butene (2M1B) and 2-Methyl 2-Butene (2M2B) - was used. From these simulations it was possible to determine operating regions for the RD of TAME as well as its stationary points. It was also found that the simplification taken holds true in most cases, but that caution must be taken to avoid erroneous analysis of the results. With regard to n-Propyl Propionate synthesis, the structure of the system did not allow for bi-dimensional representation of the residue curves and as such they were not plotted or analysed.

Using a pilot-scale reactive distillation column, which exists at the

University of Dortmund, it was possible to perform experiments for the production of n-Propyl Propionate. The column is made of glass, which is thermally insulated to allow for adiabatic operation, and has an internal diameter of 50 mm (DN50). Although the value of its actual height is larger, due to the height taken by the inter-stage distributors, it possesses an effective height of 5.846 m of which 2.646 m are reactive, 2.7 m non-reactive and 0.5 m correspond to the reboiler. The internal structure of the column is made of non-reactive separative stages containing Sulzer BX structured packings and reactive stages containing Sulzer KATAPAK SP11 structured packings filled with Amberlyst 46 catalyst. Due to a series of problems resulting from the need to reassemble the column and some other problems related with data analysis, only two experiments produced acceptable results, with a product purity in the Bottoms stream between 74% and 80%.

The data retrieved from the pilot-scale experiments was then used to validate a model for the simulation of reactive distillation. This computational model, which was developed at the University of Dortmund and implement using Aspen Custom Modeler language, uses Equilibrium (EQ) and Non-Equilibrium (NEQ) stage models to simulate the behaviour of the reactive column, together with the appropriate mass transfer correlations and reaction data. The model was found to predict with reasonable accuracy the experimental data available - considering the lack of adequate thermodynamic data for the activity and VLE calculations and the considerations that had to be made regarding the reactive packing used - and was thus validated. Using the same model, the production of TAME in a RD column with similar configuration was investigated and it was predicted that a column, operating at total reflux - simulated by a reflux ratio of 1000 and a distillate stream of 0.5% of the total feed flowrate - and at a pressure of 2.5 bar, containing 1.6 m of Sulzer BX packing above the reboiler, followed by 3.3 m of Multipak II reactive structured packing filled with Amberlyst 15wet resin and a final 0.5 m of Sulzer BX packing, being fed with an equimolar amount of Methanol - below stage 1 - and isoamylenes - below stage 2 - is able to produce an almost pure bottom stream of TAME and achieve near total conversion of the reactants (above 99%). Some considerations regarding the use of non-pure isoamylene feed stock and alternative processes are also made.

RESUMO

Neste trabalho estuda-se a produção de TAME (Éter *terc*-amilmetílico) e de Propionato de Propilo por Destilação Reactiva (DR). Dada a necessidade de possuir dados relativos à cinética reaccional dos sistemas e visto esses dados não existirem para a síntese de Propionato de Propilo, foram efectuados estudos experimentais em reactor catalítico fechado, sendo usados como reagentes 1-Propanol e Ácido Propanóico e como catalisador a resina Amberlyst 46. Por análise dos resultados obtidos, foi determinado que o sistema reaccional não apresenta resistência interna significativa, pelo que pode ser usado um modelo Pseudo-Homogéneo, para o qual foram obtidas as expressões das constantes Cinética e de Equílibrio. Estas expressões demonstraram um bom ajuste à realidade experimental, quando utilizadas em simulações de reconciliação. Foi igualmente determinada a expressão da constante cinética para uma reacção não-catalisada, a qual apresenta valores 3 ordens de grandeza inferiores aos valores obtidos para as constantes das reacções catalíticas, pelo que esta não foi considerada para o cálculo de velocidades de reacção.

Seguiu-se o cálculo dos Mapas de Curvas Residuais Reactivas (MCRRs) utilizando, no caso da síntese de TAME, um modelo UNIFAC Modificado (Dortmund) para o cálculo de actividades e Equilíbrio Líquido-Vapor (ELV). Dado o sistema de síntese de TAME ser composto por quatro componentes, foi necessário recorrer a uma simplificação que consiste em agrupar os dois isoamilenos - 2-Metil-1-Buteno (2M1B) e 2-Metil-2-Buteno (2M2B) - num só pseudo-composto. A partir dos cálculos efectuados foi possível a determinação de zonas de operação para a DR do TAME, bem como os seus pontos estacionários. Foi igualmente verificado que a simplificação referida pode ser efectuada na maioria dos casos, mas que é necessária a devida cautela na sua utilização de forma a evitar erros na análise dos resultados. Em relação ao sistema do Propionato de Propilo, não foram desenhados nem analisados MCRRs visto a sua estrutura não permitir a

representação bidimensional das curvas residuais.

Recorrendo a uma coluna piloto de destilação reactiva, existente na Universidade de Dortmund, foi possível a execução de experiências para produção de Propionato de Propilo. A coluna é feita de vidro, isolado termicamente de forma a permitir operação adiabática, e possui um diâmetro interno de 50mm (DN50). A coluna tem uma altura efectiva de 5,846 m - isto apesar da sua altura real ser superior, devido à presença de distribuidores entre os andares - da qual 2,646 m é reactiva, 2,7 m é não reactiva e 0,5 m corresponde ao reebulidor. A estrutura interna da coluna consiste em 3 andares não-reactivos contendo um enchimento estruturado BX da Sulzer e 3 andares reactivos contendo um enchimento estruturado KATAPAK SP11, também da Sulzer, cheio com resina Amberlyst 46. Devido a inúmeros problemas que ocorreram devido à necessidade de remontar a coluna e a outros problemas relacionados com a análise de dados, apenas foram obtidos resultados aceitáveis para duas experiências, nas quais o produto apresentou purezas molares de 74% a 80% na corrente de cauda.

Os dados obtidos na coluna foram utilizados para validar um modelo computacional usado para simular destilação reactiva. Esse modelo, desenvolvido na Universidade de Dortmund e implementado em Aspen Custom Modeler, recorre, juntamente com dados de transferência de massa e reacção química, a modelos de andares de Equilíbrio (EQ) e Não-Equilíbrio (NEQ), para simular o comportamento da coluna. Apesar da falta de dados termodinâmicos para o cálculo de actividades e ELV, e, tendo sido necessário adaptar as correlações existentes para simular o enchimento estruturado reactivo utilizado, a previsão dos resultados experimentais demonstrou uma precisão bastante razoável sendo o modelo validado. Recorrendo a este modelo, simulou-se a produção de TAME numa coluna similar à utilizada experimentalmente, sendo previsto que, operando a refluxo total - simulado por uma razão de refluxo igual a 1000 e um caudal de topo igual a 0,5% do total dos caudais alimentados - e a uma pressão de 2,5 bar, sendo a coluna constítuida por 1,6 m de enchimento BX acima do reebulidor, seguido por 3.3 m de de enchimento reactivo Multipak II - contendo resina Amberlyst 15wet - e um andar final com 0.5 m de enchimento BX, sendo alimentada com uma quantidade equimolar de Metanol - abaixo do andar 1 - e Isoamilenos - abaixo do andar 2 -, é obtida uma corrente de cauda contendo TAME quase puro e conversões superiores a 99% para os reagentes. Foram igualmente feitas algumas considerações relativas ao uso de alimentação não pura de isoamilenos , bem como a processos alternativos.

RESUMÉ

Dans ce travail on étudie la production de TAME (éther tert-amyl méthylique) et de propionate de propyle par distillation réactive (DR). Une fois qu'on a besoin de donnés relatifs à la cinétique réactionnelle des systèmes et ces donnés n'existent pas pour la synthèse de propionate de propyle, on a effectué des études expérimentales en réacteur catalytique fermé, en utilisant comme réactifs 1-propanol et acide propanoïque et comme catalyseur la résine Amberlyst 46. Pour l'analyse des résultats, on a déterminé qui le système est bien modélisé par une cinétique pseudo-homogène, pour laquelle on a obtenu les expressions des constantes cinétique et d'équilibre. Cettes expressions ont été capables de bien s'ajuster à la réalité expérimentale, quant elles furent utilisées en simulations de réconciliation. L'expression de la constante cinétique pour une réaction non-catalytique était aussi déterminée, laquelle présente des valeurs trois fois plus petits que ceux obtenus pour les constantes des réactions catalytiques ; par conséquent, la réaction non-catalytique n'était pas considérée pour le calcul des vitesses de réaction. En suite on a calculé les mappes de courbes résiduelles réactives (MCRRs) en utilisant, dans le cas du TAME, un modèle UNIFAC modifié (Dortmund) pour le calcul des activités et de l'équilibre liquide-vapeur (ELV). Une fois que le système de synthèse de TAME est constitué par quatre composants, on a eut besoin d'utiliser une simplification consistant en grouper les deux iso-amylènes - 2-méthyl-1-butène (2M1B) et 2-méthyl-2-butène (2M2B) - en un seul pseudo-composant. En partant des calculs effectués il était possible déterminer des zones d'opération pour la DR du TAME, aussi bien que ses points stationnaires. Il était également vérifié que la simplification référée peut être effectuée dans la plupart des cas, mais qu'on doit être soigneux quand on l'utilise de façon à éviter des erreurs quand on analyse les résultats. En ce qui concerne le propionate de propyle, on n'a pas dessiné ni analysé des MCRRs une fois que sa structure ne permet pas la représentation bidimension-

nelle des courbes résiduelles. Faisant appel à une colonne pilote de distillation réactive, existant dans l'Université de Dortmund, il était possible d'exécuter des expériences pour la production du propionate de propyle. La colonne est en glace, thermiquement isolé de façon à permettre l'opération adiabatique, avec un diamètre interne de 50 mm (DN50). La colonne a une hauteur effective de 5,846 m - malgré son hauteur réelle qui est supérieure, du à la présence de distributeurs entre les étages - desquels 2,646 m est réactive, 2,7 m est non-réactive et 0,5 m correspond au rebouilleur. La structure interne de la colonne comprend 3 étages non-réactifs avec un garnissage structuré BX de la Sulzer, et trois étages réactifs avec un garnissage structuré KATAPAK SP11, de la Sulzer aussi, rempli avec résine Amberlyst 46. À cause des nombreux problèmes qui sont arrivés du au besoin de réinstaller la colonne et d'autres relatifs à l'analyse des donnés, on a obtenu des résultats acceptables seulement pour deux des expériences, dans lesquelles le produit a présenté des puretés molaires de 74% à 80% dans le courant d'en bas. Les donnés obtenus expérimentalement dans la colonne ont été utilisés pour valider un modèle computationnel utilisé pour simuler la distillation réactive. Ce modèle, développé dans l'Université de Dortmund et implémenté en langage Aspen Custom Modeler, utilise, conjointement avec des donnés relatifs au transfert de matière et à la réaction chimique, des modèles d'étages d'équilibre (EQ) e de non-équilibre (NEQ), pour simuler le comportement de la colonne. Malgré l'absence de donnés thermodynamiques pour le calcul des activités et du ELV, et considérant qu'on a eu besoin d'adapter les corrélations existantes pour simuler le remplissage réactive structuré qu'on a utilisé, la prévision des résultats expérimentaux a montré une précision raisonnable ce qui valide le modèle. En utilisant ce modèle, on a simulé la production de TAME dans une colonne semblable à celle utilisée expérimentalement, et on a prévu que, si l'on opère a reflux totale - simulé par une raison de reflux égale à 1000 et un produit de tête correspondant à 0,5% du total des débits d'alimentation - et à pression de 2,5 bar, la colonne ayant 1,6 m de garnissage BX en dessus du rebouilleur, suivi par 3,3 m de garnissage réactif Multipak II - contenant la résine Amberlyst 15wet - et un étage final avec 0,5 m de garnissage BX, étant alimentée par une quantité équimolaire de méthanol - sous le premier étage - et iso-amylènes - sous le deuxième étage -, on doit obtenir un courant de queue contenant TAME presque pur, et avoir conversions des réactifs supérieures à 99%. On a fait quelques considérations relativement à l'utilisation d'alimentation d'iso-amylènes non pure, aussi bien qu'à des procédés alternatifs.

ACKNOWLEDGEMENTS

First and foremost, I would like to thank my supervisor, Professor José Miguel Loureiro, for catalysing so well this work towards its completion. Most especially, for, during our work together, making me feel like this was MY work and he was help. In truth, this work is greater than I alone would be able to achieve.

Second, I would like to thank the Faculty of Engineering of the University of Porto - namely the Department of Chemical Engineering - and LSRE - Laboratory for Separation and Reaction Engineering - for all the facilities and logistical help provided.

Third, I would like to thank FCT for indirectly supporting me through project POCTI/EQU/41406/2001 and for teaching me to rely on myself and not on third parties.

Finally, I would like to thank the financial support given by the European Commission within the 5th Framework Programme, Marie Curie Training Site "Reactive Separations"; Contract Nr. HPMT-CT-2001-00408, without which this work would had taken far longer.

A very special thanks to the Lehrstuhl für Thermische Verfahrenstechnik of the Fachbereich Bio- und Chemieingenieurwesen, Universität Dortmund, for providing the greater boost this work needed at the right time and in particular to Professor Andrzej Górak for the invitation to work there and for all the support provided. Serdecznie dziękuję!

Another special thanks to all the people who worked and shared their lives with me, both in Porto and Dortmund, most especially my office / lab colleagues. In Porto, Susana, Olga, Carlos, in room E416, for all the discussions we had - work related or not - which helped keep the *animus* going, and Mafalda in the lab without whom lots of things would be broken by now (well, more than those that are...). Muito Obrigado! To the rest of the people in LSRE which helped me along - Adriano, Carlos, Eduardo, Filipe, Marta, Simone, Vera and many others - my deepest thanks!

Although not in Porto any more, I wish to thank my predecessor, Manela Vilarinho, without whom this work would have been far harder than it was! The reactor still works!

In Dortmund, to Alexey - спасибо - who taught me a lot about Aspen without (like me) liking it at all (Fortran's better, right?) and to Carsten, with whom a great part of the RD part of this work was done, including those long night shifts (I'm done, now it's YOUR turn... eheheheh), Danke Sehr. To the rest of the people in Dortmund (and all of the TV-ers), most especially Daniela, Ivo and Jogi with whom I spent most of my "between-work" time and who made me feel like there's more than one home in one's life, Danke (and Mersi)!

Finally, I would like to thank the people directly or indirectly responsible for my work, Peter - my "local supervisor" and my first contact in Dormund, and also those who taken care so well of all the bureaucratic and welcoming stuff - Dorota, Judith and Silke.

My friends, from before and now and ever, which although not directly connected with this work helped me get away from it sometimes, thank you! We do need to see each other more often so that gossip doesn't build up excessively.

I would like to thank my family, my parents and brother, for keeping up with me all this time, through the easy parts and most especially the hard ones, without flinching. I can't say it was easy, but I can assure that it is done.

Finally, To Catarina, my more-than-anything and the one who kept (and keeps) me going day and night, sun or rain, I cannot thank because there is no word to express such gratitude. Ta gra agam ort.

CONTENTS

LIST OF FIGURES

LIST OF TABLES

1 INTRODUCTION

1.1 Background and Motivation

The main objective of a chemical engineer has always been the development and optimisation of processes. This is usually translated in the optimisation of profit and includes such factors as the construction cost of the project (which includes the cost of the process' units), the capital investment of operation (be it energetic, consumption of reactants or removal of undesirable side-products), the value of the products and, most recently, environmental-related costs. The overall result of these considerations leads to: a) cheaper and smaller units and as less units as possible; b) lowest energy consumption, most complete conversion of reactants with the least production of side-products; c) highest possible product yield and purity and d) least impact on the environment.

In order to tackle all of these issues at once, the old, unit-based approach to the chemical industry where specialised independent units (e.g. reactors, distillation columns, heat exchangers) operate interconnected in a mixture of parallel and serial configurations has slowly been replaced by multifunctional units, which incorporate two or more phenomena in a synergistic way, reducing operating costs (due to a higher energy efficiency or higher reactant conversion, avoiding costly recycle loops), increasing product throughput as well as its purity, or diminishing the plant's footprint. One of the most obvious possibilities for a multifunctional unit is the integration of the classic reaction and thermal separation units – the reactor and the distillation column, respectively – into one, multifunctional, reactive (or catalytic) distillation (RD) column.

The advantages of such an integration are multiple (Sundmacher and Kienle, 2003):

- Elimination of the chemical equilibrium barrier, by removing of one or more products from the reaction zone, thus increasing

conversion;

- Shift of the azeotropic points, namely saddles, allowing for better separations and/or larger working regions;
- Exploitation of the heat of reaction, if exothermic, as heat of vaporisation, reducing the column's heat demands at the reboiler;
- Drastic reduction of the plant's footprint, through elimination of recycling loops, interconnecting tubing, heat transfer equipment and the 'standard units' themselves.

Nonetheless, and as with any process, the use of reactive distillation is not always advantageous or even feasible. For simpler configurations (e.g. tubular reactor plus distillation column) which already have high efficiency, a RD column will most likely prove to be excessive and will represent higher implementation and operating costs. Also, in some systems, the conjunction of the reactive and separative phenomena may, in fact, worsen reaction and/or separation performance due to the formation of undesirable reactive azeotropes, removal of reactants from the reaction zone or excessively strong perturbations of the column's heat balance (e.g. strongly endothermic reactions).

Despite an increase in interest and visibility in recent times, reactive distillation is not a new process. A patent submitted by Backhaus (1921) and assigned to the U.S. Industrial Alcohol Co. concerning a process for the continuous production of esters, namely methyl acetate reads on lines 100-107:

> In carrying out the process, the esterification is carried out more completely and more rapidly by reason of the continual removal by distillation of the ester from the esterification zone and because of the provision of much larger quantities of an ester such as methyl alcohol than are needed for the reaction.

Although not called by the now adopted name, this is a reactive distillation operation, i.e, the removal of products from the reaction zone through distillation. Despite the early appearance of reactive distillation, the process did not have a lot of success in the subsequent years, with little to no practical use, due mainly to the added complexity of designing and operating such a column. It is only ironic that more than half-a-century after Backhaus' patent and the subsequent near-oblivion of reactive distillation, its revival arose from a process

for methyl acetate production, developed at Eastman Kodak (Agreda and Partin, 1984).

In the classic process, Methyl Acetate (MeAc) was produced in a tubular reactor and the product stream went through a several distillation processes to separate each component (Fig. 1.1). This was due to the presence of minimum azeotropes with boiling points near pure Methyl Acetate, which forced the use of azeotropic and extractive distillation techniques to separate the product stream components. The use of a reactive distillation column simplified the process considerably, by eliminating almost all of the distillation columns (keeping only two of them to remove impurities) – as can be seen on Fig. 1.2 – while maintaining a very high process performance, with almost pure Methyl Acetate (99.5 % w/w) being produced at a far lower energy comsumption rate and with far less waste.

The Eastman Kodak process for the production of Methyl Acetate became the herald of reactive distillation as a viable alternative to complex reactive-separative processes and led to a substantial increase in both research and industrial application in this area. Within a few years, more processes emerged, be it for other esterifications (Zhicai et al., 1998), etherifications (Sundmacher and Hoffmann, 1996), acetalisations (Chopade and Sharma, 1997) and others. An extensive review of the use of reactive distillation, be it industrially or conceptually, was done by Sharma and Mahajani (2003), listing roughly 100 cases, which in itself shows the importance that reactive distillation is achieving.

This work, which follows a previous one by Ferreira de Oliveira (2004), intended originally to evaluate the suitability and performance of the production of TAME in a reactive distillation column. In the course of its development, an opportunity for cooperating in the investigation of the production of Propyl Propionate by reactive distillation appeared and gained such an importance that it ended up equalling TAME in terms of time spent. This led to changing (in fact, doubling) the initial goal of analysing one reactive system and so Propyl Propionate was added to TAME.

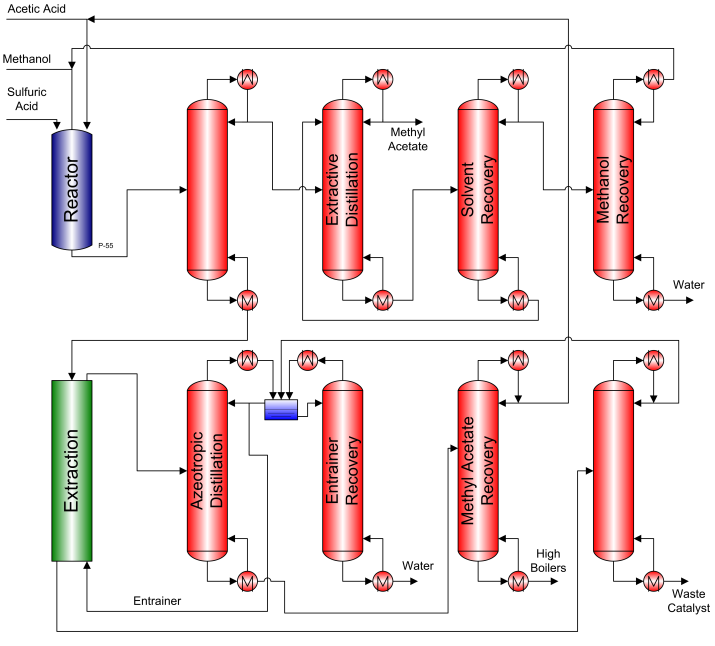

Figure 1.1: Classic production process of Methyl Acetate

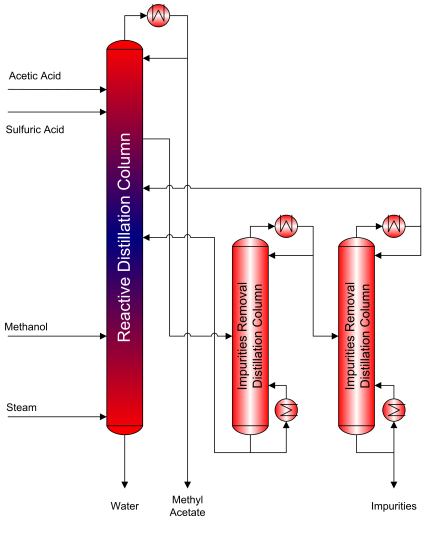

Figure 1.2: Reactive distillation process for the production of Methyl Acetate (adapted from Agreda et al. (1990))

1.2 Production and Uses of n-Propyl Propionate

n-Propyl Propionate (Fig.1.3) is a member of the propionate esters family and shares with them its basic characteristics: good performance as a solvent, good volatility, high electrical resistance, pleasant odour profile at low concentrations as well as being sensible to the taste, and no toxicity (The Dow Chemical Company, 2002a; Glancy, 1987). These characteristics define clearly the two fields where this compound is mostly used: as a solvent for paints and inks and as an additive for food and perfumes.

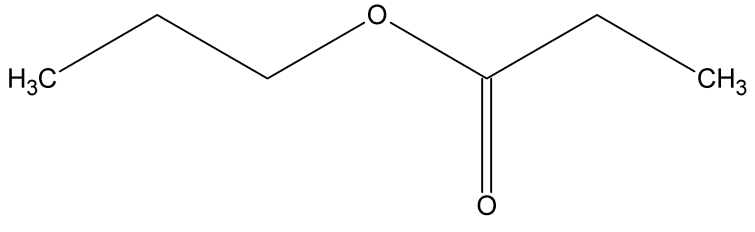

Figure 1.3: Chemical structure of n-Propyl Propionate

The main consumption market for propyl propionate is as a solvent for paints and inks. Its properties are very similar to Xylene (Table 1.1), but with several advantages:

- It is not an Hazard Air Pollutant (HAP) – as defined by the US Environmental Protection Agency (EPA) and part of the Clean Air Act (42 U.S.C. 7412);
- It is less toxic (Table 1.2);
- It emits a weaker and more 'pleasant' odour (The Dow Chemical Company, 2002a).

This sets Propyl Propionate as a viable alternative to Xylene (Tyler and Sakshaug, 2004) and might result in an increased adoption over the next years, as environmental and health legislation becomes stricter and restricts or bans replaceable HAP's.

n-Propyl Propionate has also a presence in the the food additive and perfume markets. According to *Fenaroli's Handbook of Flavor Ingredients* (Fenaroli, 2002), 'Propyl propionate has a complex, fruity odour reminiscent of apple, banana and pineapple'. At a concentration of 20 ppm, it shows a '(s)weet, lift, tropical green, fruity' taste and is reported

Table 1.1: Properties comparison between Xylene and Propyl Propionate (NTP conditions, taken from Knovel Corporation (2003) and The Dow Chemical Company (2002b))

	Xylene	Propyl Propionate
Molecular Weight	106.17	116.16
Boiling Point (°C)	138.0	122.4
Flash Point (°C)	25	24
Density (g/cm^3)	0.868	0.883
Viscosity (cP)	0.63	0.70
Surface Tension (mN/m)	28.8	24.7
Evaporation Rate (n-BuAc=1)	0.75	1.2

to have been found in white Sauvignon grape variety, fresh apple, apricot, melon, papaya, Gruyere cheese, rum, cider, popcorn, durian, olive, malt whiskey and coffee. This results in its being classified as a natural flavouring substitute – and not as an artificial flavouring – and it is recognised and registered by the JECFA (Joint Expert Committee on Food Additives) under nr. 142, the American FDA (Food and Drug Administration) under 21 CFR 172.515, the European Union on the European Comission Decision 1992/217/EC (The Comission of the European Communities, 1999), the Council of Europe under nr. 203 and the FEMA (Flavor and Extract Manufacturers Association) under nr. 2958.

Table 1.2: Toxicity results of n-Propyl Propionate and Xylene in animals (American College of Toxicology, 1992a,b; Fetsko, 1974; Hollingsworth et al., 1956)

		LD50 (mg/kg)	
Animal	Application	Propyl Propionate	Xylene
Rabbit	Skin	> 14128	> 1700
Rat	Oral	10331	4300

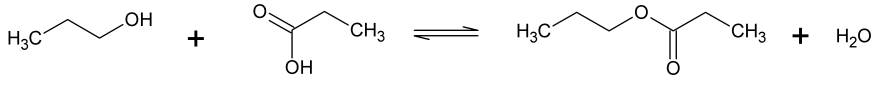

Figure 1.4: Reaction structure for Propyl Propionate synthesis

It is usually produced by liquid-phase homogeneous catalysis (using Sulphuric Acid – H_2SO_4 – or Boron Trifluoride – BF_3) in plug-flow reactors, followed by distillation in a distillation column, having as reactants 1-Propanol (POH) and Propionic Acid (ProAc) and Water as a secondary product (Fig. 1.4). It can also be produced by heterogeneous catalysis, using a strong-acid resin as a catalyst (Lilja et al., 2002), but in this case a secondary product, di-n-propyl ether (DPE), is formed from 1-Propanol inside the catalyst pores, as was proved during the catalyst pre-selection performed for this work.

1.3 Production and Uses of *tert*-Amyl Methyl Ether (TAME)

TAME (Fig.1.5), an acronym for *tert*-Amyl Methyl Ether, is a member of the oxygenated fuel additives family of which MTBE (Methyl *tert*-Butyl Ether) is the most known member. The adoption of these additives is a direct result of the Clean Air Act (42 U.S.C. 7542, 2000), which prohibited, in the United States, the use of lead-based anti-knocking additives in petrol from 1995 onwards. The European Union followed suite in October 1998, with Directive 98/70/EC (The European Parliament and The Council of the European Union, 1998) which prohibited for all member-states the commercialisation of leaded petrol in their territories from 2000 onwards. This resulted in the adoption of oxygenated additives, alcohols or long-chain esters as alternatives to lead (or, more correctly, to Lead Tetraethyl) in order to maintain the performance characteristics of the petrol, namely its octane number.

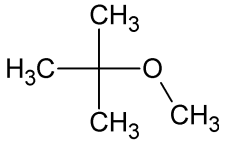

Figure 1.5: Chemical structure of TAME

The most widely adopted of these compounds is MTBE, due to being the one with the cheapest production costs (being produced from isobutene and methanol) but, since its early adoption in some US states in 1992, health problems (headaches, nausea, eye irritation) started to be reported (National Center for Environmental Assessment, 1993). This led to the conduction of further studies and subsequent

publication of a series of guidelines and warnings regarding MTBE and other oxygenated additives (Akland et al., 1996; Watson et al., 1997) and, more precisely, the appearance of MTBE in drinking water (Abernathy, 1997; Davis et al., 1998). Based on this information, nineteen U.S. States banned it partially or completely (Table 1.3). This meant that other additives had to be used, which includes TAME (with the exception of two cases). Although in Europe MTBE is still allowed, it is to be expected that in the near future EU legislation will follow the US one.

TAME already has an advantage over MTBE (and even ETBE) during the summer and in hotter climates: lower Reid vapour pressure of the blend (Table 1.4). This means that petrol containing TAME is less likely to vaporise in the summer due to temperature, thus pollutes less. Even so, its adoption has been slow at best and might be compromised in the future if, as seems likely, the ban on additives extends to all ethers.

TAME is the product of a reaction between Methanol (MeOH) and two isoamylenes (2MxB): 2-Methyl-1-Butene (2M1B) and 2-Methyl-2-Butene (2M2B), which also react by themselves forming one another (Fig. 1.6). The reaction is acid-catalysed and uses an heterogeneous catalyst – usually a strong-acid ion exchange resin – to that effect.

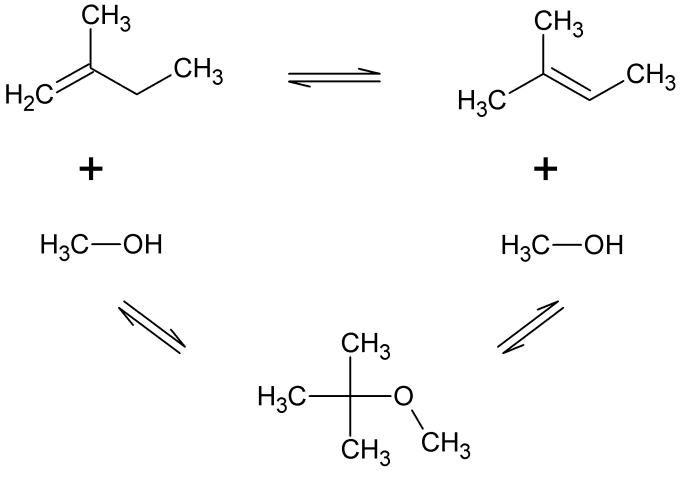

Figure 1.6: Reaction structure for TAME synthesis

The main problem with the production of TAME is a common one: low conversion. For example, Ferreira de Oliveira (2004) determined that, in an equimolar feed of isoamylenes and methanol,

Table 1.3: U.S. States which banned partially / totally MTBE (adapted from Gustafson (2004))

U.S. state	Type of Ban	Start Date	Max. Vol.
California	Complete	31/12/03	n.a.
Colorado	Complete	30/04/02	n.a.
Connecticut	Complete	01/01/04	n.a.
Michigan	Complete	01/06/03	n.a.
Minnesota	Complete[†]	02/07/05	n.a.
New York	Complete	24/05/00	n.a.
Illinois	Partial	24/07/04	0.5 %
Indiana	Partial	24/07/04	0.5 %
Iowa	Partial	01/07/00	0.5 %
Kansas	Partial	01/07/04	0.5 %
Kentucky	Partial	01/01/06	0.5 %
Maine	Partial	01/01/07	0.5 %
Missouri	Partial	31/07/05	0.5 %
Nebraska	Partial	13/07/00	1.0 %
New Hampshire	Partial[‡]	01/01/07	0.5 %
Ohio	Partial	01/07/05	0.5 %
South Dakota	Partial	01/07/01	0.5 %
Washington	Partial	01/01/04	0.6 %
Wisconsin	Partial	01/08/04	0.5 %

[†] Ban also applies to ETBE and TAME
[‡] Ban also applies to other ethers and TBA

Table 1.4: Comparison of Reid Vapour Pressures (RVP, mmHg at 100 °F (37.8 °C)) of MTBE and TAME (Council, 1993)

	MTBE	ETBE	TAME
Blend RVP	8	4	1.5

considered ideal conditions, the mass fraction of TAME at equilibrium is of roughly 0.21. If we remove the presence of the inert isopentante (iC5) from the calculation, we get a mass fraction of roughly 0.58 which corresponds to only 35% in terms of total moles. This means that the product stream from a reactor must be distilled – a reactor plus distillation column setup, of which Neste's NExTAME™ process (Fig. 1.7) is an example – or, in alternative, produced and distilled simultaneously – in a reactive distillation column, usually with a pre-reactor, as in CDTech's CDTAME™ process (Fig. 1.8).

It is interesting to note that both licensers mention the possibility of operating their technology for the production of other ethers, either simultaneously with TAME or by change of feedstock. Ferreira de Oliveira (2004) lists, in her thesis, several processes and licensers/licensees (pgs. 17-18, Tabela 1.2) and in all cases the processes are, again, indicated as being suitable for the production of more than TAME. This is due to the low demand of TAME (in comparison with other oxygenates) and the seasonality of the demand (summer months, as already mentioned). Another apparent trend is that more recently developed processes favour reactive distillation in comparison to the classic reactor plus distillation column arrangements. The reason for this seems to be more connected to the previous point, that TAME is not produced exclusively or alone, than with TAME production itself, since it can be produced quite efficiently by the classic arrangement (Neste quotes a 90% conversion for TAME, while a similar arrangement for MTBE/ETBE/TAME – e.g., Neste's NExETHERS™ process – needs an additional distillation column).

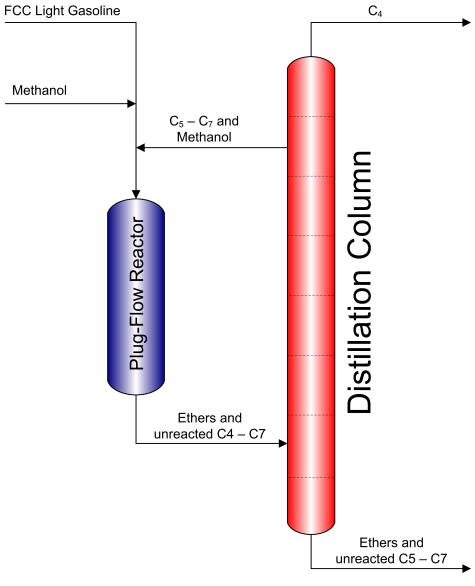

Figure 1.7: NExTAME™ process for the production of TAME (Neste Jacobs Oy, n.d.)

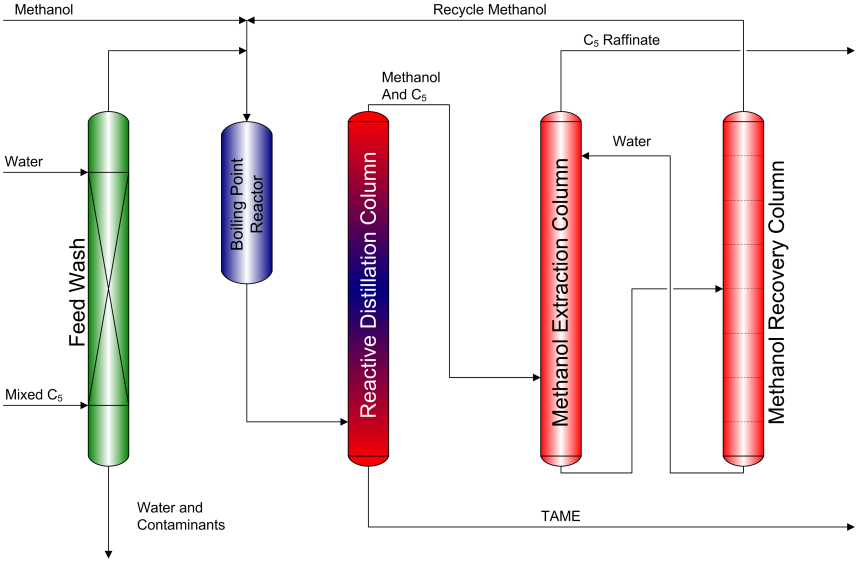

Figure 1.8: CDTAME™ process for the production of TAME (CD Tech, n.d.)

1.4 Main Aspects of Reactive Distillation

As the Methyl Acetate example presented in the beginning of this Chapter shows, Reactive Distillation began as an afterthought, i.e., 'regular' distillation columns that happened to also have reacting chemicals inside. The use of homogeneous catalysts, such as sulphuric acid, were thought to have little influence in the column behaviour and, when and if they did, adjustments were made to have the same separative performance as before.

Looking first at homogeneous catalysis, since heterogeneous catalysis represents by itself a departure from 'simple' distillation, the operating regimes for reactive and non-reactive distillation are different, if not opposite: while in non-RD columns, one wants to maximise liquid-vapour contact – which usually means small holdups as well –, in RD the main factor is the residence time of the liquid phase and inter-liquid contact – meaning large holdups. So, while non-reactive tray distillation columns are operated at high superficial velocities (spray or froth flow regimes) to favour liquid-vapour contacting, RD columns are operated at low superficial velocities (bubbly flow regime) (Krishna, 2002) and high holdups, favouring residence time instead. Despite this problem, the internal design of the column is very similar, using trays that are only modified to allow for an higher liquid holdup (and eventually some geometric changes to the tray to avoid short-circuiting and dead-zones).

With heterogeneously catalysed reactions, the departure from 'regular' distillation is far greater. The most immediate and evident problem is how to accomodate a solid catalyst, which is usually bead-like and with a small diameter, inside the column. A second one is how to maximize liquid flow through the catalyst while minimizing vapour flow through it. To address these problems, several configurations for 'packing' the catalist exist. Krishna 2003 does a quite thorough review of existent packing types, mentioning:

- Porous spheres filled with catalyst;
- Cylindrical envelopes;
- Wire gauze envelopes of diverse shapes;
- Perpendicularly disposed wire mesh tubes with catalyst;
- Cloth-wrapped catalyst bales;

- Sandwiched catalyst between corrugate wire gauze sheets;
- 'Activated' packings such as Raschig rings or monoliths;
- 'Envelopes' containing the catalyst and placed on regular trays.

Of these packings, the most commonly used ones are either bales or corrugated sheets. Bales are made of cloth, knitted to a steel wire mesh, to which pockets, containing the catalyst, are sewn into (Fig. 1.9). They are then rolled into bale-shape (hence the name) and installed into the reactive section of the column. The pioneering work into this kind of packing was done in the U.S. by the Chemical Research & Licensing Company (CR&L) and later on licensed to Catalytic Distillation Technologies (CDTECH) – which is a partnership of the aforementioned CR&L and ABB Lumus Global – for inclusion on their RD units.

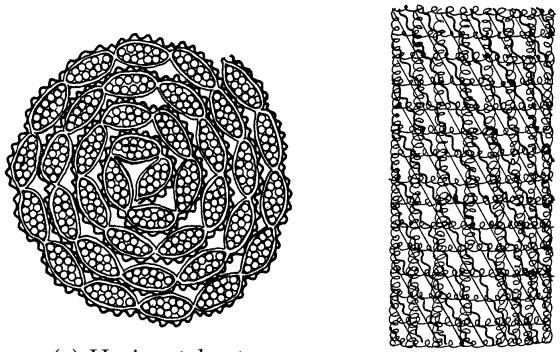

(a) Horizontal cut

(b) Vertical view

Figure 1.9: Bale-like packing (taken from Smith, Jr. (1980))

Corrugated sheets (also known as 'sandwich') packings differ from bales as they are not a continuous roll of packing, but rather individual sheets which are bound together by a gauze band. The example presented in Fig. 1.10 represents one of the more common reactive packings, Sulzer's Katapak-SP®, which is made of intercalated reactive and non-reactive sheets. The reactive sheets are specifically made for the reactive packing (the structure can be seen on Fig. 1.11) while the non-reactive ones are Sulzer's MellapakPlus® sheets (Sulzer Chemtech, 2005).

Both packing types offer similar characteristics (Table 1.5) but due to the criss-cross flow pattern of the corrugated sheets packings, they

Table 1.5: Estimated properties of bale-like and corrugated sheet packings (SI units, adapted from Lebens et al. (1999))

Property	Bales	Katapak-S
void fraction	0.75	0.75
macroscopic void fraction	0.50	0.50
catalyst loading	0.20	0.20
gas-liquid mass transfer area	169	250
catalyst surface-to-volume ratio	4000	4000
packing surface-to-volume ratio	800	800

offer a better axial dispersion and, subsequentely, better mixing. A possible indication of the superiority of this packing type versus bales is that CR&L patented their last technology in bale-like packings in 1995 (Crossland et al., 1995), which already includes a sort-of criss-cross pattern between the catalyst bags. Yet more recently, in 1998, they patented another geometry (Groten et al., 1998), which is a fixed, monolith-like structure, for holding catalyst, departing completely from bales.

When comparing with classic, unstructured, packings – such as Raschig rings, which can be activated for RD – structured packings offer better liquid-liquid contact, lower pressure drops, but a far poorer liquid-vapour contact and thus separation (Baur and Krishna, 2002). This results in the necessity of assessing previously the main focus of the RD column reaction or separation. For reaction-intensive columns (e.g. slow reactions), structured packings are preferred, even more so when they allow for longer and thiner structures – due to the low pressure drop – favouring higher conversions. For more separative columns (e.g. fast reactions), unstructured packings can be used and while they require shorter and 'stubbier' columns, due to the pressure drop, they also allow for a better separation and thus reduce the need for post-unit separative processes.

The rest of the RD column's structure is in all similar to a regular distillation column (distributors, reboilers, condensers, ...) and, for the untrained eye, looks exactly the same. There are some caveats though, which are related to the use of catalyst and the presence of structured packings. Most catalysts, especially ion-exchange resins, can become inactive if they dry up, as air gets inside the pores, blocking the active sites. This means that, even when not operating, the column must be kept wet by recirculation of, for example, the liquid in the

Figure 1.10: Katapak-SP® structured packing (taken from Sulzer Chemtech (2005))

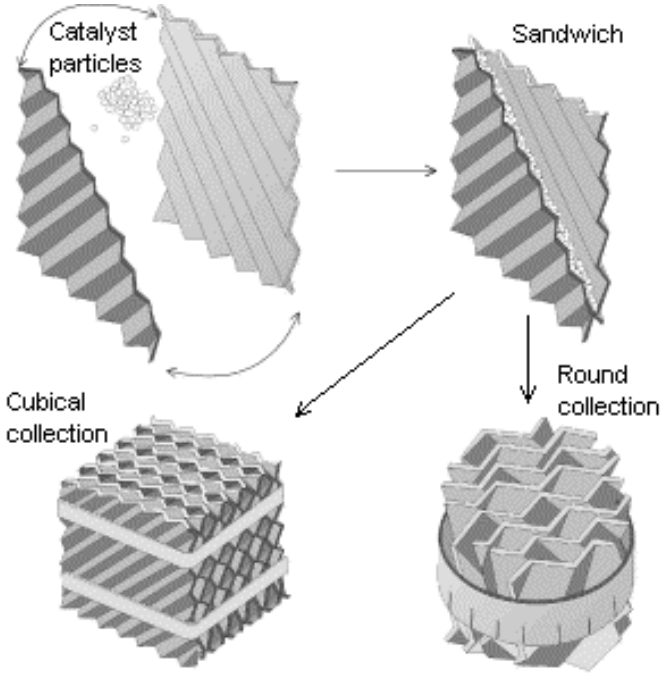

Figure 1.11: Katapak-S® sheet and structure (taken from van Baten and Krishna (2002))

reboiler. Also, before (if possible) or after (if not) the installation of the packed stages, residence time distribution (RTD) experiments should be conducted as to reduce or eliminate preferencial routes that will most certainly appear. If DTR is not possible, maximum attention should be taken to detect if excessive liquid flow is ocurring in the sides of the column. If it does happen, the packings should be reinserted or rotated. Finally, special care should be taken so that the temperature inside the catalytic zones of the column does not exceed the manufacturer's specification for the catalyst, which might render the catalyst useless or, in the case of resins, even fuse it to the packing, destroying both the catalyst and packing structure.

1.5 Structure and Objectives

The two main objectives of this work are the study of reactive distillation as a process for the production of *tert*-Amyl Methyl Ether, or TAME, and n-Propyl Propionate. As mentioned earlier, the first objective originated as a follow-up to a previous work done by Ferreira de Oliveira (2004) in which she investigates the production of TAME in batch and plug-flow reactors – determining kinetics for the process as well – and introduces the concept of Reactive Distillation through the Residue Curve Maps (RCMs). Her work, and this one as well, are also the result of two other preceding works on the production of oxygenated aditives for petrol: ETBE (Prior, 2001) and MTBE (Caetano, 1995). The second objective comes as a result of a cooperation with the University of Dortmund (UniDo) and has no relation to any previous work, as Propyl Propionate has not been the target of any consistent research up to this date.

The first step in any reaction distillation project, or in any project for that matter, is having as much preliminary data available as possible. In this case, mass transfer data are readily available from literature and previous works developed at the University of Dortmund. Reaction kinetics and related data are also available for TAME (from Ferreira and Loureiro (2004)), but none exist for Propyl Propionate using an heterogeneous ion-exchange resin as a catalyst – with the exception of the one published by Lilja et al. (2002), which only reports for only one reacting temperature (of 60°C) making it of little use. Given this, several kinetic experiments are carried out and the results analysed in order to obtain a consistent and representative kinetic law for the production of Propyl Propionate in the range expected to occur

inside a RD column. This constitutes Chapter 2.

From the available mass transfer and kinetic data, preliminary studies on the feasibility of applying RD to a certain process can be carried out. The most important of these, as it defines working regions for RD (or for distillation, if required) is the Residue Curve Map (RCM). The RCM is a theoretical simulation of a batch distillation process in which the change of composition in the liquid phase (residue) is analysed and plotted in the form of curves in a diagram (map), allowing to determine the trajectories of the distillation from a given starting point and, more importantly, the final, steady-state composition of the mixture. This allows, with little capital or time investment, to determine if a certain reactive system is likely to be adequate for RD or not, and can also give an idea of the necessary operating conditions for the column (e.g. pressure). This is dealt with, for TAME and Propyl Propionate, in Chapter 3.

The initial idea of this work was to operate the existing pilot-scale reactive distillation column, present at the University of Dortmund, for producing TAME and thus validating a computational model. Unfortuntely, TAME-synthesis requires above atmospheric pressures for proper operation and the pilot plant only operates up to 1 atm. Because of this, it was decided to carry out experiments with the n-Propyl Propionate synthesis process and with the results from those experiments, validate a computational model. The results from the sucessful experimental runs and a discussion of all the work involved is present in Chapter 4.

Using the experimental data gathered at the pilot plant, the PROFILER simulator (Klöker et al., 2005), developed at the University of Dortmund, is re-validated for n-Propyl Propionate synthesis by comparison of experimental versus computational runs. n-Propyl Propionate synthesis simulations are only carried out in the validation step, since some differences with regard to packing data exist between the simulator and the actual column and are still being studied. TAME synthesis is simulated somewhat more extensively since it does not have to conform to the existent packing structure. The simulation results, as well as an analysis of the results obtained, are described in Chapter 5.

Finally and taking into consideration the results obtained, several conclusions regarding the suitabily of RD as a process for producting TAME and Propyl Propionate are drawn and analysed, leading also to suggestions for future work. The main conclusions of this work are thus outlined in Chapter 6.

BIBLIOGRAPHY

42 U.S.C. 7412, 2000. Hazardous Air Pollutants.

42 U.S.C. 7542, 2000. Regulation of fuels.

Abernathy, C., 1997. Fact sheet: Drinking water advisory: Consumer acceptability advice and health effects analysis on methyl tertiary-butyl ether (mtbe). Tech. rep., U.S. Environmental Protection Agency.

Agreda, V. H., Partin, L. R., 1984. Reactive distillation process for the production of methyl acetate. U.S. Patent 4,435,595, assignee: Eastman Kodak Company.

Agreda, V. H., Partin, L. R., Heise, W. H., February 1990. High-purity methyl acetate via reactive distillation. Chem. Eng. Progr. 86, 40–46.

Akland, G., Auer, C., Caldwell, J., Cote, I., Davis, J. M., Dubey, S., Durkee, S., Elder, J., Farland, W., Freed, C., Goldman, L., Grant, L., Gray, J., Helmer, K., Huber, A., Oge, M., Riordan, C., Ris, C., Smith, M., Timm, G., Washington, E., 1996. Oxyfuels information needs. Tech. rep., U.S. Environmental Protection Agency.

American College of Toxicology, 1992a. Acute toxicity data. J. Am. Coll. Toxicol., Part B 1, 175.

American College of Toxicology, 1992b. Acute toxicity data. J. Am. Coll. Toxicol., Part B 1, 177.

Backhaus, A. A., 1921. Continuous process for the manufacture of esters. US Patent 1,400,849, assignee: U.S. Industrial Alcohol Co.

Baur, R., Krishna, R., 2002. Hardware selection and design aspects for reactive distillation. A case study on synthesis of TAME. Chem. Eng. Process. 41, 445–462.

Caetano, N., 1995. Síntese de MTBE: Estudo cinético em reactor fechado e simulação / operação de um reactor de leito fixo. Ph.D. thesis, Faculty of Engineering of the University of Porto.

CD Tech, n.d. Cdtame : Technology profile. www.cdtech.com.

Chopade, S. P., Sharma, M. M., 1997. Reaction of ethanol and formaldehyde: use of versatile cation-exchange resins as catalyst in batch reactors and distillation columns. Reac. Funct. Polym. 32, 53–65.

Council, U. N. P. (Ed.), 1993. U.S. Petroleum Refining: Meeting Requirements for Cleaner Fuels and Refineries. Vol. Appendix L.

Crossland, C. S., Gildert, G. R., Hearn, D., 1995. Catalytic distillation structure. US Patent 5,431,890, assignee: Chemical Research & Licensing Company.

Davis, J. M., Brophy, J., Hitzig, R., Kremer, F., Osinski, M., Prah, J. D., Schmelling, S., Speth, T. F., Swank, R., Tafuri, A. N., West, C., 1998. Oxygenates in water: Critical information and research needs. Tech. rep., U.S. Environmental Protection Agency.

Fenaroli, G., 2002. Fenaroli's Handbook of Flavor Ingredients, 4th Edition. CRC Press, Boca Raton, USA.

Ferreira, M. V., Loureiro, J. M., 2004. Number of actives sites in tame synthesis: Mechanism and kinetic modeling. Ind. Eng. Chem. Res. 43, 5156–5165.

Ferreira de Oliveira, M. M. V., 2004. TAME: Cinética em reactor fechado e simulação da produção em contínuo. Ph.D. thesis, Faculty of Engineering of the University of Porto.

Fetsko, J. M. (Ed.), 1974. Organic Solvents. Vol. 1 of NPIRI Raw Materials Data Handbook. National Printing Ink Research Institute, Bethlehem, USA.

Glancy, C. W., 1987. New solvents for high solids coatings. In: Proceedings of the Water-Borne and Higher-Solids Coatings Symposium. pp. 209–229.

Groten, W. A., Booker, D., Crossland, C. S., 1998. Catalytic distillation structure. US Patent 5,730,843, assignee: Chemical Research & Licensing Company.

Gustafson, K., 2004. State actions banning mtbe (statewide). Tech. rep., U.S. Environmental Protection Agency.

Hollingsworth, R. L., McCollister, D. D., Rowe, V. K., Wolf, M. A., 1956. Toxicological studies of certain alkylated benzenes and benzene: experiments on laboratory animals. AMA Arch. Ind. Health. 14, 387–398.

Klöker, M., Kenig, E. Y., Hoffmann, A., Kreis, P., Górak, A., Jun. 2005. Rate-based modelling and simulation of reactive separations in gas/vapour-liquid systems. Chem. Eng. Process. 44 (6), 617–629.

Knovel Corporation, 2003. Knovel critical tables. Online at Knovel Library.

Krishna, R., 2002. Reactive separations: more ways to skin a cat. Chem. Eng. Sci. 57, 1491–1504.

Krishna, R., 2003. Reactive Distillation: Status and Future Directions. Wiley VCH, Ch. 7 - Hardware Selection and Design Aspects for Reactive Distillation Columns, pp. 169–189.

Lebens, P. J. M., Kapteijn, F., Moulijn, J. A., 1999. Potentials of internally finned monoliths as a packing for multifunctional reactors. Chem. Eng. Sci. 54, 1359–165.

Lilja, J., Murzin, D., Salmi, T., Aumoa, J., Mäki-Arvela, P., Sundell, M., 2002. Esterification of different acids over heterogeneous and homogeneous catalysts and correlation with the taft equation. J. Mol. Catal. A: Chem. 182-183, 555–563.

National Center for Environmental Assessment (Ed.), 1993. Proceedings of the Conference on MTBE and other oxygenates: A Research Update.

Neste Jacobs Oy, n.d. Nextame light cracked naphta etherification. URL `www.nesteengineering.com`

Prior, J. M. V., 2001. Síntese de ETBE: Estudo cinético em reactor fechado; simulação / operação de um reactor de leito fixo. Ph.D. thesis, Faculty of Engineering of the University of Porto.

Sharma, M. M., Mahajani, S. M., 2003. Reactive Distillation: Status and Future Directions. Wiley-VCH, Ch. 1 - Industrial Applications of Reactive Distillation, pp. 3–29.

Smith, Jr., L. A., 1980. Catalyst system for separating isobutene from c4 streams. US Patent 4,215,011, assignee: Chemical Research and Licensing Company.

Sulzer Chemtech, 2005. Structured packings for distillation, absorption and reactive distillation.
URL www.sulzerchemtech.com

Sundmacher, K., Hoffmann, U., 1996. Development of a new catalytic distillation process for fuel ethers via a detailed nonequilibrium model. Chem. Eng. Sci. 51, 2359–2368.

Sundmacher, K., Kienle, A., 2003. Reactive Distillation: Status and Future Directions. Wiley-VCH, Ch. Preface, pp. XI–XVII.

The Comission of the European Communities, 1999. Commission Decision of 23 February 1999 adopting a register of flavouring substances used in or on foodstuffs drawn up in application of regulation (EC) no 2232/96 of the European Parliament and of the Council of 28 October 1996. Off. J. Eur. Comm. L 84, 20.

The Dow Chemical Company, 2002a. Oxygenated solvents: Ucar n-alkyl propionates.

The Dow Chemical Company, October 2002b. Ucar n-propyl propionate.

The European Parliament, The Council of the European Union, 1998. Directive 98/70/EC of the European Parliament and of the Council of 13 October 1998 relating to the quality of petrol and diesel fuels and amending Council Directive 93/12/CE. Off. J. Eur. Comm. L 350, 58–68.

Tyler, T., Sakshaug, L., September 2004. The search for exxate fluids replacements for solventborne coatings. Paint Coat. Ind. Mag.

van Baten, J. M., Krishna, R., 2002. Gas and liquid phase mass transfer within katapak-s structures studied using cfd simulations. Chem. Eng. Sci. 57, 1531–1536.

Watson, R. T., Bierbaum, R. M., Albritton, D. L., Canny, J. N., Fidler, S. N., Goldman, L. R., Hirsch, R., Holstein, E., Jackson, R. J., McClelland, J. W., McNutt, B., Nichols, M. D., Olden, K., Prince, R., 1997. Interagency assessment of oxygenated fuels. Tech. rep., National Science and Technology Council.

Zhicai, Y., Xianbao, C., Jing, G., 1998. Esterification-distillation of butanol and acetic acid. Chem. Eng. Sci. 53, 2081–2088.

2 Reaction Kinetics of n-Propyl Propionate Synthesis

2.1 The Reactive System

As mentioned in the section *Production and Uses of n-Propyl Propionate* of the Introduction, n-Propyl Propionate (ProPro) can be produced from the reaction of 1-Propanol (POH) with Propionic Acid (ProAc). Several secondary reactions have been identified as possible (Figs. 2.1 and 2.2), which might lead to the formation of Di-n-Propyl Ether (DPE) or Propene (Pro).

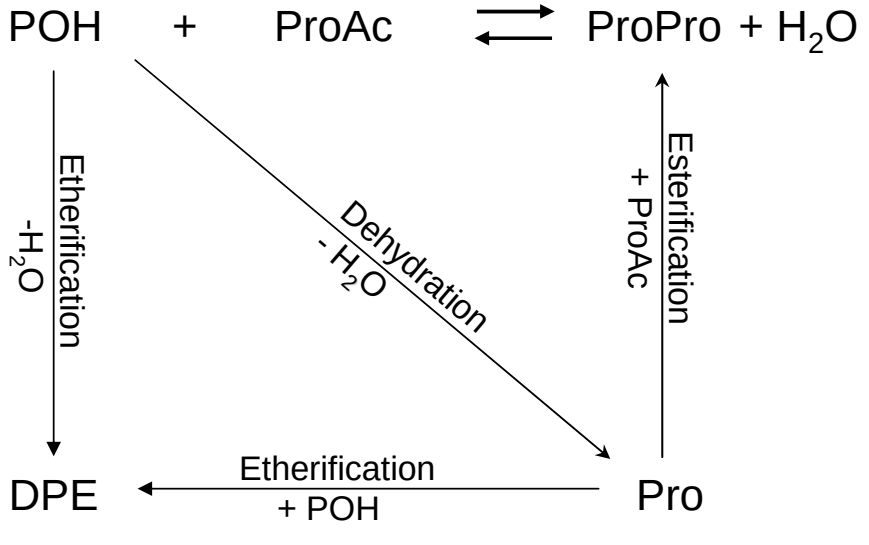

Figure 2.1: Summary diagram of n-Propyl Propionate synthesis and possible secondary reactions (adapted from Buchaly et al. (2005))

The presence of these compounds is undesirable, not only because

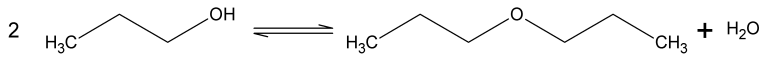

(a) Etherification of 1-Propanol to DPE

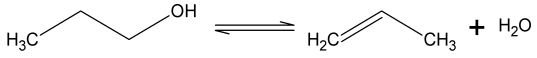

(b) Dehydration of 1-Propanol to Propene

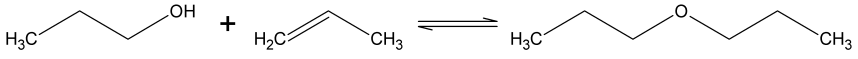

(c) Etherification of Propene to DPE

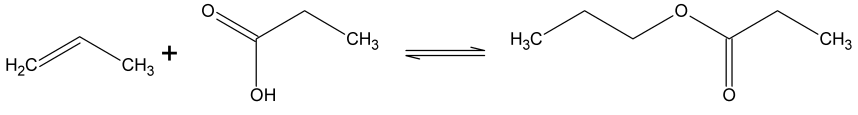

(d) Esterification of Propene to n-Propyl Propionate

Figure 2.2: Possible secondary reactions structures from n-Propyl Propionate synthesis

they represent an added cost – by consuming a reactant and having to be removed afterwards – but also because Propene is a highly flammable gas, thus posing a security risk.

The n-Propyl Propionate synthesis reaction is acid-catalysed and can be accomplished by either homogeneous or heterogeneous catalysis. In this work and since the reaction is to occur inside a RD column, only heterogeneous catalysis will be studied.

2.2 Catalysts

A proper choice of catalyst is an indispensable step in designing any apparatus where a catalytic reaction is to occur. In the case of n-Propyl Propionate synthesis, strong-acid ion exchange resins are used, due to the H^+ groups needed to catalyse the reaction. Of the commercially available catalysts, which one should be used has to be determined.

The main point in the choice of the resin is not as much speed of conversion, but rather selectivity. As mentioned in the previous Section, the main etherification reaction can be plagued by unwanted secondary reactions and their reduction and/or elimination is a primary goal. In order to tackle this issue, a catalyst screening for the n-Propyl Propionate synthesis reaction is performed.

2.2.1 Catalyst Screening Set-up

The set-up for the catalyst screening is a simple one. Since the objective is not to determine equilibrium or kinetic constants, but rather to perform an evaluation of which secondary products are obtained, as well as having a preliminary idea of the performance of the catalysts (i.e. rate of reaction), the set-up (Fig. 2.3) is made of a glass vessel (A), heated in an oil bath (B), to which the reactants and a given amount of catalyst are put into. The catalyst / reactant mixture is stirred by electromechanical means (C), at not very high rotations to avoid milling of the catalyst beads. The temperature is measured by a glass thermometer (D) and the vapour is collected through an opening in the side of the vessel, cooled down in a condenser (E) – the condensate being collected in a flask (F) – and the remaining gaseous phase is cooled down by liquid nitrogen in a final stage to collect lower condensing compounds (G). The liquid collected from the condensate and nitrogen-cooled flasks is then taken and analysed in a previously calibrated Shimadzu gas chromatograph, using Flame Ionization (FID) and Thermal Conductivity (TCD) Detectors.

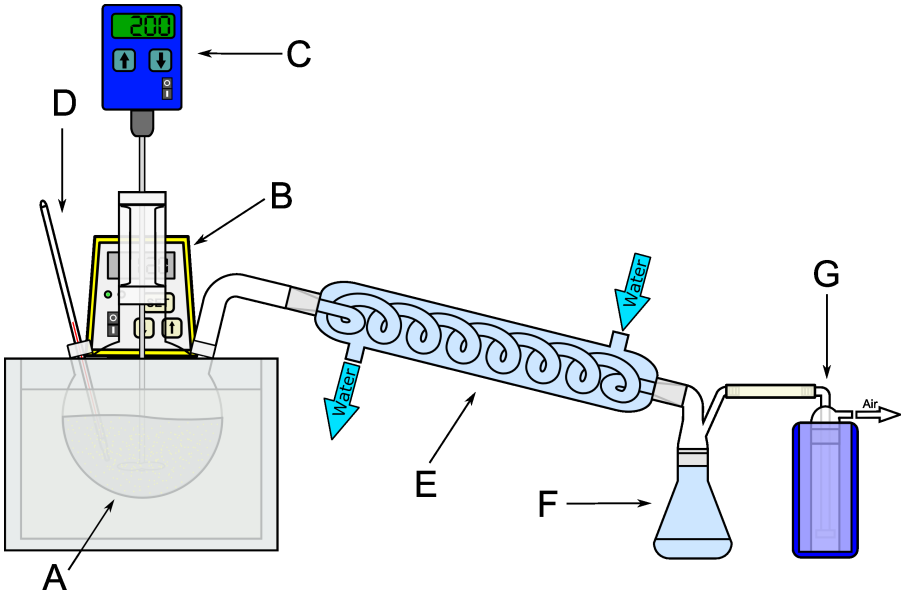

Figure 2.3: Schematic drawing of the experimental set-up for catalyst screening (A- Glass vessel; B- Oil bath; C- Stirrer; D- Thermometer; E- Condenser; F- Condensate flask; G- Nitrogen-cooled flask)

The experiments were carried out using two commercial catalysts: Amberlyst 15, the most commonly used resin catalyst, and Amberlyst 46, due to its specificity towards esterifications. Both catalysts are macroreticular, sulphonic acid, polymeric catalysts, but they differ on the location of the sulphonic active sites. While Amberlyst 15 is activated throughout the particle (i.e. surface and inside the catalyst pores), Amberlyst 46 only contains active sites on the outer catalyst surface. This results in different physical characteristics, as shown in Table 2.1.

Table 2.1: Physical properties comparison between Amberlysts 15Wet and 46 (taken from Rhom and Haas Company (2002, 2003))

	Amberlyst 15Wet	Amberlyst 46
Conc. Active Sites (eq/kg)	$\geq$4.7	0.8-1.3
Water Content (%)	52-57	26-36
Max. Oper. Temp. (°C)	120	120

According to what was expected, and using an equal amount of catalyst and reactants, the reaction was faster with Amberlyst 15 but considerable amounts of DPE were detected in the GC analysis. The experiments catalysed by Amberlyst 46 were slower to reach equilibrium, but no DPE was detected afterwards.

As mentioned before, Amberlyst 46 is a different kind of sulphonic acid catalyst, which was developed specifically for esterification reactions. The main problems with esterification reactions are, usually, secondary etherification reactions (as is the case with the formation of DPE) which occur mainly inside the pores of the catalyst bead. The solution found at Rhom-Haas was to restrict the functionalisation of the catalyst to the surface only, to avoid reaction inside the pores. Quoting Lundquist (1995) from Amberlyst 46's patent:

> While not wishing to be bound by theory, I have found evidence that indicates the strongly acidic functional groups that are more distant from the surface of the polymer contribute more to the formation of ethers during the esterification of organic acid with alcohols, while those closest to the surface are responsible for most of the esterification. I believe that the surface functional groups are accessible to all the reactants, while the functional groups deeper within the polymer are accessible only to small, polar reactants.

> When fully functionalised polymer beads are used in esterification reactions, the non-polar, organic acid and small, polar alcohol partition themselves differently within the strong acid ion exchange resin catalyst. The polar alcohol partitions into the interior of the hydrophilic polymer, which is not accessible to the non-polar, organic acid. The high concentration of alcohol and low concentration of organic acid at the functional groups within the hydrophilic polymer causes the formation of ethers through alcohol condensation. In the esterification of an organic acid with a secondary or tertiary alcohol, the high concentration of alcohol within the interior of a fully functionalised polymer bead also favours a second type of undesirable side reaction, i.e., dehydration of the alcohol to form olefinic by-products. Dehydration of the alcohol to form olefinic by-products is wasteful of the valuable alcohol. The olefinic by-products so formed contaminate the product ester and can foul the polymer beads, shortening the useful life of the beads as catalysts. Accordingly, I believe the surface-functionalised catalyst beads useful in the present invention to be those which minimize formation of ethers and other undesirable by-products while maximizing formation of esters. I believe those catalyst beads to contain aromatic nuclei bearing strongly acidic functional groups only at or near the polymer surface, with the remainder of the aromatic nuclei being unfunctionalised.

Although rate of reaction is important for any synthesis, the avoidance of undesirable (or even harmful) secondary products takes priority in this case, leading to the choice of Amberlyst 46 as catalyst for Propyl Propionate production.

2.2.2 Catalyst Characterisation

As shown in the specification sheet for Amberlyst 46 (Rhom and Haas Company, 2002), the values for the concentration of active sites and water content have a wide variation range. Furthermore, and in respect to the water content, the value is very dependent on the method used to extract excess water from the catalyst prior to weighing and loading.

In order to obtain precise experiments and diminish error, the catalyst batch used was characterised with respect to the concentration of

active sites and water content. Since the experiments for determining the concentration of active sites depend on the previous knowledge of the water content (as the concentration is calculated in dry catalyst mass basis), the water content value was determined first.

2.2.2.1 Catalyst Water Content

The set-up for this experiment is a very simple one that is also used for extracting excess water prior to catalyst loading in the experimental runs. It consists of a filtering flask connected to a vacuum aspirator installed in a faucet, to which a buchner funnel containing filter paper and the catalyst is placed on top and filled with water. The vacuum is then turned on until little to no water is observed coming into the filtering flask. A sample is taken, weighed and placed in an oven at a temperature of 105°C for 12 hours. Afterwards, the sample is removed from the oven, left to cool down on a exsiccator and weighed again. Using equation 2.1, the value for water content is obtained.

$$\text{Water Content } (\%) = \frac{m_{cat}^{wet} - m_{cat}^{dry}}{m_{cat}^{wet}} \times 100 \tag{2.1}$$

Table 2.2: Experimental values of water content for Amberlyst 46

Exp.	m_{cat}^{wet} (g)	m_{cat}^{dry} (g)	Water Content (%)
1	5.00	2.90	41.9
2	5.00	2.41	51.8

As shown on table 2.2, the two experiments have a significant difference between one another and both are above the maximum value of 36% given by the manufacturer. As a result of this discrepancy, an intermediate value of 42% was used throughout the experiments and for the determination of active sites.

Although not used during the experiments, it is quite common to load the catalyst into the reaction vessel in an alcohol phase, instead of water, to reduce product contamination. To accommodate this possibility, experiments to determine 1-Propanol content for the catalyst were performed, following a similar protocol to the water experiments. The results are presented on Table 2.3.

Table 2.3: Experimental values of 1-Propanol content for Amberlyst 46

Exp.	m_{cat}^{wet} (g)	m_{cat}^{dry} (g)	1-Propanol Content (%)
1	5.00	2.67	46.5
2	5.00	2.14	57.1

2.2.2.2 Concentration of Active Sites

After determining the water content of the catalyst, the experiments for obtaining the concentration of active sites can be performed. Several methods for this are available, but the simplest, although not quickest, is to titrate a new or enerated load of catalyst with a strong base, such as Sodium Hydroxide (NaOH). To do so, a known mass of catalyst, after removal of excess water and weighing, is placed inside an Erlenmeyer flask containing distilled water and a few drops of phenolphtalein. A burete containing a solution of NaOH of known concentration is placed above the flask.

When NaOH is added to the Erlenmeyer, the Na^+ ions are adsorbed by the resin, "liberating" H^+ which will neutralize the OH^- resulting from the dissociation of Sodium Hydroxide. When the resin saturates (i.e. all the active sites contain Sodium ions), the remaining Sodium Hydroxide in the solution is enough to raise the pH of the solution above 7, thus turning it to purple due to the phenolphtalein. Throughout this whole process, the contents of the flask should be stirred to promote the contact between the ions and the resin and the solution is considered saturated when no colour change (i.e. no return from purple to transparent) occurs for at least 5 minutes.

In these particular experiments, no solution of NaOH was readily available, so one was prepared from solid Sodium Hydroxide, which was titrated with a 1N solution of Hydrochloric Acid (HCl) to determine its exact concentration, found to be of 0.1 N. The solution was then used to titrate the catalyst, the results being presented on Table 2.4.

As can be observed from the error obtained, the value of 0.95 - rounded to just two digits in order to follow the manufacturer's format of specification - is reasonably accurate. This value was used throughout the rest of the experiments and simulations as the catalyst batch used was either the same (for the kinetic experiments) or found to have an equal value for the concentration of active sites (for the reactive distillation experiments). Nonetheless, it is wise to remind

Table 2.4: Amberlyst 46 titration results

Exp.	m_{cat}^{wet} (g)	V NaOH (ml)	Capacity (eq/L)
1	2.093	11.50	0.9473
2	2.007	10.93	0.9392
3	2.008	11.30	0.9701
		Average	0.9522
		Standard Deviation	0.01603
		Error (%)	1.68

once again that due to the specificity of the manufacturing method of the catalyst, its capacity (i.e. concentration of active sites) as well as the water content (or content of the liquid in which the catalyst is saturated prior to loading) must be determined for each batch of catalyst used, in order to reduce errors.

2.3 Kinetic Experiments

2.3.1 Experimental Set-up

The experimental set-up (Fig. 2.4) for determining the kinetic and equilibrium constants is composed of a stirred jacketed batch reactor, which contains a catalyst basket in the stirrer shaft; a gas chromatograph (GC), connected on-line to the reactor; a thermostatic bath, for heating the reactor, with thermal oil as heating fluid; several gas lines - hydrogen, nitrogen and air connected to the GC and helium connected to both GC and reactor; and a control / data acquisition apparatus, consisting of a computer, data acquisition (DAQ) card, terminator box and connecting cabling.

The DAQ acquires FID signals from the chromatograph, pressure from a pressure transducer connected to the reactor and temperature from a T thermocouple, whose tip is located near the end of one of the baffles. It controls directly the Start/Stop signals going to the chromatograph and the stirrer motor. Valves V1 and V2, which control the admission of samples to the chromatograph, are controlled by the chromatograph. The temperature is set using the oil bath controls and the pressure is set one time at the beginning.

Although the batch reactor is a simple apparatus, the structure surrounding it is slightly more complex (Fig. 2.5) and requires a closer

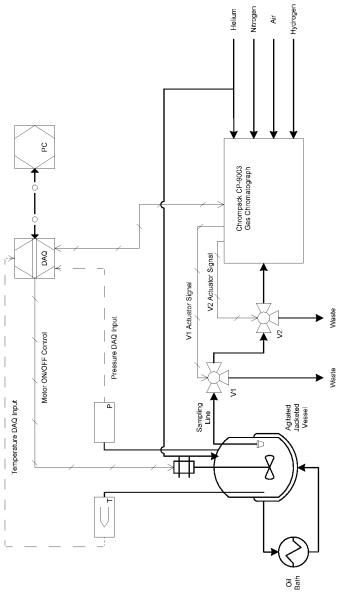

Figure 2.4: Experimental set-up for obtaining kinetic data

look. The main unit of the batch reactor is the jacketed reaction vessel (**A**), made by Büchi Glas Uster, and corresponding to Type 1 of the BEP280 model. This vessel is constructed out of borosilicate glass and has a capacity of 1 dm^3. The vessel is rated by the manufacturer as having a maximum operating temperature of 200°C and a maximum operating pressure of 12 bar.

The reactive mixture is stirred by a three-bladed impeller (**C**) screwed into a metallic shaft (**G**) and powered by an external three-phase motor (**H**), built by Loher Gmbh, with an output of 0.25 kW. The rotational velocity of the shaft is controlled by a Planetroll variable speed gearbox (**I**). Two metallic baffles (**E**) exist to further promote homogeneous mixing of the fluid within the vessel. The catalyst to be used in the reaction is placed inside a metal basket (**B**), which is screwed into the impeller shaft. Before start-up, the basket is screwed all the way to the top, resting above the reacting mixture. When the experiment starts, the rotation of the stirrer is sufficient to make the basket fall (resting on top of the impeller) and start the reaction.

To avoid unwanted vaporisation of the components, it is normally necessary to increase the operating pressure. In order to do so, an outside gas - Helium, in this case - is inserted into the reaction vessel, after it has been properly closed and tightened. In order to control the admission of gas, which is only performed at start-up, two valves (**M**) in series are used. The pressure of the system at any time can be checked by analog means by reading the value in the manometer (**L**). At the end of the experiment or in the case of an undesired increase in pressure (which happens, for example, when a temperature rise occurs), the pressure can be lowered by opening valve **N**. If for some reason the pressure increases over 12 bar, an automatic safety valve (**O**) rated at that pressure opens. During operation, pressure is read and transmitted to the data acquisition set-up by a Foxboro 841-GM pressure transducer (**K**).

The temperature of the system is controlled externally, by means of a Lauda Ecoline RE104 thermostatic bath, rated with a maximum operating temperature of 120°C. The heating fluid used is a synthetic thermal oil, Julabo Thermal M, rated with a temperature operating interval of 40-170°C. This fluid is heated or cooled according to necessities by the thermostatic bath, which is also responsible for pumping it into the circuit. The fluid enters the jacketed vessel at the bottom and exits near the top, proceeding to a metal plate to which the vessel is sealed against and then returns to the bath. Except for the vessel and the metal plate, the whole circuit is thermally isolated. The tem-

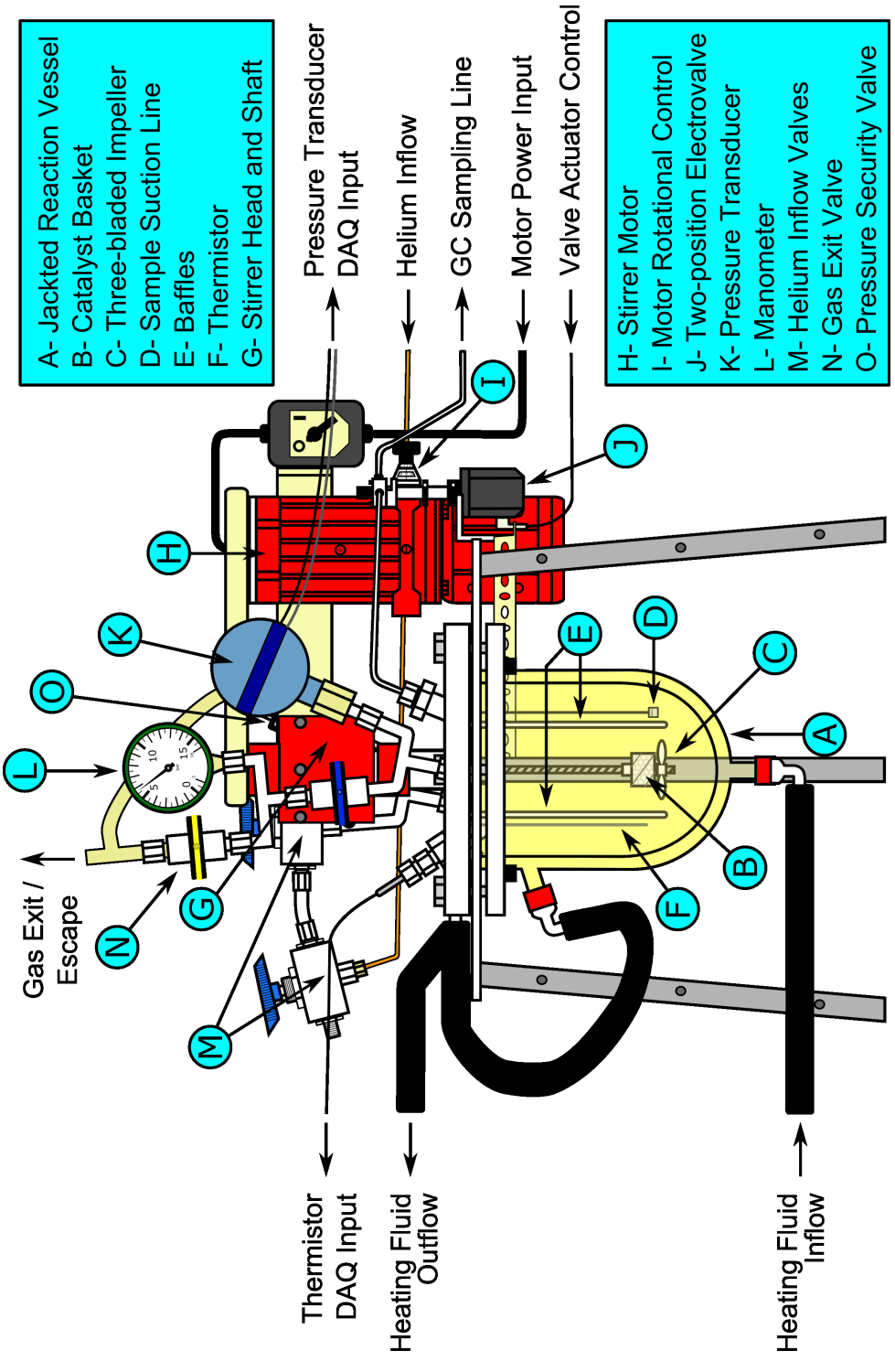

Figure 2.5: Diagram of the batch reactor set-up

perature of the reacting mixture is read by means of a T thermocouple (**F**), which is connected to the DAQ system. At low temperatures, little to no discrepancy between values in the bath and in the vessel exists but at higher temperatures, some heat is dissipated and the temperature in the bath is always higher, so some manual control must be performed (e.g., setting the bath temperature higher) to obtain the desired temperature for the reacting mixture.

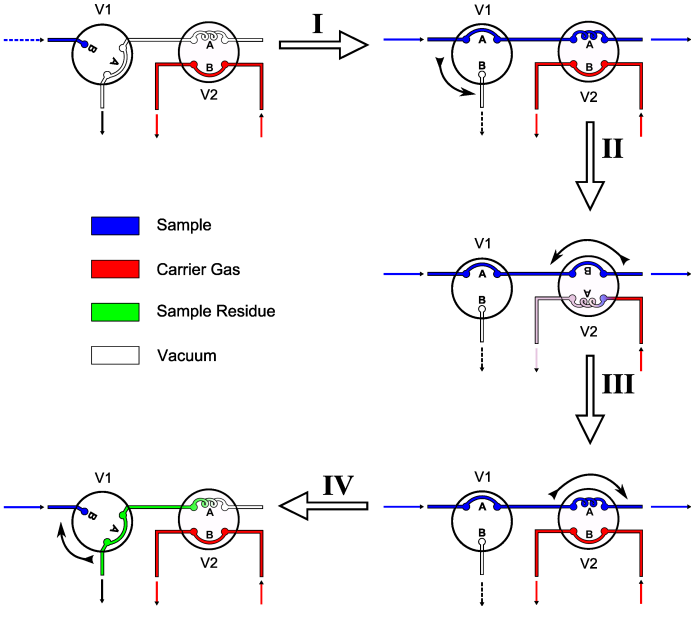

Figure 2.6: Sample injection cycle: I- Clean / Fill Loop; II-III - Sample injection IV- Sample Line Purge

The sampling of the reacting mixture is done automatically. A suction line (**D**) is always in contact with the fluid and when valves V1 (**J**) and V2 (Fig. 2.4) open, the pressure difference between the vessel and the purge of the chromatograph is enough to feed liquid into a sample injection loop, contained inside V2. Figure 2.6 exemplifies the process of injecting a sample into the GC: first (**I**), valve V1 rotates, admitting fluid (A position) into the sample line and V2 loop (A position). Second (**II**), V2 rotates placing the loop in contact with the GC carrier gas (B position) for some seconds and rotates back again (**III**), the injection being completed. Finally (**IV**), V1 rotates to its original position (B) and the sample line is purged by vacuum. All the liquid exiting V2 and not being injected into the GC is purged to

an outside residue container, which is emptied between experiments.

Analysis of the samples taken throughout the experimental runs are done by the gas chromatograph, a Chrompack CP-9003. This unit is equipped with a Varian Porabond-Q capillary column, with a total length of 25 m and an outside diameter of 0.53 mm. On the detection side, the GC has two detectors available: a Flame Ionization Detector (FID), which is suitable for detection of most compounds and usually gives better results, and a Thermal Conductivity Detector (TCD) which, although far less sensible to compounds, is able to detect water.

Although at first, the TCD seems to be an obvious choice, the results from the calibration runs (Appendix A) show that its peaks are very small and, as such, more prone to errors. An alternative solution is to use both detectors in series; since the TCD does not destroy the sample, the output from it could be fed into the FID thus detecting and quantifying water in the TCD and the other three compounds in the FID. Unfortunately and due to limitations in the DAQ set-up, only one output channel could be captured at a time, preventing the use of this solution. The third solution, which was the one used, makes two assumptions: a), no products exist inside the reactor at time of loading nor are the reactants contaminated by any product; and b), given a) and the reaction stoichiometry, the number of moles of Water at any given time is always equal to the number of moles of n-Propyl Propionate. This solution, although far from perfect, has a smaller probability of error than just using a TCD, especially since, as can be seen in Appendix A, considerable peak tailing exists.

The whole system is controlled by a computer program, written in BASIC originally by Caetano (1995) and modified by Prior (2001). The program communicates with the set-up through a Data Translation DT-2805 DAQ board, installed inside the computer, which connects to a Data Translation DT707-T terminator - to where all the inputs and output signals are connected. The DAQ receives analog signals from the pressure transducer, the thermocouple and the GC detector in use. It sends out two digital signals: one to start/stop the stirrer motor and another to start/stop the GC run. The control of the valve injection cycle (Fig. 2.6) and the temperature rise program of the GC oven is performed by the GC itself, through the construction and use of an internal program (Appendix A). The BASIC program mentioned before was altered for these runs for several reasons: first, an waiting period between sample injection and data collection, necessary in previous uses, was removed and second, due to an unexpected bug,

the time between samples had to be changed according to the run time since the program crashes after 335 samples are taken.

2.3.2 Theoretical Modelling

2.3.2.1 Reaction Model

The modelling of the reactive system can be divided into two parts: first, the model of the reaction *per se*, which includes kinetic, equilibria and adsorption constants; and second, the model of the batch reactor. Regarding the reaction model, several possibilities exist for heterogeneously catalysed reactions. The simplest of these is the so-called "pseudo-homogeneous" model: it assumes that the behaviour of the reactive mixture in presence of an heterogeneous catalyst is equal to the behaviour in the presence of an homogeneous catalyst. As such, it does not take into account the physical/chemical processes associated with adsorption/desorption phenomena, thus dispensing the use of adsorption constants.

As it has been mentioned earlier, the Propyl Propionate synthesis is a reversible reaction. This means that at any given time there is production of Propyl Propionate and Water from 1-Propanol and Propionic Acid (Eq. 2.2) with rate constant k_1 and destruction of Propyl Propionate and water to 1-Propanol and Propionic Acid (Eq. 2.3) with a rate constant k_{-1}.

$$POH + ProAc \overset{k_1}{\rightarrow} ProPro + H_2O \tag{2.2}$$

$$ProPro + H_2O \overset{k_{-1}}{\rightarrow} POH + ProAc \tag{2.3}$$

So, at any given time, the rate of formation of Propyl Propionate is given by

$$r_{ProPro} = k_1\ a_{POH}\ a_{ProAc} - k_{-1}\ a_{ProPro}\ a_{H_2O} \tag{2.4}$$

When the rate of reaction of Propyl Propionate is equal to zero, it means the reaction has reached an equilibrium point, no species being formed or consumed because the rate of formation of any compound is equal to the rate of its disappearance (Eq. 2.5).

$$k_1\ a_{POH}\ a_{ProAc} = k_{-1}\ a_{ProPro}\ a_{H_2O} \tag{2.5}$$

Rearranging Eq. 2.5, the equilibrium constant *Keq* can be defined as:

$$Keq = \frac{k_1}{k_{-1}} = \frac{a_{ProPro}\ a_{H_2O}}{a_{POH}\ a_{ProAc}} \tag{2.6}$$

Returning to Eq. 2.4, the kinetic constant of the direct reaction can be put in evidence,

$$r_{ProPro} = k_1 \left(a_{POH}\ a_{ProAc} - \frac{k_{-1}\ a_{ProPro}\ a_{H_2O}}{k_1} \right) \tag{2.7}$$

and the definition of equilibrium constant as given by Eq. 2.6 can be applied, resulting in a final reaction rate for n-Propyl Propionate of

$$r_{ProPro} = k_1 \left(a_{POH}\ a_{ProAc} - \frac{a_{ProPro}\ a_{H_2O}}{Keq} \right) \tag{2.8}$$

It is widely accepted in the reaction engineering world that the centenary Arrhenius equation (Eq. 2.9) - proposed first in 1889 by Svante Arrhenius - is still capable of predicting temperature-dependence of kinetic and equilibrium constants. The equation is composed of two parameters: the pre-exponential factor, k_0, and the activation energy, E, and is dependent only of the system temperature. The exponential structure of the equation lends itself easy for regression, after linearisation (Eq. 2.10).

$$k = k_0\ e^{-\frac{E}{RT}} \tag{2.9}$$

$$\ln(k) = \ln(k_0) + \left(-\frac{E}{R} \right) \frac{1}{T} \tag{2.10}$$

2.3.2.2 Batch Reactor Model

Performing a mass conservation balance to generic species i inside a batch reactor, for a time interval between t and $t + \mathrm{d}t$,

$$n_{i,t+\mathrm{d}t} = n_{i,t} + \nu_i\ r\ L\ m_{cat}^{dry}\ \mathrm{d}t \tag{2.11}$$

in which n corresponds to the number of moles of i at any given time in [mol], ν_i to the stoichiometric coefficient of each component i, r to the reaction rate in [mol.s^{-1}.eq^{-1}], L to the concentration of active sites in $\left[eq.\ \left(kg_{cat}^{dry}\right)^{-1}\right]$, $\mathrm{m_{cat}}$ to the dry mass of catalyst

$$\frac{n_{i,t+\mathrm{d}t} - n_{i,t}}{\mathrm{d}t} = \nu_i\ r_i\ L\ m_{cat}^{dry} \tag{2.12}$$

and simplified to a differential form

$$\frac{\mathrm{d}n_i}{\mathrm{d}t} = \nu_i \; r \; L \; m_{cat}^{dry} \tag{2.13}$$

Furthermore, and since the number of moles of i is a fraction x_i of the total moles in the system, N_T, Equation 2.13 can be rewritten as

$$\frac{\mathrm{d}\left(x_i \; N_T\right)}{\mathrm{d}t} = \nu_i \; r \; L \; m_{cat}^{dry} \tag{2.14}$$

In the case of Propyl Propionate synthesis and since the reaction is of the $A + B \rightleftharpoons C + D$ type, the total number of moles in the system does not change and N_T can be taken outside of the differential term as it is not time-dependent. Doing so and rearranging,

$$\frac{\mathrm{d}x_i}{\mathrm{d}t} = \nu_i \; r \frac{L \; m_{cat}^{dry}}{N_T} \tag{2.15}$$

a specific version of the mass balance is obtained.

Since the dry catalyst mass is not measured directly, but rather calculated from Equation 2.1, the mass balance to be used in the models is rewritten as

$$\frac{\mathrm{d}x_i}{\mathrm{d}t} = \nu_i \; r \frac{L \; m_{cat}^{wet} \; (1 - hum)}{N_T} \tag{2.16}$$

with hum standing for the water content as a fraction of the total wet catalyst weight.

2.3.2.3 Thermodynamic modelling: Activity Coefficients

Although it is common to represent the rate law as a function of molar fractions or concentrations, this is only true when the thermodynamic behaviour of the species in the mixture approaches ideality because then the activity of the molecules in the liquid phase is equal to their molar fraction. When the mixture is non-ideal a correction factor, known as activity coefficient (φ), needs to be introduced (Eq. 2.17).

$$a_i = \varphi_i \; x_i \tag{2.17}$$

Several methods exist for estimating activity coefficients in multi-component liquid phases, but the most currently used and popular are the ones based on the concept of local composition, as introduced by Wilson (1964). This concept states that, quoting from Smith and Van

Ness (1987a), "(w)ithin a liquid solution, local compositions, different from the overall mixture composition, are presumed to account for the short-range order and non-random molecular orientations that result from differences in molecular size and intermolecular forces." Further models based on the same concept were developed, including the NRTL (Non-Random Two-Liquid) (Renon and Prausnitz, 1968) and UNIQUAC (UNIversal QUAsi-Chemical) models (Abrams and Prausnitz, 1975). All of these models require the availability of vapour-liquid (VLE) or liquid-liquid (LLE) equilibrium data in order to obtain the necessary parameters. In some cases, that data is not readily available and from that the need of group-contribution methods, derived from UNIQUAC, arose. These methods take into account the molecular structure of the components, dividing them into groups, and try to estimate the interaction between them. The first, most famous and more widely used of these is the UNIFAC (UNIQUAC Functional-group Activity Coefficient) method, proposed first by Fredenslund et al. (1975) and further developed by Fredenslund et al. (1977). In this work, the UNIQUAC method was used as it tends to be the most accurate if parameters exist for each component pair. A comprehensive discussion of the UNIQUAC and UNIFAC method can be found in Smith and Van Ness (1987b), so only the basic equations will be treated here.

The UNIQUAC method divides the contribution for the activity coefficient into two parts: a combinatory part, φ^C, which accounts for molecular size and shape differences and a residual part, φ^R, which accounts for molecular interactions. So, the activity coefficient is defined as

$$\ln\varphi_i = \ln\varphi_i^C + \ln\varphi_i^R \tag{2.18}$$

with $\ln\varphi_i^C$ and $\ln\varphi_i^R$ being given by

$$\ln\varphi_i^C = 1 - J_i + \ln J_i - 5q_i\left(1 - \frac{J_i}{L_i} + \ln\frac{J_i}{L_i}\right) \tag{2.19}$$

$$\ln\varphi_i^R = q_i\left(1 - \ln L_i\right) - \sum_j\left(\theta\frac{s_{j,i}}{\eta_j} - q_i\ln\frac{s_{j,i}}{\eta_j}\right) \tag{2.20}$$

The parameters for these two equations are calculated as follows:

$$J_i = \frac{r_i}{\sum_j r_j\, x_j} \tag{2.21}$$

$$L_i = \frac{q_i}{\sum_j \; q_j \; x_j} \tag{2.22}$$

$$\theta = \sum_i \; q_i \; x_i \tag{2.23}$$

$$s_{j,i} = \sum_m \; q_i \; \tau_{m,j} \tag{2.24}$$

$$\eta_j = \sum_i \; s_{j,i} \; x_i \tag{2.25}$$

$$\tau_{m,j} = e^{\frac{-\left(v_{m,j} - v_{i,i}\right)}{R\,T}} \tag{2.26}$$

where x_i corresponds to the molar fraction of component i in the mixture, R to the universal gas constant and T to temperature. The values for parameters r_i, q_i and $\left(v_{m,j} - v_{i,i}\right)$ are to be found in literature or regressed from VLE data. When no data exists, the interaction parameters for that specific binary pair can be estimated from UNIFAC, as mentioned earlier.

In this work, the source for the UNIQUAC parameters used, their type and validity range are presented on Table 2.5. Of the binary pairs, the two possibly problematic cases are the Propyl Propionate / Propanol and Propyl Propionate / Propionic Acid pairs. In the first case, Liquid-Liquid Equilibrium data is used instead of Vapour-Liquid Equilibrium, and with a maximum applicable temperature of 40°C. In the second, no data whatsoever was available, so the coefficients were estimated by UNIFAC.

As can be easily understood, the data set used is far from ideal and this should reflect in deviations from theoretical values and goodness of fit when used for modelling of experimental values. Nevertheless, it was considered better to use experimental data, when available, instead of using approximation models (such as UNIFAC), as the errors, although present, tend to be lower.

2.3.2.4 Thermodynamic Modelling: Equilibrium Constant

The thermodynamic definition of chemical equilibria is given through the chemical system's total Gibbs energy, G^t. The application of the Laws of Thermodynamics to the system's total Gibbs energy imply that that energy, in a closed system at constant temperature and pressure, will tend towards its lowest value possible, or stated in a mathematical form,

Table 2.5: Source and applicability range of UNIQUAC parameters data

Binary Pair	Source	Min. Temp.	Max. Temp.
ProPro/POH	LLE-Lit	20.0	40.0
POH/ProAc	VLE-HOC	99.5	140.0
ProPro/Water	VLE-IG	88.9	114.3
POH/Water	VLE-HOC	25.0	100.0
ProAc/Water	DECHEMA	99.9	137.5
ProPro/ProAc	UNIFAC	N/A	N/A

Lit- Dortmund Data Series (Aspen Data banks); IG- Fitted by Aspentech, Ideal Gas model; HOC- Fitted by Aspentech, Hayden-O'Connel model; DECHEMA- taken from DECHEMA data series; UNIFAC- Estimated by UNIFAC. T is in °C

$$\left[\frac{\mathrm{d}G^t}{\epsilon}\right]_{T,P} = 0 \tag{2.27}$$

with ϵ corresponding to the reaction coordinate (a measure of extent of reaction) of the system.

The expression for the differential of Gibbs energy in a closed system is given by

$$\mathrm{d}\,(n\ G) = (n\ V)\,\mathrm{d}P - (n\ S)\,\mathrm{d}T + \sum \mu_i\ \mathrm{d}n_i \tag{2.28}$$

in which n corresponds to the number of moles, G to the Gibbs energy, V to volume, P to pressure, S to entropy, T to temperature and μ to the chemical potential. Since, by definition, at equilibrium temperature and pressure are constant and knowing that the number of moles of species i is dependent of the stoichiometric coefficient ν and the reaction coordinate,

$$\mathrm{d}n_i = \nu_i\ \mathrm{d}\epsilon \tag{2.29}$$

Eq. 2.28 can be rearranged to

$$\sum \nu_i\ \mu_i = \left[\frac{\mathrm{d}G^t}{\epsilon}\right]_{T,P} = 0 \tag{2.30}$$

From the Ideal Gas Law and Eq. 2.28, the formula for the partial Gibbs energy of i in a mixture can be derived,

$$\mathrm{d}\bar{G}_i = R\ T\ \ln \hat{f}_i \tag{2.31}$$

and since, by definition, $\bar{G}_i = \mu_i$, the previous equation can be integrated at a constant temperature from a standard state (superscript $\circ$) to the actual state and rearranged to

$$\mu_i - G_i^\circ = R\ T\ \ln \frac{\hat{f}_i}{f_i^\circ} \tag{2.32}$$

or

$$\mu_i - G_i^\circ = R\ T\ \ln \hat{a}_i \tag{2.33}$$

because activity is defined as the ratio between the fugacity of the species in solution at current and standard conditions. Solving the equation in order to the chemical potential and combining with Eq. 2.30, thus eliminating μ_i, results in

$$\sum \nu_i \left(G_i^\circ + R\ T\ \ln \hat{a}_i\right) = 0 \tag{2.34}$$

Expanding and transforming the sum of the natural logarithm into a product, solving in order to it (Eq. 2.35), and finally recalling Eq. 2.6, formulated in a general manner, the thermodynamic definition of equilibrium constant is found.

$$\prod \left(\hat{a}_i\right)^{\nu_i} = e^{\frac{-\sum \nu_i\ G_i^\circ}{R\ T}} \tag{2.35}$$

$$Keq = e^{\frac{-\sum \nu_i\ G_i^\circ}{R\ T}} \tag{2.36}$$

From this equation, defining the standard Gibbs heat of reaction as $\Delta G^\circ = \sum \nu_i\ G_i^\circ$, using Eq. 2.28 with a constant total number of moles (as in equilibrium) and the definition of Gibbs energy, $G = H - T\ S$, it is possible to arrive at an equation which gives the dependence of the equilibrium constant in order to the temperature. This equation (Eq. 2.37) was first proposed in 1884 and is now known by its author name as the (Jacobus Henricus) van't Hoff equation.

$$\frac{\mathrm{d}\ \ln Keq}{\mathrm{d}T} = \frac{\Delta H^\circ}{R\ T^2} \tag{2.37}$$

The determination of the equilibrium constant by theoretical means (using Eq. 2.37) requires the knowledge of the heat of reaction (ΔH°) at the actual temperature. That information is usually not available and

so an alternative route needs to be taken. If the van't Hoff equation is integrated in order to temperature,

$$\ln Keq = \int \frac{\Delta H^\circ}{R\ T^2} \mathrm{d}T + I \tag{2.38}$$

where I is a constant of integration and knowing that the heat of reaction can be calculated from

$$\Delta H^\circ = \int \Delta Cp^\circ\ \mathrm{d}T + J \tag{2.39}$$

- J being another integration constant and Cp being calculated using one of many available temperature-dependent correlations - it is possible, together with Eq. 2.36, to calculate a temperature-dependent expression for the equilibrium constant since data for heat and standard Gibbs energy of formation, at a standard temperature (usually 298 K), is available for most compounds.

In the case of n-Propyl Propionate synthesis, using the correlation provided in DIPPR 801 (1998) (Eq. 2.40) for calculation of heat capacities, Eq. 2.39 can be expanded into Eq.s 2.41 and 2.36 into Eq. 2.43. Applying Eq. 2.38 to Eq. 2.41, an expression for a system-specific expression for the equilibrium constant is obtained (Eq. 2.42) which can be solved by applying the values given in Table 2.6 to finally obtain the integration constants J and I (Table 2.7).

$$Cp = A + B\ T + C\ T^2 + D\ T^3 + E\ T^4 \tag{2.40}$$

$$\Delta H^\circ = \Delta A\ T + \frac{\Delta B}{2} T^2 + \frac{\Delta C}{3} T^3 + \frac{\Delta D}{4} T^4 + \frac{\Delta E}{5} T^5 + J \tag{2.41}$$

$$\ln K = \frac{1}{R}\left(\Delta A \ln T + \frac{\Delta B}{2} T + \frac{\Delta C}{6} T^2 + \frac{\Delta D}{12} T^3 + \frac{\Delta E}{20} T^4 - \frac{J}{T}\right) + I \tag{2.42}$$

$$\Delta G^\circ = J - R\ T\left(\Delta A \ln T + \frac{\Delta B}{2} T + \frac{\Delta C}{6} T^2 + \frac{\Delta D}{12} T^3 + \frac{\Delta E}{20} T^4 + I\right) \tag{2.43}$$

It should be noted that Δ was used to represent the stoichiometric sum of the parameters (e.g. $\Delta A = \sum \nu_i\ A_i$), as is this sum that is used

Table 2.6: Heat of reaction (at 298.15 K), standard Gibbs energy of formation (at 298.15 K) and heat capacity coefficients for the species involved in n-Propyl Propionate synthesis (DIPPR 801, 1998)

	POH	ProAc	ProPro	Water
A	1.59×10^5	2.14×10^5	0.892×10^5	2.76×10^5
B	-6.35×10^2	-7.03×10^2	3.20×10^2	-20.9×10^2
C	1.97	1.66	0.476	8.13
D	0	0	0	-1.41×10^{-2}
E	0	0	0	9.37×10^{-6}
ΔH°	-3.03×10^8	-5.09×10^8	-5.28×10^8	-2.86×10^8
ΔG°	-1.69×10^8	-3.82×10^8	-3.21×10^8	-2.37×10^8

Units: A [J.kmol^{-1}.K^{-1}] ; B [J.kmol^{-1}.K^{-2}] ; C [J.kmol^{-1}.K^{-3}] ; D [J.kmol^{-1}.K^{-4}] ; E [J.kmol^{-1}.K^{-5}] ; ΔH°, ΔG° [J.kmol^{-1}]

Table 2.7: Integration constants

J	-1.4317×10^6	[J.kmol^{-1}]
I	9.2344	[-]

Table 2.8: Theoretical equilibrium constants for n-Propyl Propionate synthesis

T [K]	Keq
233	17.2
243	16.8
253	16.4
263	16.0
273	15.6
283	15.2
293	14.8

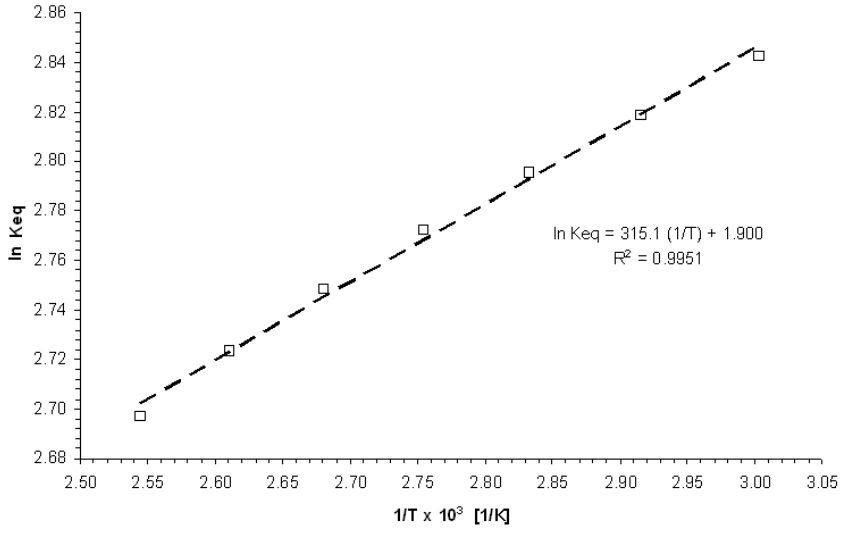

Figure 2.7: Linearised regression of Arrhenius equation for the theoretical determined equilibrium constant

to calculate the enthalpy and standard Gibbs energy of formation and the kinetic constant.

Using Eq. 2.42, with the appropriate parameters, the value of the equilibrium constant was calculated for a 60 K range (from 233 to 393 K) (Table 2.8) and plotted in x-y graphic (Fig. 2.7), according to the linearised form of the Arrhenius equation (Eq. 2.10). From the linear regression, it is possible to obtain the values of the activation energy, E, and the value of the pre-exponential factor, k_0, and arrive at a final expression for the theoretical chemical equilibrium constant of the n-Propyl Propionate synthesis (Eq. 2.44, T in Kelvin, R in SI units).

$$Keq = 6.686\, e^{\frac{2.620\times10^6}{R\,T}} \tag{2.44}$$

2.3.3 Experimental Runs

2.3.3.1 Plan of experiments

In order to obtain the value of the experimental kinetic and equilibrium constants, a series of experiments, under different conditions, were devised. Since the driving force behind obtaining this data was to use it further on in reactive distillation modelling, the conditions at

which the data was collected were chosen to approach the conditions under which the reactions are expected to occur inside a RD column. As such, a temperature range of 60-120 °C , with a 10°C interval between experiments, was chosen and both equimolar and excess (2:1) Propanol loads were tested.

Two sets of runs were performed with roughly one year between them. The first set was run in 2004 and consists of 10 catalytic experiments and 3 non-catalytic experiments, for determining if the non-catalysed reaction was strong enough to influence the process, all of them with equimolar loads of 1-Propanol and Propionic Acid. This set was analysed in a similar way to the set run later on, but the GC column used was an Hewlett-Packard HP-1. An analysis of the results perfomed after the conclusion of the experiments permited the extraction of preliminary kinets (Duarte et al., 2006), but since the first analysis of the results obtained with these runs were considered insufficient, further experiments were carried on in 2005. This consisted of a total of 14 experiments - the first experiment was repeated thrice. Experiment 6 was disregarded in the analysis since a problem occurred during the run, invalidating intermediate data points.

For these experiments, the initial planning suffered adjustments: it was found out that the maximum constant temperature attainable in the reacting mixture was of 115°C and a necessity for testing loads with excess Propionic Acid (1:2) appeared . Also, it was found that equilibrium at lower temperatures took a long time to be reached and so non-equimolar experiments were only performed from 80°C upwards. A fourth adjustment, of lesser significance, was the change of catalyst load (m_{cat}) at 115°C, which was reduced to half as to have a slower reaction and more data points. Finally, the volume of total liquid load was also reduced as the experiments proceeded, to save reactants and increase speed (the initial experiments had a load of approximately 725 ml and the last ones of 650 ml).

The complete listing of experimental runs and the conditions at which they were taken can be found in Table 2.9. The liquid loads are not presented because they are not used in the models. Instead, total number of moles (N_T), calculated from the mass loads of each reactant, is shown.

2.3.3.2 Experimental Results: Catalytic Runs

Before trying to adjust a theoretical model to the experimental data, it is useful to show the overall aspect of it and how the change in

Table 2.9: Listing of experimental runs performed

Run	Year	POH:ProAc	Temp. (°C)	m_{cat} (g)	N_T (mol)
1	2004	1:1	100	10	6.75
2	2004	1:1	100	10	6.75
3	2004	1:1	100	10	6.75
4	2004	1:1	90	10	8.10
5	2004	1:1	110	15	8.10
6	2004	2:1	90	12	8.10
7	2004	2:1	100	12	8.10
8	2004	2:1	110	12	8.10
9	2004	2:1	70	12	8.10
10	2004	1:1	90	12	8.10
nc1	2004	1:1	100	0	6.75
nc2	2004	1:1	100	0	6.75
nc3	2004	1:1	90	0	6.75
nc4	2004	1:1	110	0	6.75
1a	2005	1:1	60	10.02	9.70
1b	2005	1:1	60	10.01	9.69
1c	2005	1:1	60	10.00	10.0
2	2005	1:1	60	9.70	9.69
3	2005	1:1	70	10.03	9.70
4	2005	1:1	70	10.03	9.70
5	2005	1:1	80	10.06	9.69
6	2005	1:1	80	10.20	9.69
7	2005	1:1	115	10.04	9.69
8	2005	1:1	115	4.98	7.46
9	2005	2:1	80	10.00	9.27
10	2005	2:1	100	10.06	9.27
11	2005	2:1	115	5.07	9.26
12	2005	1:2	80	10.02	8.65
13	2005	1:2	100	10.00	8.65
14	2005	1:2	115	5.03	8.63

experimental conditions, namely temperature, affects the progress of the reaction. In Figure 2.8, one experiment with equimolar load at each of the used temperatures is shown (with the exception of 100°C, because no equimolar run was run at that temperature). Only experiments from 2005 are presented, since they contain more data points and have longer runtimes, thus giving a better picture of the reaction system.

Looking at the presented plots, some immediate comparisons can be made. Taking as a "measuring point" the approximate time at which the product curves cross the reactant curves (i.e. when the molar fractions are equal, around 0.25), a relative rate of reaction can be calculated. At 60°C, the curves do not cross and appear to start touching around 1700-1800 minutes. At 70°C, the crossing occurs at around 1200 min, at 80°C at 1000 min and at 115°C and - with half the catalyst - the crossing occurs at roughly 140 minutes. A first conclusion that can be taken from just observing the experimental results is that the speed of reaction increases with temperature, as expected.

Looking now at the concentrations in equilibrium, the conclusions are harder to take. Experiment 1c is not even near steady-state, so nothing can be concluded from it. The remaining three experiments seem to be near or in equilibrium, with an average value of 0.3 for the products and 0.2 for the reactants in Exp.s 3 and 5, and 0.32 for the products and 0.18 in Exp. 8. If the rest of the experiments are observed (Appendix B), no pattern whatsoever seems to emerge, with the equilibrium compositions varying somewhat independently of temperature.

Comparing now two non-equimolar experiments at an equal temperature of 100°C (Fig. 2.9), their behaviour is similar with regard to the rate of reaction, with the limiting reactant curve crossing the products at around 130 minutes but their equilibrium concentrations differing, more reactants being consumed when there is an excess of acid. This can be more easily seen on a plot of both experiments (Fig. 2.10), with a maximum time of 1600 minutes.

This can be attributed not only to the non-ideality of the mixture, which might play some part, but mainly to analytical error. As described in Appendix A, the propionic acid peak tails significantly. When the concentration of this compound is low, a large part of the tail merges with the baseline and cannot be assessed correctly by the integrator, thus under-evaluating the real concentration of acid. Since the molar fractions are calculated from mass fractions, which in turn are calculated from the ratio of peak areas, an under-evaluated ProAc

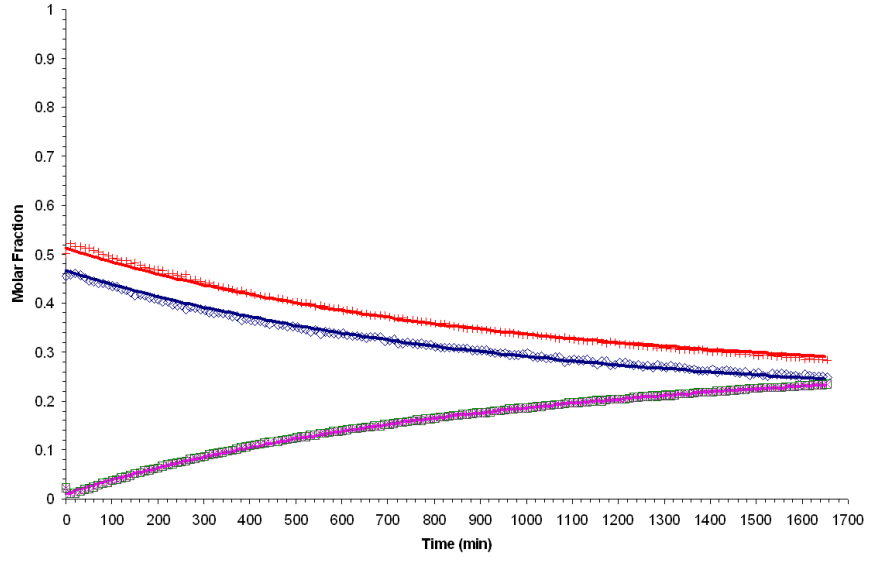

(a) Exp. 1c (60°C)

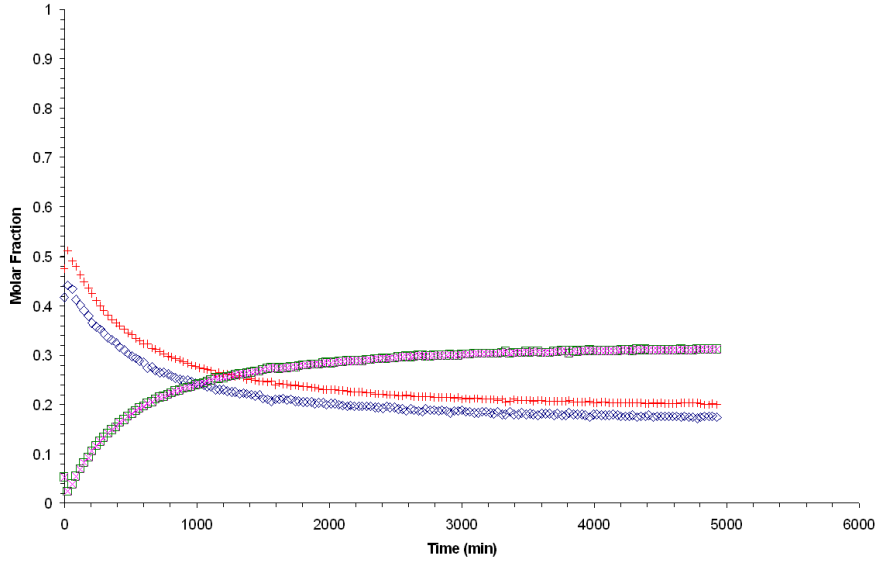

(b) Exp. 3 (70°C)

Figure 2.8: Plots of equimolar-loaded runs at different temperatures (◊- POH; +- ProAc; □- ProPro; ×- Water)

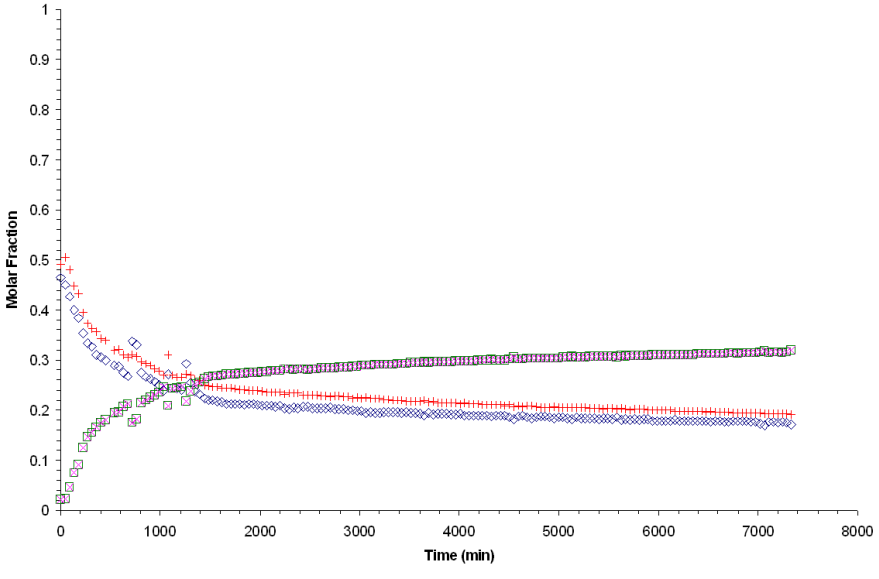

(c) Exp. 5 (80°C)

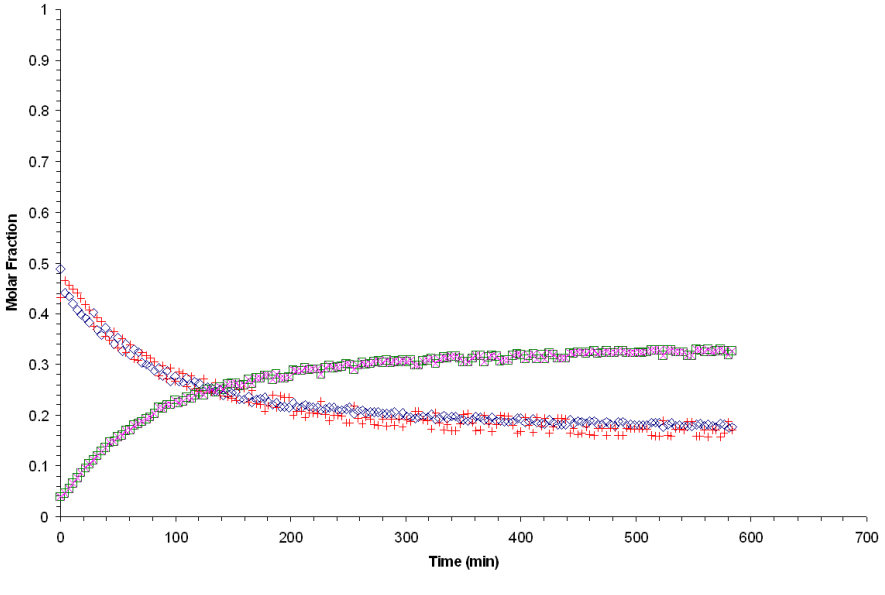

(d) Exp. 8 (115°C)

Figure 2.8: Plots of equimolar-loaded runs at different temperatures (Continued) (◊- POH; +- ProAc; □- ProPro; ×- Water)

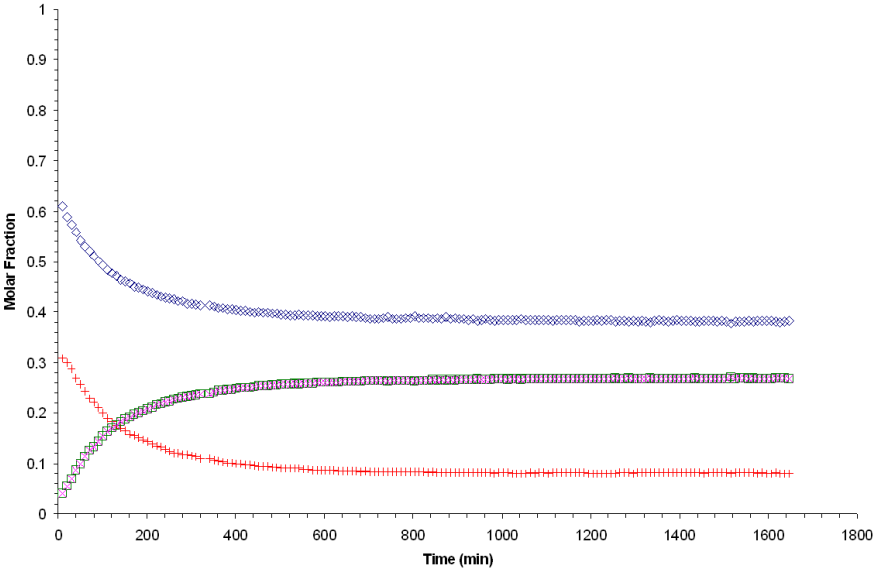

(a) Exp. 10 (2:1 POH:ProAc Ratio)

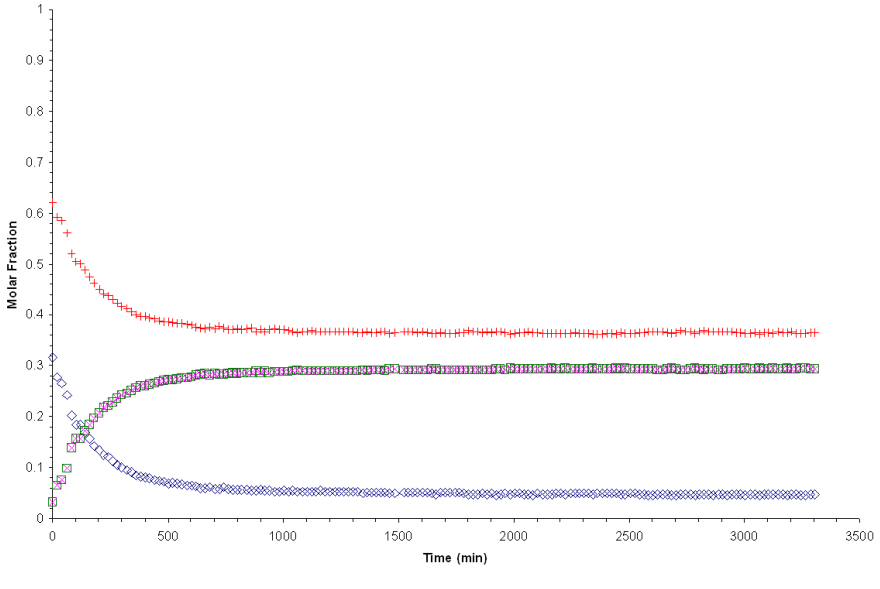

(b) Exp. 13 (1:2 POH:ProAc Ratio)

Figure 2.9: Plot of non-equimolar runs at 100°C (◊- POH; +- ProAc; □- ProPro; ×- Water)

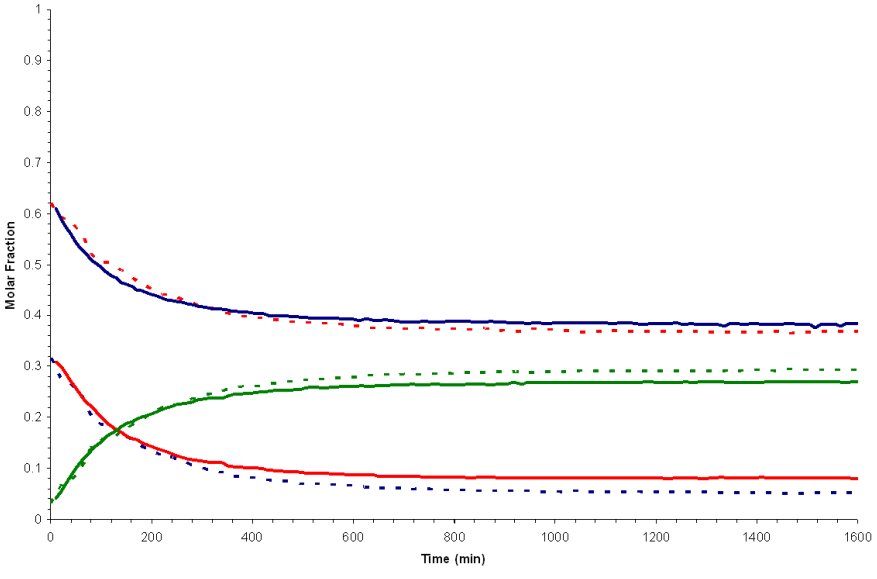

Figure 2.10: Simultaneous plot of non-equimolar runs at 100°C (— 2:1 POH:ProAc molar ratio; - - 1:2 POH:ProAc molar ratio; — POH; — ProAc; — ProAc; — Water)

peak results in a lower-than-real molar fraction reading for the acid and a slight increase of the others. This problem only occurs at low concentration of acid, so the rest of the curve is good enough for data regression analysis and the full data set was used to that end.

2.3.3.3 Experimental Results: Non-Catalytic Runs

The non-catalytic runs present very similar results to the catalytic ones, albeit with an expected slower progression of the reaction. Fig. 2.11 presents all four non-catalytic runs performed. It should be noted that in Exp. nc4, depressurisation of the reaction vessel occurred during the run which lead to a loss of the most volatile component - 1-Propanol. This can be easily seen in the corresponding plot, by a sudden increase of the molar fraction of propanoic acid and decrease of the alcohol.

A common aspect of all experiments is that due to their low reaction rate, no run neared equilibrium conditions. Since equilibrium, by definition, should not depend on whether the reaction is catalysed or not, this is not a problem as the kinetic constant can still be obtained from the initial data points.

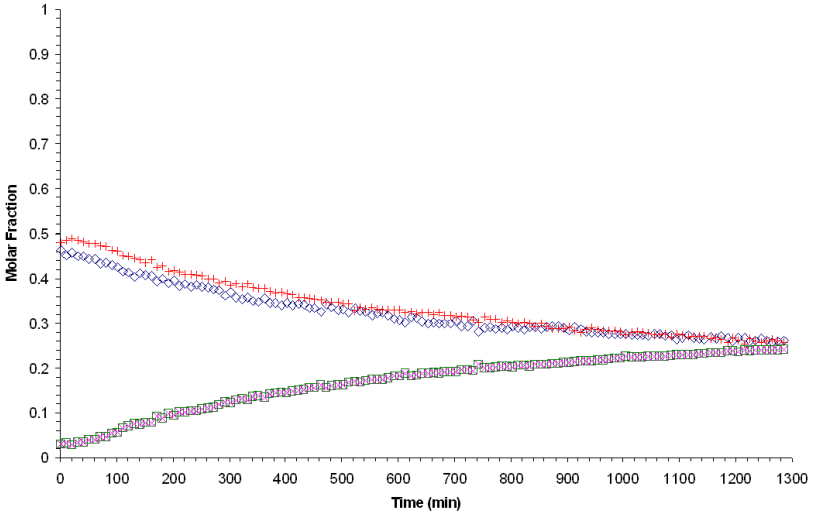

(a) Exp. nc1 (100°C)

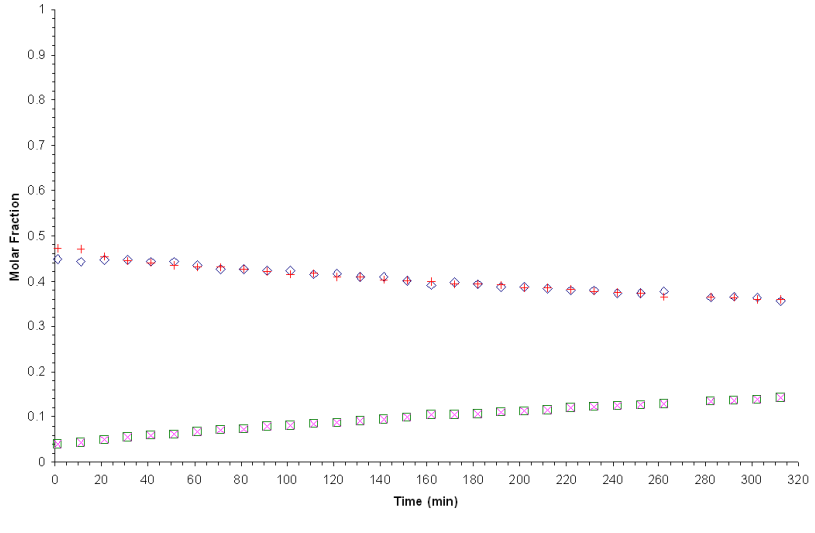

(b) Exp. nc2 (100°C)

Figure 2.11: Plots of non-catalytic runs at different temperatures (◊- POH; +- ProAc; □- ProPro; ×- Water)

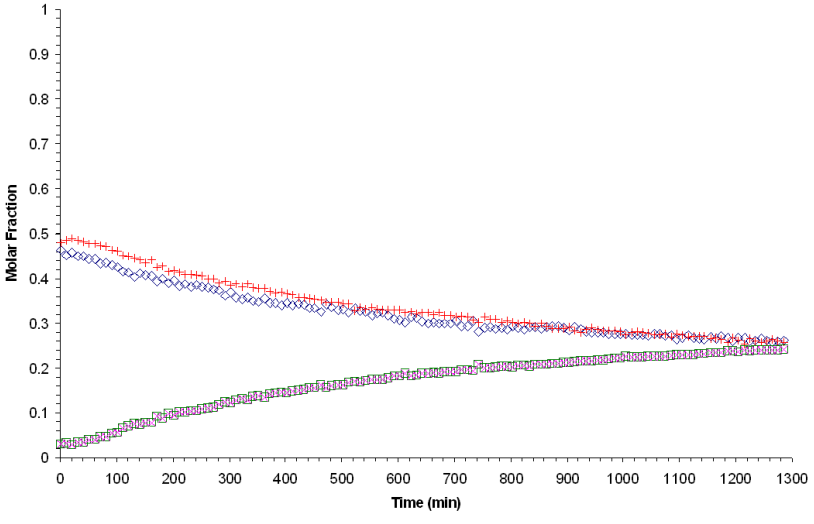

(c) Exp. nc3 (90°C)

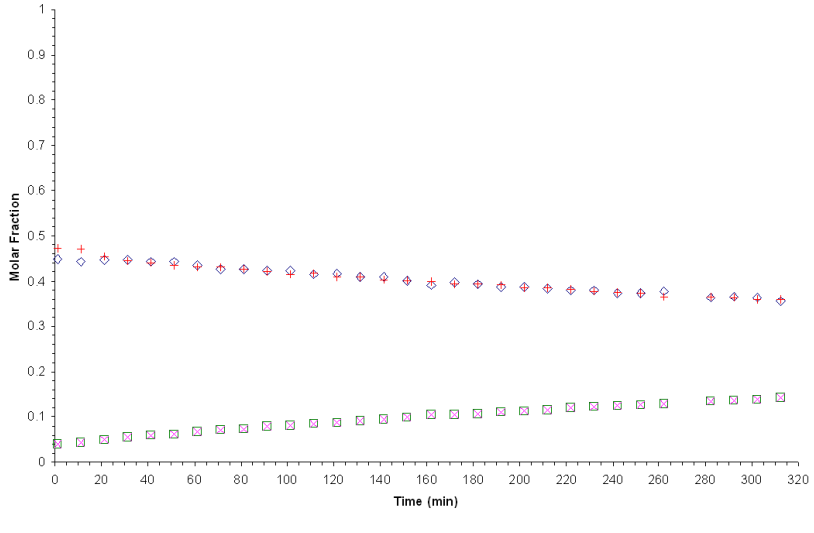

(d) Exp. nc4 (110°C)

Figure 2.11: Plots of non-catalytic runs at different temperatures (Continued) (◊- POH; +- ProAc; □- ProPro; ×- Water)

2.3.4 Data Fitting and Analysis: Catalytic Experiments

2.3.4.1 Data Regression

Using the software package Aspen Custom Modeler (ACM) as a modelling base, an isothermal batch reactor was modelled (Eq. 2.16). For each run, fixed values (total number of moles, mass of catalyst, catalyst water content and concentration of active sites, operating temperature and pressure) and initial compositions (mass fractions for POH, ProAc, ProPro and Water) are entered in the model set-up. Estimated values for the kinetic and equilibrium constants are also given as initial guesses.

The experimental data for each run (time-molar fraction data) are introduced into ACM Estimation model and the kinetic and equilibrium constants are set as estimated variables. The estimation simulation is then run, up to the maximum experimental time, in order to maximise the logarithmic likelihood (Cameron and Trivedi, 1998; Aspentech, 2005) of the regressed curve in order to the experimental data points.

One problem discovered when using ACM to fit the kinetic and equilibrium constants to the experimental data is that ACM considers the initial composition points (i.e. at t=0) to be correct and all the fitted curves start from those points. Since the initial points are also estimated from the initial load of catalyst, not taking into account possible losses in the loading process and lag between the start of reaction and data collection, this problem amounted to having not the best fit, but only the best fit at the initially predicted starting compositions.

To circumvent this problem, a Microsoft Excel macro, using Excel Solver as a base, was built to maximize the value of Logarithmic Likelihood obtained from ACM by changing the initial compositions. This macro gives an initial composition input to ACM and retrieves Logarithmic Likelihoods when the data fitting run ends. It then iterates new compositions in order to maximize the Likelihood value, stopping at the maximum value attained.

The results (i.e. initial composition, kinetic and equilibrium constants and Maximum Logarithmic Likelihood) for the experimental runs performed are presented on Table 2.10. It should be noted that the goodness of the fit cannot be compared in absolute terms, as the likelihood value depends on the number of points used for the regression.

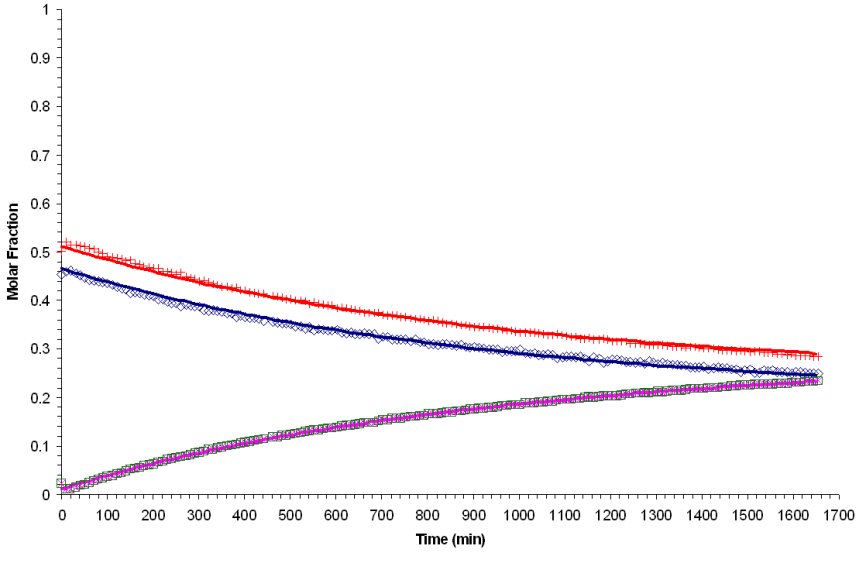

(a) Exp. 1c (60°C, 1:1 POH:ProAc Load Ratio)

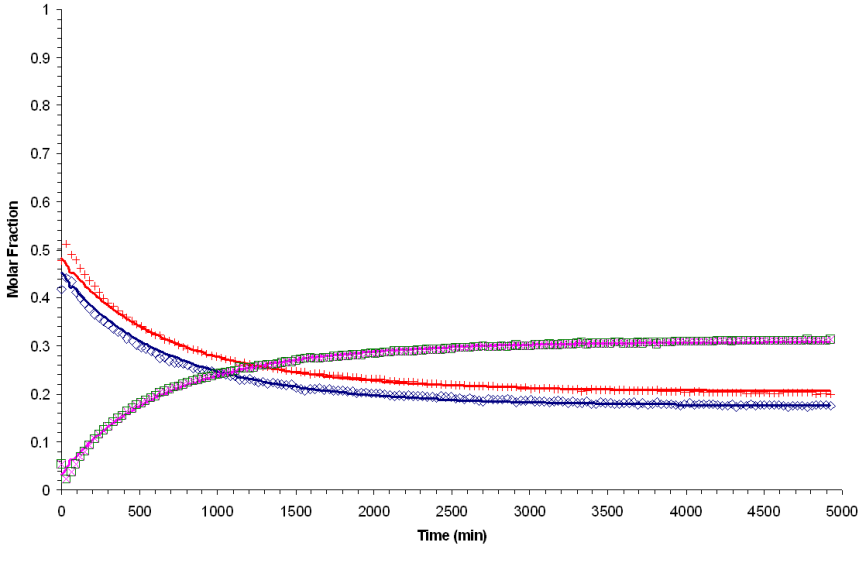

(b) Exp. 3 (70°C, 1:1 POH:ProAc Load Ratio)

Figure 2.12: Time-composition plots of experimental vs. regressed data points (Experimental data: ◊- POH; +- ProAc; □- ProPro; ×- Water. Regressed data: —, same colour codes as experimental points)

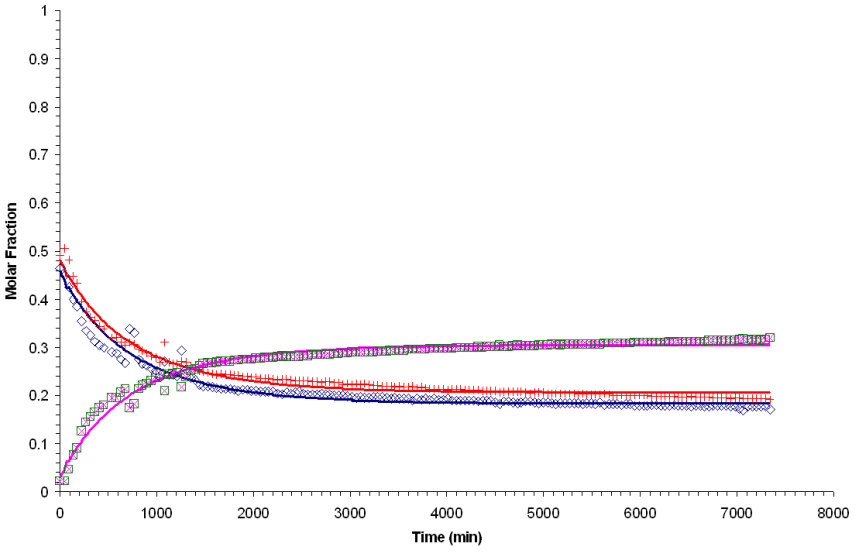

(c) Exp. 5 (80°C, 1:1 POH:ProAc Load Ratio)

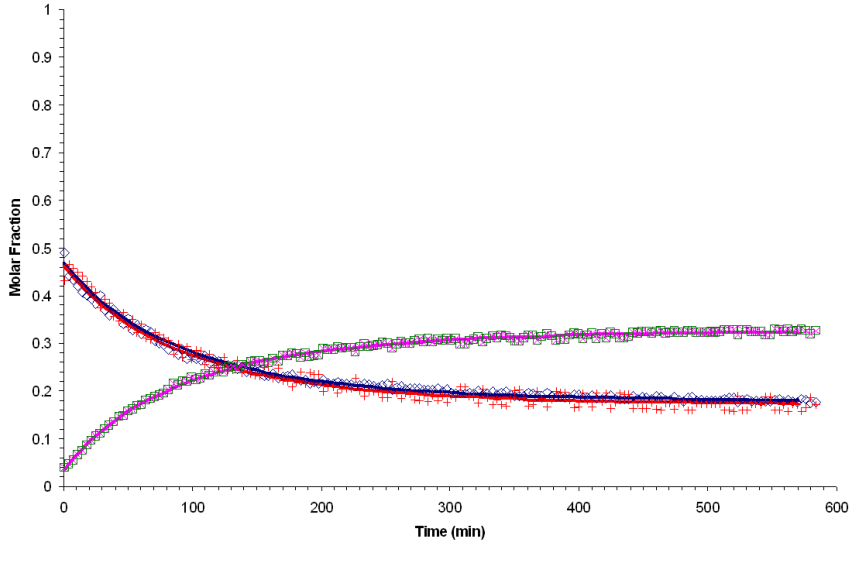

(d) Exp. 8 (115°C, 1:1 POH:ProAc Load Ratio)

Figure 2.12: Time-composition plots of experimental vs. regressed data points (Continued) (Experimental data: ◊- POH; +- ProAc; □- ProPro; ×- Water. Regressed data: —, same colour codes as experimental points)

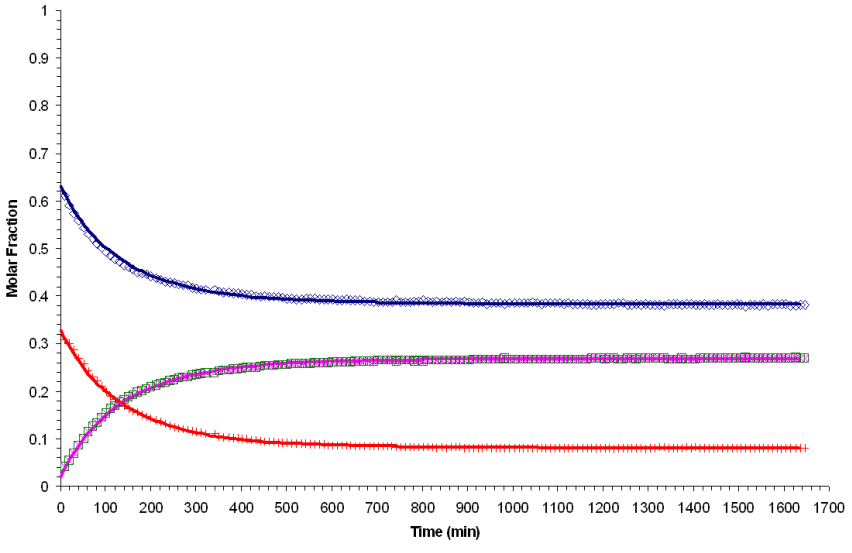

(e) Exp. 10 (100°C, 2:1 POH:ProAc Load Ratio)

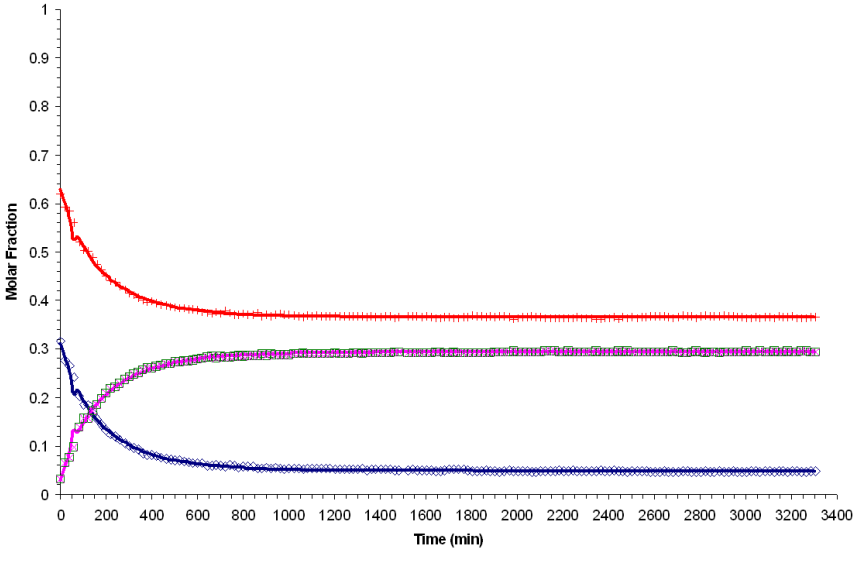

(f) Exp. 13 (100°C, 1:2 POH:ProAc Load Ratio)

Figure 2.12: Time-composition plots of experimental vs. regressed data points (Continued) (Experimental data: ◊- POH; +- ProAc; □- ProPro; ×- Water. Regressed data: —, same colour codes as experimental points)

Table 2.10: Data fitting results for catalytic experimental data

Run	Year	T	k $\times 10^2$	Keq	x_0^{POH}	x_0^{ProAc}	x_0^{ProPro}	L.L.
1c	2005	60	5.159	24.90	0.466	0.512	0.011	2667
2	2005	60	2.294	7.03	0.437	0.469	0.047	2229
3	2005	70	8.051	34.93	0.452	0.483	0.033	2409
4	2005	70	7.751	15.12	0.464	0.501	0.018	1776
5	2005	80	7.310	27.52	0.458	0.482	0.030	2015
7	2005	115	81.86	27.66	0.485	0.493	0.011	543
8	2005	115	93.89	22.48	0.469	0.462	0.034	2450
9	2005	80	12.64	29.30	0.638	0.316	0.023	2947
10	2005	100	36.51	19.51	0.630	0.328	0.021	3059
11	2005	115	94.02	34.71	0.577	0.213	0.105	2860
12	2005	80	18.13	59.56	0.322	0.649	0.015	1030
13	2005	100	30.82	36.48	0.312	0.628	0.030	2976
14	2005	115	100.0	28.06	0.273	0.606	0.060	2918
1	2004	100	33.31	39.49	0.498	0.470	0.009	2070
2	2004	100	40.47	26.67	0.488	0.493	0.018	1401
3	2004	100	35.09	31.18	0.487	0.471	0.021	2845
4	2004	90	20.14	24.72	0.482	0.482	0.018	848
5	2004	110	51.86	26.60	0.469	0.450	0.040	1153
6	2004	90	16.31	27.96	0.656	0.319	0.017	2281
7	2004	100	24.59	25.88	0.619	0.285	0.048	2387
8	2004	110	42.95	21.38	0.642	0.298	0.030	1622
9	2004	70	8.244	44.29	0.431	0.500	0.027	2169
10	2004	90	18.83	38.47	0.465	0.449	0.043	2483

T in °C; k in $mol.s^{-1}.eq^{-1}$; $x_0^{Water} = x_0^{ProPro}$; L.L.- Logarithmic Likelihood

In order to judge the goodness of the fit, reconciliation runs were performed and the results from those runs plotted against the experimental values. In order to allow a more consistent comparison, the plots of experimental vs. regressed values for the runs first presented in Fig.s 2.8 and 2.9 are shown in Fig. 2.12. The rest of the plots are available in Appendix B. As can be seen from observing the plots, the fit between experimental and regressed values is usually good, but some exceptions exist. These exceptions occur at lower temperature (Exp. 2 and the start of the ProAc curve in Exp. 3) or, in a specific case, when the experimental error is larger (Exp. 5). While the second case is self-explanatory, the first is due to the lower precision of the equilibrium constant. Since the equilibrium constant depends of the existence of equilibrium points or points near those, the fit of the experiments at lower temperatures might suffer, since those points are not available. A repetition of said experiments, with a longer runtime, would probably solve the situation, but since both are outside the operating range intended (80-120 °C), it was deemed as unnecessary to repeat them and the values obtained were used in the constants regression phase.

2.3.4.2 Kinetic and Equilibrium Constants Regression

As referenced before, the kinetic and equilibrium constants are assumed to follow the Arrhenius equation (Eq. 2.9) structure. In order to obtain the necessary parameters, one has to do a linear regression of the data, in accordance to linearised version of the equation (Eq. 2.10). Transforming the experimental data (temperature and constants) presented in Table 2.10 into a regression-ready form (Table 2.11) and plotting them for the kinetic (Fig. 2.13) and equilibrium (Fig 2.14) constants, a first analysis, previous to actual regression, can be made.

While the plot for the kinetic constant shows a strong linear tendency, with the kinetic constant increasing with temperature (in the plot, the negative logarithm of the kinetic constant increasing with the inverse of the temperature), the equilibrium constant shows no linear tendency at all, with the points following more of an oscillatory pattern. Since the theoretical thermodynamic equilibrium constant is known (Eq. 2.44) and the lower the temperature, the more inexact the determination of the equilibrium constant is, the solution found to minimise the errors in the regression of the equilibrium constant is to remove data points at lower temperatures, until the aspect of the regression line for the experimental data is the most similar to the the-

Table 2.11: Regression-ready values for temperature, kinetic and equilibrium constants, sorted by ascending temperature

Run	Year	$1/T \times 10^3$ (1/K)	-ln k	ln Keq
1c	2005	3.00	2.964	3.22
2	2005	3.00	3.775	1.95
3	2005	2.91	2.519	3.55
4	2005	2.91	2.557	2.72
9	2004	2.91	2.496	3.79
5	2005	2.83	2.616	3.32
9	2005	2.83	2.069	3.38
12	2005	2.83	1.707	4.09
4	2004	2.75	1.602	3.21
6	2004	2.75	1.813	3.33
10	2004	2.75	1.670	3.65
10	2005	2.68	1.008	2.97
13	2005	2.68	1.177	3.60
1	2004	2.68	1.099	3.68
2	2004	2.68	0.905	3.28
3	2004	2.68	1.047	3.44
7	2004	2.68	1.403	3.25
5	2004	2.61	0.657	3.28
8	2004	2.61	0.845	3.06
7	2005	2.58	0.200	3.32
8	2005	2.58	0.063	3.11
11	2005	2.58	0.062	3.55
14	2005	2.58	0.000	3.33

oretical one. This led to the removal of two data points corresponding to the lowest temperature, 60°C. Another possible approach to this problem is to just average the constants, since they appear to fluctuate around a middle value, again removing the two points at 60°C.

Calculating first the regression for the kinetic constant (Fig. 2.15), it is verifiable that the fit is good, both by visual inspection of the plot and through the value of the correlation coefficient.

Turning now to the equilibrium constant (Fig. 2.16), the fit is obviously poor. The vale of the correlation coefficient itself indicates that no apparent correlation exists. Nevertheless, and by comparison with the theoretical values for the constant, the regression line is very similar, being mostly shifted up (which indicates a difference in the

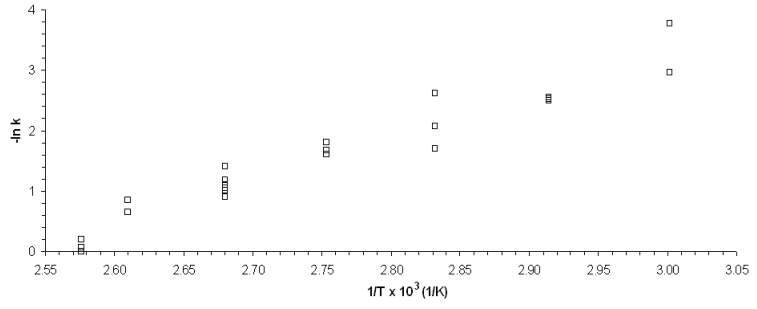

Figure 2.13: Linearised plot of experimental kinetic constants in order to temperature

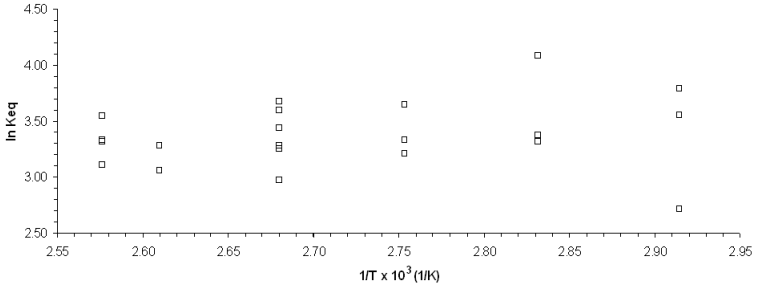

Figure 2.14: Linearised plot of experimental equilibrium constants in order to temperature

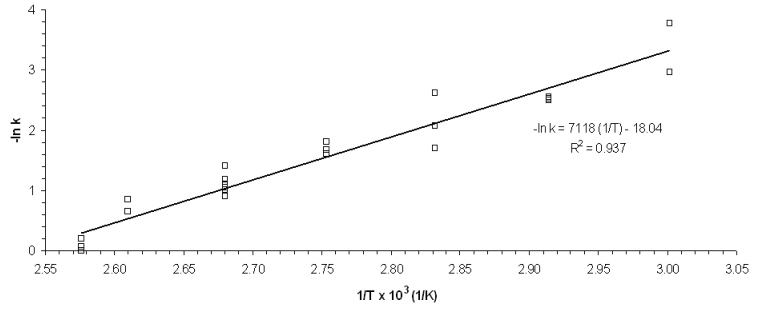

Figure 2.15: Linear regression for the kinetic constant

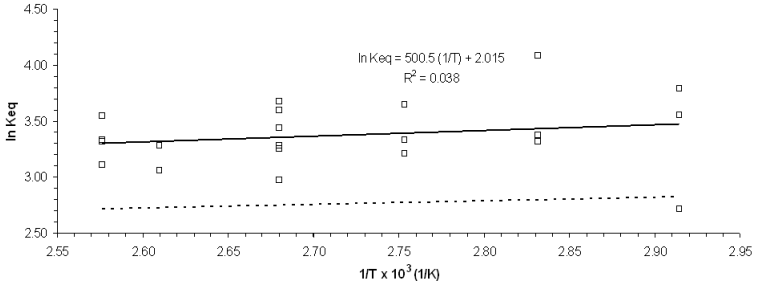

Figure 2.16: Linear regression for the equilibrium constant (— Linear regression; - - Theoretical constant)

Table 2.12: Pre-exponential factors and activation energies for the kinetic and equilibrium constants

	k	Keq
k_0	6.848×10^7	7.504
E	5.918×10^4	-4.161×10^3

k_0 in $[mol.s^{-1}.eq^{-1}]$ for k; E in $[J.mol^{-1}]$

pre-exponential factor).

Extracting the values of the pre-exponential factors and activation energies for both constants (Table 2.12) and applying them to the Arrhenius equation (Eq. 2.9) temperature-dependent expressions for the kinetic (Eq 2.45) and equilibrium (Eq. 2.46) constants are obtained. It should be noted that although in Table 2.12, a parameter E is presented for the equilibrium constant, it in fact corresponds to ΔH.

$$k = 6.848 \times 10^7 e^{-\frac{5.918 \times 10^4}{R\,T}} \tag{2.45}$$

$$Keq = 7.504\, e^{\frac{4.161 \times 10^3}{R\,T}} \tag{2.46}$$

Finally, and for comparison purposes, the average value of the equilibrium constant was calculated and compared with the values given, at each temperature, by Eq. 2.46. The comparison is presented on Table 2.13 and shows that the difference between both methods is minimal. In either case, and comparing to the constants obtained from

Table 2.13: Regressed and average values for the equilibrium constant

	Keq	
T (°C)	Regressed	Average
70	32.26	30.57
80	30.96	
90	29.77	
100	28.69	
110	27.71	
115	27.24	

the data fitting (Table 2.10), it is easy to see that the error between experimental and calculated constants is far greater than between the calculated constants themselves.

2.3.5 Data Fitting and Analysis: Non-Catalytic Experiments

2.3.5.1 Data Regression

The regression performed on the non-catalytic experimental data is similar to the ones performed on catalytic data. The batch reactor model (Eq. 2.16) was changed, in order to reflect the reaction occurring throughout the liquid phase and not only on the active sites of the catalyst (Eq. 2.47).

$$\frac{\mathrm{d}x_i}{\mathrm{d}t} = \frac{\nu_i \, r}{N_T} \tag{2.47}$$

Also, and since none of the experimental data obtained approached equilibrium, the equilibrium constant was not regressed. Instead, values taken from Eq. 2.44 were used and the fitting was only performed in order to the kinetic constant (k_{nc}). The results of the regression are presented on Table 2.14 and the plots of the regression curves versus the experimental data points on Fig. 2.17.

2.3.5.2 Kinetic Constant Regression

Using the same procedure described for the catalytic experiments, the logarithm of the experimental kinetic constants were calculated (Table 2.15) and plotted in order to the inverse of the absolute temperature (Fig. 2.18. The four data points were then fitted to a linear function

Table 2.14: Data fitting results for non-catalytic experimental data

Run	T	$k_{nc} \times 10^4$	x_0^{POH}	x_0^{ProAc}	x_0^{ProPro}	L.L.
nc1	100	2.469	0.467	0.480	0.026	1846
nc2	100	3.572	0.459	0.459	0.041	603
nc3	90	1.961	0.492	0.489	0.009	2724
nc4	110	4.135	0.479	0.499	0.011	1464

T in °C; k_{nc} in $mol.s^{-1}$; $x_0^{Water} = x_0^{ProPro}$; L.L.- Logarithmic Likelihood

(Fig. 2.19), from which the value for the activation energy and the pre-exponential factor of the non-catalytic reaction were obtained (Table 2.16).

This result can now be written in the familiar Arrhenius form (2.9), using the parameters obtained through regression:

$$k_{nc} = 3.267 \times 10^2 e^{-\frac{4.322 \times 10^4}{R\,T}} \tag{2.48}$$

2.3.6 Data Reconciliation and Conclusions

From the parameters obtained in the previous subsection, it is possible to calculate kinetic and equilibrium constants at the temperatures used in the experimental work (Table 2.17). Using these constants and running reconciliation simulations, with the same conditions as the experimental runs, it is possible to compare the model predicted data points with the actual experimental points. Using again, as a reference, Run nr.s 1c, 3, 5, 8, 10 and 13 for the catalytic experiments and all four non-catalytic experiments, a visual inspection of the goodness of fit can be done (Fig.s 2.20 and 2.21).

Unlike the individual regressions, the use of the constants from the overall regression of data does not give almost uniformly good results. In fact, for most of the runs (see Appendix B for all the plots), the fit is not good, especially when relating to the concentrations in equilibrium. The explanation for this behaviour is quite simple and has to do with the low quality of the linear fit to the equilibrium constants. Tables 2.18 and 2.19 compare the experimental and regressed constants for each run which was reconciled / plotted and calculates the deviation of the experimental values to the modelled ones.

Although the kinetic constant appears to have errors almost as high as the equilibrium constant, with the average absolute error of

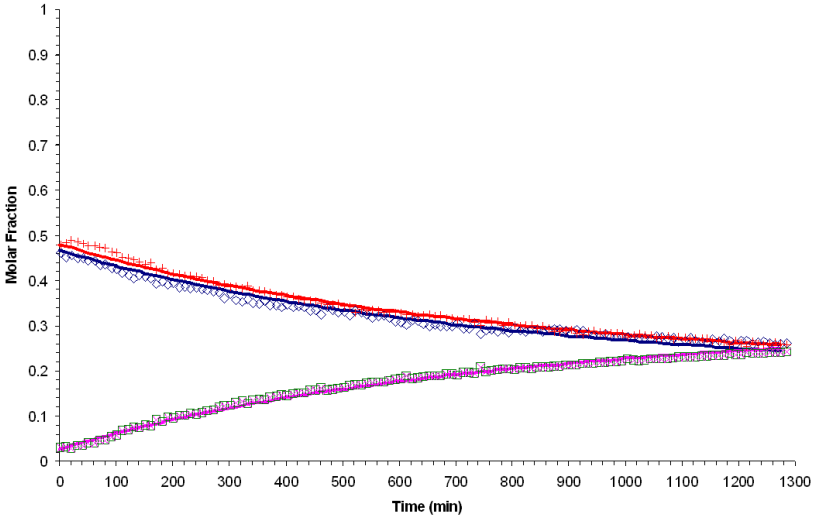

(a) Exp. nc1 (100°C)

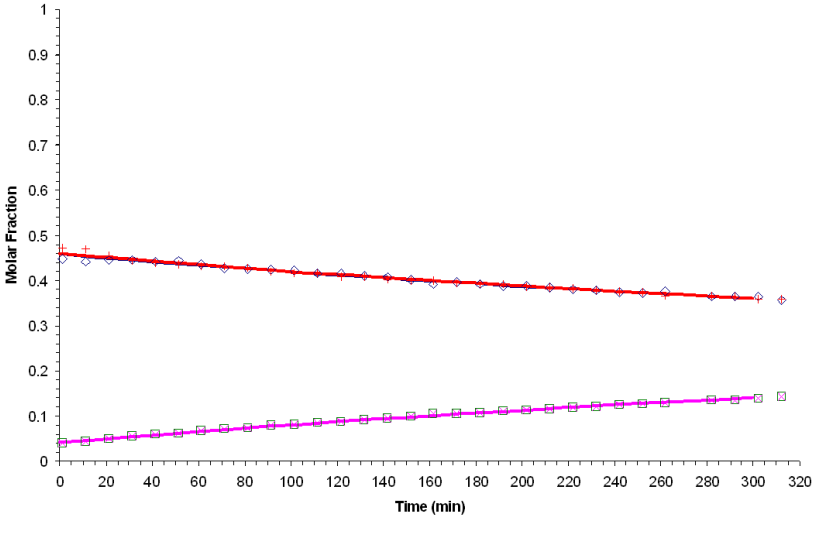

(b) Exp. nc2 (100°C)

Figure 2.17: Time-composition plots of experimental vs. regressed data points for non-catalytic experiments (Experimental data: ◊- POH; +- ProAc; □- ProPro; ×- Water. Regressed data: —, same colour codes as experimental points)

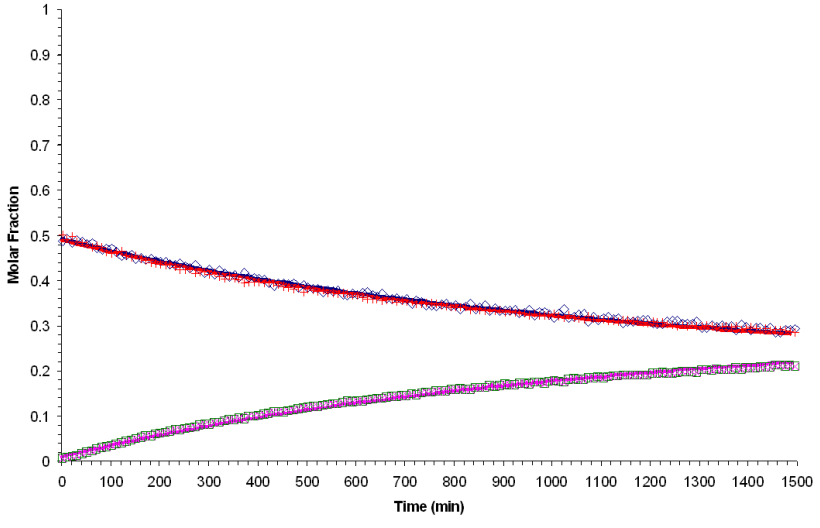

(c) Exp. nc3 (90°C)

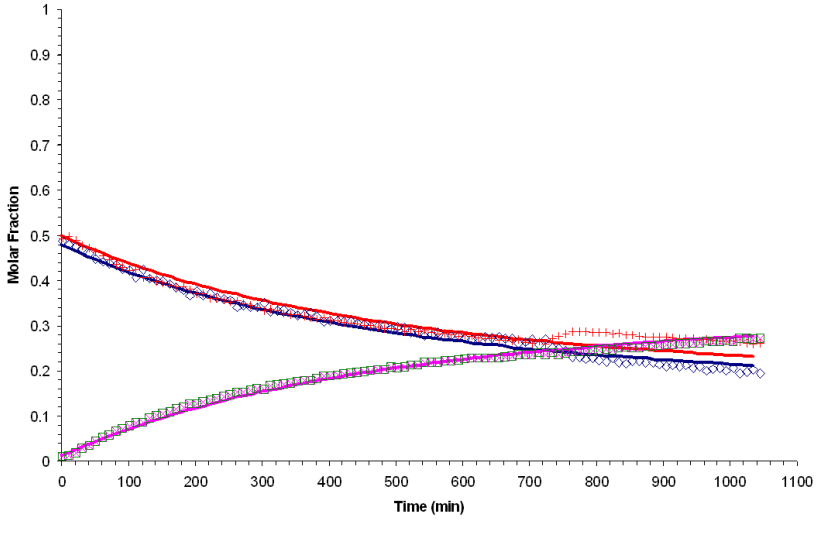

(d) Exp. nc4 (110°C)

Figure 2.17: Time-composition plots of experimental vs. regressed data points for non-catalytic experiments (Continued) (Experimental data: ◊- POH; +- ProAc; □- ProPro; ×- Water. Regressed data: —, same colour codes as experimental points)

Table 2.15: Regression-ready values for temperature and kinetic constant, sorted by ascending temperature (non-catalytic)

Run	1/T (1/K)	-ln k_{nc}
nc3	2.75×10^{-3}	1.961×10^{4}
nc1	2.68×10^{-3}	2.469×10^{4}
nc2	2.68×10^{-3}	3.572×10^{4}
nc4	2.61×10^{-3}	4.135×10^{4}

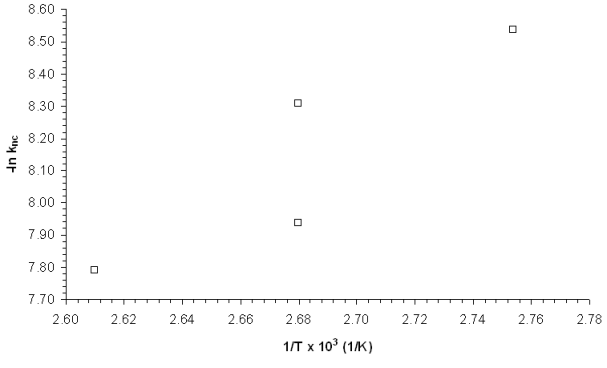

Figure 2.18: Linearised plot of experimental non-catalytic kinetic constant in order to temperature

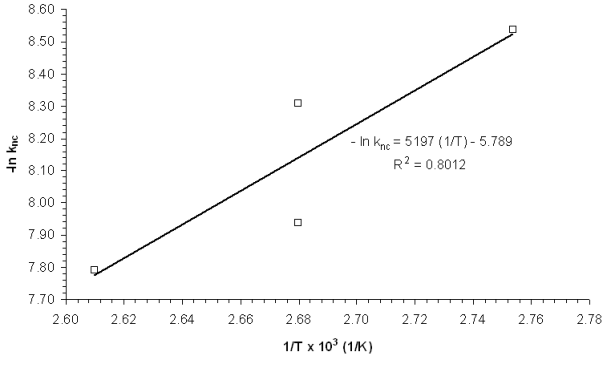

Figure 2.19: Linear regression for the non-catalytic kinetic constant

Table 2.16: Pre-exponential factors and activation energies for the non-catalytic kinetic constant

k_{nc0}	3.267×10^2
E_{nc}	4.322×10^4

k_{nc0} in $[mol.s^{-1}]$; E_{nc} in $[J.mol^{-1}]$

the kinetic constant being of 20.6% and of the equilibrium constant of 24.5%, one has to remember that the variation of the kinetic constant in the temperature range studied is of approximately 20 times, while the equilibrium constant is near invariant. This means that while the errors in the kinetic constant are perfectly included in the errors associate with the structure of the model, namely the water content of the catalyst, the liquid load in the reactor or even the mass load of catalyst and concentration of active sites, the errors in the equilibrium constant are of a different sort, since the it does not depend of any of the mentioned parameters. It should be noted that, in the case of the four non-catalytic experiments, the errors presented are merely presented for the sake of completeness. The number of experiences is too low for the values obtained to be considered accurate and the error due to undersampling is, likely, large.

The reason for the discrepancy of the equilibrium constants is not known and although several factors might contribute to it, two stand out as most likely candidates:

- The equilibrium constant is very sensible to variations which, although large in relative terms, are small in absolute terms. A variation of a low concentration component, which might be sub- or over-evaluated is such a case. This variation can be attributed to deficiencies in the GC analysis, already mentioned, which include the inability to properly quantify one of the products and the tailing of two peaks (Propionic Acid and n-Propyl Propionate).

- The equilibrium constant, more than the kinetic constant, is sensible to the thermodynamic model used. Since the model used is far from perfect, especially in the case of two binary pairs, the activity coefficients calculated probably do not represent reality correctly. The difference between the thermodynamically

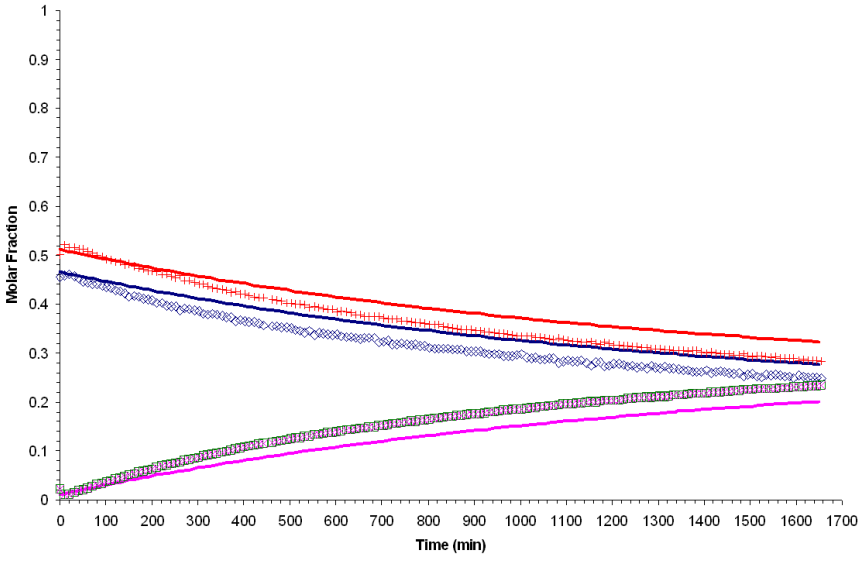

(a) Exp. 1c (60°C, 1:1 POH:ProAc Load Ratio)

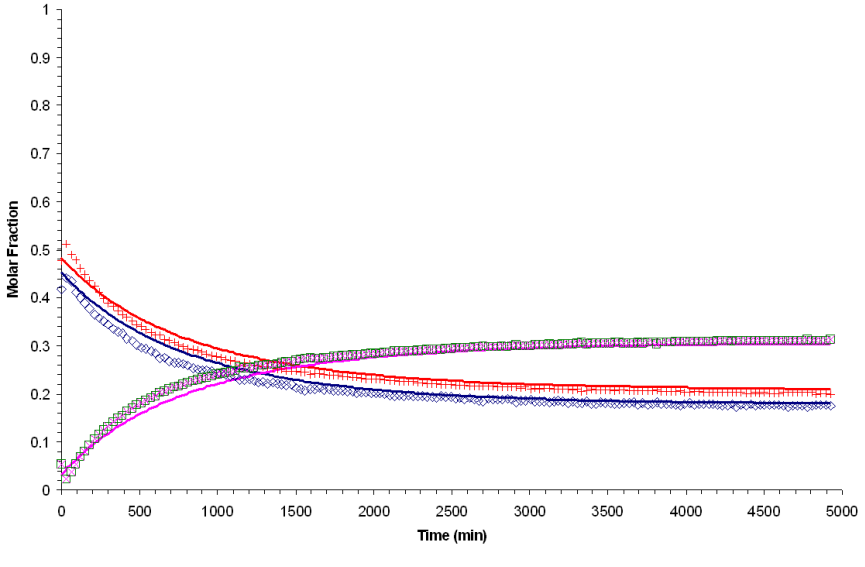

(b) Exp. 3 (70°C, 1:1 POH:ProAc Load Ratio)

Figure 2.20: Time-composition plots of experimental vs. regressed data points (Catalytic experiments) (Experimental data: ◊- POH; +- ProAc; □- ProPro; ×- Water. Regressed data: —, same colour codes as experimental points)

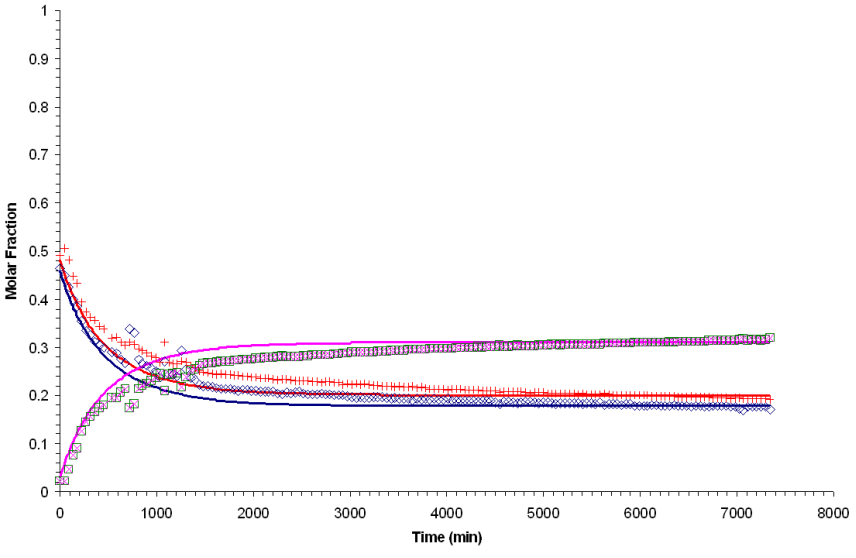

(c) Exp. 5 (80°C, 1:1 POH:ProAc Load Ratio)

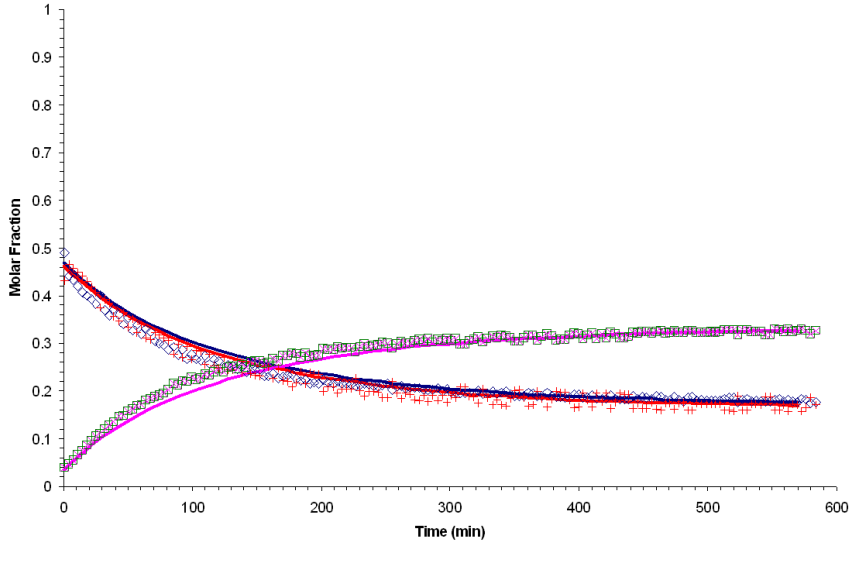

(d) Exp. 8 (115°C, 1:1 POH:ProAc Load Ratio)

Figure 2.20: Time-composition plots of experimental vs. regressed data points (Catalytic experiments) (Continued) (Experimental data: ◇- POH; +- ProAc; □- ProPro; ×- Water. Regressed data: —, same colour codes as experimental points)

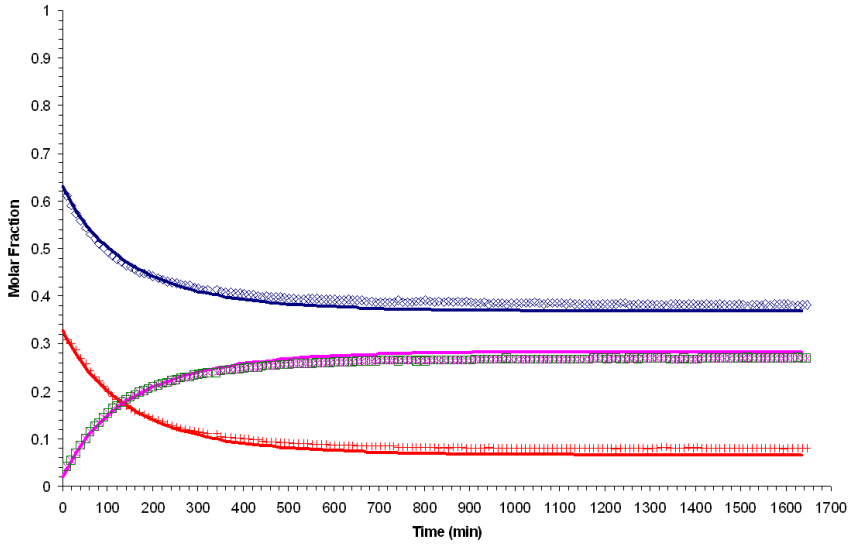

(e) Exp. 10 (100°C, 2:1 POH:ProAc Load Ratio)

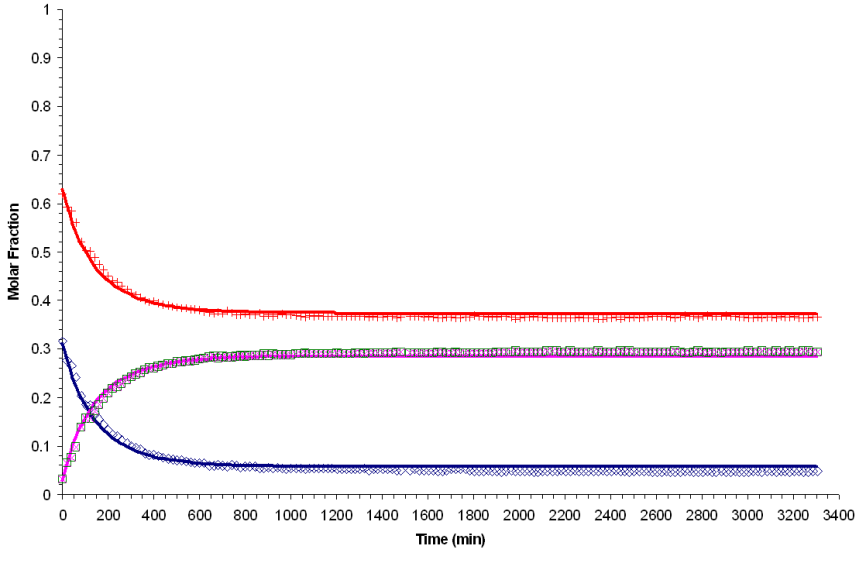

(f) Exp. 13 (100°C, 1:2 POH:ProAc Load Ratio)

Figure 2.20: Time-composition plots of experimental vs. regressed data points (Catalytic experiments) (Continued) (Experimental data: ◊- POH; +- ProAc; □- ProPro; ×- Water. Regressed data: —, same colour codes as experimental points)

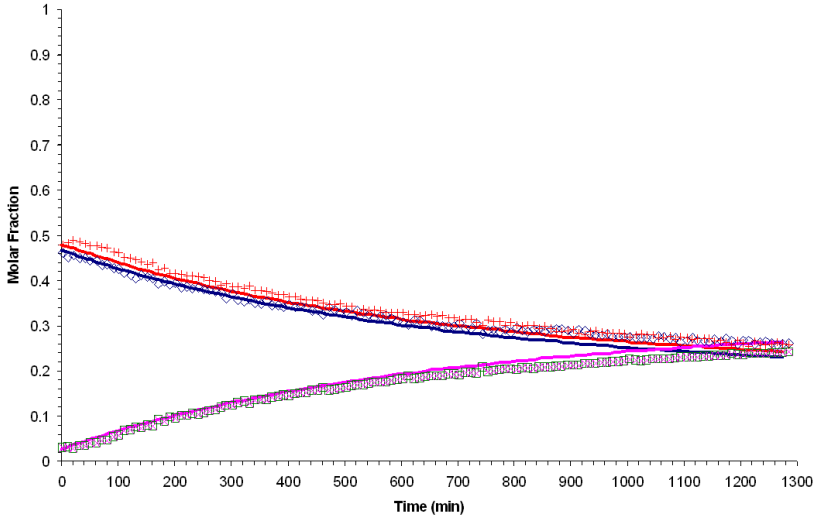

(a) Exp. nc1 (100°C)

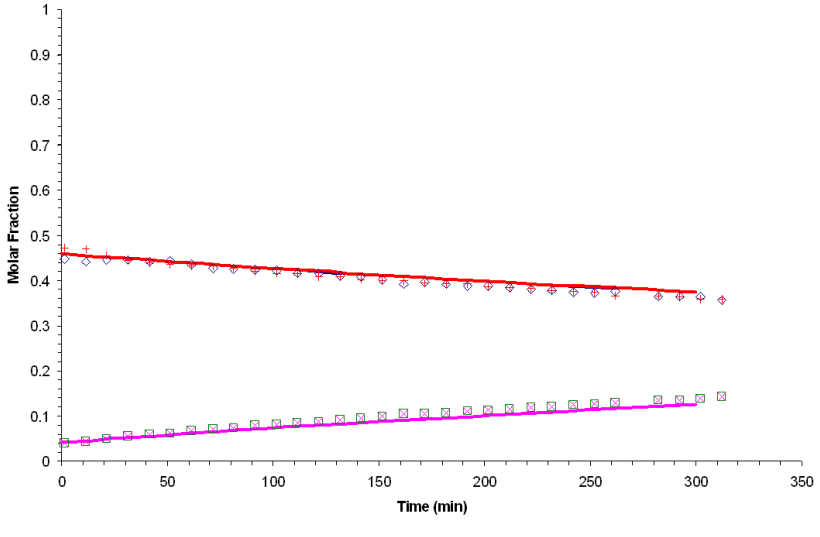

(b) Exp. nc2 (100°C)

Figure 2.21: Time-composition plots of experimental vs. regressed data points (Non-catalytic experiments) (Experimental data: ◊- POH; +- ProAc; □- ProPro; ×- Water. Regressed data: —, same colour codes as experimental points)

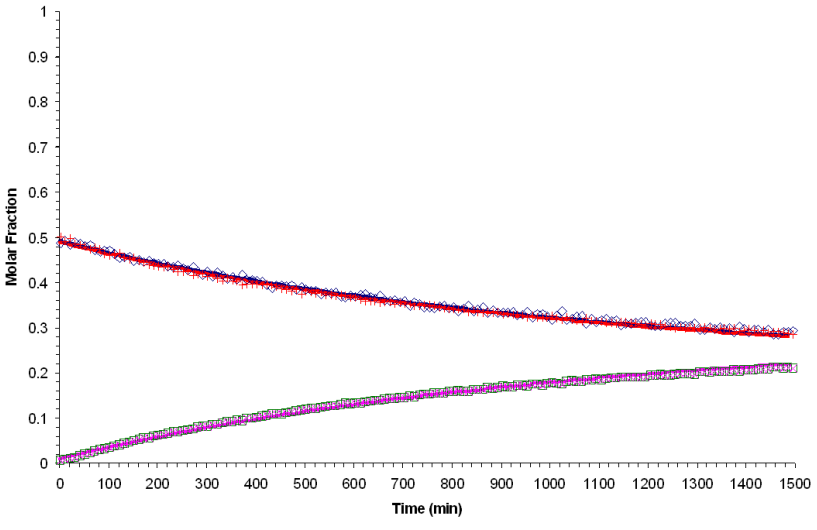

(c) Exp. nc3 (90°C)

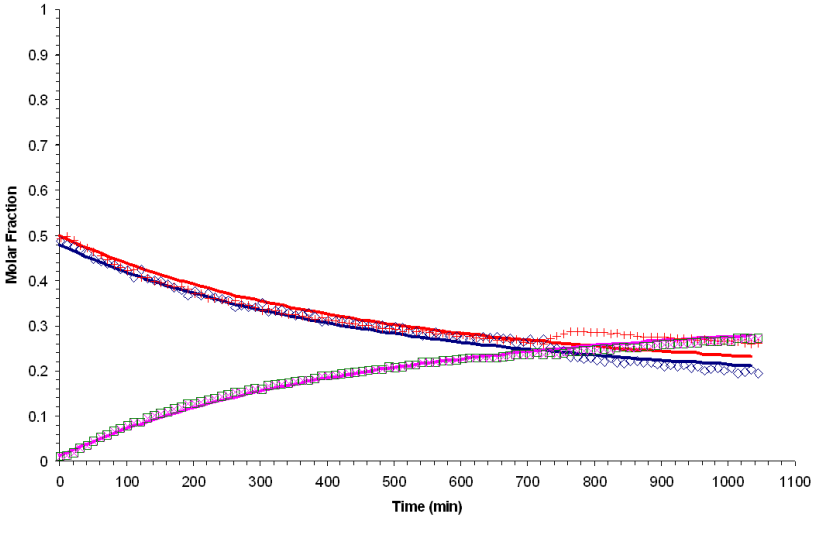

(d) Exp. nc4 (110°C)

Figure 2.21: Time-composition plots of experimental vs. regressed data points (Non-catalytic experiments) (Continued) (Experimental data: ◇- POH; +- ProAc; □- ProPro; ×- Water. Regressed data: —, same colour codes as experimental points)

Table 2.17: Kinetic and equilibrium constants at experimental temperatures

T	Keq	k	k_{nc}
60	$33.71^{\dagger}$	3.597×10^{-2}	$5.457 \times 10^{-5\dagger}$
70	32.26	6.175×10^{-2}	$9.364 \times 10^{-5\dagger}$
80	30.96	1.116×10^{-1}	$1.435 \times 10^{-4\dagger}$
90	29.77	1.952×10^{-1}	2.148×10^{-4}
100	28.69	3.315×10^{-1}	3.147×10^{-4}
110	27.71	5.474×10^{-1}	4.518×10^{-4}
115	27.24	6.967×10^{-1}	$5.337 \times 10^{-4\dagger}$

T in [°C]; k in $[mol.s^{-1}.eq^{-1}]$; † Extrapolated values

calculated constants and the regressed ones might be a symptom of the same problem.

Although an evaluation of the errors associated with the use of the regressed kinetic constant is already presented in Tables 2.18 and 2.19, it might be useful to determine the actual error of the equilibrium composition. To do so, the deviation between the values given by the model at or near equilibrium (which include all valid experiments, with the exception of Runs 1 and 2) are compared with the values taken experimentally, using the last point taken. The local relative (i.e. the deviation between model and experimental values, in terms of experimental values - $\frac{x_{mod}-x_{exp}}{x_{exp}}$) and relative system (since the sum of x is always 1, the relative system error is equal to the difference between model and experimental values) deviations / errors are presented on Tables 2.20 and 2.21, with the exception of water, since water, by definition of the analytical conditions, has always an equal molar fraction to Propyl Propionate.

Looking at the values obtained, it is easily seen that while in some cases the local relative deviation is high (over 50% in one case), that deviation is always low in system terms, being always lower than 4%. Even if the criteria is tightned (considering that the "average" molar fraction for an equimolar feed is roughly of 0.333), the maximum error obtained will be of less than 10%, well inside an acceptable region of trust.

The conclusion that can be taken from the conjunction of the data presented on the previous tables and the reconciliation plots is that

Table 2.18: Comparison of individually regressed vs. modelled values for the catalytic kinetic and equilibrium constants

		$k \times 10^2$			Keq		
Run	Year	Exp.	Mod.	Dev.	Exp.	Mod.	Dev.
1c	2005	5.159	3.597	43.4	24.90	33.71	-26.1
2	2005	2.294	3.597	-36.2	7.03	33.71	-79.1
3	2005	8.051	6.705	20.1	34.93	32.26	8.3
4	2005	7.751	6.705	15.6	15.12	32.26	-53.1
5	2005	7.310	12.06	-39.4	27.52	30.96	-11.1
7	2005	81.86	74.28	10.2	27.66	27.24	1.5
8	2005	93.89	74.28	26.4	22.48	27.24	-17.5
9	2005	12.64	12.06	4.7	29.30	30.96	-5.4
10	2005	36.51	35.54	2.7	19.51	28.69	-32.0
11	2005	94.02	74.28	26.6	34.71	27.24	27.4
12	2005	18.13	12.06	50.3	59.56	30.96	92.4
13	2005	30.82	35.54	-13.3	36.48	28.69	27.1
14	2005	100.0	74.28	34.6	28.06	27.24	3.0
1	2004	33.31	35.54	-6.3	39.49	28.69	37.6
2	2004	40.47	35.54	13.9	26.67	28.69	-7.1
3	2004	35.09	35.54	-1.3	31.18	28.69	8.7
4	2004	20.14	21.02	-4.2	24.72	29.77	-17.0
5	2004	51.86	58.47	-11.3	26.60	27.71	-4.0
6	2004	16.31	21.02	-22.4	27.96	29.77	-6.1
7	2004	24.59	35.54	-30.8	25.88	28.69	-9.8
8	2004	42.95	58.47	-26.5	21.38	27.71	-22.8
9	2004	8.244	6.705	23.0	44.29	32.26	37.3
10	2004	18.83	21.02	-10.4	38.47	29.77	29.2
		Aver. Dev.		3.0	Aver. Dev.		-0.9
		Aver. Abs. Dev.		20.6	Aver. Abs. Dev.		24.5

k in $[mol.s^{-1}.eq^{-1}]$; Dev. in %; Exp.- Experimental; Mod.- Modelised; Dev.- Deviation; Abs.- Absolute

Table 2.19: Comparison of individually regressed vs. modelled values for the non-catalytic kinetic constant

	$k \times 10^4$		
Run	Exp.	Mod.	Rel. Dev.
nc1	2.469	2.907	-15.1
nc2	3.572	2.907	22.9
nc3	1.961	1.981	-1.0
nc4	4.135	4.181	-1.1
	Aver. Rel. Dev.		1.4
	Aver. Abs. Dev.		10.0

k in $[mol.s^{-1}]$; Rel Dev. in %; Exp.- Experimental; Mod.- Modelised; Dev.- Deviation; Rel.- Relative; Abs.- Absolute

although deviations exist between the experimental and model results, that deviation is, with the exceptions noted, small and the impact in the actual results is not very significant. As such, the parameters modelled in these experiments are considered as adequate for use later on in other modelling experiments, namely obtaining of RCMs (Residue Curve Maps) and the computer simulation of the reactive distillation column.

A second conclusion is that the pseudo-homogeneous model fits the system well, eliminating the need for using other, more complex, reaction models such as Langmuir-Hinshelwood. It also means that there is no need to determine adsorption constants, as they are not used despite the phenomena existing.

A third and last conclusion, with regard to the comparison between catalytic and non-catalytic kinetics, is that the reaction occurs even without catalyst at a reasonable pace. Nevertheless, when catalyst does exist in the system, the difference between the order of magnitude of both constants (10^3) is large enough that the reaction occurring in the liquid can be disregarded. Another interesting point which arises from comparing the results - although, has been mentioned before, the non-catalytic kinetic constant likely has a significant error due to undersampling - is that both expressions have similar activation energies, the main difference being the pre-exponential factor which indicates that the simplification mentioned before - disregard for the non-catalytic reaction when the catalyst exists - can be most likely

Table 2.20: Relative local and relative system error of the equilibrium compositions (2005 Experiments)

	Experimental			Model			Loc. Rel. Dev.			Rel. Sys. Dev.		
Run	x_{POH}	x_{ProAc}	x_{ProPro}	x_{POH}	x_{ProAc}	x_{ProPro}	x_{POH}	x_{ProAc}	x_{ProPro}	x_{POH}	x_{ProAc}	x_{ProPro}
3	0.174	0.200	0.313	0.181	0.211	0.304	3.9	5.7	-2.9	0.7	1.1	-0.9
4	0.200	0.245	0.278	0.177	0.214	0.305	-11.7	-12.6	9.8	-2.3	-3.1	2.7
5	0.171	0.191	0.319	0.178	0.201	0.310	4.3	5.4	-2.8	0.7	1.0	-0.9
7	0.158	0.169	0.336	0.161	0.169	0.335	1.8	0.0	-0.4	0.3	0.0	-0.1
8	0.177	0.171	0.326	0.175	0.168	0.328	-0.9	-1.5	0.6	-0.2	-0.3	0.2
9	0.394	0.073	0.266	0.393	0.071	0.268	-0.4	-2.8	0.7	-0.2	-0.2	0.2
10	0.382	0.080	0.269	0.369	0.067	0.282	-3.4	-16.8	4.9	-1.3	-1.3	1.3
11	0.399	0.038	0.282	0.410	0.045	0.272	2.8	20.8	-3.4	1.1	0.8	-0.9
12	0.039	0.370	0.296	0.060	0.387	0.277	53.9	4.6	-6.5	2.1	1.7	-1.9
13	0.047	0.365	0.294	0.057	0.373	0.285	20.1	2.2	-3.0	0.9	0.8	-0.9
14	0.046	0.380	0.287	0.048	0.381	0.286	3.5	0.3	-0.5	0.2	0.1	-0.1

Deviations in %; (Loc.) Rel. (Sys.) Dev.- (Local) Relative (System) Deviation

Table 2.21: Relative local and relative system error of the equilibrium compositions (2004 Experiments)

	Experimental			Model			Loc. Rel. Dev.			Rel. Sys. Dev.		
Run	x_{POH}	x_{ProAc}	x_{ProPro}	x_{POH}	x_{ProAc}	x_{ProPro}	x_{POH}	x_{ProAc}	x_{ProPro}	x_{POH}	x_{ProAc}	x_{ProPro}
1	0.192	0.173	0.318	0.198	0.169	0.310	3.1	-2.4	-2.4	0.6	-0.4	-0.8
2	0.195	0.179	0.313	0.198	0.203	0.307	1.5	13.0	-1.6	0.3	2.3	-0.5
3	0.183	0.167	0.325	0.188	0.172	0.320	2.9	2.9	-1.6	0.5	0.5	-0.5
4	0.255	0.246	0.249	0.246	0.246	0.254	-3.8	-0.2	2.1	-1.0	-0.1	0.5
5	0.183	0.159	0.329	0.179	0.161	0.330	-1.9	1.1	0.3	-0.3	0.2	0.1
6	0.414	0.066	0.260	0.402	0.065	0.271	-2.9	-1.8	4.4	-1.2	-0.1	1.1
7	0.402	0.065	0.267	0.393	0.059	0.274	-2.2	-8.7	2.7	-0.9	-0.6	0.7
8	0.410	0.060	0.265	0.396	0.052	0.276	-3.2	-13.1	4.0	-1.3	-0.8	1.1
9	0.190	0.262	0.274	0.205	0.274	0.253	8.0	4.3	-7.5	1.5	1.1	-2.1
10	0.183	0.166	0.325	0.193	0.178	0.314	5.6	7.0	-3.3	1.0	1.2	-1.1
nc1	0.259	0.260	0.240	0.230	0.242	0.264	-11.3	-6.9	9.9	-2.9	-1.8	2.4
nc2	0.364	0.359	0.138	0.374	0.375	0.125	2.8	4.3	-9.3	1.0	1.6	-1.3
nc3	0.291	0.287	0.211	0.282	0.279	0.219	-2.8	-2.6	3.7	-0.8	-0.7	0.8
nc4	0.203	0.259	0.269	0.211	0.231	0.279	4.4	-10.8	3.5	0.9	-2.8	1.0

Deviations in %; (Loc.) Rel. (Sys.) Dev.- (Local) Relative (System) Deviation

extended beyond the temperature range studied in this work.

NOMENCLATURE

Variables / Constants

A	Heat Capacity correlation parameter	$[J.kmol^{-1}.K^{-1}]$
a_i	Liquid-phase activity of species i	[-]
B	Heat Capacity correlation parameter	$[J.kmol^{-1}.K^{-2}]$
C	Heat Capacity correlation parameter	$[J.kmol^{-1}.K^{-3}]$
Cp	Heat Capacity	$[J.kmol^{-1}.K^{-1}]$
D	Heat Capacity correlation parameter	$[J.kmol^{-1}.K^{-4}]$
E	Activation Energy	$[J.mol^{-1}]$
E	Heat Capacity correlation parameter	$[J.kmol^{-1}.K^{-5}]$
f	Fugacity	$[Pa]$
G	Standard Gibbs energy	$[J]$
G_i	Standard Gibbs energy of species i	$[J.mol^{-1}]$
G^t	Total system Gibbs energy	$[J]$
ΔG°	Standard Gibbs energy of formation	$[J.kmol^{-1}]$
H	Enthalpy	$[J]$
ΔH°	Enthalpy of reaction	$[J.kmol^{-1}]$
hum	Wet catalyst total water content	[-]
I	Enthalpy integration constant	$[J.kmol^{-1}]$
J	Equilibrium constant integration constant	[-]
J_i	UNIQUAC / UNIFAC parameter	[-]
Keq	Equilibrium constant	[-]
k	Kinetic constant	$[mol.s^{-1}.eq^{-1}]$
k_0	Pre-exponential factor (k)	$[mol.s^{-1}.eq^{-1}]$
k_0	Pre-exponential factor (Keq)	[-] for Keq
L	Concentration of active sites (Capacity)	$[eq.\left(kg^{dry}\right)^{-1}]$
L_i	UNIQUAC / UNIFAC parameter	[-]

m_cat	Catalyst mass	[g]/[kg]
N_T	Total number of moles	$[mol]$
n_i	Number of moles of species i	$[mol]$
P	Pressure	$[Pa]$
q_i	UNIQUAC / UNIFAC parameter	[-]
R	Universal Gas Constant = 8.314	$[J.mol^{-1}.K^{-1}]$
r_i	Reaction rate	$[mol.s^{-1}.eq^{-1}]$
r_i	UNIQUAC / UNIFAC parameter	[-]
S	Entropy	$[J.K^{-1}]$
$s_{j,i}$	UNIQUAC / UNIFAC parameter	[-]
T	Temperature	$[K]$
t	Time	$[s]$
V	Volume	$[m^3]$
x_i	Molar fraction of species i	[-]

Greek Letters

Δ	Variation	N/A
ϵ	Reaction coordinate	$[mol]$
η_j	UNIQUAC / UNIFAC parameter	[-]
θ	UNIQUAC / UNIFAC parameter	[-]
μ_i	Chemical potential	$[J.mol^{-1}]$
ν_i	Stoichiometric coefficient of species i	[-]
$\tau_{m,j}$	UNIQUAC / UNIFAC parameter	[-]
$\upsilon_{i,i}$	UNIQUAC / UNIFAC parameter	[-]
$\upsilon_{m,j}$	UNIQUAC / UNIFAC parameter	[-]
φ_i	Liquid-phase activity coefficient of species i	[-]
φ_i^C	Liquid-phase activity coefficient (combinatory part) of species i	[-]
φ_i^R	Liquid-phase activity coefficient (residual part) of species i	[-]

Indexes

Superscript

dry	Dry catalyst
wet	Wet catalyst
$\bar{}$	Partial property
$\hat{}$	Property of a species in solution
$\circ$	Standard state property

Subscript

cat	Catalyst
i	Dummy argument, usually representing chemical species
nc	Non-catalytic (for the kinetic constant)
t	Property at time t
$t + \mathrm{d}t$	Property at time t+dt
0	Initial condition (at t=0)
1	For k, direct reaction
-1	For k, inverse reaction

Abbreviations and Acronyms

DAQ	Data AcQuisition
DPE	Di-n-Propyl Ether
FID	Flame Ionisation Detector
GC	Gas Chromatograph
LLE	Liquid-Liquid Equilibrium
NRTL	Non-Random Two-Liquid
POH	1-Propanol
Pro	Propene
ProAc	Propionic Acid
ProPro	n-Propyl Propionate
TCD	Thermal Conductivity Detector
UNIFAC	UNIQUAC Functional-group Activity Coefficient
UNIQUAC	UNIversal QUAsi-Chemical
VLE	Vapour-Liquid Equilibrium

BIBLIOGRAPHY

Abrams, D. S., Prausnitz, J., 1975. Statistical thermodynamics of liquid-mixtures - new expression for excess gibbs energy of partly or completely miscible systems. AIChE J 21, 116–128.

Aspentech, 2005. Aspen Custom Modeler 2004.1 - Aspen Modeler Reference Guide. Aspen Technology Inc.

Buchaly, C., Duarte, C., Loureiro, J. M., Kreis, P., September 2005. Process intensification of n-propyl propionate synthesis using reactive distillation over a novel catalyst. In: ChemPor 2005 - 9th International Chemical Conference. Coimbra, Portugal.

Caetano, N., 1995. Síntese de MTBE: Estudo cinético em reactor fechado e simulação / operação de um reactor de leito fixo. Ph.D. thesis, Faculty of Engineering of the University of Porto.

Cameron, A. C., Trivedi, P. K., 1998. Regression Analysis of Count Data. Cambridge University Press, Ch. 2 - Model Specification, pp. 22–27.

DIPPR 801, 1998. DIPPR Project 801 Evaluated Thermophysical Property Database. DIPPR Themophysical Properties Laboratory.

Duarte, C., Buchaly, C., Kreis, P., M., L. J., 2006. Esterification of propionic acid with n-propanol catalytic and non-catalytic kinetic study. Inz. Chem. Procesowa 27, 273–286.

Fredenslund, A., Gmehling, J., Rasmussen, P., 1977. Vapor-Liquid Equilibrium using UNIFAC. Elsevier, Amsterdam.

Fredenslund, A., Jones, R. L., Prausnitz, J. M., 1975. Group-contribution estimation of activity-coefficients in nonideal liquid-mixtures. AIChE J. 21, 1086–1099.

Lundquist, E. G., 1995. Catalyzed esterification process. US Patent 5,426,199, assignee: Rohm and Haas Company.

Prior, J. M. V., 2001. Síntese de ETBE: Estudo cinético em reactor fechado; simulação / operação de um reactor de leito fixo. Ph.D. thesis, Faculty of Engineering of the University of Porto.

Renon, H., Prausnitz, J. M., 1968. Local compositions in thermodynamic excess functions for liquid mixtures. AIChE J. 14, 135.

Rhom and Haas Company, 2002. Amberlyst 46 product data sheet.

Rhom and Haas Company, 2003. Amberlyst 15wet product data sheet.

Smith, J. M., Van Ness, H. C., 1987a. Introduction to Chemical Engineering Thermodynamics, 4th Edition. McGraw-Hill Book Company, Ch. Twelve, p. 379.

Smith, J. M., Van Ness, H. C., 1987b. Introduction to Chemical Engineering Thermodynamics, 4th Edition. McGraw-Hill Book Company, Ch. Appendix D, pp. 676–681.

Wilson, G. M., 1964. Vapor-liquid equilibrium. xi. a new expression for the excess free energy of mixing. J. Am. Chem. Soc. 86, 127–130.

3 RESIDUE CURVE MAPS

3.1 Introduction to Residue Curve Maps: Theory and Practice

The complexity and associated cost of designing, building and operating a distillation column is nowadays somewhat simplified by the use of powerful computational tools, which allow the persons responsible for such a project to complete it faster, more efficiently and with lower error. This advantage has not always been so and for almost a century, chemical processes were built on personal experience, empirical knowledge of the process, hand-made calculations and the theory of thermal separation processes.

One of the oldest tools available, which allowed for a first feasibility study of the separation intended, is the Residue Curve Map. The idea behind it is quite simple: a single-stage, batch distillation, from which the vapour phase is removed - which happens naturally - is analysed with respect to the composition of the remaining ("Residual") liquid phase over time. The results are then plotted on graphics and a curve is drawn over the composition points taken, resulting on a "Curve Map" - hence Residue Curve Map (RCM).

The simplicity of the process is accompanied by the simplicity of the model. It is usually assumed that the composition of the vapour phase is in equilibrium with the liquid phase and, because of this, the relationship between compositions and the variation of the liquid phase remaining on the stage is given by Vapour-Liquid Equilibrium (VLE).

From the data gathered from the RCMs, it is possible to determine if separate distillation regions exist, where are the boundaries of those regions and design some specific types of columns from that data only (Foucher et al., 1991).

Analogous to the construction of the normal distillation RCMs, so can reactive distillation RCMs be obtained. The work initiated by Bar-

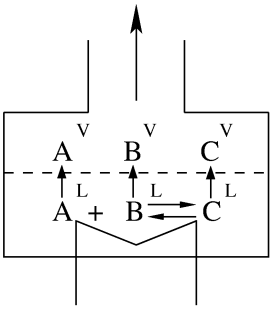

Figure 3.1: Schematic of a heated still used for RCM determination

bosa and Doherty (1988) and continued, in the most part, by Doherty - e.g. Ung and Doherty (1995); Venimadhavan et al. (1994); Foucher et al. (1991); Chen et al. (2000) - helped to mature the knowledge of this tool.

3.1.1 RCM Model

The apparatus used to experimentally determine the RCM of a reactive system is similar to the one used for non-reactive RCMs. It consists of a heated still - which can contain catalyst, as is the case that will be modelled - where a reacting mixture is placed, samples being taken from the liquid phase at given intervals and the resulting vapour phase being removed continuously.

Figure 3.1 represents such an apparatus. In terms of model parameters and variables, it contains the liquid mixture hold-up (H), which is heated at a variable heat input Q in order to vaporise part of the solution - with a vapour flow rate of $\dot{V}$. The reaction is assumed to occur only in the liquid phase - as is normally the case - between the chemical species present, each having a molar fraction x_i (i representing the species). The composition of the vapour phase is represented by y_i and is assumed to be in equilibrium with the liquid phase composition.

Performing a mass balance to the liquid present at any given time in the still, in order to a generic component i (Venimadhavan et al., 1994),

$$\frac{\mathrm{d}\,(H\,x_i)}{\mathrm{d}\,t} = -\dot{V}\,y_i + \rho\frac{V_{cat}}{H^0}H\sum_{j=1}^{M}\left(\nu_{i,j}\,r_j\right) \tag{3.1}$$

in which ρ represents the density of the catalyst, V_{cat} the volume of active catalyst inside the still, H^0 the initial load of liquid, $\nu_{i,j}$ the stoichiometric coefficient of species i in reaction j and r_j the rate of reaction j. Summing the individual mass balances of each component, an overall mass balance to the still is obtained.

$$\frac{\mathrm{d}H}{\mathrm{d}t} = -\dot{V} + \rho\frac{V_{cat}}{H^0}H\sum_{i=1}^{N}\sum_{j=1}^{M}\left(\nu_{i,j}\,r_j\right) \tag{3.2}$$

Expanding the left-hand term of Eq. 3.1, replacing $\frac{\mathrm{d}H}{\mathrm{d}t}$ with Eq. 3.2, rearranging and dividing the resulting expression by the liquid hold-up, a species dependent expression is obtained.

$$\frac{\mathrm{d}x_i}{\mathrm{d}t} = \frac{\dot{V}}{H}\left(x_i - y_i\right) + \rho\frac{V_{cat}}{H^0}\left[\sum_{j=1}^{M}\left(\nu_{i,j}\,r_j\right) - x_i\sum_{i=1}^{N}\sum_{j=1}^{M}\left(\nu_{i,j}\,r_j\right)\right] \tag{3.3}$$

In order to simplify the model, a further assumption regarding the heating policy is made. It is considered that the control of the heating element of the still is such that the ratio between the molar vapour flow rate and the molar liquid hold-up is constant throughout the experiment, i.e.,

$$\frac{\dot{V}}{H}\left(=\frac{\dot{V}^0}{H^0}\right) = R_{V/L} \tag{3.4}$$

As it is obvious by inspection, $R_{V/L}$ has units of reciprocal time, so it can be used to obtain a dimensionless time τ, which is defined as

$$\tau = \frac{\dot{V}}{H}t \tag{3.5}$$

Substituting Eq. 3.5 into Eq. 3.3 and taking into account the equality defined by Eq. 3.4, the expression is simplified. Introducing the Damköhler number, defined as the ratio between the rate of reaction - given by a kinetic constant at a standard temperature, k_{ref} - and rate of mass transfer - given by the initial vapour flow rate $\dot{V}^0$ -,

$$\mathcal{D}a = \rho \frac{V_{cat}}{\dot{V}^0} k_{ref} \tag{3.6}$$

Eq. 3.3 becomes

$$\frac{\mathrm{d}x_i}{\mathrm{d}\tau} = (x_i - y_i) + \frac{\mathcal{D}a}{k_{ref}} \left[\sum_{j=1}^{M} \left(\nu_{i,j}\, r_j \right) - x_i \sum_{i=1}^{N} \sum_{j=1}^{M} \left(\nu_{i,j}\, r_j \right) \right] \tag{3.7}$$

which is the final structure of the mass balance to the still.

3.1.2 RCM Plotting

For a ternary system (e.g. $A + B \rightleftharpoons C$), the method of representation used is the ternary diagram (Fig. 3.2). It consists of an triangular (preferably equilateral) plot with each vertex representing a pure component (i.e. $x_i = 1$). Since the sum of the molar fractions is always equal to one, only two variables are independent at a time, allowing for a bi-dimensional representation of three variables.

The curves are plotted in a parametric way (since the curve's points are taken sequentially, at timed intervals, they should be represented in that way, starting from the initial point up to the end point - corresponding usually to a stable node), sometimes including arrows to indicate the direction of the temporal progression of the composition. The stationary points (discussed in detail further on) and possibly their boiling temperatures (the curves always progress from lower to higher temperatures, so the representation of arrows can be avoided by just observing the temperatures) should also be plotted in the maps. Finally, if distillation regions exist, the separation line - separatrix (Widagdo and Seider, 1996) - which divides them should also be drawn in order to facilitate the interpretation of data.

When more than three components are involved, the graphical representation of the RCMs becomes more difficult. For four component systems, it is always possible to plot the data in three-dimensional (3D) form (a triangular pyramid made of equilateral triangles). Unfortunately, reading data in 3D is hard and becomes even harder if distillation regions exist, since they become delimited by bidimensional surfaces and not curves. Several hypothesis exist, from lumping similar compounds together (Thiel et al., 1997) to following topographical strategies of representing 2D planar cuts and projections of the pyramid (Blagov and Hesse, 2002) or removing one of the components

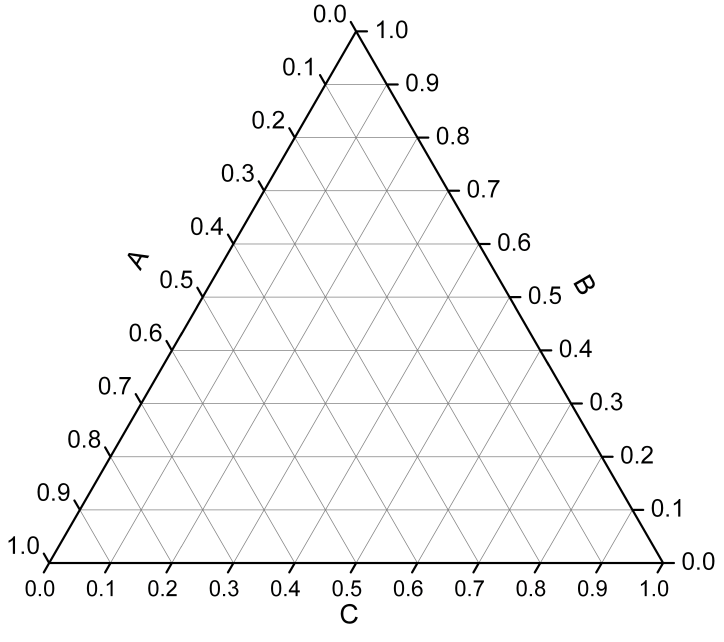

Figure 3.2: Example of ternary RCM plot

and recalculating molar fractions, collapsing the 3D RCM to one of its sides. Nevertheless, these methods are cumbersome and may lead to errors in analysis, as will be shown with the case of TAME further on. If more than 4 components exist, not even 3D representation is a hypothesis and only topographical analysis of data is possible.

3.1.3 Stationary Points and Distillation Regions

The concept of distillation azeotrope - a point where the liquid and vapour phases have the same composition and, because of that, it is not possible to distil further - also exists applied to reactive distillation. The base principle is the same - a point from where no further change in the composition of liquid and vapour phases occur - but, due to the effect of reaction, the composition of the phases can differ.

Looking at Eq. 3.7, if no reaction occurs (simple distillation, $\nu_{i,j}\, r_j = 0$), then the equation becomes

$$\frac{\mathrm{d}x_i}{\mathrm{d}\tau} = (x_i - y_i) \tag{3.8}$$

which is the same to say that, if no change in composition occurs ($\frac{\mathrm{d}x_i}{\mathrm{d}\tau} = 0$) then $x_i = y_i$, which corresponds to the definition of non-reactive azeotrope given before.

On the other hand, if reaction is occurring but the system is stationary (i.e. no change in composition over time), Eq. 3.7 simplifies to

$$(x_i - y_i) = -\frac{\mathcal{D}a}{k_{ref}} \left[\sum_{j=1}^{M} \left(\nu_{i,j}\, r_j \right) - x_i \sum_{i=1}^{N} \sum_{j=1}^{M} \left(\nu_{i,j}\, r_j \right) \right] \tag{3.9}$$

which is the same to say that the composition changes occurring from mass transfer (left-hand side) are compensated by composition changes deriving from reaction (right-hand size), i.e., that the vapour-liquid mass transfer is in equilibrium with the liquid phase reaction and results in a stationary composition of the mixture, which is called a reactive azeotrope.

Azeotropes, be they reactive or not, are classified as nodes or saddles. Nodes represent the highest (stable) or lowest (unstable) boiling stationary points in a given distillation region while saddles represent the intermediate boiling points. The existence of several of these points define distillation regions, which are separated by separatrixes - composition lines, in three-component mixtures, that cannot be usually crossed.

Foucher et al. (1991) presents a very good algorithm for classifying stationary points and drawing the basic structure of a RCM, which can be applied to three-component systems. It consists of eight steps - to be taken in order to build the diagram - and two rules - used to classify the stationary points. For completeness' sake, the algorithm will be reproduced here, with some additional comments and clarifications.

1. *Fill in the edges of the triangle.* Knowing the boiling temperatures of the pure components and binary azeotropes, arrows should be drawn on the sides of the digram, pointing in the direction of an increase in temperature.

2. *Determine the nature of the Pure Component vertices* A pure component vertex is a saddle if one of the adjacent pure components or binary azeotropes (whichever is closest) has a higher boiling temperature and the other a lower boiling temperature (i.e. if

the vertex is an intermediate boiler in relation to the two closest pure or binary stationary points).

A pure component vertex is a stable node if the two adjacent pure or binary stationary points boil at a lower temperature. It is an unstable node if they boil at a higher temperature.

3. *Determine the nature of the ternary azeotrope* In order for the ternary azeotrope to be a saddle, it has to be able to originate from two lower boiling points and to connect to two higher boiling points. This means that, for a ternary saddle to exist, four pure component or binary nodes must exist. If more than four points in this situation exist, then an indetermination occurs.

   In order for it to be a node, the total number of binary azeotropes plus pure component nodes must be less than four and / or, excluding pure component saddles, it must be the highest, second highest, lowest or second lowest boiling species. In the first case, and remembering what has been said before, it is a stable node. In the second case, an unstable node.

4. *Make connections to the ternary saddle* If no indetermination occurs, connect the pure component nodes and binary azeotropes to the ternary saddle.

5. *Determine the number of binary nodes and saddles if no ternary saddle exists* If no ternary saddle exists, the number of binary nodes and saddles can be calculated from Eq.s 3.10 and 3.11, where N_2 represents the number of binary nodes, B the total number of binary azeotropes, N_1 the number of pure component nodes, N_3 the number of ternary nodes, S_3 the number of ternary saddles (equal to 0, in this case) and S_2 the number of binary saddles.

$$N_2 = \frac{(2 + B - N_1 - 2N_3 + 2S_3)}{2} \tag{3.10}$$

$$S_2 = B - N_2 \tag{3.11}$$

6. *Check the consistency of the data* By definition, the lowest or highest boiling azeotropes in the system must be nodes. Also, N_2 - determined from Eq. 3.10 if no ternary saddle occurs - must be equal to the total number of binary nodes. So, if the highest

and/or lowest azeotropes are binary and they are in number greater than N_2, the result is not consistent.

The remaining number of binary azeotropes (intermediate boilers) cannot be larger than the number of binary saddles, as determines by Eq. 3.11. If this occurs, the result is inconsistent.

7. *Indeterminations* Indeterminations can occur if the the sum of pure component nodes and binary azeotropes is greater than four or if the number of intermediate boiling binary azeotropes is greater than the number of binary saddles. In this case, the maps must be calculated first (by simulation) and the classification of the azeotropes in doubt is done in accordance with the behaviour of the curves (i.e. if they originate close to them, they are unstable nodes, if they terminate in them, stable nodes and if they approach and then deviate from them, saddles).

8. *Final connections* If no indetermination exists, connect the remaining points, namely, ternary nodes to binary saddles (if the saddle has a lower boiling point than the node). Then, infeasible connections to the binary saddles are ruled out (e.g. a connection originating from a lower boiling stable node) and the remaining connections made.

Having all the data regarding stationary points and distillation regions, it is then possible to draw a sketch of the ternary map. The exact location of the separatrix, when existent, is hard to determine. The easiest way is to calculate curves with trajectories which approach a distillation boundary and then, from their behaviour, estimate the location and draw the separatrix. This method usually works quite well and is fast but, as with any estimation, is more subject to errors.

One further aspect that needs to be considered has to do with the specificity of each map to the conditions under which it was calculated. Looking at Eq. 3.7, it is easily seen that the balance depends directly on the value of the Damköhler number and indirectly, through the VLE calculations, of the operating pressure of the system. The change of either of these values leads to a shift of the location of the stationary points. This concept has already been tested in non-reactive separations (Holland et al., 2004a,b; Tapp et al., 2004) and there are reasons to believe it is expandable to reactive distillations.

From a chemical and mathematical perspective, the RCMs are influenced by both stationary and dynamic factors. The stationary factors,

dealing with the location, number and classification of the stationary points appear to be influenced by the number of chemical-physical phenomena present in the process. In a normal distillation, such phenomena can be usually reduced to vapour-liquid mass transfer (represented in the mass balance by the $x_i - y_i$ term and calculated via VLE procedures). If reaction occurs, one or two phenomena need to be accounted for: for homogeneous reactions (catalytic or not), the liquid phase reaction rate as quantified by the kinetic law and the kinetic and equilibrium constants. For heterogeneous catalysed reactions, the effect of adsorption is also accounted for, either discretely by inclusion in the kinetic and equilibrium constants - for pseudo-homogeneous models -, or explicitly, by the adsorption constant. Despite this, in most of the literature dealing with heterogeneously-catalysed reactive distillations, the influence of adsorption is ignored and considered to be part of the reaction. This is incorrect and should be avoided. The influence that adsorption has on the stationary points is independent of the influence of reaction "per se". If the system was non-reactive but the adsorbent still existed, the system-wide adsorption equilibria would need to be taken into account and would most certainly influence the location of the stationary points.

Regarding the dynamic factors, they are represented by the differential term of the mass balance, which, since it is based on the variation of the liquid phase, takes into account both mass transfer and, when it exists, reaction. Once again, the apparent transparency of the model can be misleading. One point that must not be forgotten when looking at the RCMs is that the curves represent a dynamic variation and their points are time-dependent. Because of this, and for the plotting of the curves, all transient phenomena needs to be accounted and, once more, adsorption usually is not. During the process leading to this work, the effect of adsorption of heterogeneous catalysed reactive distillation processes, more specifically the synthesis of TAME, was investigated (Duarte and Loureiro, 2004).

$$\left[1+\frac{\mathcal{D}a}{k_{ref}}R_{V/L}\frac{K_i\,\gamma_i}{\left(1+K_i\,a_i\right)^2}\right]\frac{\mathrm{d}x_i}{\mathrm{d}\tau}- \frac{\mathcal{D}a}{k_{ref}}R_{V/L}\sum_{i=1}^{N}\left[\frac{K_i\,\gamma_i}{\left(1+K_i\,a_i\right)^2}\frac{\mathrm{d}x_i}{\mathrm{d}\tau}\right]x_i = (x_i-y_i)+\frac{\mathcal{D}a}{k_{ref}}\left[\sum_{j=1}^{M}\left(\nu_{i,j}\,r_j\right)-x_i\sum_{i=1}^{N}\sum_{j=1}^{M}\left(\nu_{i,j}\,r_j\right)\right] \quad (3.12)$$

As was expected, the adsorption phenomena had an impact on the trajectories of the curves, ranging from the small - when the Damköhler number and pressure were low - to the significant - when reaction gained importance. In terms of mass balance, and as an example, a simple visual comparison can be made between Eq. 3.7, which does not account for adsorption and Eq. 3.12 - which takes into account adsorption using a simple, non-competitive, Langmuir model (K_i being the adsorption constant of species i).

Finally, the operating conditions chosen for each map determines the actual map, by affecting almost all variables of the process. Of the two parameters affecting the RCMs, one is evident - pressure - while the other is not - Damköhler number. The pressure is usually a process variable of any distillation process, controlling the temperature range in effect and, through it, the VLE and, in reactive distillation, the reaction rate. In most cases, low pressure (i.e. as near atmospheric as possible) is wanted for separation, because it reduces the boiling point of the mixtures, thus being cheaper and, in the case of atmospheric distillation, eliminates the need for pressurising equipment. Reaction, on the other hand, is usually favoured by high temperatures and hence, higher pressures. A cost / benefit equilibrium needs to be found when determining the operating conditions of any reactive distillation process.

The Damköhler number, on the other hand, is rather a consequence of the modelling conditions than an actual project parameter. It depends mainly on the initial vapour flow rate and represents the ratio between reaction and separation. High Damköhlers mean than the process is limited by separation - usually reaction is in equilibrium - while low Damköhler numbers result in little to no reaction occurring, thus making the process approach the conditions of a simple separation. The upper ($\mathcal{D}a \to \infty$) and lower ($\mathcal{D}a = 0$) limits are important

in defining the location of all viable stationary points under a given operating pressure.

In fact, and since only P and $\mathcal{D}a$ have an influence in the location of the stationary points, it is useful to know the location of all the possible stationary points under the desired operating conditions. This means fixing an operating pressure - which is a process parameter - while varying the Damköhler number from its lower value of zero to infinity. This can be done by solving the mass balance, using continuation methods (Rheinboldt, 1980; Heijer and Rheinboldt, 1981) to change the value of $\mathcal{D}a$ for a fixed pressure and obtain the resulting stationary points at each $\mathcal{D}a$ calculated and from them plot the trajectories of the stationary points. This calculation was not achieved in this work, due to numerical problems using the continuation routines.

3.2 Calculation of the Residue Curve Maps

In order to obtain the desired RCMs, two computational programs were developed using Fortran 90. The first one calculates the stationary points and the second one the curves themselves. Both programs share a similar structure, being system-specific implementations of the molar mass balances, given by Eq.s 3.7 and 3.9, and VLE. The stationary points are calculated using a Fortran 90 implementation of Broyden's Method (Press et al., 1992) while the curves are obtained using a differential-algebraic solver routine, DDASPK (Petzold et al., 1996). It was decided to use the simple model, which does not take into account adsorption, since the interest lays mainly with the location of the stationary points rather than with the shape of the curves. Furthermore, n-Propyl Propionate synthesis is well described by a pseudo-homogeneous model and because of it no experimental work to obtain adsorption data was performed. In regard to TAME, the kinetics used are different from the ones used in (Duarte and Loureiro, 2004) and only take into account the adsorption of Methanol, since the other constants are not obtainable easily and can give erroneous results.

3.2.1 Stationary Points

The algorithm for the determination of the stationary points is presented on Fig. 3.3 and is a very simple one. The user first inputs an estimation of the liquid phase composition and its boiling tempera-

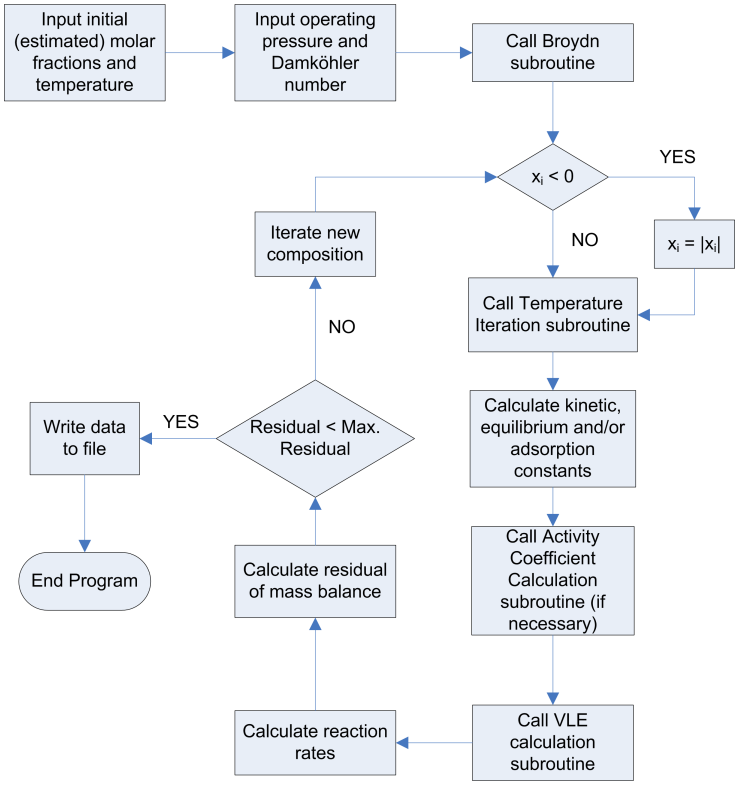

Figure 3.3: Algorithm of the program used to find stationary points

ture; he then inserts the operating conditions (operating pressure and Damköhler number) and the iteration begins.

The first step of the iteration consists on verifying if the values of x_i are greater than zero. If that is not the case, then x_i is set to be equal to its modulus. This step is necessary since during iteration, Broyden's method will overshoot the bounds. While this is not a problem with values of x_i greater than one, values less than zero can cause an indetermination error in the activity coefficient calculation subroutine, since the natural logarithm of the molar fraction is calculated.

The second step consists on a Runge-Kutta iteration (Fig. 3.4) of the boiling temperature, using as a convergence parameter the sum of the vapour phase molar fractions - which must be equal to 1.

After calculating the correct boiling temperature of the liquid under the used operating conditions, the values for the kinetic, equilibrium and / or adsorption constants are calculated and from them, the

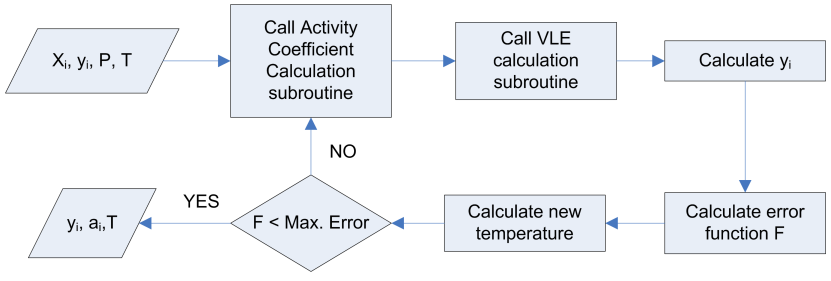

Figure 3.4: Algorithm of the boiling temperature calculation subroutine

reaction rate of each reaction.

Finally, a residual error function of Eq. 3.9 is calculated. If that error function obeys (i.e. is lower than) the set absolute and relative convergence parameters, the iteration ends and the results are written to a text file. If the contrary is the case, then the Broyden's Method subroutine iterates a new composition for the liquid phase and the process starts again, until convergence.

Although not directly related to the general algorithm of the program, it was found during its use that when one of the components' molar fraction was equal to zero, it was necessary to set its activity coefficient equal to a constant value. This results from the subroutines used to calculate the liquid phase activity data which calculates the logarithm of the composition. By bypassing the calculation of the activity coefficient for values of molar fraction equal to zero, a mathematical indetermination - and subsequent program crash - is avoided.

3.2.2 Residue Curves

The algorithm used for the calculation of the residue curves (Fig. 3.5) is very similar to the one used for the stationary points (Fig. 3.3). Comparing the two algorithms, the main difference (besides the mathematical ones, of course) is that the stationary points algorithm ends after finding the solution, while the curves algorithm runs up to the inputed runtime, increasing the actual time in each step.

In detail, the user is first required to input the starting point composition and an estimative of that composition's boiling temperature. He then inputs the operating conditions (operating pressure and Damköhler number), total runtime of the experience and sampling time - i.e., the time at which data is written to file (this is not shown

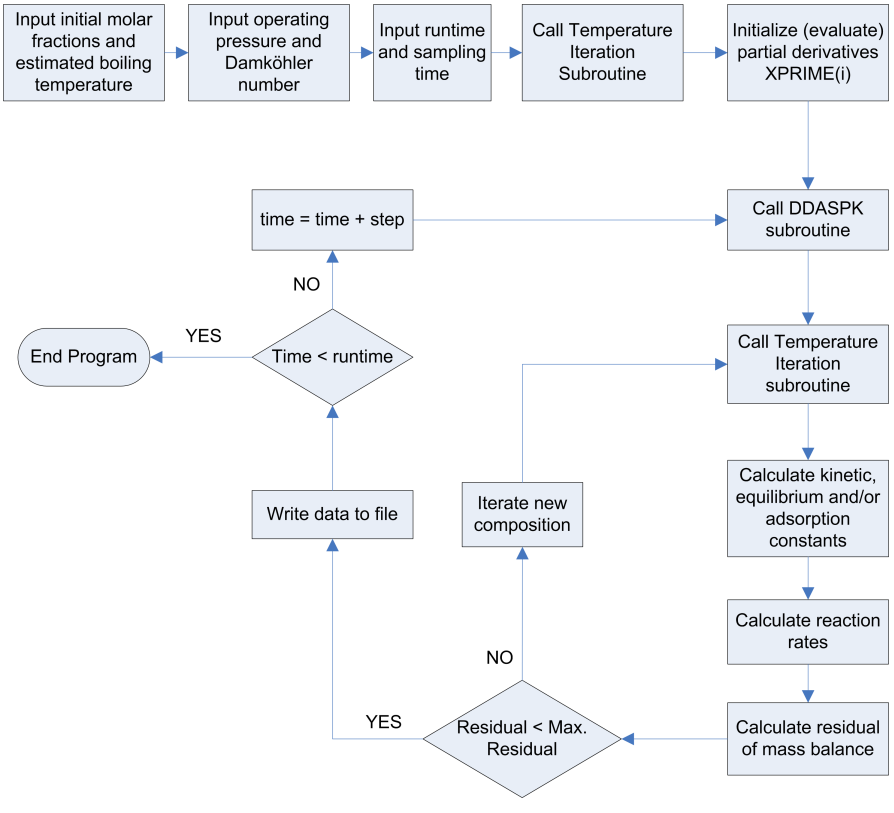

Figure 3.5: Algorithm of the program used to calculate residue curves

in the algorithm, to avoid cluttering the diagram; it is "assumed" that the sampling time is equal to the time between steps). The program calculates the time between steps using runtime$\times 1 \times 10^{-8}$.

The calculation part of the program then starts by calling the boiling temperature calculation subroutine (Fig. 3.4) and initialising the partial derivatives of the molar fractions in order to time. To that end, they are considered to be equal to the solution of Eq. 3.7 and are iterated after this point by the solver subroutine. This initialisation was found to be necessary, since initial runs performed with a fixed initialisation value showed convergence problems. After all the needed variables and constants are inputed or calculated, the differential-algebraic solver subroutine (DDASPK) is called and the iterative runs begin.

The first step of the iteration consists in the calculation of the boiling temperature of the liquid phase composition (via the Runge-Kutta

subroutine which was already mentioned). With that temperature, the kinetic, equilibrium and / or adsorption constants are calculated and from them, the reaction rates of each chemical reaction.

Using the system species' dynamic mass balances (Eq.3.7), a residual value is calculated (the residual being equal to the inequality of the equation). If that residual is lower than the set relative and absolute limits, then the subroutine outputs the converged results. If not, new partial derivatives are iterated and the process resumes up to convergence.

When a convergence point is found, it is either written to a file - if it corresponds to a sampling time - or used in the next run. These runs are performed, with the actual time being increased one time step after every converged run, until the limit runtime inputed by the user is reached. When that happens, the program ends.

3.3 TAME Residue Curve Maps

3.3.1 Chemical Reaction Model

3.3.1.1 Reactive System

TAME (*tert*-Amyl Methyl Ether) is produced from the reaction of 2M1B (2-Methyl 1-Butene) or 2M2B (2-Methyl 2-Butene) with Methanol (MeOH). Since 2M1B and 2M2B are isomers, the isomerisation reaction occurs simultaneously with the ether synthesis. The full reaction structure of this chemical system can be found on Fig. 1.6 but each individual reaction is also presented here (Eq.s 3.13-3.15).

$$2M1B + MeOH \overset{k_1}{\rightleftharpoons} TAME \quad \text{(Reaction 1)} \tag{3.13}$$

$$2M2B + MeOH \overset{k_2}{\rightleftharpoons} TAME \quad \text{(Reaction 2)} \tag{3.14}$$

$$2M1B \overset{k_3}{\rightleftharpoons} 2M2B \quad \text{(Reaction 3)} \tag{3.15}$$

In order to facilitate the computational treatment of the system, each component was given an index number i - 2M1B (1), 2M2B (2), MeOH (3) and TAME (4) - and each reaction an index number j - the numbers being equal to the reaction numbers presented on Eq.s 3.13-3.15. The stoichiometric number of each component in each reaction

($\nu_{i,j}$) and the reaction's total stoichiometric balance (represented by Σ) are presented on Table 3.1.

Using Eq. 3.7 and applying the appropriate stoichiometric values from Table 3.1, the mass balance with respect to each one of the components is given by

$$\frac{\mathrm{d}x_1}{\mathrm{d}\tau} = (x_1 - y_1) + \frac{\mathcal{D}a}{k_{ref}} \left[-r_1 \left(1 - x_1\right) - r_3 + r_2 \, x_1\right] \tag{3.16}$$

$$\frac{\mathrm{d}x_2}{\mathrm{d}\tau} = (x_2 - y_2) + \frac{\mathcal{D}a}{k_{ref}} \left[-r_2 \left(1 - x_2\right) + r_3 + r_1 \, x_2\right] \tag{3.17}$$

$$\frac{\mathrm{d}x_3}{\mathrm{d}\tau} = (x_3 - y_3) + \frac{\mathcal{D}a}{k_{ref}} \left[-r_1 \left(1 - x_3\right) - r_2 \left(1 - x_3\right)\right] \tag{3.18}$$

$$\frac{\mathrm{d}x_4}{\mathrm{d}\tau} = (x_4 - y_4) + \frac{\mathcal{D}a}{k_{ref}} \left[r_1 \left(1 + x_4\right) + r_2 \left(1 + x_4\right)\right] \tag{3.19}$$

k_{ref} being the value of the kinetic constant of reaction 1 (k_1) at 298 K.

The reaction rates (r_j - Eq.s 3.20-3.22) used in the calculation of the RCMs - and throughout this work - are taken from Ferreira de Oliveira (2004), as well as the values for the kinetic (k_j - Eq.s 3.23-3.25), equilibrium (Keq_j - Eq.s 3.26-3.28) and adsorption constants (K_M - Eq. 3.29). In regard to the adsorption constant, the model considers that the adsorption of Methanol is larger than the adsorption of the other compounds and so they can be disregarded.

$$r_1 = k_1 \, {K_M}^2 \, \frac{a_1 \, a_3 - \frac{a_4}{Keq_1}}{\left(1 + K_M \, a_3\right)^2} \tag{3.20}$$

Table 3.1: Stoichiometry of TAME synthesis

$\nu_{i,j}$	1	2	3	4	Σ
1	-1	0	-1	1	-1
2	0	-1	-1	1	-1
3	-1	1	0	0	0

$$r_2 = k_2 \; {K_M}^2 \; \frac{a_2 \; a_3 - \frac{a_4}{Keq_2}}{\left(1 + K_M \; a_3\right)^2} \tag{3.21}$$

$$r_3 = k_3 \; K_M \; \frac{a_1 - \frac{a_2}{Keq_3}}{1 + K_M \; a_3} \tag{3.22}$$

$$k_1 = 7.03 \times 10^{14} \; e^{\frac{-106 \times 10^3}{R \; T}} \tag{3.23}$$

$$k_2 = 2.64 \times 10^{12} \; e^{\frac{-92.5 \times 10^3}{R \; T}} \tag{3.24}$$

$$k_3 = 1.51 \times 10^{11} \; e^{\frac{-82.4 \times 10^3}{R \; T}} \tag{3.25}$$

$$Keq_1 = e^{\frac{4.63 \times 10^3}{T} - 9.875} \tag{3.26}$$

$$Keq_2 = e^{\frac{3.57 \times 10^3}{T} - 9.382} \tag{3.27}$$

$$Keq_3 = \frac{Keq_1}{Keq_2} \tag{3.28}$$

$$K_M = 8.34 \times 10^{-2} e^{\frac{17 \times 10^3}{R \; T}} \tag{3.29}$$

3.3.1.2 Thermodynamic Model

Since the TAME synthesis system is non-ideal, it is necessary to introduce the use of activities (a_i) in order to compensate for that non-ideality. Ferreira de Oliveira (2004) used, in her work leading to the determination of the constants described before, the Modified (Dortmund) UNIFAC method (Gmehling et al., 1993).

This method constitutes an improvement over the original UNIFAC method - which in turn is a predictive subset of the UNIQUAC method, as described on pages 40-42 of Chapter 2 - by taking into account the variation of the activity coefficient over a wider temperature range.

The UNIFAC method is based on the interaction between molecules and their chemical groups. It is thus necessary to break up each of the molecules present in the system into their respective groups. This division, and the number of groups each molecule contains, is presented on Table 3.2.

Table 3.2: Chemical groups of the species involved in TAME synthesis

Group\Species		2M1B	2M2B	MeOH	TAME
1	CH_3	2	3	0	3
2	CH_2	1	0	0	1
4	C	0	0	0	1
7	$C = CH_2$	1	0	0	0
8	$C = CH$	0	1	0	0
15	$HOCH_3$	0	0	1	0
24	OCH_3	0	0	0	1

3.3.1.3 VLE Model

The composition relation between liquid and vapour phase can be determined by Raoult's Law (Eq. 3.30), which establishes that the ratio between the vapour - y_i - and liquid - x_i - phase compositions is equal to the ratio between the species partial saturation pressure - P_i^{sat} - and the total system pressure - P. It is assumed that, in this system, the vapour phase behaves near ideality while the non-ideality of the liquid phase is predicted by the UNIFAC method described before and the subsequent use of the activity coefficient - γ_i.

$$y_i \, P = P_i^{sat} \, \gamma_i \, x_i \tag{3.30}$$

The value of the partial saturation pressure can be obtained from an Antoine-like correlation (Eq. 3.31) and each species' specific parameters for it, taken from DIPPR 801 (1998).

$$\ln P_i^{sat} = A_i + \frac{B_i}{T} + C_i \ln T + D_i \, T^{E_i} \tag{3.31}$$

3.3.2 Methodology

Since TAME is a quaternary system, a simplification needs to be performed in order to allow for bi-dimensional representation of the maps (as mentioned before). Thiel et al. (1997), in their work regarding the RCMs of MTBE and TAME synthesis, refer to a previous work by Oost and Hoffmann (1995) in which a kinetic expression for a "lumped" (*sic*) synthesis of TAME, i.e. simultaneous formation of TAME from both 2M1B and 2M2B, is obtained. Because of this, they decide to "lump" together the isoamylenes into a pseudo-component "IA".

In this work, and because the system under study is the same although with different kinetics, it was decided to follow a similar procedure of combining both isoamylenes into a single pseudo-component "2MxB'". Nevertheless, the curves and stationary points are calculated with the full kinetics and no "lumping" of the kinetic expression is performed.

In order to observe the effect of both Pressure and Damköhler number, six RCMs were constructed at two different pressures - 1 and 10 bar - and three Damköhler numbers - 10^{-4}, 10^{-2} and 1.

3.3.2.1 Stationary Points

Since no continuation method or full spatial search method is used, but rather the result of single iterations using Broyden's Method, the stationary point to which it converges depends fully on the initial point given. As such, for each set of operating conditions ($\mathcal{D}a$ and P), 32 runs were performed using the initial points shown in Fig. 3.6. As was explained before, the isoamylene points are lumped together and so the distribution of points seems to be skewed in the direction of higher isoamylene fractions when, in fact, it is pretty evened out.

Due to numerical errors, the number of stationary points obtained in each run was always higher than the number of actual azeotropes, with very small differences between them (usually less than 1°C). This constituted a problem, since there was no sure way of verifying which points were more precise, even more so when the errors originated from the activity coefficient calculation come into play.

The solution found was, in a first step, to plot all points obtained and then, according to the behaviour of the residual curves, eliminate those who did not fit in.

3.3.2.2 Residual Curves

The residual curves were plotted starting from points either a) near the unstable node, or; b) in a point opposite to the node when a clear zone separation existed, in order to "define" the location of the separatrix. They were always run until finish (i.e. stable node location), by increasing the total runtime when necessary. As mentioned, the separatrix was constructed by the use of both the location of the stationary points (unstable nodes and saddles) and the trajectory of the curves.

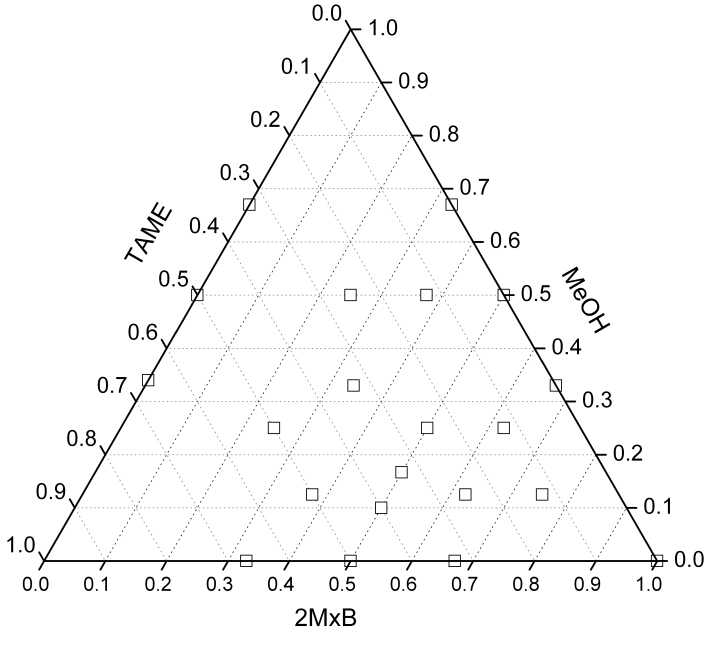

Figure 3.6: Distribution of initial points used for stationary point search

3.3.3 Plots and Analysis

The RCMs computed, in accordance to the operating conditions already mentioned, are presented in Fig. 3.7. The first point that should be made is that all maps share a similar structure of two distillation regions, with an unstable node in the MeOH-2MxB axis (i.e. the unstable node is always a mixture of methanol and isoamylenes. In fact, and if the isoamylenes are separated, of methanol and one of the isoamylenes), a moving saddle point, a stable node at pure methanol and another stable node that "travels" from pure TAME to pure isoamylenes.

The second point is that analysis should not be made between runs at the same Damköhler number, but rather between runs at the same pressure. This is mainly due to the influence that the system pressure has on the reaction rate being larger than the influence of the Damköhler number itself. In fact, if we compare the run performed at $P = 1$ bar and $\mathcal{D}a = 1$ with the run performed at $P = 10$ bar

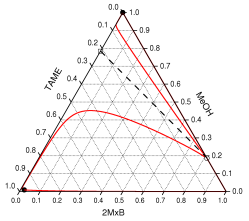

(a) $Da = 10^{-4}$; $P = 1$

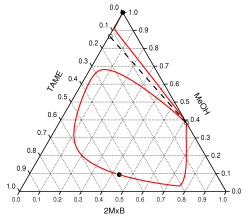

(b) $Da = 10^{-4}$; $P = 10$

Figure 3.7: Reactive Residue Curve Maps of TAME synthesis (P in bar) (◯: Unstable Node; □: Saddle; ●: Stable Node; - -: Separatrix; —: Residue Curve

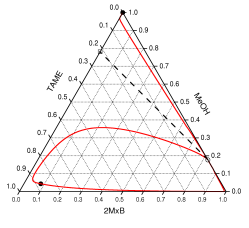

(c) $Da = 10^{-2}$; $P = 1$

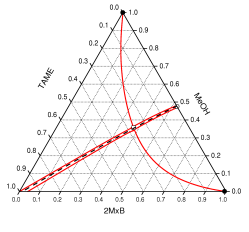

(d) $Da = 10^{-2}$; $P = 10$

Figure 3.7: Reactive Residue Curve Maps of TAME synthesis (Continued) (P in bar) (◯: Unstable Node; □: Saddle; ●: Stable Node; - -: Separatrix; —: Residue Curve

and $\mathcal{D}a = 10^{-4}$, they present greater similarities between themselves than any runs with the same Damköhler number; this is the result of a large Damköhler number on one of the runs being, in a way, "compensated" by a higher pressure in the other, despite having the lowest $\mathcal{D}a$ simulated.

Looking first at the simulations run at atmospheric pressure (which is roughly of 1 bar) and starting from $\mathcal{D}a = 10^{-4}$, there is a large region with a stable node near pure TAME and a smaller region with the MeOH stable node. When the importance of the reaction increases with respect to separation ($Da = 10^{-2}$), the bottom node moves from near-pure TAME to a mixed composition with a TAME molar fraction of roughly 87%. Increasing again the Damköhler number, not only the bottom node moves away again from the pure TAME vertex, but the upper distillation region increases in size. This behaviour is explained by the competition that exists between reaction and distillation: when reaction is slow and mass transfer fast, the reactants, being lighter boilers than the products, distil quickly into the vapour phase, leaving the product in the liquid phase before the reaction equilibrium has a chance to be corrected (and when that happens, the reactants produced are vapourised once more). When the opposite starts ocurring, the equilibrium between reactants and products gains some importance and the residual liquid in the still approaches equilibrium concentrations.

If the pressure is increased to 10 bar, while the ratio between reaction and mass transfer decreased to 10^{-4}, the situation remains similar, but the bottom node moved again to a position with less TAME (approximately 48%), this time due to a reduction of the value of the equilibrium constant. If the mass transfer is decreased ($\mathcal{D}a = 10^{-2}$ or 1), then the nodes move completely away from the product vertex to pure isoamylene. This phenomenon is probably the result of constant removal of reactants and the almost imediate reseting of the equilibrium conditions, up to the limit where no product is able to exist.

In all the maps, the upper region in which curves terminate in pure MeOH is easily explained. Since Methanol is an intermediate boiler, the other reactants are being removed first and because of that removal, any TAME formed ends reacting back to isoamylens and methanol. The more important the reaction versus mass transfer (either by the means of a higher Damköhler or a higher pressure) the lower the fraction of methanol needed for this phenomenon to occur.

If only the location of the stationary points was the object of

analysis, the conclusion taken would probably be a simple one: the reactive distillation of TAME is favoured by high mass transfers and low pressures. But in fact, things are not so simple. The pure TAME point exists at almost residual TAME concentrations and thus is anti-economical, as it requires large amounts of reactants for very little product. Also, it should be mentioned that residue curve maps should not, in most cases, be used to extrapolate the behaviour of full columns (Krolikowski (2006) discusses this problem in some detail and proves that even the assumption that an RCM can predict the behaviour of a full reflux column via distillation boundaries (Van Dogen and Doherty, 1985; Wahnschafft et al., 1992) can be inaccurate) but rather to obtain a first idea of the feasibility of the process. It is necessary to proceed to a full-scale simulation of the column in order to have a correct idea of its behaviour and adequate operating conditions.

Finally, the simplification of lumping the isoamylenes in order to allow for a 2D graphical representation of the RCM needs to be analysed - and the conclusion is that the simplification can be made, but is not fully correct. In fact, and although it was not represented, the 2M1B to 2M2B ratio has an influence in the trajectory of the curves, with curves starting from an equal value of 2MxB ("lumped" isoamylenes) terminating in different nodes if the fraction of one was larger than the other. Also other stationary points with varying molar fractions of 2M1B and 2M2B to the same fraction of MeOH appear to exist, but this hypothesis was not verified. Nevertheless, these effects are, in most cases, small, further more since the isoamylenes are likely to be fed at equilibrium concentrations and their distillation profile (low difference between boiling points) is not favourable for good separation when other compounds with a completely different boiling point exist. But when the species are not chemically and thermodynamically similar, great care should be taken before applying such a simplification, since the graphical representation of the RCM will easily and likely induce error.

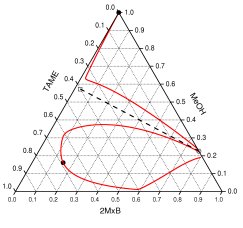

(e) $Da = 1$; $P = 1$

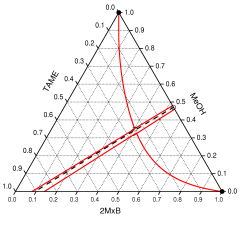

(f) $Da = 1$; $P = 10$

Figure 3.7: Reactive Residue Curve Maps of TAME synthesis (Continued) (P in bar) (◯: Unstable Node; □: Saddle; ●: Stable Node; - -: Separatrix; —: Residue Curve

3.4 n-Propyl Propionate Residue Curve Maps

The construction of the n-Propyl Propionate synthesis residue curve maps is more problematic than the construction of the TAME RCMs. The chemical system is similar in terms of number of components, four, if simple in reactional terms with only one reaction. But the components present, be them reactants or products, are very dissimilar between each other which eliminates the possibility of "lumping". The other possibility of removing one of the components, recalculating the molar fractions and then plotting them also cannot be done: the only component which could be removed - Water, because it is a side-product - appears in some binary azeotropes. Its removal might lead to the false assumption of, e.g., pure product azeotropes when, in fact, they do not exist. 3D plotting is always possible, but, as it has been mentioned, interpretation of the 3D plots is extremely hard to perform, especially if distillation regions exist, as the location of curved bi-dimensional boundaries needs to be found.

The already mentioned work done by Blagov and Hesse (2002) addresses the problem of quaternary (or higher dimension) systems and how to represent and analyse them from a sound topological point of view, but only refers to non-reactive distillation. The transition to a reactive distillation system appears to be feasible but with an added layer of complexity deriving from reaction(s) present. The adaptation of the method described to reactive distillation or the construction of a new method are judged to be out of the scope of this work, as it focus primarily on the analysis of two specific chemical systems and their suitability for reactive distillation.

If no tools for simulating the system existed or if the system was, at the time of analysis, still being evaluated for reactive distillation, then the plotting of the RCMs would be most likely needed as a preliminary feasibility study. Since it was decided from the start to perform full-scale simulations and pilot-plant experiments on the system, the need for RCMs is reduced and can be seen more as a "historical" part of study regarding the applicability of reactive distillation than an actual necessity. Because of all this factors, and since the concept of RCMs and their interpretation was already presented and applied in the specific case of TAME synthesis, it was decided not to represent the RCMs of the n-Propyl Propionate system and leave it for a future work which could be more focused on the RCMs themselves.

NOMENCLATURE

Variables / Constants

A_i	Saturation pressure parameter	$[Pa]$
a_i	Liquid-phase activity of species i	[-]
B	Total number of binary stationary points	[-]
B_i	Saturation pressure parameter	$[Pa.K]$
C_i	Saturation pressure parameter	$[Pa]$
D_i	Saturation pressure parameter	$[Pa.K^{-E_i}]$
$\mathcal{D}a$	Damköhler number	[-]
E_i	Saturation pressure parameter	[-]
H	Liquid hold-up in the still	$[mol]$
K_j	Adsorption constant of reaction j	$[m^3.mol^{-1}]$
K_M	Adsorption constant of methanol	$[m^3.mol^{-1}]$
Keq	Equilibrium constant	[-]
k_j	Kinetic constant of reaction j	$[mol.s^{-1}.kg_{cat}^{-1}]$
N_1	Number of pure component nodes	[-]
N_2	Number of binary nodes	[-]
P	Pressure	$[Pa]$
P_i^{sat}	Saturation pressure of species i	$[Pa]$
Q	Heat input	[w]
R	Universal Gas Constant = 8.314	$[J.mol^{-1}.K^{-1}]$
$R_{V/L}$	Time constant	$[s^{-1}]$
r_j	Reaction rate of reaction j	$[mol.s^{-1}.kg_{cat}^{-1}]$
S_2	Number of binary saddles	[-]
S_3	Number of ternary saddles	[-]
T	Temperature	$[K]$
t	Time	$[s]$
$\dot{V}$	Vapour flow rate	$[mol.s^{-1}]$
V_{cat}	Volume of catalyst	$[m^3]$
x_i	Liquid phase molar fraction of species i	[-]
y_i	Vapour phase molar fraction of species i	[-]

Greek Letters

γ_i	Liquid phase activity coefficient of species i	[-]
$\nu_{i,j}$	Stoichiometric coefficient of species i in reaction j	[-]
ρ	Density of the catalyst	$[kg.m^{-3}]$
τ	Dimensionless time	[-]

Indexes

Superscript

0	At initial conditions (t=0)
L	Liquid phase
M	Total number of reactions
N	Total number of species
V	Vapour phase

Subscript

cat	Catalyst
i	Chemical species number
j	Reaction number
ref	At reference conditions (for k_{ref}, T=298 K)

Abbreviations and Acronyms

2M1B	2-Methyl 1-Butene
2M2B	2-Methyl 2-Butene
MeOH	Methanol
RCM	Residue Curve Map
TAME	Tertiary Amyl Methyl Ether
UNIFAC	UNIQUAC Functional-group Activity Coefficient
UNIQUAC	UNIversal QUAsi-Chemical
VLE	Vapour-Liquid Equilibrium

BIBLIOGRAPHY

Barbosa, D., Doherty, M. F., 1988. The simple distillation of homogeneous reactive mixtures. Chem. Eng. Sci. 43, 541–550.

Blagov, S., Hesse, H., 2002. Topological analysis of vapor-liquid equilibrium diagrams for distillation process design. Phys. Chem. Chem. Phys. 4, 896–908.

Chen, F., Huss, R. S., Malone, M. F., Doherty, M. F., 2000. Simulation of kinetic effects in reactive distillation. Comp. Chem. Eng. 24, 2457–2472.

DIPPR 801, 1998. DIPPR Project 801 Evaluated Thermophysical Property Database. DIPPR Themophysical Properties Laboratory.

Duarte, C., Loureiro, J. M., 2004. Effect of adsorption on residue curve maps for heterogeneously catalytic distillation systems. Ind. Eng. Chem. Res. 23, 3242–3250.

Ferreira de Oliveira, M. M. V., 2004. TAME: Cinética em reactor fechado e simulação da produção em contínuo. Ph.D. thesis, Faculty of Engineering of the University of Porto.

Foucher, E. R., Doherty, M. F., Malone, M. F., 1991. Automatic screening of entrainers for homogeneous azeotropic distillation. Ind. Eng. Chem. Res. 30, 760–772, 2364.

Gmehling, J., Li, J., Schiller, M., 1993. Modified unifac model. 2. present parameter matrix and results for different thermodynamic properties. Ind. Eng. Chem. Res. 32, 178–193.

Heijer, C. D., Rheinboldt, W. C., 1981. On steplenght algorithms for a class of continuation methods. SIAM J. Numer. Anal. 18, 925–948, continuation Methods. Without much interest.

Holland, S. T., Tapp, M., Hildebrandt, D., Glasser, D., 2004a. Column profile maps. 2. singular points and phase diagram behaviour in ideal and nonideal systems. Ind. Eng. Chem. Res. 43, 3590–3603.

Holland, S. T., Tapp, M., Hildebrandt, D., Glasser, D., Hausberger, B., 2004b. Novel separation system design using "moving triangles". Comput. Chem. Eng. 29, 181–189.

Krolikowski, L. J., 2006. Determination of distillation regions for non-ideal ternary mixtures. AIChE J. 52, 532–544.

Oost, C., Hoffmann, U., 1995. The synthesis of tertiary amyl methyl ether (TAME): microkinetics of the reactions. Chem. Eng. Sci. 51, 329–340.

Petzold, L. R., Brown, P. N., Hindmarsh, A. C., Ulrich, C. W., 1996. DDASPK. Center for Computational Sciences & Engineering, Lawrence Livermore National Laboratory, Livermore, USA.

Press, W. H., Teukolsky, S. A., Vetterling, W. T., Flannery, B. P., 1992. Numerical Recipes in FORTRAN: The Art of Scientific Computing, 2nd Edition. Cambridge University Press, New York, USA, pp. 382–385.

Rheinboldt, W. C., 1980. Solution fields of nonlinear equations and continuation methods. SIAM J. Numer. Anal. 17, 221–237, continuation methods. Without much interest.

Tapp, M., Holland, S. T., Hildebrandt, D., Glasser, D., 2004. Column profile maps. 1. derivation and interpretation. Ind. Eng. Chem. Res. 43, 364–374.

Thiel, C., Sundmacher, K., Hoffmann, U., 1997. Residue curve maps for heterogeneously catalysed reactive distillation of fuel ethers MTBE and TAME. Chem. Eng. Sci. 52, 993–1005.

Ung, S., Doherty, M. F., 1995. Calculation of residue curve maps for mixtures with multiple equilibrium chemical reactions. Ind. Eng. Chem. Res. 34, 3195–3202.

Van Dogen, D. B., Doherty, M. F., 1985. Design and synthesis of homogeneous azeotropic distillation. 1. problem formulation for single column. Ind. Eng. Chem. Fundam. 24, 454–463.

Venimadhavan, G., Buzad, G., Doherty, M. F., Malone, M. F., 1994. Effect of kinetics on residue curve maps for reactive distillation. AIChE J. 40, 1814–1824.

Wahnschafft, O. M., Koehler, J. W., Blass, E., Westberg, W., 1992. The product composition regions of single-feed azeotropic distillation columns. Ind. Eng. Chem. Res. 31, 2345–2362.

Widagdo, S., Seider, W. S., 1996. Azeotropic distillation. AIChE J. 42, 96–130.

4 Pilot-Scale Production of n-Propyl Propionate

4.1 Pilot Plant Description

In order to conduct experiments for the synthesis of n-Propyl Propionate via Reactive Distillation, a DN50 (50 mm diameter) glass column operating at the University of Dortmund was used. In Fig. 4.1 a simple schematic drawing of the column is presented.

The column is made up of three non-reactive separation stages - one at the bottom and two at the top-, and three consecutive reactive stages. The non-reactive stages contain Sulzer BX (Sulzer Chemtech, 2005) structured packings while the reactive stages are made of Sulzer Katapak SP11 (Sulzer Chemtech, 2005) structured packings, filled with Amberlyst 46 (Rhom and Haas Company, 2002) catalyst. Distributors are placed between stages in order to allow for flexible feed / sidedraw configurations serving as well as sample collection points.

At the top of the column, a simple cooling circuit - using running tap water as coolant - is used as a condenser while at the bottom a reservoir-like vessel, heated by a heating coil in which heating oil - heated outside the column by electric resistances - circulates, serves as a reboiler. In terms of effective column height, it is calculated from the combined heights of reactive and non-reactive sections plus the reboiler. The distributors do not count towards the effective height since they have little to no effect in the separative or reactive process (they can be seen as a boundary element with a height of zero). The total height of the column is then of 5.846 m of which 2.646 m are reactive, 2.7 m non-reactive and 0.5 m correspond to the reboiler. Both stages and distributors are numbered from top to bottom (i.e. the distributor just below the condenser is distributor 1 and the stage below it, stage 1; the distributor just above the reboiler is distributor 7 and the stage above it stage 6. The number of distributors is always

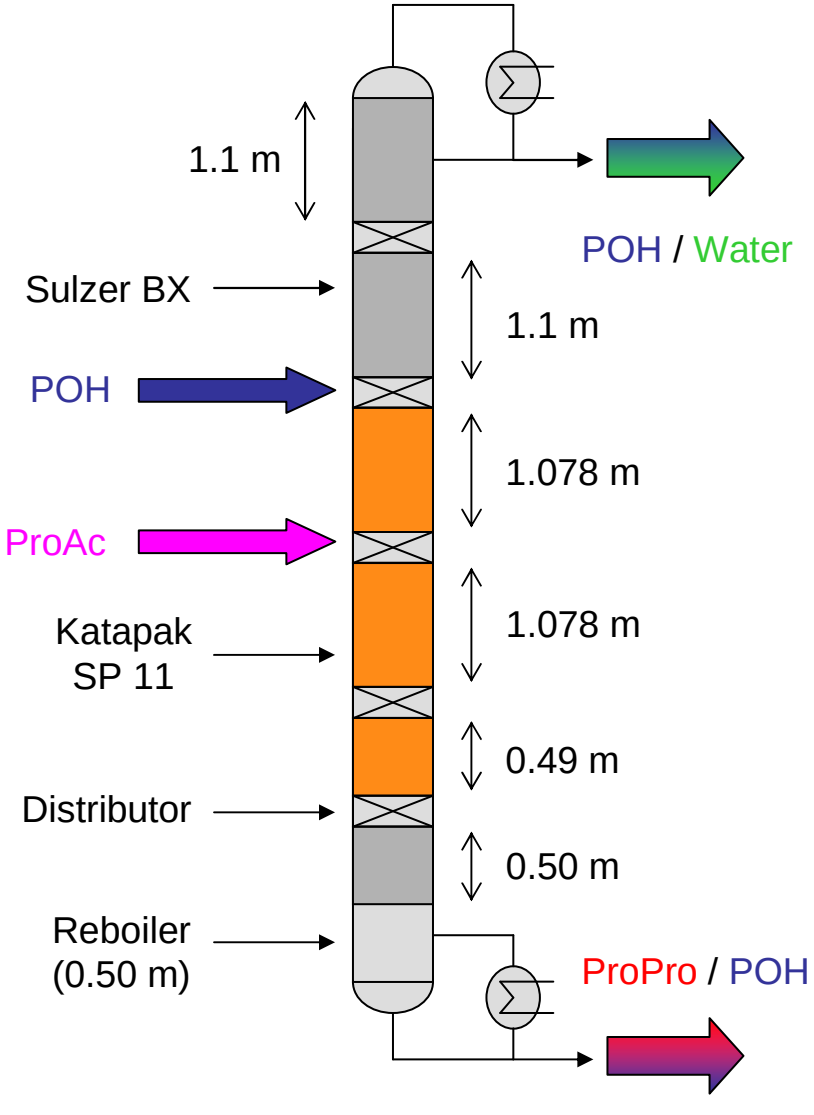

Figure 4.1: Schematic drawing of the pilot distillation column (adapted from Buchaly et al. (2005))

equal to the number of stages plus one).

The whole installation is thermally insulated with two layers of insulating material and, between the layers and in each stage, an automatic-controlled electric heating element helps insure adiabatic operation. The bottom and top (distillate) streams as well as their reflux ratios are measured and controlled via two precision scales connected to mass flow differential integrators. The reflux pump-arounds are done by diaphragm and peristaltic pumps connected to the process control system, while each of the reactants' feeds use a diaphragm pump connected to mass flow controllers. The column temperature profile is measured by thermocouples, in contact with the liquid phase, which are placed inside each distributor. The pressure drop is measured automatically via a pressure transducer and also manually by a water U-manometer. The whole system is computer-controlled via a custom engineered control scheme which acquires data from the measuring instruments and controls valves, pumps and heating elements. The pre-heating of the feed as well as the feed mass flow are controlled independently.

In order to insure safe and reliable operation of the plant, over-heating alarms are installed in the process control system as well as a manual emergency button which, when pressed, initiates the circulation of water throughout the outside of the column. Also, and since the production of below-zero boiling point ethers was a possibility, a cooling trap using liquid nitrogen was placed in the gas vent at the top - the gas vent being present in order to insure atmospheric operation - to condensate such compounds, which would likely accumulate and present a health hazard. To guarantee the adequate operation of the column, both feeds pass through an ion-exchange bed designed to adsorb metallic ions - which could be present as an impurity - and thus reduce the risk of catalyst poisoning. Also, when the column is not operating, a pump-around system is started to maintain the catalyst wet, as recommended by the manufacturer.

The operation of the pilot plant is done mainly through interaction with the computerised control system, by setting the desired operating conditions (e.g. distillate reflux rate, heat duty, top and bottom product flow, ...). As mentioned before, the feed flow rate as well as their temperature are set independently, the flow rate being set in mass flow controllers attached to the diaphragm pumps and the temperature by assigning a set-point to the heating baths which pre-heat the feeds.

Samples collection is done by inserting gas-tight needles in the distributors - which are septum-sealed - and collecting a sample of

the liquid phase. These samples collection is only performed when steady-state operation is assumed (usually when temperature is stable within 1°C) and the volume of each sample is kept small, usually near the minimum needed for the preparation of three gas chromatograph samples. These steps are needed because samples collection has a measurable impact on the column operation stability and can represent a delay of several hours towards achieving steady-state, when it has not yet occurred, or even break the current steady state. The samples are then cooled down in a refrigerator to reduce non-catalytic reaction and prepared for GC analysis by adding an internal standard. GC analysis and processing is done using Shimadzu's GCs and peak acquisition / analysis software. The liquid-phase composition is obtained by comparison of the samples' peak areas with those of standards used for calibration.

The time needed from start-up to steady state, under normal conditions and no perturbations, is of roughly one day (24 hours) for the operation conditions tested. When changing conditions in order to migrate from one steady-state to another, it takes less time, usually around 12 hours. The whole column is extremely sensitive to perturbations - as the mass balance perturbations introduced by sample collection -, which can result in delays of several hours. The most common type of perturbation found to happen during regular use were abnormal variations in the scales present at top and bottom - which are used to calculate the mass flow rate of the product streams and reflux ratios - resulting from vibrations caused by walking near them or by leaning on the column support structure. Because of this, and since the condenser scale was more sensitive due to lower rigidity of the metal structure at the top, walking in the upper floor was avoided and movement of heavy weight materials (e.g. by wheeled cart) was not allowed.

4.2 Experimental Runs and Results

4.2.1 Experimental Runs

The initial time frame allocated for the experimental runs was of four months, being preceded by training in its operation with another system. These four months also encompassed the revamping of the column from the transesterification process it was running to the Propyl Propionate synthesis. This meant emptying the column, disassembling it, changing the feed locations, reassembling and testing

Table 4.1: Operating conditions of experiments 2 and 3

Exp.	R.R.	POH F.F.	ProAc F.F.	D.F.	B.F.	Pressure
2	2	1.21	0.79	0.77	1.23	996
3	2	1.33	0.67	0.85	1.15	996

R.R.- Reflux Rate; F.F.- Feed Flowrate; D.F.- Distillate Flowrate; B.F.- Bottoms Flowrate; Flowrates in [$kg.h^{-1}$]; Pressure in [mbar]

it prior to actual operation. Due to unexpected problems - namely leakages - the column had to be partially disassembled several times, which led to more delays.

After assembling and testing was completed sucessfully, another problem surfaced. The first series of experiments conducted showed the presence of two-phase liquid mixtures in the top stream, which was undesirable, since from an industrial point of view it represents an added separation cost. So several preliminary runs - both experimental and computational and which proved somewhat time-consuming - were performed in order to move away the system from that two-phase region.

In the end, only three experiments were carried out successfully and of these three, the first, was later on disregarded due to the loss of the experimental samples taken during operation. In fact, the analysis of the compositions was only performed successfully some months after the completion of the runs due to calibration problems on the GC. The two successful runs for which data exist are very similar in respect to their operating conditions (Table 4.1), but different enough so that the change in conditions had an impact on the results.

4.2.2 Experimental Results

The experimental results can be divided into two types: steady-state profiles and time-dependent results. Usually, the results that are considered of interest and reflect the operating capacity of the column are the steady-state profiles of composition and temperature. They show what is to be expected from a column operating at the set operating conditions, what is its throughput and if a configuration change is needed or advisable. But since the column is a very sensitive dynamic system, it is important to analyse the variable temporal evolution in order to determine if steady state was reached and its

robustness to small variations of the operating conditions. To this end, time-dependent plots of several operating variables are also presented, at assumed steady state or near it.

4.2.2.1 Experiment 2

4.2.2.2 Composition and Temperature Profiles

In order to ensure steady-state data was collected, three samples with a varying time interval between them were taken when steady-state was assumed from observing the variation of directly-measured system parameters (namely temperature). Since the time-dependent data that will be used were taken for roughly 32 hours - starting from 15:51 on the 5^{th} of July up to 23:59 on the 6^{th} of the same month -, when the system was thought to be reaching steady-state, it is important to mention the time at which the sampling was performed.

The three samples were collected at 01:00, 20:30 and 23:15 on the 6^{th} of July 2005 (Samples 1, 2 and 3, respectively). The time of sampling is approximate, because since each sample had to be collected manually, it took around 15 minutes to cover the whole column. The samples were then analysed by internal standard GC and the molar fractions extracted by comparison of the data with previously obtained calibration curves. During this step, doubts regarding the accuracy of the water measuring by the TCD detector arose. Because of this, the last sample (3) was also the object of Karl Fischer titration for determining the exact water content - which was found to be much lower than given by the GC. In order to try and compensate this error, sample 2 was treated mathematically, by calculating water content from the other components rather than direct measurement. As will be shown, this step was enough to eliminate most of the error present. Experiment 1 was not treated in any way to demonstrate the deviation occurring from GC analysis.

Fig. 4.2 presents the mass fractions obtained from the GC analysis without any adjustment. If a close look is taken at the water molar fraction, it is never lower than 0.1. Initial simulations performed at the University of Dortmund indicated that little to no water was to be expected, so this result caused some surprise. When the data was treated mathematically (Exp. 2) or water content measured independently (Exp. 3), the results are different at low water concentrations, as Fig. 4.3 shows, with water molar fraction in the lower part of the column being zero or close to it. At higher concentrations, this difference

ranges from the small to the more significative in one point (the top of the column), but overall the GC analysis appears to be more accurate.

Regarding inter-sample accuracy, it can be considered good. Experiment 1 needs to be disregarded due to the already mentioned GC analysis error. Experiments 2 and 3, although their data treatment method is different, present overlapping points, which can be seen as a validation of the steady-state. It also means that mathematically treating the data, by disregarding water, leads to correct results, equal to those given by direct measuring.

Looking at the results themselves, they are reasonable, with an almost total conversion of the highest boiler (Propionic Acid) and separation of the products - Water comes out on the distillate stream, Propyl Propionate in the bottom stream. The purity of the desired product is not very high (around 80%), but that stream could hypothetically be fed into a normal column upstream where total separation would be achieved. Another hypothesis is increasing the number or height of the separation stages at the bottom - the last meter of the column, including reboiler, raise the molar fraction of Propyl Propionate from around 0.3 to 0.8 -, but this would result in more Propanol in the distillate stream, which needs to be separated later on from water in order to recirculate it to the process.

The temperature profile of the system (Fig. 4.4) is as expected, presenting a similar shape to that of the Propyl Propionate molar fraction. This can be explained by almost no Acid existing and the difference between the boiling point of Propyl Propionate and the other two components being large (while the difference between Water and Propionic Acid boiling points is far smaller), thus resulting in the temperature profile mimicking the concentration profiles. When comparing the temperature profiles at the time corresponding to the three samples taken, they are almost the same, with some small variations which had no effect on the system's composition. The only exception is the temperature of distributor 2, which is lower 1.5°C in experiment 3. As will be shown later, this corresponds to a temperature perturbation in the system, most likely caused by the sampling itself, but it had no effect on the composition since such an effect would only be observed afterwards.

4.2.2.3 Time-Dependent Profiles

In order to initiate a sampling run, which introduces significant perturbations in the column, the operator should have a reasonable degree

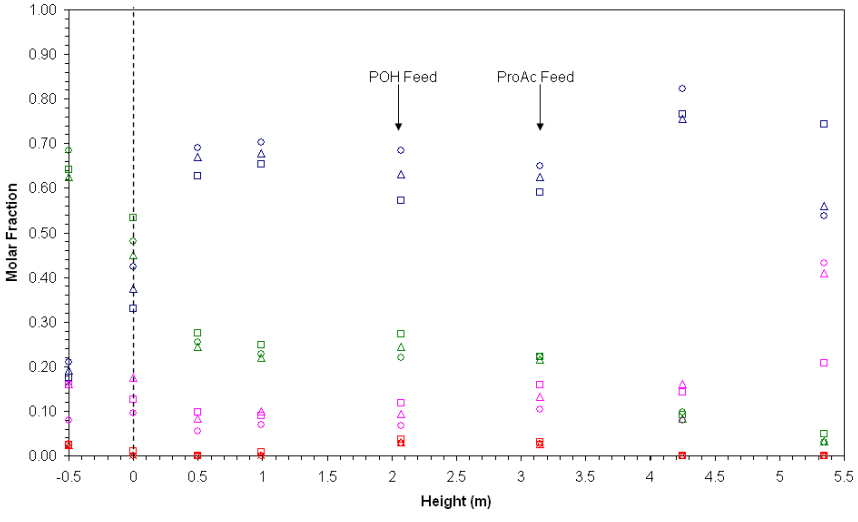

Figure 4.2: Experiment 2 steady-state composition (Original Data) (Symbols: □ - Sample 1; ◯ - Sample 2; Δ - Sample 3. Colours: ■ POH: ■ ProAc; ■ ProPro; ■ Water)

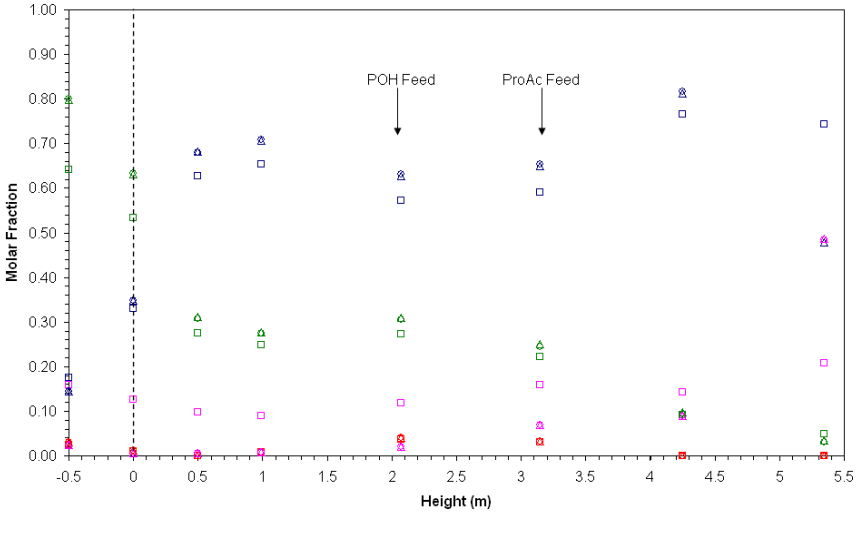

Figure 4.3: Experiment 2 steady-state composition (Treated Data) (Symbols: □ - Sample 1; ◯ - Sample 2; Δ - Sample 3. Colours: ■ POH; ■ ProAc; ■ ProPro; ■ Water)

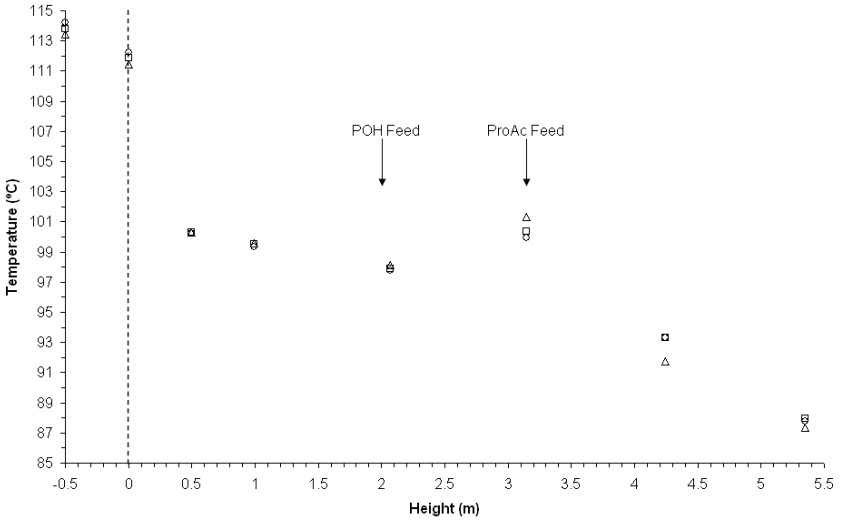

Figure 4.4: Experiment 2 steady-state temperature profile (Symbols: □ - Sample 1; ◯ - Sample 2; Δ - Sample 3)

of certainty whether the column is in steady-state. The best way to do so is to verify if the temperature profile across the column and the mass flowrates are stable within a reasonable time frame. In Fig. 4.5 the temperature profile of the column in order to time, starting from 16:00 on the 5th July 2005 up to the 24:00 the next day, is presented.

As can be seen from the figures, most temperatures are extremely stable from around 18:00 on the 5th July up to 23:10 the next day, with variations within 0.5°C. The only exception is the bottom temperature, right after the reboiler, which has a 3°C variation during the whole process, varying roughly 0.5°C per hour. This happens because the temperature difference measured between distributors 6 and 7 is quite large (10-13°C) for a very short stage (0.5 m), making it extremely sensitive to small variations in composition or reboiler heat duty. At the time of the last sample taken (23:15), there was an instability introduced into the system, which caused some fluctuation in the temperatures (and in most of the other variables). This was most likely caused by mass balance perturbations introduced either by sampling (e.g. sampling syringe clean-up performed too fast, too much sample taken at a point) or the sampling process (e.g. vibration in the scales by walking too fast / heavy, leaning on the metal support structure). The perturbation had little effect since the experiment was considered

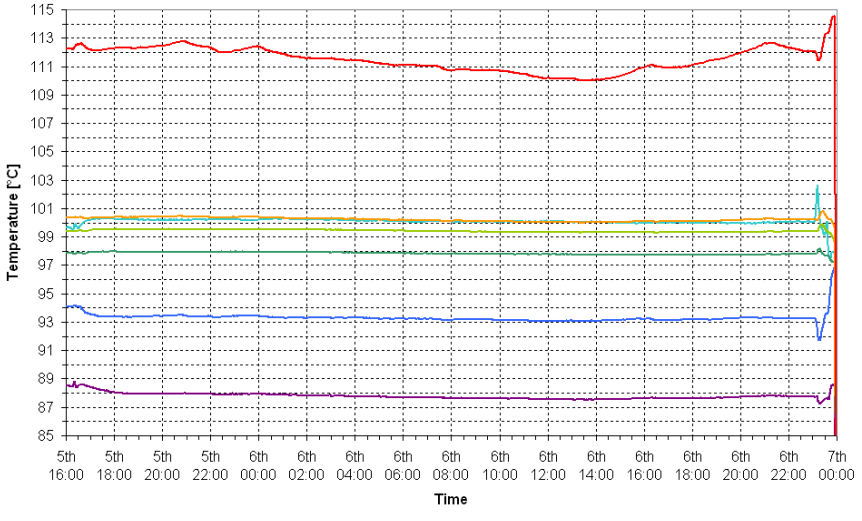

Figure 4.5: Temperature-Time profile across the RD column (Experiment 2) (– Dist. 1; – Dist. 2; – Dist. 3; – Dist. 4; – Dist. 5; – Dist. 6; – Dist. 7)

as over short afterwards and the last sample taken did not reflect it.

The next variables that should be verified to determine if steady-state is near or has been reached are those related to mass. In Fig. 4.6, the flowrates of top and bottom products, top reflux stream, condenser vapour inflow and, more importantly, the overall column mass balance, are presented. Both top and bottom product show a very steady behaviour, with some normal fluctuations that occur in any process of this scale. There is a very small sympathetic variation of top product, accompanying the decrease of the reboiler temperature, which is compensated by the variation of the bottom product - which increases slightly, as expected, since less liquid is reboiled. This effect is more evident in the decrease of inflow of vapour to the condenser when reboiler temperature lowers, compensated somewhat by the lowering of reflux to the column. In terms of overall mass balance, which might indicate leakages or holdup build-up, it is slightly above the optimal value of zero which can be attributed to measuring errors or, in the worst case, to a very small leak in the column. Nevertheless, this value is very small and can be safely disregarded.

This stability of mass flows and compensation patterns to the temperature change in the reboiler are a signal of an also stable reflux

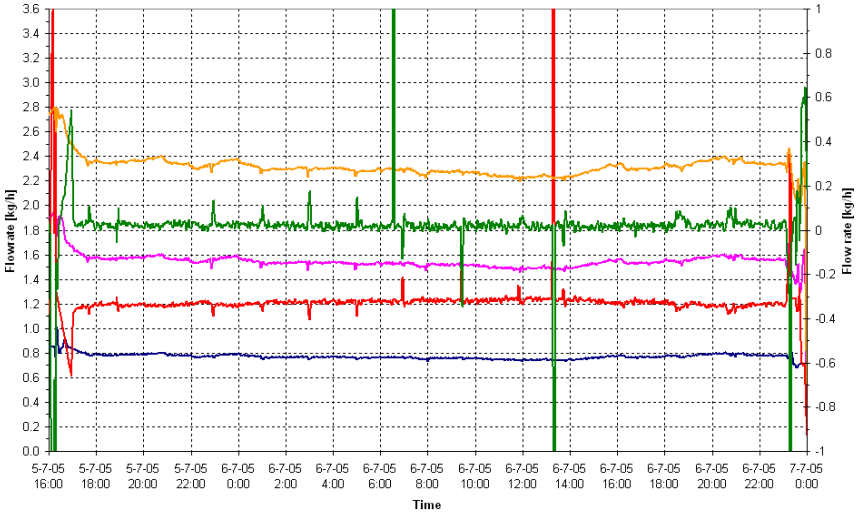

Figure 4.6: Mass Flow-Time profile in the RD column (Experiment 2) (Left Axis (Streams):– Top Product (Distillate); – Bottom Product; – Reflux; – Condenser Vapour Inflow; –. Right Axis: System Mass Balance)

ratio across the time interval analysed. This can be seen in Fig. 4.7, with the instant value of the reflux ratio varying slightly and in average fashion around the operating value of 2. The Distillate / Feed ratio, also represented, follows the reboiler temperature trend, as expected.

Regarding the variation of the temperature in the reboiler, it is useful to analyse the heat duty of the oil bath heating the reboiler as well as the temperatures of the oil before entering the reboiler and after leaving it. In Fig. 4.8 these data are represented together with the temperature of the reboiler itself. The interesting thing to notice is not that the trend is similar in all variables, as this was expected, but rather that it appears first on the temperatures of the heating oil (and less noticeably due to variation, in the heat duty) and after in the reboiler temperature itself, which means that the temperature variation in the reboiler is a consequence of a variation in the heat duty, probably commanded by the control system in order to maintain the system within the operating conditions given.

Finally, and although no effect was noticed, it is always advisable to check if the atmospheric pressure variation was significative or not, since the column operates at it. In Fig. 4.9 the variation of the

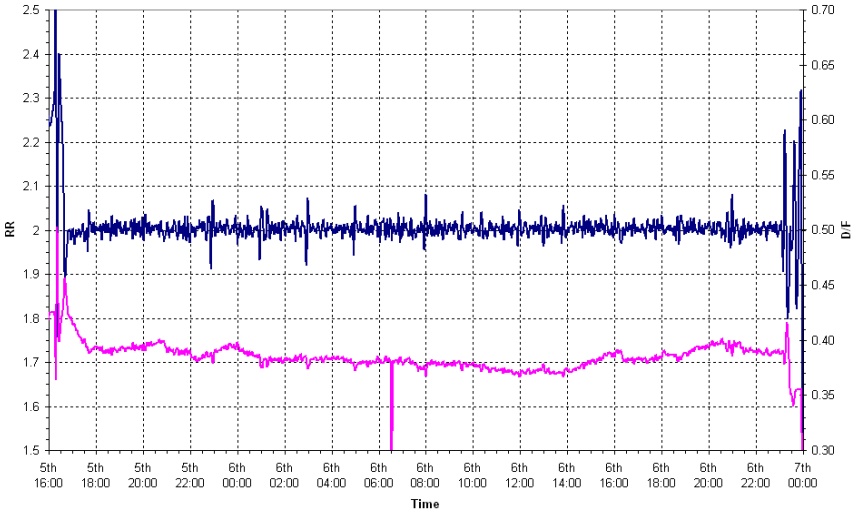

Figure 4.7: reflux ratio and Distillate/Feed Ratio Time profiles in the RD column (Experiment 2) (Left Axis: – reflux ratio. Right Axis: – Distillate / Feed Ratio)

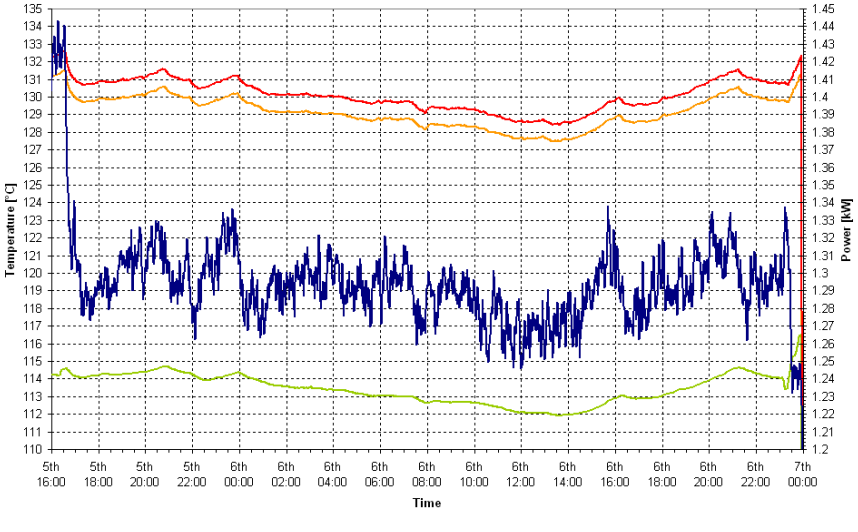

Figure 4.8: Reboiler Heat and Temperature variables during Experiment 2 (Left Axis: – Reboiler Temperature; – Inflow temperature of the heating oil; – Outflow temperature of the heating oil. Right Axis: – Heat Duty of the oil bath)

atmospheric pressure during the time interval analysed is plotted. As can be seen, there was a decrease in pressure from the start to the end, totalling a maximum of 9 mbar. This variation is negligible and had, as mentioned, no effect whatsoever on the operation of the column.

4.2.2.4 Experiment 3

4.2.2.5 Composition and Temperature Profiles

The procedure adopted for Experiment 3 is the same one of Experiment 2. Experiment 3 ran for 24 hours, picking up, in fact, from the end of Experiment 2, stabilizing - Experiment 2 finished with some instability in the mass flows - and changing the feed flowrates at 06:40 on the 7th of July. Sampling was performed later on, after the system stabilised, at 19:10, 21:10 and 22:30. Following the same procedure as before, Fig. 4.10 presents the original data measured by the GC and Fig. 4.11 the data after treatment, as done in Experiment 2. The observations that can be drawn from comparing both plots remain the same, with a significative amount of water appearing in the bottom stream. When the corrections are applied, the water value drops to near zero in reboiler, as expected and as would be correct. Intersample variation is very low - negligible even - with the points for samples 2 and 3 overlapping, which is an indication that steady-state had been reached.

The experiment itself shows overall worse results than Experiment 2. The even greater excess of Propanol to Propionic Acid in the column results in more propanol in the bottom and top streams, but without any effect on the concentration of Acid across the column. The molar fraction of n-Propyl Propionate drops to roughly 0.75 (from 0.8 on Exp. 2) in the bottom stream and the only possible positive consequence of the change of the operating conditions was the reduction of the residual water concentration at the bottom from 0.025 to 0.005. Once more, an increase in purity of the Propyl Propionate could be achieved by distilling the bottom stream in a separate column or, possibly, by increasing the height or number of separation stages at the bottom.

The temperature profile (Fig. 4.12) is very similar to that taken during Experiment 2, but with better intersampling results - the points measured at the three sampling times overlapping - and a somewhat tighter temperature range - less than 22°C when compared with the average value of 26°C of Exp. 2 - due to the increase of Propanol in all the streams (Propanol is the light boiler at the bottom but the

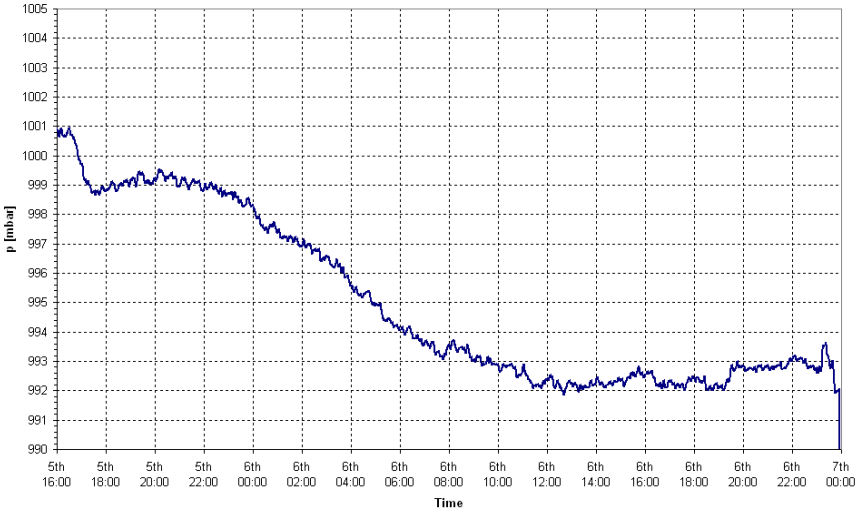

Figure 4.9: Atmospheric Pressure variation during Experiment 2

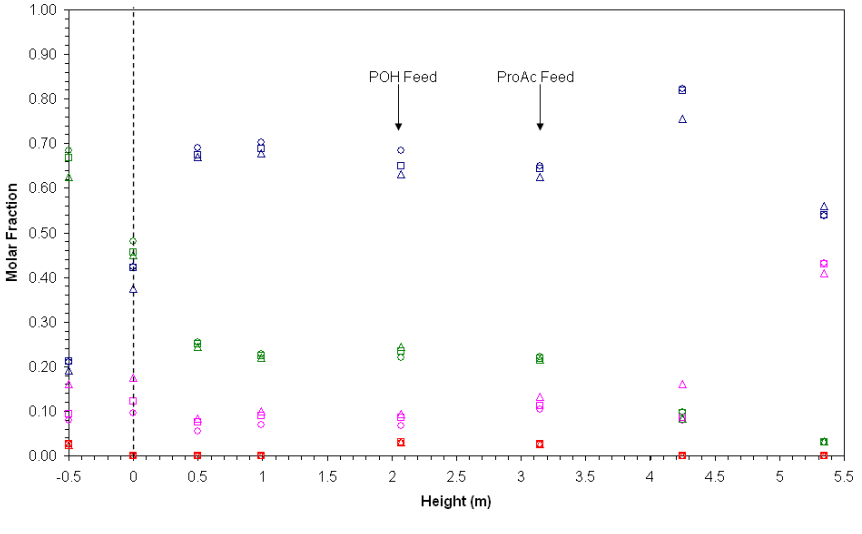

Figure 4.10: Experiment 3 steady-state composition (Original Data) (Symbols: □ - Sample 1; ◯ - Sample 2; Δ - Sample 3. Colours: ■ POH: ■ ProAc; ■ ProPro; ■ Water)

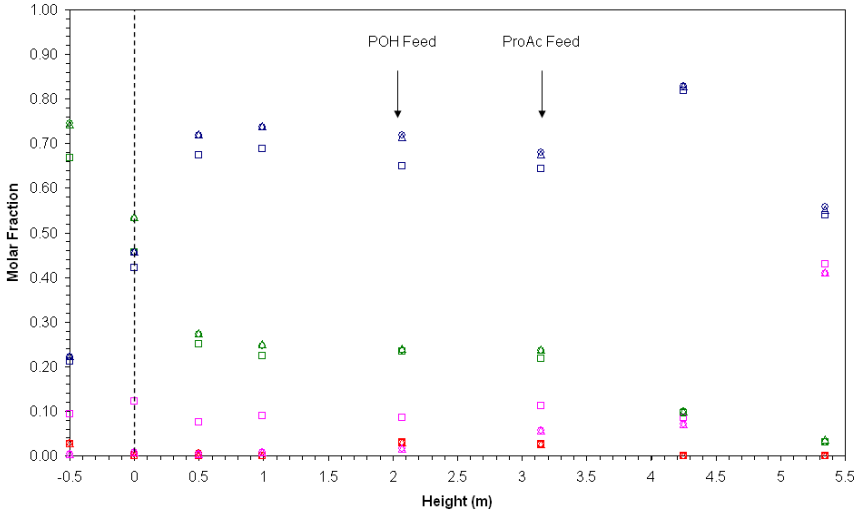

Figure 4.11: Experiment 3 steady-state composition (Treated Data) (Symbols: □ - Sample 1; ◯ - Sample 2; Δ - Sample 3. Colours: ■ POH; ■ ProAc; ■ ProPro; ■ Water)

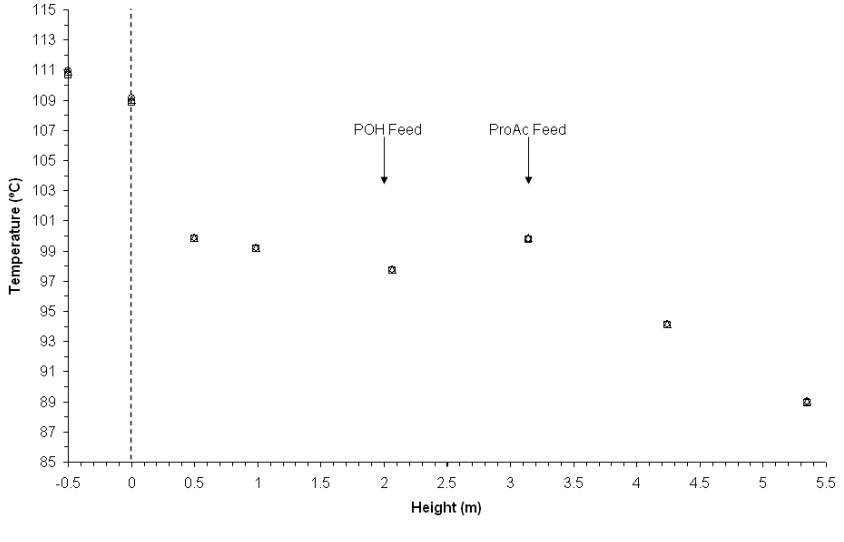

Figure 4.12: Experiment 3 steady-state temperature profile (Symbols: □ - Sample 1; ◯ - Sample 2; Δ - Sample 3)

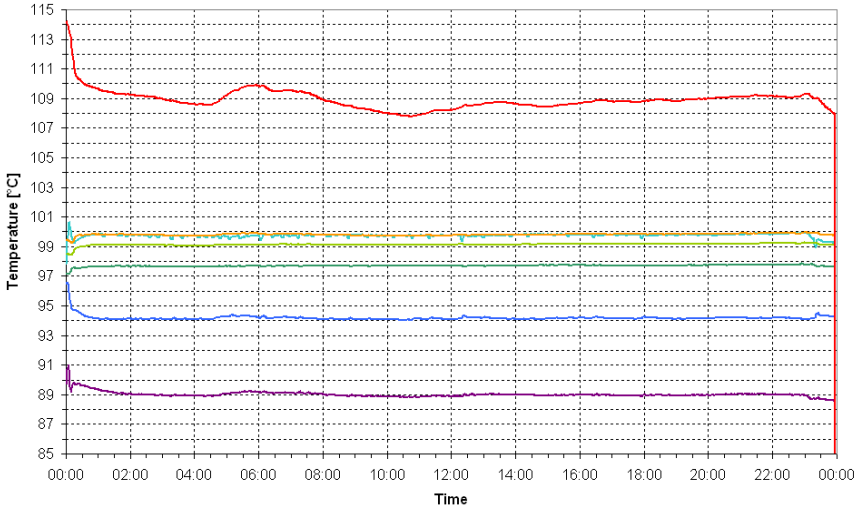

Figure 4.13: Temperature-Time profile across the RD column (Experiment 3) (– Dist. 1; – Dist. 2; – Dist. 3; – Dist. 4; – Dist. 5; – Dist. 6; – Dist. 7)

heavy boiler at the top, so an increase in its concentration reduces the temperature at the bottom but increases it at the top).

4.2.2.6 Time-Dependent Profiles

The time-temperature profile of the column (Fig. 4.13) resembles that of Experiment 2. There is slightly more "noise" in the profiles, but they are more stable on the long term. The temperature above the reboiler is, due to the temperature difference to the next distributor, more prone to fluctuations, but after sharp fluctuations in the beginning, it reaches a steady profile - possibly with a small long-term increase tendency. The fact that the overall temperature variation of the column decreased helped, since the difference between the temperatures in Distributors 7 and 6 lowered from the 10-13°C of Experiment 2 to 8-9 °C in this experiment, after the column assumed a more stable behaviour (11:00 onwards) in temperature terms.

In terms of mass, there are more significant differences between both experiments. In Fig. 4.14 we can observe that the oscillation of the mass flowrates across the column are more pronounced, even after some stability of the vapour inflow to the condenser was achieved

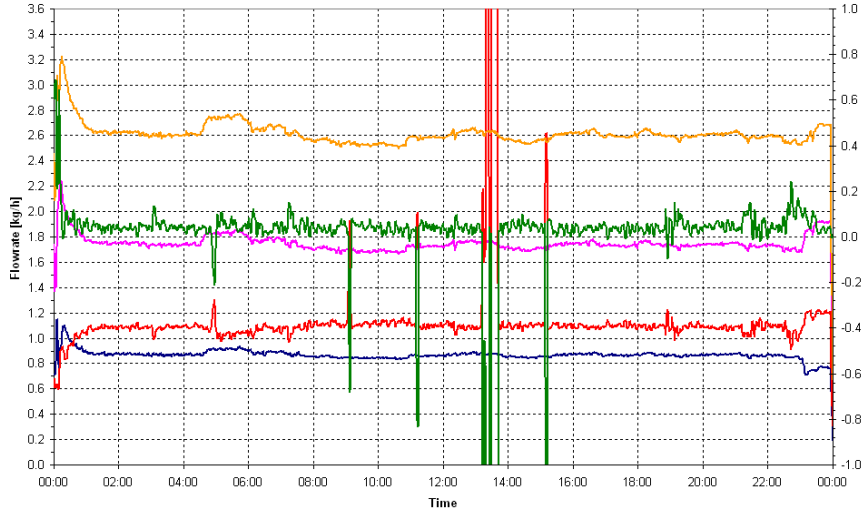

Figure 4.14: Mass Flow-Time profile in the RD column (Experiment 3) (Left Axis (Streams):– Top Product (Distillate); – Bottom Product; – Reflux; – Condenser Vapour Inflow; –. Right Axis: System Mass Balance)

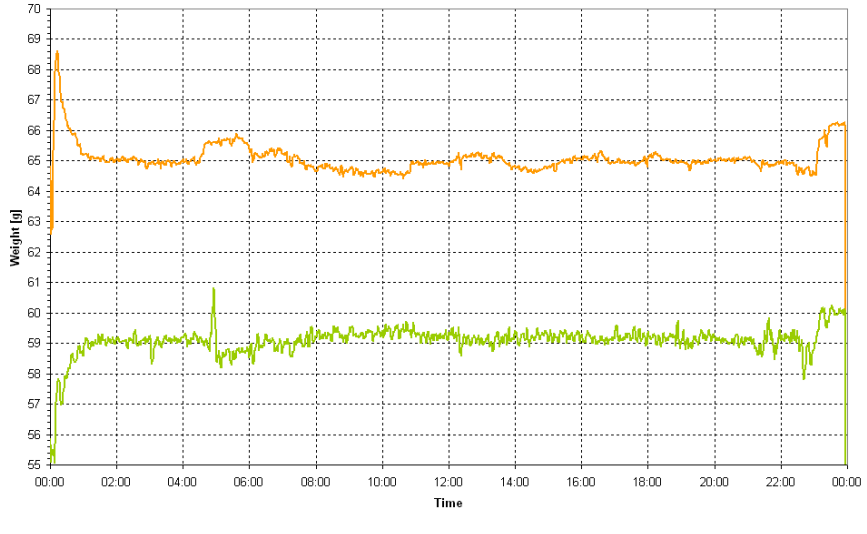

Figure 4.15: Time-weight profile at the top and bottom scales used for flowrate measurement (– Top Scale; – Bottom Scale)

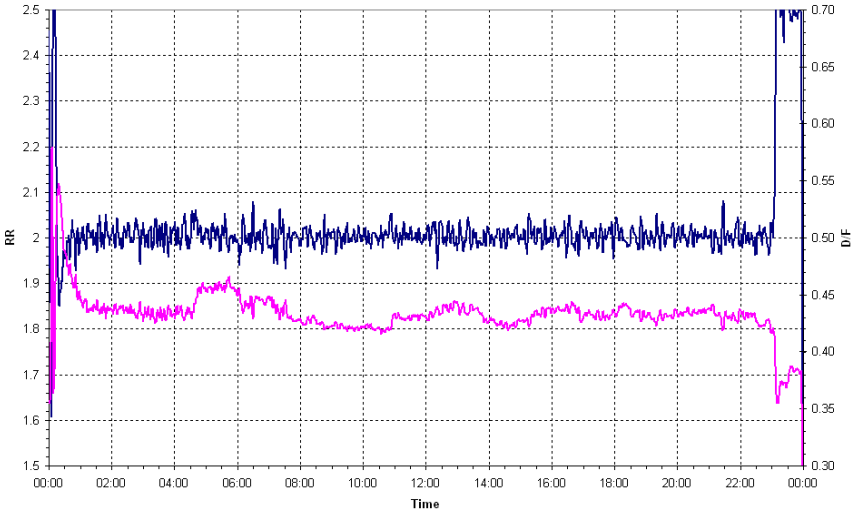

Figure 4.16: reflux ratio and Distillate/Feed Ratio Time profiles in the RD column (Experiment 3) (Left Axis: – reflux ratio. Right Axis: – Distillate / Feed Ratio)

(around 11:00). There is also a long-term fluctuation of the feeds, similar to the preceding experiment, and a series of measuring errors in the bottom flow rate, occurring from 15:15 to 15:45, which affected the mass balance calculation. These errors originated from problems in the flowrate differential integrator connected to the measuring scale at the bottom and not from the column or the scale itself - as can be seen in Fig. 4.15. A more serious problem of the mass analysis is the constant mass imbalance of the system, which increased from Experiment 2. This is an indication of a leak somewhere in the column and will most likely influence the fitting of these results to a theoretical model.

The oscillations seen on the mass profile are amplified in the reflux ratio and Distillate/Feed plots (Fig. 4.16), with the reflux ratio, although averaging around the operating set point of 2, showing wider variations than in Experiment 2, where the variations have lower amplitude. The Distillate/Feed Ratio plot shows these oscillations very clearly as well, with the line showing wide and high peaks, besides an overall fluctuation which seems to be diminishing its amplitude with time. This could be seen as an indication that the system was not in true steady state, but very near it. Although the composition and

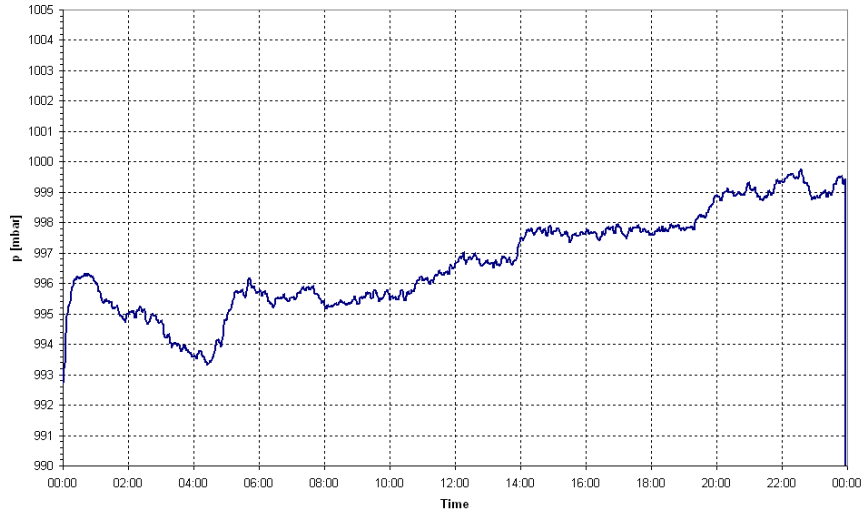

Figure 4.17: Atmospheric Pressure variation during Experiment 3

temperatures taken during sampling show invariance, other variables appear to do not. In practical terms, this is of little to no consequence since the objective are steady top and bottom products and small variations inside the column are irrelevant. The only precaution that should be kept in mind is that, since the system is near steady state and not in it, the column is more vulnerable to outside perturbations.

In terms of system pressure (Fig. 4.17), it varies from a minimum of 993.4 mbar at around 04:30 to a maximum of 999.7 mbar at 22:35, thus being able to be considered invariant for operating or even simulation analysis.

BIBLIOGRAPHY

Buchaly, C., Duarte, C., Loureiro, J. M., Kreis, P., September 2005. Process intensification of n-propyl propionate synthesis using reactive distillation over a novel catalyst. In: ChemPor 2005 - 9th International Chemical Conference. Coimbra, Portugal.

Rhom and Haas Company, 2002. Amberlyst 46 product data sheet.

Sulzer Chemtech, 2005. Structured packings for distillation, absorption and reactive distillation.
URL www.sulzerchemtech.com

5 Reactive Distillation Modelling and Simulation

5.1 Reactive Distillation Column Model

5.1.1 Introduction to RD Column Modelling

5.1.1.1 Equilibrium Stage Model

Reactive distillation, for the most part of its history and even today, has been seen as a subset of distillation rather than an independent process. Most of its development has been the work of persons who have an history in the thermal separation field and this reflects on the way modelling of the reactive distillation process was approached.

The first, simpler, and probably most widely used model for simulating a regular distillation column is the equilibrium stage model. This model assumes that the column can be divided into stages (transversal cuts of the column, for packed columns), where all the relevant mass transfer operations occur. It also assumes that the liquid and vapour leaving the stage are in thermodynamic equilibrium with each other. For reactive distillation, it also takes into account liquid phase reaction.

In Fig. 5.1 a simple schematic of an equilibrium stage can be seen. The equations used to describe this stage (Taylor and Krishna, 2003) are the so-called MESH equations, for Mass, (phase) Equilibrium, Summation (molar/mass fractions) and entHalphy. The Mass equations are made of a simple mass conservation balance to the liquid phase holdup, both component-wise and global. Starting with the component-specific mass balance,

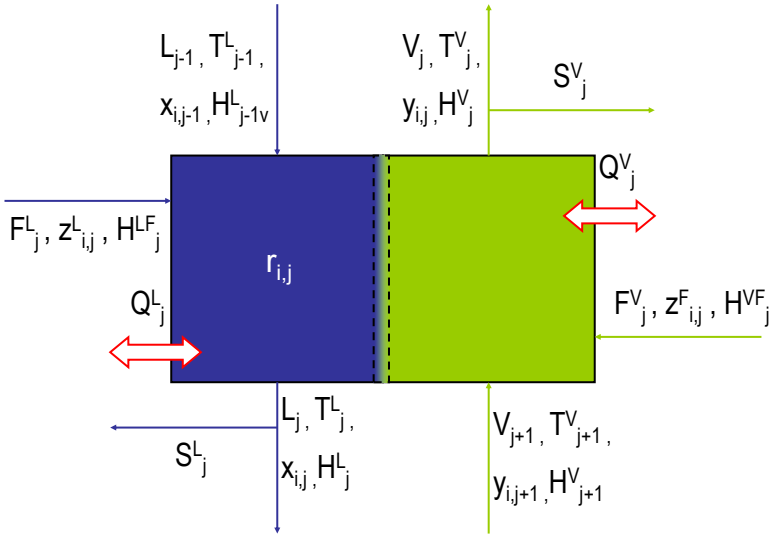

Figure 5.1: Equilibrium stage model (adapted from Taylor and Krishna (2003) (Blue: Liquid, Green: Vapour)

$$\frac{\mathrm{d}U_j\, x_{i,j}}{\mathrm{d}t} = V_{j+1}\, y_{i,j+1} + L_{j-1}\, x_{i,j-1} + F_j\, z_{i,j} + \left(S_j^V + V_j\right) y_{i,j} + \left(S_j^L + L_j\right) x_{i,j} + \sum_{n=1}^{m} \left(\nu_{i,n}\, r_{n,j}\right) \quad (5.1)$$

where U_j is the stage liquid holdup, $x_{i,j}$ the stage liquid phase molar fraction of component i, t time, V_{j+1} the molar vapour inflow, $y_{i,j+1}$ the molar fraction of component i in the vapour inflow, L_{j-1} the liquid vapour inflow, $x_{i,j-1}$ the molar fraction of component i in the liquid inflow, F_j the molar feed (both liquid and vapour), $z_{i,j}$ the molar fraction of component i in the feed, S_j^V the molar flowrate of the vapour sidedraw, V_j the molar vapour outflow, $y_{i,j}$ the molar fraction of component i in the vapour outflow, S_j^L the molar flowrate of the liquid sidedraw, L_j the molar liquid outflow, $\nu_{i,n}$ the stoichiometric coefficient of component i in reaction n, $r_{n,j}$ the reaction rate of reaction n and index m the total number of reactions.

By summing all the component-specific mass fractions, an overall balance to the liquid holdup on the stage can be obtained,

$$\frac{\mathrm{d}U_j}{\mathrm{d}t} = V_{j+1} + L_{j-1} + F_j + \left(S_j^V + V_j\right) + \left(S_j^L + L_j\right) + \sum_{n=1}^{m}\sum_{i=1}^{nc}\left(\nu_{i,n}\, r_{n,j}\right) \tag{5.2}$$

where the index *nc* represents the total number of components in the system.

The phase Equilibrium equations are simple and given by vapour-liquid equilibrium (VLE) type relationships,

$$y_{i,j} = K_{i,j}\, x_{i,j} \tag{5.3}$$

where $K_{i,j}$ represents a generic, phase-equilibrium, constant.

The Summation equations are nothing more than the normal conditions that the sum of the molar fractions (liquid and vapour), must always be equal to one.

$$\sum_{i=1}^{nc} x_{i,j} = \sum_{i=1}^{nc} y_{i,j} = 1 \tag{5.4}$$

Finally, the heat balance equations (or entHalphy balance equations) are given by

$$\begin{aligned}\frac{\mathrm{d}U_j\, H_j}{\mathrm{d}t} = {} & V_{j+1}\, H_{j+1}^V + L_{j-1}\, H_{j-1}^L + F_j\, H_j^F \\ & - \left(S_j^V + V_j\right) H_j^V - \left(S_j^L + L_j\right) H_j^L - Q_j\end{aligned} \tag{5.5}$$

where H_j is the stage's enthalpy (liquid-phase), H_j^V and H_j^L the vapour and liquid phase enthalpies of the stage and outflows, H_{j+1}^V and H_{j-1}^L the enthalpies of the vapour and liquid inflows, H_j^F the enthalpy of the feed and Q_j the heat exchange with the outside. Usually, this heat transfer represents a loss of system heat and because of this it is represented as subtracting from the balance. This also means that the direction of the transfer is assumed to be FROM the column TO the outside. If the outside is at an higher temperature than the column, the direction should be maintained and the value of Q would be negative.

5.1.1.2 Non-Equilibrium Stage Model

Although the Equilibrium Stage (EQ) Model is able to simulate a large number of distillation systems, it suffers from its main assumption:

that the liquid and vapour streams leaving the stage are in equilibrium when, in fact, normally they are not. The solution to this problem was suggested by Murphree (1925), by the introduction of "stage efficiency" concept or Murphree Efficiency (η, using the notation found in Seader et al. (1997)), as given by Eq. 5.6 ($y^*_{i,j}$ is the vapour molar fraction of component i that is in equilibrium with the liquid phase, while the other molar fractions are actual values leaving or entering the stage).

$$\eta = \frac{y_{i,j} - y_{i,j-1}}{y^*_{i,j} - y_{i,j-1}} \tag{5.6}$$

The concept of stage efficiency mitigates somewhat the error associated with the use of an EQ model, but it requires the previous knowledge of the efficiency value, which usually can only be determined experimentally. This, of course, reduces the usefulness of the model when no data is available.

Another alternative to the use of the EQ model is to take into account the non-equilibrium of the vapour and liquid outflows. Krishnamurthy and Taylor (1985a,b,c) did exactly this by introducing the concept of Non-Equilibrium Stage (NEQ) Model. The structure of the model for non-reactive systems is similar to that of the Equilibrium Stage Model, as can be seen in Fig. 5.2. The two main differences are the addition of a two-film model (Lewis and Whitman, 1924) (Fig. 5.3), which is responsible for modelling the temperature and mass differences between phases, and the inclusion of interphase mass and heat transfer ($N_{i,j}$ and e_j, respectively).

Later on, Taylor et al. (1994) expanded the model in order to include other factors, such as pressure drop, giving birth to the extended MERSHQ model (MERSHQ for Mass, Energy, transfer Rate, Summation, Hydraulic (pressure drop) and interface eQuilibrium). Because this non-equilibrium models are based on the rate of mass and heat transfer between phases, rather than equilibrium, they are also known as Rate-based Models.

The equations of this model are similar to those of the MESH model (Eqs. 5.1-5.5), but each phase is the object of an independent mass and energy balance (instead of an overall balance to the stage). The balance, in order to be simpler, is done in steady-state and no reaction is included, since this is the basic, non-reactive model. Also, Krishnamurthy and Taylor (1985a) considers as positive the outflows and negative the inflows. For consistency's sake, the other way around will be presented here.

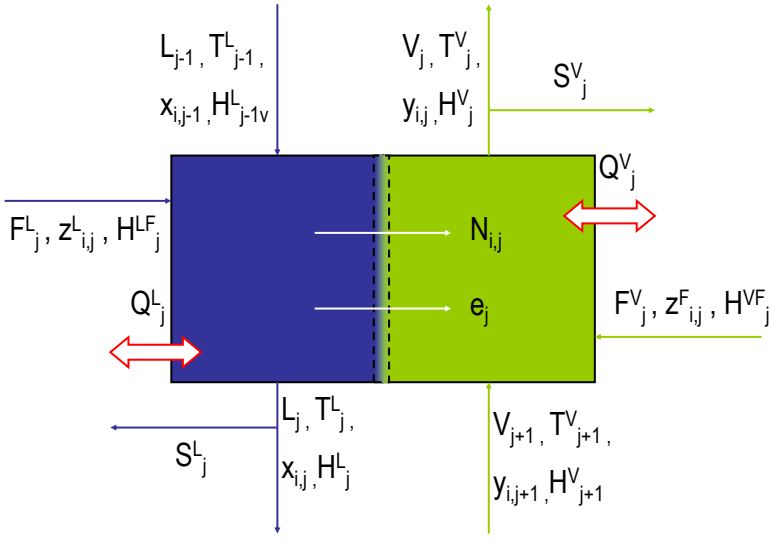

Figure 5.2: Non-Equilibrium Stage Model (adapted from Krishnamurthy and Taylor (1985a)) (Blue: Liquid Phase; Green: Vapour phase; - - -: Film / Bulk interface)

The vapour and liquid phase Mass balances are given by

$$V_{j+1}\, y_{i,j+1} + F_j^V\, z_{i,j}^V + \left(S_j^V + V_j\right) y_{i,j} - N_{i,j}^V = 0 \tag{5.7}$$

$$L_{j-1}\, x_{i,j-1} + F_j^L\, z_{i,j}^L + \left(S_j^L + L_j\right) x_{i,j} + N_{i,j}^L = 0 \tag{5.8}$$

with $N_{i,j}^V$ and $N_{i,j}^L$ representing the vapour-to-liquid molar transfer of component i at the interface.

The Energy balances have a similar structure,

$$V_{j+1}\, H_{j+1}^V + F_j^V\, H_j^{VF} - \left(S_j^V + V_j\right) H_j^V - E_j^V - Q_j = 0 \tag{5.9}$$

$$L_{j-1}\, H_{j-1}^L + F_j^L\, H_j^{LF} - \left(S_j^L + L_j\right) H_j^L + E_j^L - Q_j = 0 \tag{5.10}$$

the vapour-to-liquid energy transfer being represented by $E_{i,j}^V$ and $E_{i,j}^L$.

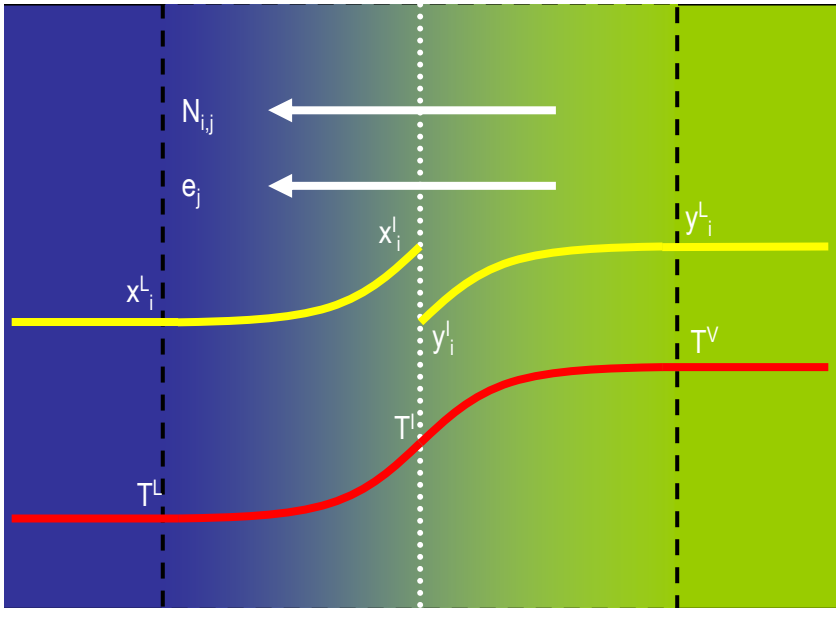

Figure 5.3: Non-Equilibrium Stage Model - Typical Composition and Temperature Interface Profiles (adapted from Krishnamurthy and Taylor (1985a)) (Blue: Liquid Phase; Green: Vapour phase; - - -: Film / Bulk interface; · · ·: Vapour / Liquid interface)

In order to evaluate the Mass and Energy balance, the interphase transfer of mass and heat needs to be accounted for. The Rate equations,

$$N_{i,j}^V - N_{i,j}^L = 0 \tag{5.11}$$

$$E_j^V - E_j^L = 0 \tag{5.12}$$

define the boundary conditions between the liquid and vapour films, by saying that the mass and heat flowing out of one film are equal to the mass and heat flowing in the other.

The Summation conditions remain unaltered, but are now applied to the interface rather than the whole stage:

$$\sum_{i=1}^{nc} x_{i,j}^I - 1 = \sum_{i=1}^{nc} y_{i,j}^I - 1 = 0 \tag{5.13}$$

The Hydrodynamic conditions take into account the pressure drop in the stage, stating that the difference between the pressure on the current stage (p_j) and the pressure in the preceding stage (p_{j-1}) is equal to the pressure drop occurring from the previous stage to the current one (Δp_{j-1})), or

$$p_j - p_{j-1} - \Delta p_{j-1} = 0 \tag{5.14}$$

Finally, the interface eQuilibrium equations were originally given in a similar way to the MESH model, by simple VLE at the interface,

$$K_{i,j}\ x^I_{i,j} - y^I_{i,j} = 0 \tag{5.15}$$

.

This model requires, as can be observed from its equations, the knowledge of mass and heat transfer at the interface. Krishnamurthy and Taylor (1985a) refer to the work of Krishna (1979), which was the object of further developments in more recent times (Taylor and Krishna, 1993; Krishna and Wesselingh, 1997) and which verses on the mass and heat transfer coefficients as given by the Maxwell-Stefan theory.

According to that work, the vapour and liquid phase mass transfer rates can be obtained by the use of

$$\frac{y_i}{R\ T^V}\frac{\partial \mu^V_i}{\partial z} = \sum_{k=1}^{nc} \frac{y_i\ N^V_k - y_k\ N^V_i}{c^V_t\ Đ^V_{i,k}} \tag{5.16}$$

for the vapour phase and

$$\frac{x_i}{R\ T^L}\frac{\partial \mu^L_i}{\partial z} = \sum_{k=1}^{nc} \frac{x_i\ N^L_k - x_k\ N^L_i}{c^L_t\ Đ^L_{i,k}} \tag{5.17}$$

for the liquid phase. c^V_t and c^L_t represent the total concentration in the vapour and liquid phases (in $\left[mol.m^{-3}\right]$), and $Đ^V_{i,k}$ and $Đ^L_{i,k}$ the Maxwell-Stefen diffusivity of the i,k pair in the vapour and liquid phases, respectively. The value of the Maxwell-Stefan diffusivity can be calculated using the techniques presented in Taylor and Krishna (1993).

The energy flux at the interface can be evaluated by summing both conductive and convective contributions, resulting in

$$E^L_j = -\lambda^L_j \frac{\partial T^L}{\partial \eta^L} + \sum_{i=1}^{nc} N^L_{i,j}\ H^L_{i,j} \tag{5.18}$$

for the liquid phase and

$$E_j^L = -\lambda_j^V \frac{\partial T^V}{\partial \eta^L} + \sum_{i=1}^{nc} N_{i,j}^V \, H_{i,j}^V \tag{5.19}$$

for the vapour phase, where λ_j^L and λ_j^V are the convection driving forces - which can be defined as $\frac{h_j}{a_j}$, h_j being the heat transfer coefficient (in the liquid or vapour phase, as appropriate) and a_j the area of the interface - and η is the measure of thickness of the liquid film - starting from zero at the film / bulk interface and ending at the liquid/vapour films interface.

In the case of reactive distillation, the model is further complicated by the reaction -i.e., type of catalysis (or absence of it), location of the reaction, ... For homogeneous systems (catalytic or not), a simple term similar to the one existing in the MESH model (Eq. 5.2) suffices for modelling the liquid bulk phase. If the reaction is fast enough (as compared to mass transfer, i.e., high Damköhler numbers), then the reaction in the film needs to be taken into account (Taylor and Krishna, 2003),

$$\frac{\partial N_i}{\partial z} = \sum_{i=1}^{m} \nu_{i,n} \, r_{n,j} \tag{5.20}$$

When the catalysis is non-homogeneous (and non-pseudo homogeneous, obviously), the mass transfer, adsorption or other physical phenomena involving the catalyst need to be evaluated. There are several ways to do so, depending on the type of catalyst and its supporting structure (i.e. bed, unstructured packing, structured packing, ...) and the analysis should be performed case-by-case. Studies on the mass transfer properties of the packings can be found in Rocha et al. (1993, 1996); Billet and Schultes (1999); Górak and Hoffmann (2001); Kołodziej et al. (2001); van Baten and Krishna (2002); Miller and Kaibel (2004); Egorov et al. (2005); Kołodziej et al. (2005).

5.1.2 The PROFILER model

The PROFILER model, which was used in the course of this work to simulate reactive distillation columns, is the object of a continued work carried out at the Chair of Fluid Separation Processes of the Department of Biochemical and Chemical Engineering of the University of Dortmund. One of the most recent publications detailing the

model, written by Klöker et al. (2005), will be used as a basis for this subsection.

PROFILER, at its core, is a computer implementation of the work of Górak and Hoffmann (2001) and Hoffmann et al. (2004), which are themselves improvements over the rate-based models for reactive distillation. It is written in Aspen Custom Modeler (ACM) and uses this software's mathematical capabilities for solving the model's equations. Since the software was developed in the framework of the INTINT (INTelligent column INTernals for reactive separations) project, it is especially targetted towards packed columns, making extensive use of correlations such as the ones mentioned previously.

In order to facilitate convergence of the more complex runs, and also add flexibility to the program, PROFILER contains besides the rate-based model, two simpler models. One, rate-based, which uses internally calculated effective diffusivities, instead of Maxwell-Stefan diffusivities and another which uses an equilibrium stage model (MESH-like). The model also accommodates a no-mass transfer model and special initialisation conditions, which are used solely for convergence purposes. A typical run of the model would start with no reaction, no mass transfer and initialisation on. Upon convergence, the complexity would be increased to Simple (equilibrium stage), then the initialisation conditions are turned off, then reaction turned on (eventually in increasing steps, starting with a reaction rate of 1% of the real rate and increase it step by step) and then the first rate-model is used (Complex). Finally, upon convergence, Maxwell-Stefan can be used in full. With each step, the tolerances used for calculation are also tightened. The whole process is usually automated via the use of ACM's scripting capabillity.

In this work, the simulation runs were executed up to the Complex model. The reason for this was two-fold: first, some problems with the Maxwell-Stefan model were detected and were in the process of being corrected, their use not being advisable for actual runs; second, modelling runs performed previously showed that few differences existed between the results obtained using the Complex model and the Maxwell-Stefan Model, probably due to the good quality of Aspen's internal correlations for the calculation of diffusivities.

Regarding the model's structure, PROFILER has a tree-like appearance (Fig. 5.4), being composed of "top" Flowsheet model, which defines the overall conditions of the simulation such as feed and product streams, the three basic modelling blocks - Condenser, Column and Reboiler - and allows for optional blocks such as reactors or mem-

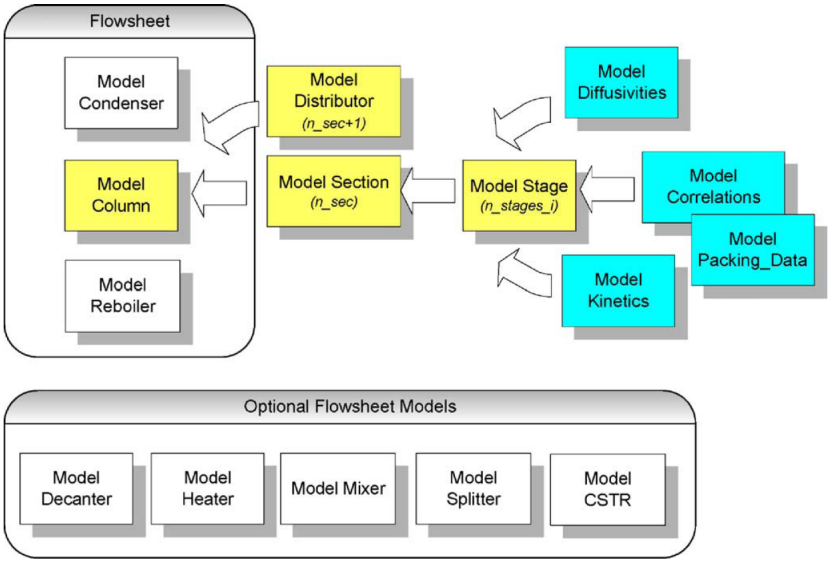

Figure 5.4: PROFILER model structure (taken from Klöker et al. (2005))

brane modules. Of the three basic blocks, the Column is subdivided into Sections and Distributors (mimicking an actual column), each Section - which is placed between two distributors - being made of discrete Stages. The actual mass and energy balances are made in and between Stages, which call upon three submodels: Diffusivities - for determining Maxwell-Stefan diffusivities -, Kinetics - for calculating the reaction rates, when reaction occurs - and Correlations - which contains the needed mass transfer correlations and has a submodel of its own containing the necessary data, Packing_Data.

5.2 n-Propyl Propionate Simulation and Data Reconciliation

5.2.1 Model setup considerations

In order to simulate n-Propyl Propionate synthesis via reactive distillation, and since experimental results exist, it was decided to try and simulate the actual column configuration and operating conditions which were used to obtain the experimental results, in order to validate the model. This task was eased considerably because PROFILER was, in a way, built around the column used, since this is the primary

column used at the University of Dortmund for experimental data gathering.

Most of the configuration was successfully introduced into the model, but one problem existed. The column used for the experimental work used, as reactive packing, Sulzer's KATAPAK SP11 but PROFILER does not contain any data for this packing. Although experiments for determining relevant data for KATAPAK SP11 are currently underway, they are not complete and as such, are prone to error.

For the original simulation runs performed at the University of Dortmund, used to define an optimum operating region for Propyl Propionate synthesis, it was decided to use the correlations for the MULTIPAK-II packings. First results - verified with preliminary kinetics - showed good agreement (Buchaly et al., 2005) and the MULTIPAK correlations continued to be used throughout the work. More recently, at higher flowrates than those originally used, some problems appeared related with the reaction rate in the packing. In order to try and reduce error, the amount of dry catalyst present in each packing was corrected from the original MULTIPAK-II values to the already determined values for KATAPAK SP11. This "modified" version of MULTIPAK was used in this work for the reconciliation runs of Propyl Propionate.

5.2.2 Simulation and Data Reconciliation

In order to run the simulations, PROFILER needs the user to introduce the operating conditions of the simulation run. Most of these conditions are similar to those which are set for an experiment but, in order to ease convergence, some are not - pressure is a clear example, since during actual atmospheric operation the pressure changes, but for simulation purposes it is set constant. The simulation operating conditions are presented on Table 5.1.

Since experimental results already exist, a comparison between simulation and experimental results can be made immediately. Figures 5.5 and 5.6 present the composition and temperature profiles for experiments 2 and 3, given by the PROFILER simulations and by the actual experimental runs (which where already presented in the previous Chapter).

Analysing first the composition profiles along the column, and discounting the results for Sample 1 for the reasons given in the previous Chapter, the fit of the simulation to the experimental data

Table 5.1: Operating conditions for Propyl Propionate reactive distillation simulations

	Experiment 2	Experiment 3
Pressure [bar]	0.992	0.997
Reflux Ratio	2.0	2.0
POH Feed Flowrate [kg.h^{-1}]	1.29	1.33
POH Feed Temperatute [°C]	90	90
POH Feed Stage	4	4
ProAc Feed Flowrate [kg.h^{-1}]	0.71	0.67
ProAc Feed Temperatute [°C]	90	90
ProAc Feed Stage	3	3
Distillate Flowrate [kg.h^{-1}]	0.77	0.85
Stage 1 Packing	Sulzer BX	Sulzer BX
Stage 1 Height [m]	1.100	1.100
Stage 2 Packing	Sulzer BX	Sulzer BX
Stage 2 Height [m]	1.100	1.100
Stage 3 Packing	Multipak II	Multipak II
Stage 3 Height [m]	1.078	1.078
Stage 4 Packing	Multipak II	Multipak II
Stage 4 Height [m]	0.078	1.078
Stage 5 Packing	Multipak II	Multipak II
Stage 5 Height [m]	0.490	0.490
Stage 1 Packing	Sulzer BX	Sulzer BX
Stage 1 Height [m]	0.500	0.500

Note: Multipak II is the modified Multipak II with KATAPAK SP11 dry catalyst mass

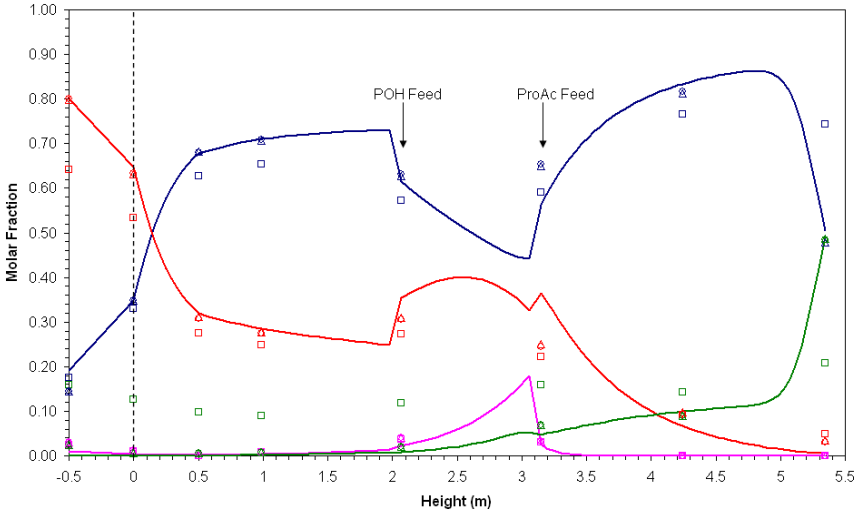

(a) Experiment 2

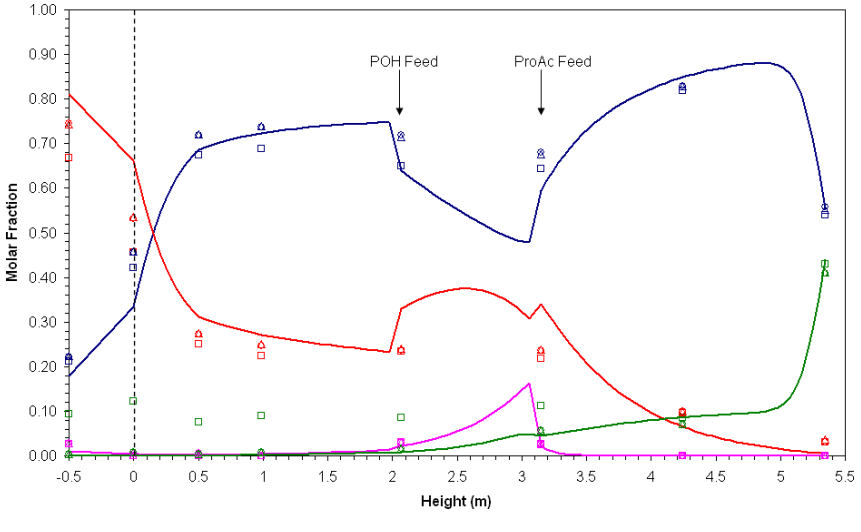

(b) Experiment 3

Figure 5.5: Data reconciliation for Propyl Propionate Production: Composition Profiles (Symbols - Experimental Data: □ - Sample 1; ○ - Sample 2; Δ - Sample 3; Simulation Data: —. Colours: ■ POH; ■ ProAc; ■ ProPro; ■ Water)

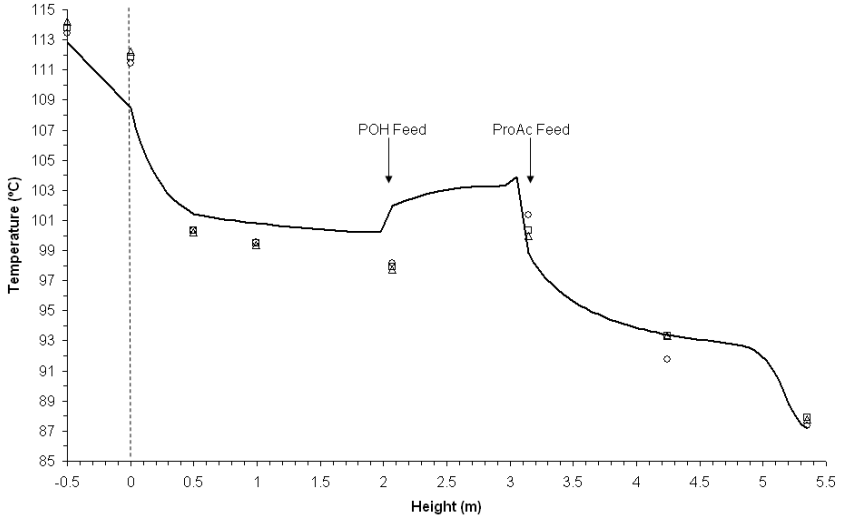

(a) Experiment 2

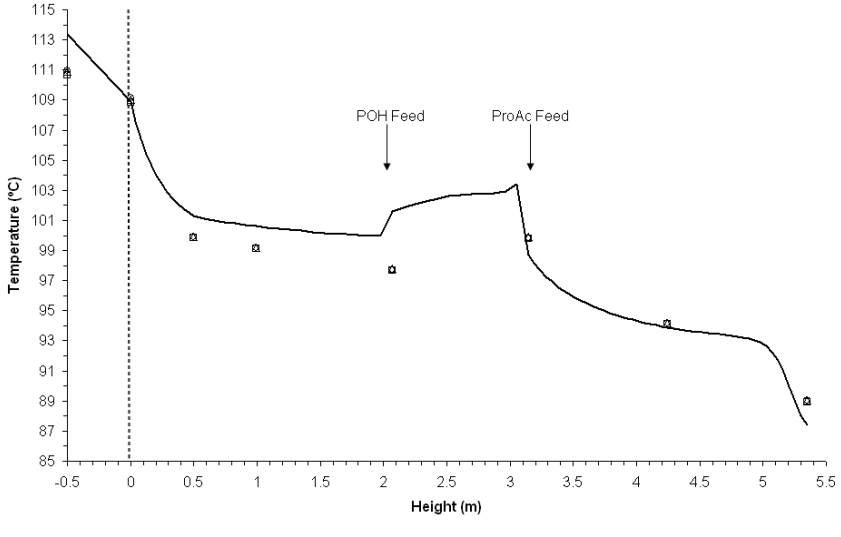

(b) Experiment 3

Figure 5.6: Data reconciliation for Propyl Propionate Production: Temperature Profiles (Symbols - Experimental Data: □ - Sample 1; ◯ - Sample 2; Δ - Sample 3; —: Simulation Data)

appears to be very reasonable. Problems still exist, but they are minor, as will be discussed.

The first of these problems, common to both experiments, is the molar fractions of Stage 3, with Propyl Propionate being over-evaluated and Propanol under-evaluated. There is no easy explanation for this, but it should be noticed that the distributor from where the sample is collected is also where the Propionic Acid stream is fed into, which can result in the sample collected not being well mixed, but rather containing a part of the feed. The fact that the rest of the profile fits far better than this single point helps supporting this theory.

The second problem is related to Experiment 3. There is constant deviation of the Propanol and Propyl Propionate simulated composition profiles to the experimental data points and this situation is particularly noticeable in the reboiler, with absolute errors of 5%. As discussed in the previous Chapter, Experiment 3 suffered some problems, most importantly an undetected leak. Although the leak was small, with a an average value of 0.05 $kg.h^{-1}$ - 2.5% of the feed flowrate - this value is sufficient to disturb the reconciliation of the model with the actual data (e.g. changing the feed molar fractions from 0.67 to 0.65 for Propionic Acid and 1.33 to 1.35 for Propanol results in the bottom product composition matching the experimental values, which can mean that the acid feed was lower than what was measured).

Finally, there is a small deviation in the top stream, with the simulation predicting less Propyl Propionate than it actually exists. Once more, no immediate explanation exists, but two factors might contribute: first, existing VLE data are far from ideal (as mentioned in Chapter 2) and second, these concentrations are near the binary liquid phase region so it is possible that binary phases exist in parts of the the packing section, situation which is not accurately predicted by the model.

Regarding the temperature profiles, there are far more deviations, with the reactive section of the column being off by 1°C and the reboiler temperatures (before and after) having deviations of up to 3°C. The main explanation for this, besides possible mis-calibration of the thermocouples at higher temperatures, is related entirely to the error which the VLE data introduces into the system.

Despite these small problems, product streams are predicted with an acceptable error from an industrial standpoint - and this with patent inaccuracies in the VLE and packing data -and the work that is continuing to be done in both chemical system and model will iron

them out. All and all, the model proves to be quite robust and the overall experience (e.g. Klöker et al. (2005)) with its use has been positive, especially when accurate hydro- and thermodynamic data exists.

5.3 TAME Simulation

5.3.1 Model Setup

For the TAME reactive distillation, a similar column to the one used for the Propyl Propionate experiences will be simulated. The structure of the column will suffer some changes, as will be detailed further on, and the kinetics for TAME synthesis determined by Ferreira de Oliveira (2004) will be used. Analogous to what was done in Chapter 3, the Modified (Dortmund) UNIFAC model (Gmehling et al., 1993) will be used for activity coefficient determination and VLE calculations.

5.3.2 Column Parameters' Evaluation and Optimization

Since no optimisation method was implemented, the search for optimal column configurations had to be performed manually. In order to establish a methodology and explain how the search was executed, a "test configuration" will be investigated with regard to how process parameters affect the column's performance.

The "test configuration" consists of a similar column to that used in the Propyl Propionate synthesis, containing a total of six stages with heights of 1.1 m in each of the first four stages and 0.5 m in each of the last two. The starting configuration contains two reactive Multipack II packings, in stages 3 and 4, and Sulzer BX packings in the remaining stages. Two streams are fed into the column, above stage 3 and below stage 4 (Distributors 3 and 5), with the topmost stream (Feed1) containing pure Methanol and the bottom feed stream (Feed2) containing an equimolar mixture of 2-Methyl-1-Butene and 2-Methyl-2-Butene. The mass flowrates of each stream has a value of 1 $kg.h^{-1}$ and a feed temperature of 90°C. The initial reflux ratio was set to 1 and the distillate stream to 1 $kg.h^{-1}$. The operating pressure of the column is of 5 bar.

The search methodology involves changing one parameter at a time - with the exception of the feed flowrates, because the total inflow had to be constant; this means that, e.g., changing Feed1 from 1 to 0.9 $kg.h^{-1}$ results in changing Feed2 from 1 to 1.1 $kg.h^{-1}$ - in order

to be able to establish the influence of that parameter upon the initial configuration. In Table C.1, available in Appendix C, the conditions under which each simulation was run are presented.

To better evaluate the performance of the column, a set of benchmark parameters were calculated. They consist of absolute performance parameters - conversion of the reactants (Eq. 5.21) and TAME's yield (Eq. 5.22), mass-based purity (equal to TAME's mass fraction in the bottom stream) and molar-based purity (equal to TAME's molar fraction in the bottom stream) in the Bottoms stream - and their differential, or "delta", to the initial configuration. All the values are given, for convenience, in percentages and x_i^D corresponds to the molar fraction of i in the Distillate stream, x_i^B to the molar fraction of i in the Bottoms stream, x_i^1 and x_i^2 to the molar fractions of i in Feed1 and Feed2 streams, d to the molar flowrate of the Distillate stream, b to the molar flowrate of the bottoms stream and f1 and f2 to the molar flowrates of the Feed1 and Feed2 streams. These values, together with top and bottom compositions and the reboiler heat duty, are presented in Table C.2 of Appendix C.

$$Conv_i = 1 - \frac{x_i^D\ d + x_i^B\ b}{x_i^1\ f1 + x_i^2\ f2} \tag{5.21}$$

$$Yield = \frac{x_{TAME}^B\ f}{x_{TAME}^D\ d + x_{TAME}^B\ b} \tag{5.22}$$

The first parameter analysed to determine its influence in the column behaviour was the Distillate flowrate - or, more correctly, the ratio between Distillate and Bottoms flowrates, since the sum of both is always equal to 2 kg.h^{-1}. In Fig. 5.7 it can be seen that any change to the Distillate flowrate worsens the results of the column. The only parameter that increases with a change in this flowrate - a decrease, to be more precise - is the yield of TAME at the bottom, which is obvious since less is coming out at the top. Also, the conversion of 2M1B is not affected much by changes in the distillate flowrate - except when it falls to 0.7 kg.h^{-1}. All the other parameters decrease when the distillate flowrate is changed, especially the conversion of 2M2B which reaches negative conversion - i.e., overall, 2M2B is produced (from 2M1B) and not consumed.

The second parameter deals with another flowrate ratio, the MeOH / 2MxB ratio (or, Feed1 / Feed2 ratio). For convenience's sake, the results presented in Fig. 5.8 are in order to the Methanol flowrate, since the sum of both feeds is always constant and equal to 2 kg.h^{-1}.

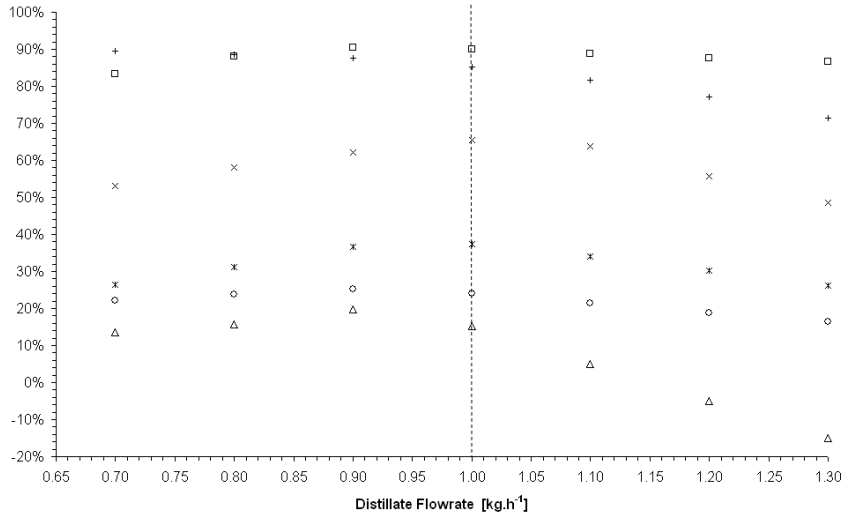

Figure 5.7: Influence of the Distillate Flowrate in the "Test Column" behaviour (Conversion: □ - 2M1B; Δ - 2M2B; ◯ - MEOH. TAME (Bottoms): + - Yield; × - Mass-based Purity; ∗ - Mole-based Purity). - - -: Starting Configuration

The most obvious - and expected - trend in this case is Methanol conversion, which increases when the Methanol Feed decreases. TAME's purity in the Bottoms stream also increases - again, as expected, since most of the Bottoms stream is composed by a MeOH-TAME mixture - but this effect "appears" to affect only molar purity. This is due to TAME having the highest molecular mass in the system, especially when compared to Methanol. The conversion of the isoamylenes is reduced by either an increase or decrease of the Methanol feed stream, which is related to an increase in their own feed flowrate into the system.

The last flow-related parameter which was investigated is the Reflux Ratio - which is defined as the ratio between condensate refluxing into the column and condensate being withdrawn from the column. Fig. 5.9 presents the results obtained when this parameter is changed. The decrease of the reflux ratio seems to have little effect in the process, although a small increase of all the parameters is obtained when it is reduced from 1 to 0.9. The increase of the reflux ratio, on the other hand, has a strong effect in the column's results, with all the relevant parameters - except for TAME yield, which decreases and

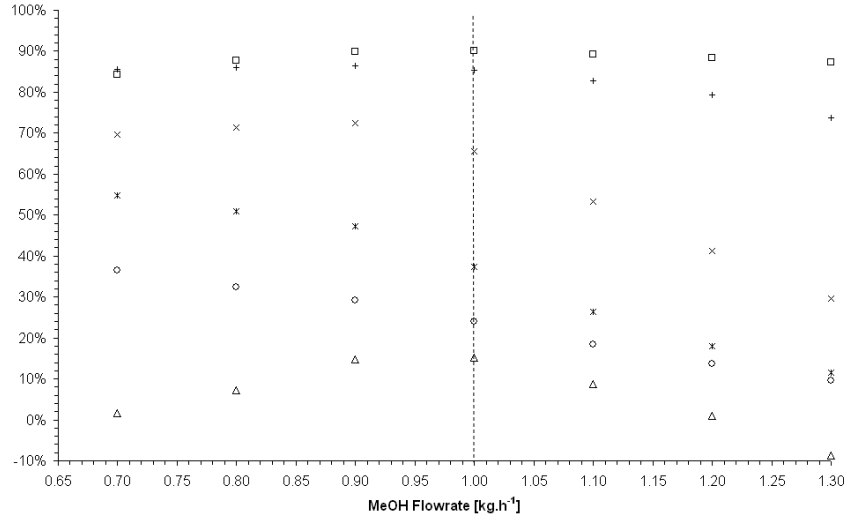

Figure 5.8: Influence of the MeOH/2MxB Feed Ratio in the "Test Column" behaviour (Conversion: □ - 2M1B; Δ - 2M2B; ◯ - MEOH. TAME (Bottoms): + - Yield; × - Mass-based Purity; ∗ - Mole-based Purity). - - -: Starting Configuration

then increases - falling sharply.

Finally, the effect of the operating pressure was also investigated. It should be noted that, in this case, only a decrease of pressure would be of value for actual use, since an increase would result in overall higher temperatures which would almost certainly exceed the maximum recommended operating temperature for the catalyst. Either way, the results are presented in Fig. 5.10 and, as can be seen, the effect is small in most parameters, except when the pressure goes down to atmospheric values, in which case the performance of the column falls sharply.

Together with the operating conditions, structural changes to the column were investigated. Simulations 25A to 29A deal with those changes. These changes involved changing the location of the feed streams and changing the type of packing from non-reactive to reactive. Table 5.2 presents the results, where it can be seen that the change of location for the feed streams resulted always in a decrease of column performance, most noticeably when the feeds where merged into a single one, fed to the middle of the column. Adding packings, on the other hand, resulted in a slight increase of performance.

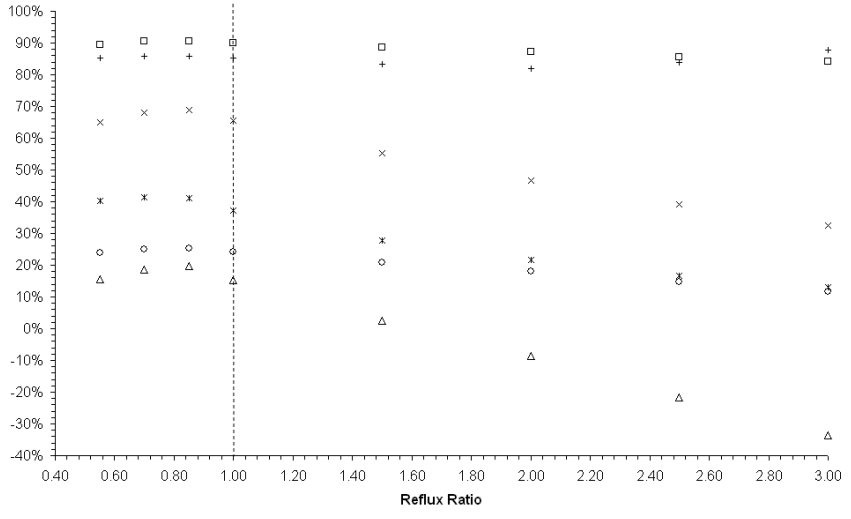

Figure 5.9: Influence of the Reflux Ratio in the "Test Column" behaviour (Conversion: □ - 2M1B; Δ - 2M2B; ◯ - MEOH. TAME (Bottoms): + - Yield; × - Mass-based Purity; ∗ - Mole-based Purity). - - -: Starting Configuration

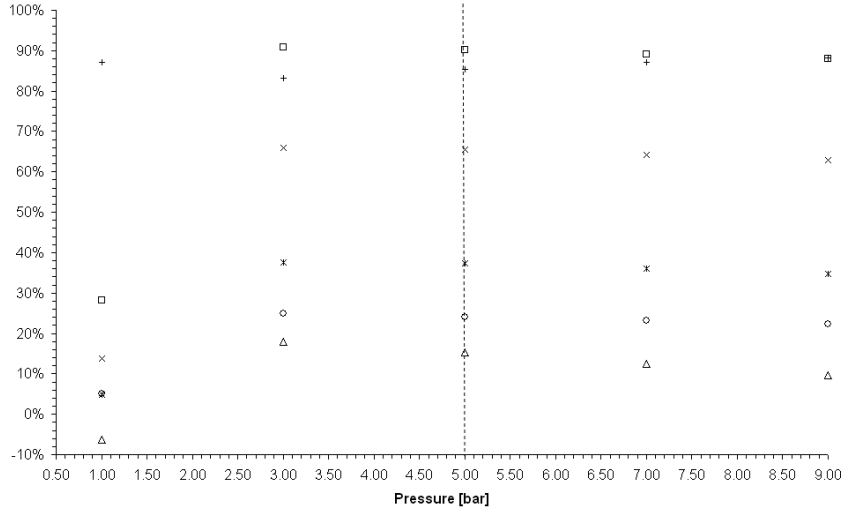

Figure 5.10: Influence of the Pressure in the "Test Column" behaviour (Conversion: □ - 2M1B; Δ - 2M2B; ◯ - MEOH. TAME (Bottoms): + - Yield; × - Mass-based Purity; ∗ - Mole-based Purity). - - -: Starting Configuration

Table 5.2: Effect of Structural Changes in the "Test Column" behaviour

		25A	26A	27A	28A	29A
	Change Made:	Feed 1 → St.4	Feed 2 → St. 4	Feeds 1+2 → St. 4	St. 5 → MP-II	St.5+2 → MP-II
Conv.	2M1B	89.03	89.10	85.67	90.27	90.26
	2M2B	06.67	08.10	-23.30	16.17	16.85
	MeOH	21.86	22.20	14.27	24.32	24.47
TAME	Yield	82.86	83.77	84.74	85.55	85.20
	Mol. P.	30.01	31.37	16.43	38.21	38.35
	Mass P.	57.76	59.31	38.53	66.34	66.47
ΔConv.	2M1B	-01.07	-00.99	-04.43	00.18	00.16
	2M2B	-08.61	-07.18	-38.58	00.89	01.57
	MeOH	-02.21	-01.87	-09.80	00.24	00.39
ΔTAME	Yield	-02.47	-01.56	-00.60	00.22	-00.13
	Mol. P.	-07.31	-05.95	-20.89	00.89	01.03
	Mass P.	-07.74	-06.19	-26.97	00.84	00.97

Conv. - Conversion; Mol. P. - Molar-based Purity; Mass P. - Mass-based Purity; MP-II - Multipak II; St. - Stage; Conv., TAME, ΔConv., ΔTAME in [%]

In terms of actual search pattern, it would start by adopting a condition change that resulted in an increase of the desired parameters (e.g. decreasing the MeOH / 2MxB ratio) and then re-evaluate the effect of the other conditions. After a new increase is found, that change is adopted and the process is repeated until no improvement can be made or until the cost of improving the process exceeds the benefit of changing (e.g. refluxing, recirculating or heat costs). This process, in more simple terms, can be compared with a single parameter search algorithm, with parameter change at the end of each step. It is, of course, less efficient than an automated method which comprises a search vector, thus being able to adjust several variables at once, but has the advantage of better convergence because the process is followed closely. The main problem with automated optimisation methods are the discrete parameters, usually related to the column structure, which cannot easily be optimised, even more so when a change in column structure usually requires a full run (i.e. from the

simpler to the more complex models) to be executed.

5.3.3 Optimised Configurations

5.3.3.1 Pure Isoamylenes Feed

Using the method presented previously, it is possible to reach an optimised configuration for the column, but what is the "optimal" needs to be established first. The "perfect" optimal point for an RD column is full conversion and full separation at the lowest cost (i.e. lowest reflux and lowest heat duty) possible. This is for most processes, of course, unattainable. TAME synthesis, if done from pure reactants, has two advantages in this aspect: one, there is only one product of reaction, and two, TAME is the highest boiler. This means that TAME will always go downwards and that no other product needs to be separated. So, ideally, the column should be fed the reactants and return a pure TAME stream at the bottom. Since no product comes out at the top, the column would operate at total reflux.

Since PROFILER does not directly support total reflux, without extensive remodelling, an approximation was used. The Reflux Ratio was set at 1000 and a "purge" distillate stream with a flowrate of 0.5% of the total feed (i.e. 0.01 $kg.h^{-1}$ and resulting in a reflux flowrate of 10 $kg.h^{-1}$) was allowed. Also, the top stage was reduced in height (from 1.1 m to 0.5 m) while stage 4 was heightned (from 0.5 m to 1.1 m), since almost no separation is needed in the upper stages (the 0.5 m separative stage was kept in order to help convergence). In accordance with this principle, Stage 2 was also "equipped" with Multipak II reactive packings and the feed streams moved up. The full structural configuration of the column can be seen in Table 5.5

These assumptions are not without some possible problems, however. Since the reflux flowrate is calculated from the reflux ratio and the distillate stream, by setting both it forces the column to provide the necessary flowrate and it does so by increasing the heat duty of the reboiler to "boil up" more liquid. So, the energy spending increases significantly. One way to decrease costs is to reduce the operating pressure, since the liquid phase will boil at lower temperatures, but this decrease has to be well monitored to avoid: a) unwanted boilup (if the boiling temperature falls below room temperature) and b) reducing excessively the reaction rate. For this simulation, the pressure was reduced in half, from 5 bar to 2.5 bar. The operating parameters used and resulting reboiler heat duty can be found in Table 5.3.

Table 5.3: General operating parameters of the column

Pressure	Reflux Ratio	Heat Duty
2.50	500.0	462.1

Pressure in [bar]; (Reboiler) Heat Duty in [W]

Table 5.4: Column streams compositions and flowrates

	Feed1	Feed2	Distillate	Bottoms
T [°C]	60.00	60.00	55.02	118.62
x_{2M1B}	0.000	0.500	0.559	0.000
x_{2M2B}	0.000	0.500	0.216	0.000
x_{MeOH}	1.000	0.000	0.225	0.004
x_{TAME}	0.000	0.000	0.000	0.996
Flowrate	0.627	1.373	0.010	1.990

Flowrates in [$kg.h^{-1}$]

Table 5.5: Column Structure

	Packing	Height [m]	Inflows
Stage 1	Sulzer BX	0.50	-
Stage 2	Multipak II	1.10	Feed1
Stage 3	Multipak II	1.10	Feed2
Stage 4	Multipak II	1.10	-
Stage 5	Sulzer BX	1.10	-
Stage 6	Sulzer BX	0.50	-

Table 5.6: Benchmark results

Conversion			TAME
2M1B	99.07	Yield	100.0
2M2B	99.64	Molar Pur.	99.58
MeOH	99.40	Mass Pur.	99.86

Pur. - Purity; All values in [%]

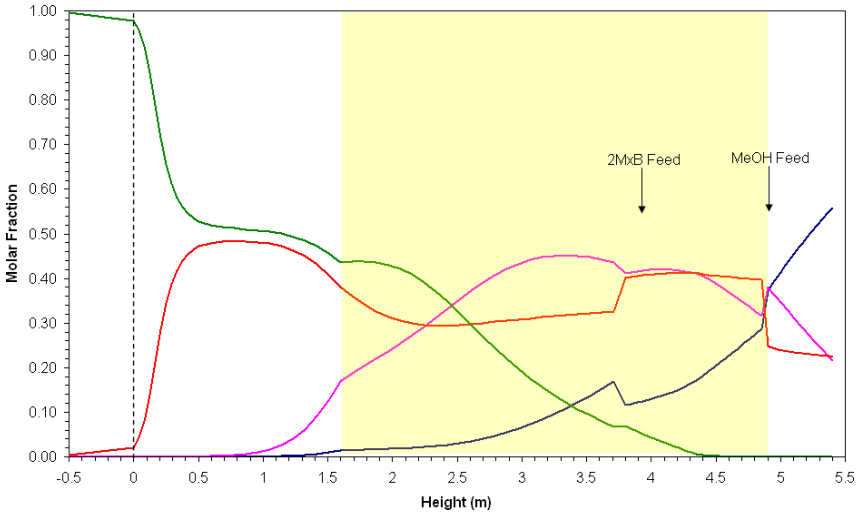

Figure 5.11: Composition profile of the full-reflux equimass column (— 2M1B: — 2M2B; — TAME; — MeOH; — Reboiler boundary; Yellow Area: Reactive Section)

As can be seen from the bottom composition (Table 5.4), it is composed of mostly TAME with a small residue of Methanol. In terms of the benchmark parameters established before, they all exceed 99%, with the yield of TAME being of 100% and its purity, molar- or mass-based, being over 99.5%. The top distillate stream - which is, for all effects, a purge stream - contains only reactants. The feed streams composition is exactly equimolar in terms of a 2MxB/MeOH ratio which confirms what was stated by Ferreira de Oliveira (2004) for plug-flow reactors - that an equimolar feed ratio is the ideal ratio for TAME synthesis - and extends this conclusion to reactive distillation.

The composition profile of the column (Fig. 5.11) is straightforward to analyse. TAME is being constantly removed downwards from the reactive section, while the isoamylenes are being pushed up. Methanol, as an intermediate boiler has a more even distribution along the column, with the exception of the lower stage (Stage 6) where it is separated from TAME. This results in high concentrations of reactants in the reactive region, thus explaining the very high conversions. This composition distribution results in a very steep temperature profile (Fig. 5.12) with a total variation of over 60°C, which, in a way, can be seen as the driving force behind the separation.

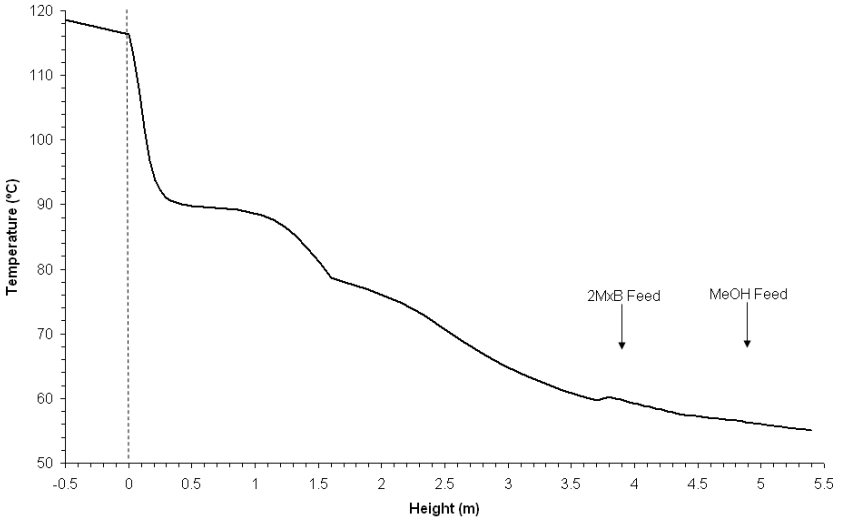

Figure 5.12: Temperature profile of the full-reflux equimass column

A final consideration regarding these simulations should me made. It was assumed, together with the column structure, that the total feed flowrate (and, in consequence, the total product flowrate) is equal to 2 kg.h^{-1}. This value was chosen because all the Propyl Propionate simulations and experimental runs were done with it, but it does not, in any way, correspond to an optimum flowrate for the column. In fact, and for example, increasing the total flowrate to 3 kg.h^{-1}, while maintaining the feed ratios and the "purge" percentage equal, results in a substantial decrease of TAME purity at the Bottoms stream from 99.58% to 80.64%, mole-based) and conversion of the reactants (from 99.64% to 79.05% for 2M2B and from 99.40% to 88.93% for MeOH). This can be corrected by increasing the column's temperature (via an increase in the operating pressure). In the example given, an increase of 0.1 bar is sufficient to bring the system back to good results. This correction is not always sucessful because, eventually, the positive and negative effects of a pressure increase even out, on one hand, and the packings ability to efficiently contact and transfer mass as well as the catalyst capacity will start to saturate, on the other.

During this work, a total mass flowrate of up to 6 kg.h^{-1} was found to be attainable with similar benchmark parameter results to the main simulation, using an operating pressure of 3.37 bar. This, of course, implies also higher operating costs, namely a reflux stream of

15 kg.h^{-1} and a reboiler heat duty of 1300 W. Above these flowrates - and assuming always a minimum increase of 1 kg.h^{-1} the purity of TAME and the conversion of the reactants start to reduce more significantly.

Despite these good results, a warning should be made that the model was not tested thoroughly at higher pressures and, as such, some correlations used might not apply.

5.3.4 Other Impure Isoamylenes Feeds

One of the problems when studying the feasibility of a chemical being produced by any process are the differences that exist between the operating conditions which are assumed for research purposes and the actual conditions under which an industrial process would be implemented. One of the most usually overlooked aspects is the purity of the feed streams and TAME synthesis is a perfect example of that.

Oost and Hoffmann (1995) mention, in their work, that most TAME is not produced from pure isoamylene stock, but rather from C_5 cuts taken from FCC or steam cracking. These cuts contain, in weight, around 25% reactive isoamylenes (Krause and Hammarstrom, 1987; Oost and Hoffmann, 1995) and the rest is made of non-reactive C_5 compounds and some residue C_4 and C_6 compounds as well (Piccoli and Lovisi, 1995; Ferreira de Oliveira, 2004).

The introduction of a feed stream, with high amounts of impurities (75% weight) into a reactive distillation column will result in a drastic deacrese of production efficiency, because a large part of the available separation capacity will be "dedicated" to removing the impurities, rather than removing Methanol and 2MxB from the bottom stream. Also, since boiling points will change, the reaction will also be affected. It is true that the problem can be solved by distilling the bottoms stream further on, since the higher boiling point of TAME will likely allow for full separation, but this requires the existence of a reflux stream. Another possibility is the previous purification of the isoamylenes stream, which will likely prove difficult - or expensive - due to the compounds sharing a similar basic chemical structure, resulting in a narrow range of boiling points.

5.4 Alternatives to Reactive Distillation

5.4.1 Pre-reactor

Although not an alternative *per se*, the introduction of a Pre-reactor usually helps the process by reducing the number of reactive stages and/or the amount of catalyst spent in the process. In the case of TAME with pure isoamylenes as feed, although it is likely it would help, it is unnecessary since full conversion and product purity are easily attainable.

In the case of a non-pure isoamylenes feed, it will likely prove very helpful, since it will help create an adequate temperature profile across the column due to the existence of significant amounts of TAME from the start. Although no simulations were run to this end, it is expectable that very good product purity - or at least, easily separable two-component compositions - will be reached in the Bottoms stream. Also, some reaction of the remaining reactants is also likely to occur, increasing the process conversion when compared with a single reactor scheme. Recycle streams will be needed, of course, but the system can be expected to operate adequately.

A good example of this configuration is CDTech's CDTAME process (Chapter 1, Fig. 1.8) which includes a pre-reactor and operates in excess methanol, which is recovered later on and recycled back into the system. Although no information regarding the isoamylenes exist, the structure of the process indicates that total or near-total conversion occurs - which can be obtained with the right amount of Methanol to shift the chemical reaction.

5.4.2 Reactor plus Distillation Column

This alternative represents a classic setup of Process Engineering, with reaction occurring followed by product separation. It consists of reactor (usually plug-flow) followed by a distillation column where the product is separated (in this case in the bottoms streams) and the remaining recycled back to the reacting step. In the case of TAME, there is an additional need for removal of the non-reactive components of the C_5 cut, or else they will accumulate. This can be done via an additional distillation column, in which Methanol is separated from the others. If, as in the example given before, excess Methanol is used, good isoamylene conversion can be expected and reactant loss will not be very large.

Neste's NExTAME process (Chapter 1, Fig. 1.7) is similar in concept (reactor plus distillation column) but with a different schematic, since a sidedraw is taken from the column and recycled back to the reactor - which contains most of the unreacted methanol - while TAME exits via the Bottoms stream, together with unreacted compounds and the lighter compounds are removed in the distillate. It is expectable that TAME is purified further upstream by means of distillation processes. This process has a different approach towards TAME's production compared to CDTAME, since here Methanol is fully reacted while in CDTAME's case, the isoamylenes are the ones which are expected to be fully converted.

NOMENCLATURE

Variables / Constants

a_j	Interfacial area	$[m^{-2}]$
b	Molar Bottoms flowrate	$[mol.s^{-1}]$
c_t	Total molar concentration	$[mol.m^{-3}]$
$Đ_{i,k}^{V}$	Maxwell-Stefan diffusivity of the binary component pair i, j	$[m^2.s^{-1}]$
d	Molar Distillate flowrate	$[mol.s^{-1}]$
E_j/e_j	Interfacial heat flux in stage j	$[J.m^{-2}.s^{-1}]$
F_j	Liquid / Vapour Feedstream flowrate in stage j	$[mol.s^{-}1]$
$f1/f2$	Molar Feed1/Feed2 flowrates	$[mol.s^{-1}]$
H_j	Liquid / Vapour Molar Enthalpy in stage j	$[J.mol^{-1}]$
h_j	Interfacial Heat transfer coefficient of stage j	$[J.K^{-1}.s^{-1}]$
$K_{i,j}$	Vapour-Liquid Equilibrium constant for component i in stage j	[-]
L_j	Liquid flowrate exiting stage j	$[mol.s^{-1}]$
$N_{i,j}$	Molar interfacial flux of component i in stage j	$[mol.m^{-2}.s-1]$
p_j	Pressure in stage j	$[Pa]$
Q_j	Liquid / Vapour transfer in/out of stage j	$[W]$
R	Universal Gas Constant = 8.314	$[J.mol^{-1}.K^{-1}]$
$r_{n,j}$	Rate of reaction n in stage j	$[mol.s^{-1}]$
S_j	Liquid / Vapour Sidedraw flowrate in stage j	$[mol.s^{-1}]$

T	Temperature	$[K]$
t	Time	$[s]$
U_j	Liquid holdup in stage j	$[mol]$
V_j	Vapour flowrate exiting stage j	$[mol.s^{-1}]$
$x_{i,j}$	Liquid-phase molar fraction of component i in stage j	[-]
$y_{i,j}$	Vapour-phase molar fraction of component i in stage j	[-]
$z_{i,j}$	Liquid-/Vapour-phase molar fraction of component i in the feedstream of stage j	[-]

Greek Letters

η	Relative Film Thickness (Maxwell-Stefan)	[-]
η	Murphree Efficiency	[-]
λ_j	Convection Driving Force in stage j	$[W.m^{-2}.K^{-1}]$
μ_i	Chemical Potential of component i	$[J.mol^{-1}]$
$\nu_{i,n}$	Stoichiometric Coefficient of component i in reaction n	[-]

Indexes

Superscript

*	In Vapour-Liquid Equilibrium
1	Feed1
2	Feed2
B	Bottoms Stream
D	Distillate Stream
F	Feed Stream
I	At the Interface
L	Liquid phase
V	Vapour phase

Subscript

i	Dummy argument for component
j	Stage number
n	Reaction number
nc	Total number of components in system
m	Total number of chemical reactions

Abbreviations and Acronyms

2M1B	2-Methyl 1-Butene
2M2B	2-Methyl 2-Butene
2MxB	Isoamylenes (2M1B+2M2B)
EQ	EQuilibrium stage model
MeOH	Methanol
MERSHQ	Mass, Energy, transfer Rate, Summation, Hydraulic and interface eQuilibrium distillation model
MESH	Mass, phase Equilibrium, Summation and entHalpy distillation model
NEQ	Non-EQuilibrium stage model
TAME	Tertiary-Amyl Methyl Ether
VLE	Vapour-Liquid Equilibrium

BIBLIOGRAPHY

Billet, R., Schultes, M., 1999. Prediction of mass transfer columns with dumped and arranged packings. Trans. IChemE 77 (Part A), 498–504.

Buchaly, C., Duarte, C., Loureiro, J. M., Kreis, P., September 2005. Process intensification of n-propyl propionate synthesis using reactive distillation over a novel catalyst. In: ChemPor 2005 - 9th International Chemical Conference. Coimbra, Portugal.

Egorov, Y., Menter, F., Klöker, M., Kenig, E. Y., 2005. On the combination of cfd and rate-based modelling in the simulation of reactive separation processes. Chem. Eng. Process. 44, 631–644.

Ferreira de Oliveira, M. M. V., 2004. TAME: Cinética em reactor fechado e simulação da produção em contínuo. Ph.D. thesis, Faculty of Engineering of the University of Porto.

Gmehling, J., Li, J., Schiller, M., 1993. Modified unifac model. 2. present parameter matrix and results for different thermodynamic properties. Ind. Eng. Chem. Res. 32, 178–193.

Górak, A., Hoffmann, A., 2001. Catalytic distillation in structured packings: methyl acetate synthesis. AIChE J. 47, 1067–1076.

Hoffmann, A., Noeres, C., Górak, A., 2004. Scale-up of reactive distillation columns with catalytic packigns. Chem. Eng. Process. 43, 383–395.

Klöker, M., Kenig, E. Y., Hoffmann, A., Kreis, P., Górak, A., Jun. 2005. Rate-based modelling and simulation of reactive separations in gas/vapour-liquid systems. Chem. Eng. Process. 44 (6), 617–629.

Kołodziej, A., Jaroszyński, M., Hoffmann, A., Górak, A., 2001. Determination of catalytic packing characteristics for reactive distillation. Catal. Today 69, 75–85.

Kołodziej, A., Jaroszyński, M., Schoenmakers, H., Althaus, K., Geißler, E., Übler, C., Klöker, M., 2005. Dynamic tracer study of column packings for catalytic distillation. Chem. Eng. Process. 44, 661–670.

Krause, A. O. I., Hammarstrom, L. G., 1987. Etherification of isoamylenes with methanol. Appl. Catal. 30, 313–324.

Krishna, R., 1979. Mass and energy transfer in multicomponent systems. Chem. Eng. Commun. 3, 201–275.

Krishna, R., Wesselingh, J., 1997. Maxwell-stefan approach to mass transfer. Chem. Eng. Sci. 52, 861–911.

Krishnamurthy, R., Taylor, R., 1985a. A nonequilibrium stage model of multicomponent separation processes. part i: model description and method of solution. AIChE J. 31, 449–456.

Krishnamurthy, R., Taylor, R., 1985b. A nonequilibrium stage model of multicomponent separation processes. part ii: comparison with experiment. AIChE J. 31, 456–465.

Krishnamurthy, R., Taylor, R., 1985c. A nonequilibrium stage model of multicomponent separation processes. part iii: the influence of unequal component efficiencies in process design problems. AIChE J. 31, 1973–1985.

Lewis, W. K., Whitman, W. G., 1924. Principles of gas absorption. Ind. Eng. Chem. 16, 1215–1220.

Miller, C., Kaibel, G., 2004. Packings for fixed bed reactors and reactive distillation. Chem. Eng. Sci. 59, 5373–5379.

Murphree, E. V., 1925. Rectifying column calculations with particular reference to n component mixtures. Ing. Eng. Chem. 17, 747–750.

Oost, C., Hoffmann, U., 1995. The synthesis of tertiary amyl methyl ether (TAME): microkinetics of the reactions. Chem. Eng. Sci. 51, 329–340.

Piccoli, R. L., Lovisi, H. R., 1995. Kinet and thermodynamic study of the liquid-phase etherification of isoamylenes with methanol. Ind. Eng. Chem. Res. 34, 510–515.

Rocha, J. A., Bravo, J. L., Fair, J. R., 1993. Distillation columns containing structured packings: a comprehensive model for their performance. 1. hydraulic models. Ind. Eng. Chem. Res. 32, 641–651.

Rocha, J. A., Bravo, J. L., Fair, J. R., 1996. Distillation columns containing structured packings: a comprehensive model for their performance. 2. mass-transfer model. Ind. Eng. Chem. Res. 35, 1660–1667.

Seader, J. D., Siirola, J. J., Barnicki, S. D., 1997. Perry's Chemical Engineers' Handbook, 7th Edition. McGraw-Hill, Ch. 13 Distillation.

Taylor, R., Kooijman, H. A., Hung, J. S., 1994. A 2nd generation nonequilibrium model for computer-simulation of multicomponent separation processes. Comp. Chem. Engng. 18, 205–217.

Taylor, R., Krishna, R., 1993. Multicomponent Mass Transfer. John Wiley, New York.

Taylor, R., Krishna, R., 2003. Reactive Distillation - Status and Future Directions. Wiley-VCH, Ch. 9 Modelling of Homogeneous and Heterogeneous Reactive Distillation Processes, pp. 217–240.

van Baten, J. M., Krishna, R., 2002. Gas and liquid phase mass transfer within katapak-s structures studied using cfd simulations. Chem. Eng. Sci. 57, 1531–1536.

6 Conclusions and Future Work

6.1 Conclusions

The first set of conclusions that should be taken relate to the title of this work, *Production of TAME and n-Propyl Propionate by Reactive Distillation*, or more precisely, the feasibility of the production of both compounds by Reactive Distillation. Both chemical systems present themselves, at first glance, as suitable for Reactive Distillation (RD).

TAME is produced from three other components (2-Methyl 1-Butene, 2-Methyl 2-Butene and Methanol) and no secondary products exist. Furthermore, TAME is the highest boiler, which points towards the possibility of total separation. Although experiments were not carried out for TAME synthesis, the use of the PROFILER model - which proved itself reliable - show that if the isoamylene feed is pure, full conversion and purity are possible (Chapter 5). It also shows that good modelling tools are becoming indispensable in designing, building and operating reactive distillation columns, since, as was shown in the Chapter dealing with it, small variations of the operating conditions can have significant effects on the distribution of products and column performance.

The use of preliminary modelling tools, such as Reactive Residue Curve Maps (RRCMs) - dealt with in Chapter 3 - can be a helpful tool in evaluating if a system is feasible for reactive distillation and under which conditions it should be operated, by defining the existing stationary points in the system and the distillation boundaries at any given set of operating conditions. Nevertheless, the simplification methods used to allow for bi-dimensional plotting of systems with more than three components should be approached with care. Although in the case of TAME, the curves were for the most part helpful, crossing of distillation boundaries under certain conditions were

shown to occur. In the case of a system such as Propyl Propionate, this was found to be impossible without significant treatment of the data or by sacrificing the ability to visually inspect the diagram.

The main constraint in using RRCMs for feasibility studies is their inability to deal with non-reactive packings, especially in columns which are known, beforehand, that the reactive section will be packed between two non-reactive sections. It does allow, however, when coupled with non-reactive RCMs to help determine if a certain composition is adequate for reaction, if its products can be separated or if it needs to suffer some kind of separation first.

All the simulation work (preliminary and full-scale) on TAME synthesis would qualify it for production by RD was it not the actual conditions under which it is produced, namely the use of C_5 cuts as feed stock. Nevertheless, industrial processes for the production of TAME both by reactive distillation and combined reactive and separative units exist. Also, the problem of the restriction being placed on the use of oxygenated petrol additives and the more popular MTBE and ETBE present a problem. An idea, and since TAME is a "summer additive" is to have a common structure for producing all of these compounds, just by switching feedstocks or even produce a blended additive. Several industrial processes, although designed primarily for MTBE production, already contemplate this possibility.

Propyl Propionate, on the other hand, is a compound which is only now finding its way into large-scale markets, such as paint additives. Propyl Propionate has the advantage, over its competitors, of being almost non-toxic, as its use as a food additive or its presence in fruits demonstrates. It can be produced from Propionic Acid and 1-Propanol - the system which was studied in this work -, but the reactive system has the disadvantage of, when using standard industry catalysts, producing by-products. The use of a novel catalyst was part of the research done in the course of this work and led to a new kinetic law which was never studied previously (Chapter 2). This kinetic law, which was found to fit a pseudo-homogeneous model thus eliminating the need for adsorptive data, shows that Propyl Propionate synthesis is favoured kinetically by higher temperatures, despite the reaction equilibrium suffering somewhat with temperature increase. It also shows that a kinetic law with a reasonable fit to experimental values can be determined even with indirect measuring of some components and a lack of good thermodynamic data.

Propyl Propionate's production by Reactive Distillation is favoured by the thermodynamic structure of the system, with Propyl Propi-

onate being the second highest boiler. By using an adequate ratio between the feedstocks, it is possible to obtain Propyl Propionate with a high degree of purity and reasonable conversions. The low number of experiments obtained for analysis (Chapter 4) do not allow the drawing of many conclusions to what are the ideal column conditions for the production of Propyl Propionate, although other incomplete experiences and the work which was continued at the University of Dortmund point towards pure Propyl Propionate streams being obtainable. What they can show is that PROFILER, the ACM model used for simulation, proves itself to be reliable and trustworthy, even with the poor quality thermodynamic data available (Chapter 5), having only small deviations from the experimental data and, even then, under specific conditions such as packing boundary regions.

6.2 Future Work

Regarding Propyl Propionate, work on its production by reactive distillation is still being carried out at the University of Dortmund and further experimental results are both expected and needed. Work on its RRCMs should also proceed, using topographical models to represent it in an efficient and intelligible way. The idea should be to establish a - if possible, computational - model which is able to extract and plot maps pertaining to important and significant operating regions. The evaluation of the process, by inclusion of pre- or side-reactors is also of interest, in order to evaluate a possible productivity increase, which will require modelling and experimental work with plug-flow and other type of chemical reactors. Finally, other catalysts should be tested and kinetic laws for them derived. This will require an evaluation of intraparticular mass transfer, including the adsorptive phenomenon.

For TAME, the step of carrying out experimental work remains to be done. This requires a column capable of operating at higher pressures - the column used was limited to atmospheric pressure and no other column was available - and the capability to sustain it. The interest of this research is limited, though. With the expected increase of the ban on oxygenated compounds as fuel additives and since TAME has no other known use, the interest in producing it is reducing day by day. It is acceptable to believe that TAME will be produced for some time longer, using the already installed industrial base and having as primary market developing countries which are

now abandoning lead-based additives, but this will not create any need for further research.

Regarding Reactive Distillation as a whole, there should be a more balanced equilibrium between separation and reaction. This is particularly important since distillation is, by definition, a dynamic process. Column start-up, shutdown and the impact of a change in the operating conditions are in need of further research, by the development of advanced unsteady-state models which include the most important transient phenomena in both mass transfer and reaction. This will likely help to reduce the time the column takes to get to a stationary state and thus increase its profitability.

Appendices

A GC CALIBRATION

A.1 GC Parameter Calibration

Before preparing calibration standards, which relate the peaks obtained in a chromatogram with the composition of the mixture being analysed, it is necessary to determine which operating parameters are the most adequate for the operation of the Gas Chromatograph (GC). These parameters include the volumetric flow of the gases (Carrier gas - Helium (He); Make-up gas - Nitrogen (N_2); Comburent gas: Air; Combustible gas: Hydrogen (H_2)), the temperature of the GC oven and the range of the detectors.

The volumetric flowrate of three of the gases (N_2, Air and H_2) are set in the chromatograph via manual needle valves while the flowrate of the carrier gas (He, in this case) is controlled in the GC software by setting the pressure in the capillary column. All of the flowrates are verified and calibrated with the help of a bubble meter.

The flowrates for each gas depend on two factors. The detector used, which sets the flowrates for the combustion gases (Air and Hydrogen) and the make-up gas; and the column used, which sets the value for the carrier gas. The correct settings for gas flowrates, according to the chromatograph's manufacturer specifications for the use of a Flame Ionisation Detector (FID) and a capillary column with an internal diameter of 0.53 mm and a total length of 25 m, are presented in Table A.1.

In reality, these flows were not controlled as exactly as they appear to be. The flowrate of hydrogen, for example, was adjusted in order to have a response from the detector, without any sample passing through it, of around 10 at range 1. The flowrate of the carrier gas was near the end of the value recommended by the manufacturer, in order to speed up analysis and avoid setting too low a pressure in the column (the pressure used was of 10 kPa). These small adjustments were necessary to improve the quality of the analysis, which was not

Table A.1: Gas flowrate specifications (Chrompack)

Gas	Flowrate
N_2	30
H_2	30
Air	250
He	1.45-2.15

Flowrates in ml/min

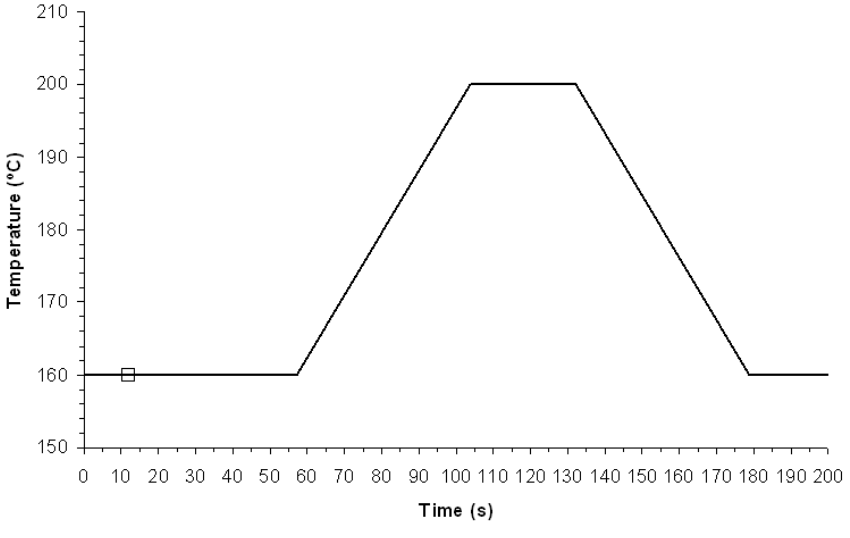

Figure A.1: Temperature programming of the GC (□ - Time of injection)

very good to start with.

Another parameter that needs to be set is the temperature of the oven. This value is limited upwards by the specification of the column and downwards by the speed of analysis. Usually, the higher the temperature, the fastest the analysis but also the poorer the separation. In this particular case, it was decided not to use a fixed temperature for analysis, but rather a "ramped" temperature. By ramped temperature one means that the temperature is increased and/or decreased during the experiment in order to speed up / separate better. The program used in this case is presented in a graphical form in Fig. A.1.

Finally, the range of the detector must be set. The range determines on which power of 10 (i.e. 10^{range}) will the detector work, in order to a), obtain good peaks (i.e. not too small) and b), not overload the detector (i.e. the analog signal not exceeding 1000 mV). The range used with the FID detector was constant throughout the experiments and had a value of 2.

A.2 Calibration Planning

In order to calibrate the FID of the GC, it is necessary to prepare standardised mixtures, with different compositions. These compositions are chosen to emulate real concentrations that are expected to exist at any given time inside the reactor.

Since the reaction will only occur in the forward direction (Eq. 2.2) and given the stoichiometry of the reaction, even if full conversion of the reactants was to occur, the maximum molar fraction of each one of the products would be of 0.5. So, no standard was prepared with a molar fraction of Water or n-Propyl Propionate over this value. The first 11 standards try to follow the progression of a (theoretical) irreversible reaction from an initial equimolar load of reactants (1-Propanol and Propionic Acid) to full conversion. The last three standards exist to accomodate non-equimolar loads, especially excess of alcohol. Although during the actual experiments initial loads with excess acid were deemed necessary (see page 48 of Chapter 2), no standards contemplating this situation exist, so all the values with a Propionic Acid molar fraction over 0.5 are extrapolated from the calibration curves.

The standards, for reasons of accuracy and precision, are prepared in mass basis and the resulting molar composition calculated from them. They were all prepared with a precision scale and from fresh pure components, to avoid contamination. Table A.2 presents the standards prepared and used in the calibration of the GC.

These standards were injected into the loop of valve V2, using a similar injection cycle as shown in Fig. 2.6 of Chapter 2, each sample being injected five times. A chromatograph of each standard is shown in Fig. A.2, with the order of the peaks being 1-Propanol first (starting at approximately 36 s), followed by Propionic Acid (starting at approximately 56 s) and finally n-Propyl Propionate (starting after 110 s, the exact starting point depending on its concentration).

Table A.2: GC calibration standards

	Mass fraction (w_i)				Molar fraction (x_i)			
Standard	POH	ProAc	ProPro	Water	POH	ProAc	ProPro	Water
1	0.4417	0.5583	0.0000	0.0000	0.4937	0.5063	0.0000	0.0000
2	0.4190	0.4798	0.0845	0.0167	0.4616	0.4289	0.0482	0.0613
3	0.3579	0.4415	0.1732	0.0274	0.3990	0.3993	0.0999	0.1018
4	0.3143	0.3861	0.2595	0.0402	0.3508	0.3496	0.1499	0.1497
5	0.2709	0.3132	0.3483	0.0677	0.2910	0.2730	0.1936	0.2425
6	0.2238	0.2786	0.4300	0.0677	0.2492	0.2517	0.2477	0.2514
7	0.1833	0.2198	0.5165	0.0804	0.2043	0.1989	0.2980	0.2988
8	0.1339	0.1690	0.5962	0.1009	0.1462	0.1497	0.3367	0.3674
9	0.0961	0.1113	0.6850	0.1076	0.1068	0.1004	0.3939	0.3989
10	0.0474	0.0555	0.7507	0.1464	0.0489	0.0465	0.4008	0.5038
11	0.0000	0.0000	0.8456	0.1544	0.0000	0.0000	0.4593	0.5407
12	0.5494	0.4506	0.0000	0.0000	0.6005	0.3995	0.0000	0.0000
13	0.6512	0.3488	0.0000	0.0000	0.6971	0.3029	0.0000	0.0000
14	0.7714	0.2286	0.0000	0.0000	0.8062	0.1938	0.0000	0.0000

POH: 1-Propanol; ProAc: Propionic Acid; ProPro: n-Propyl Propionate

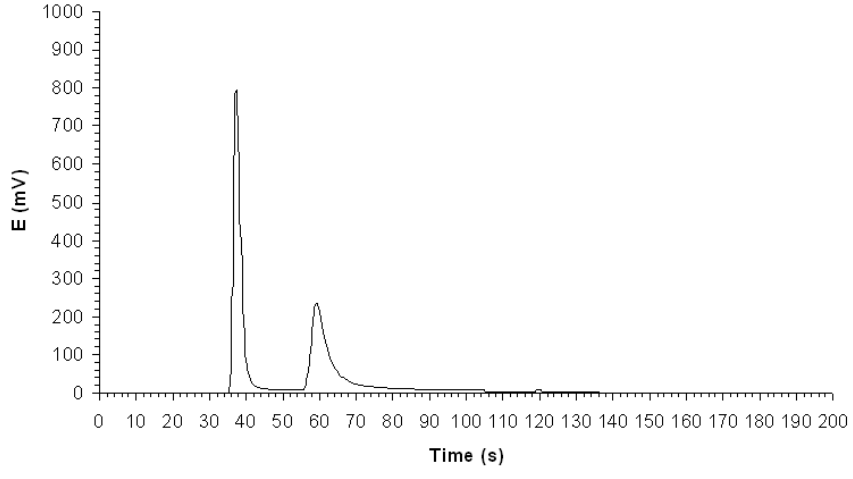

(a) P1 standard

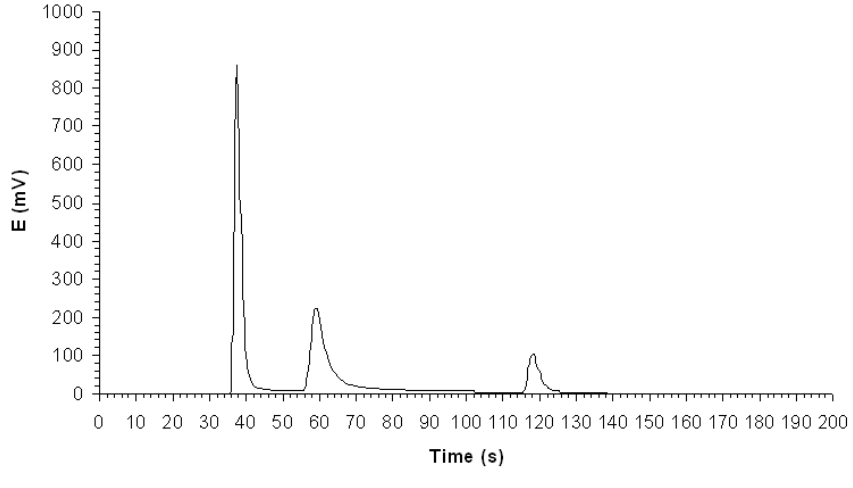

(b) P2 standard

Figure A.2: Chromatograms of the calibration standards

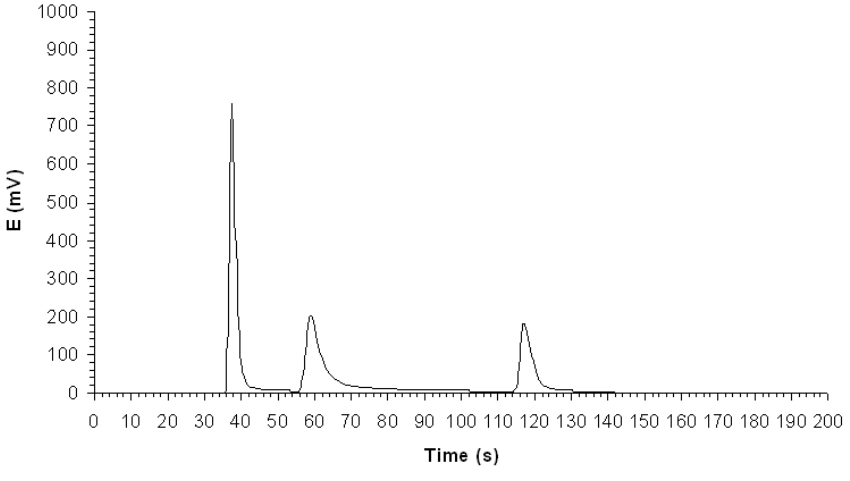

(c) P3 standard

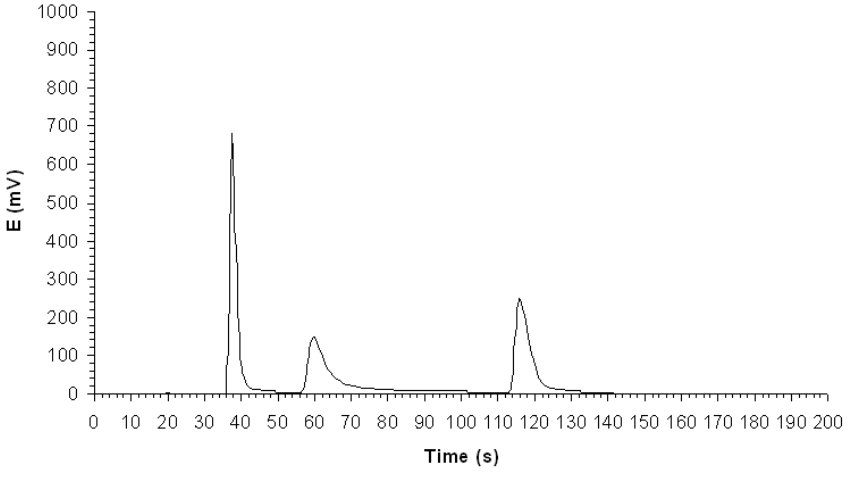

(d) P4 standard

Figure A.2: Chromatograms of the calibration standards (Continued)

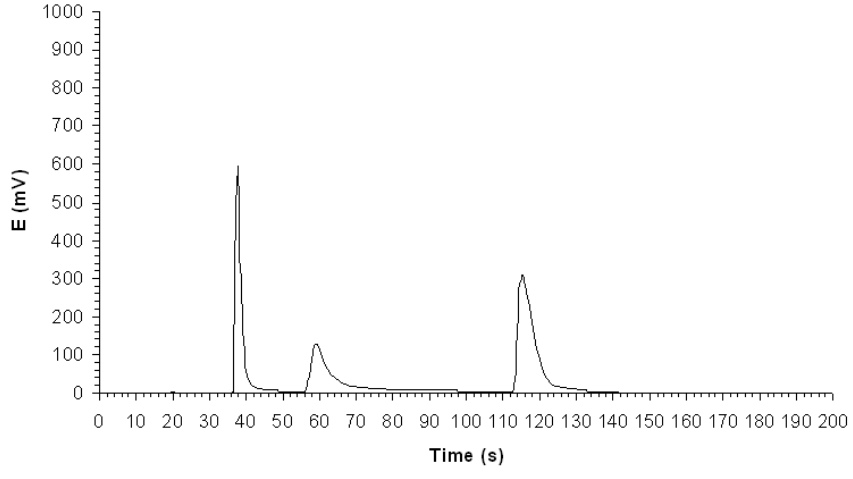

(e) P5 standard

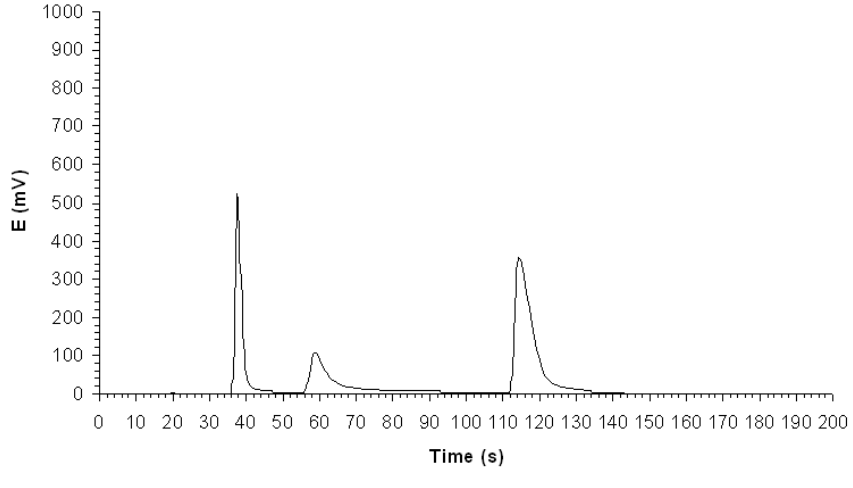

(f) P6 standard

Figure A.2: Chromatograms of the calibration standards (Continued)

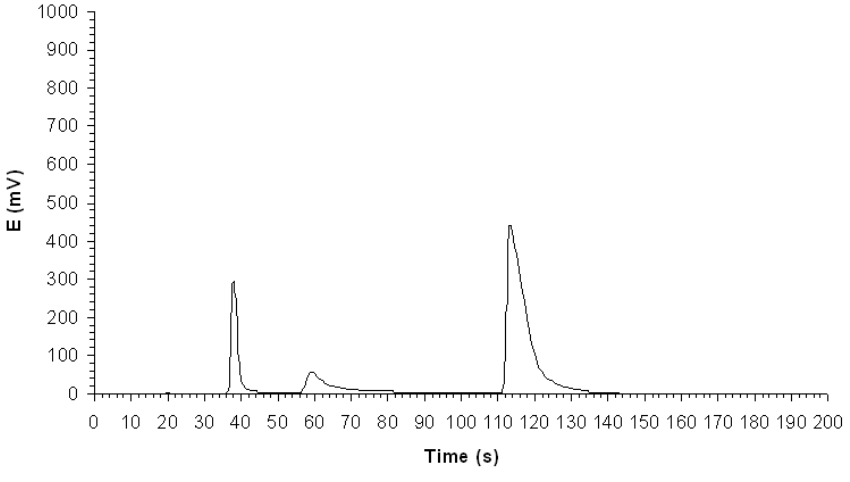

(g) P7 standard

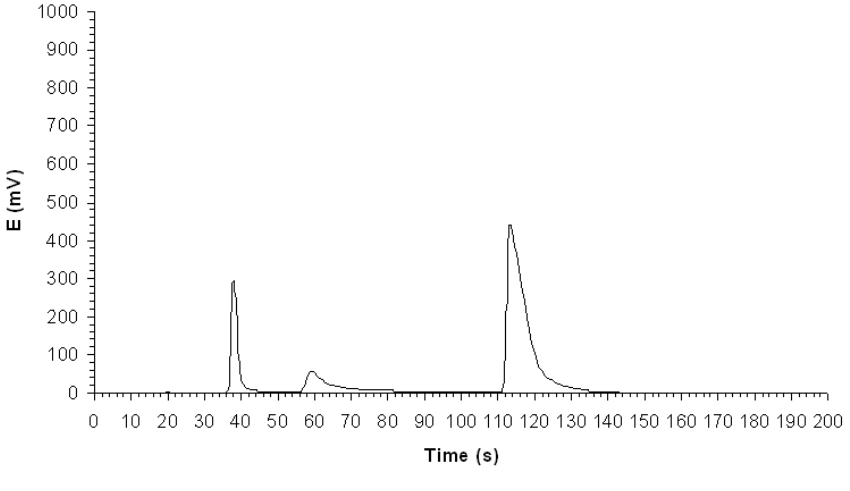

(h) P8 standard

Figure A.2: Chromatograms of the calibration standards (Continued)

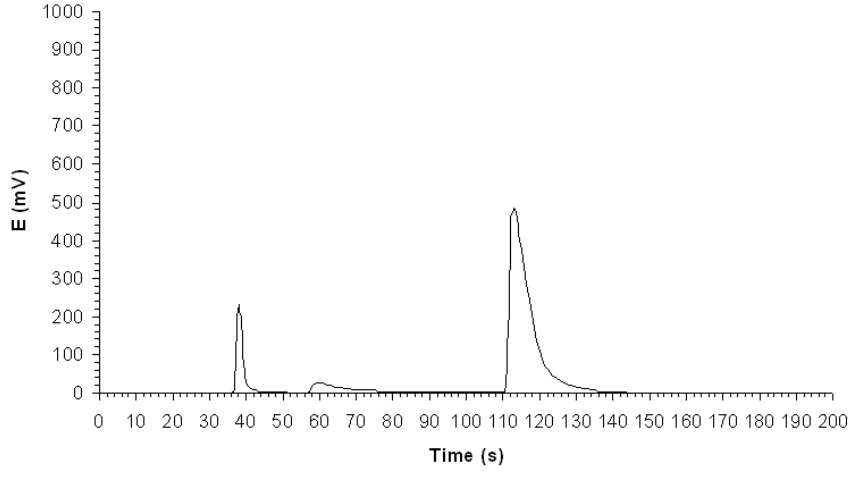

(i) P9 standard

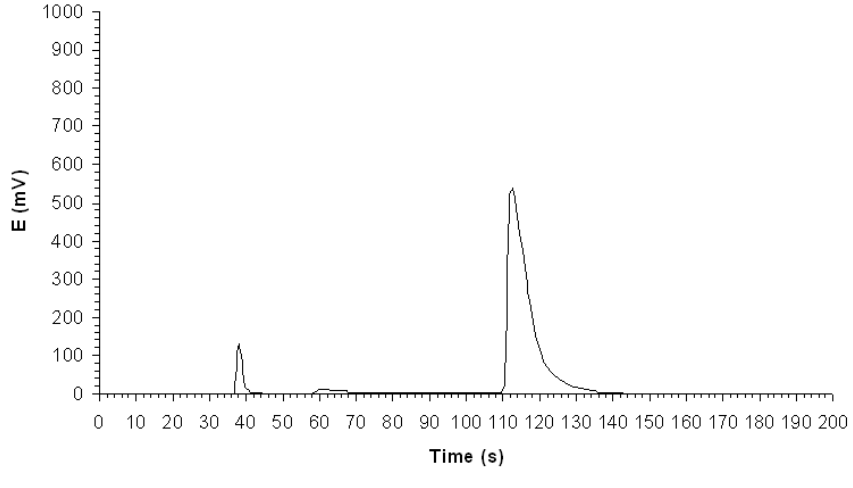

(j) P10 standard

Figure A.2: Chromatograms of the calibration standards (Continued)

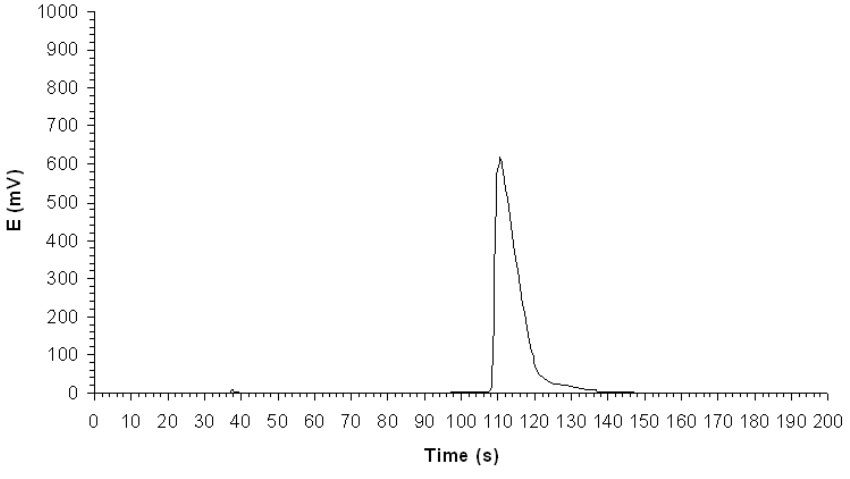

(k) P11 standard

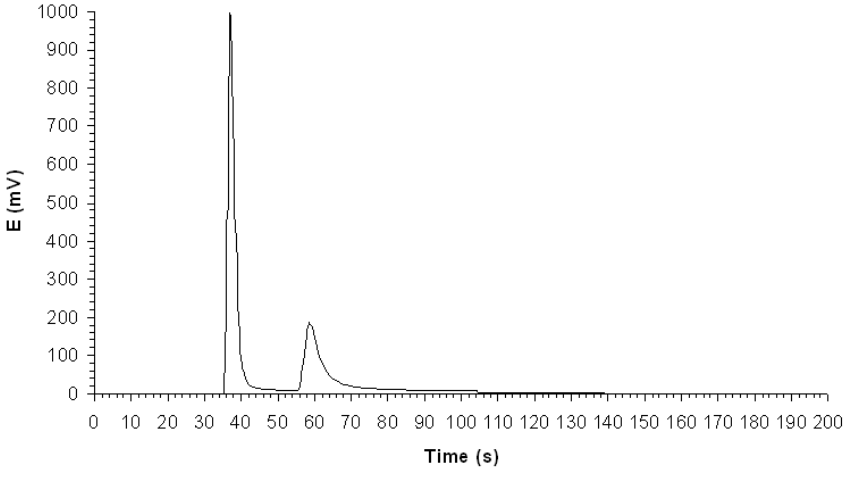

(l) P12 standard

Figure A.2: Chromatograms of the calibration standards (Continued)

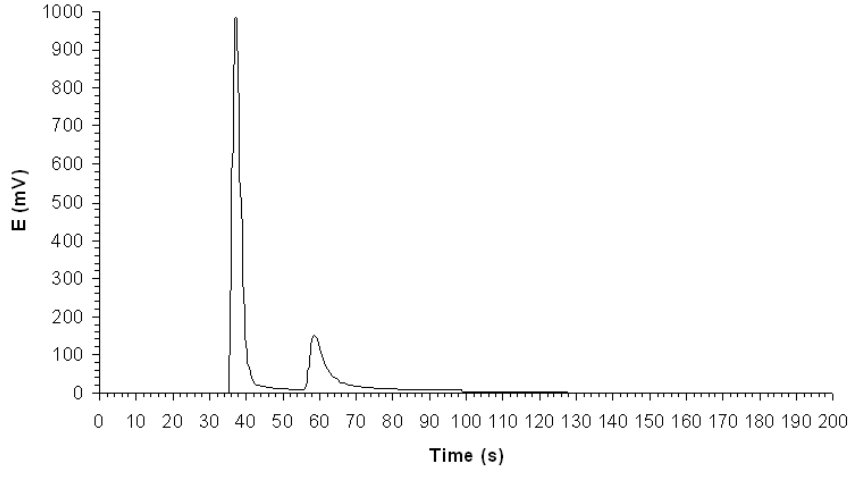

(m) P13 standard

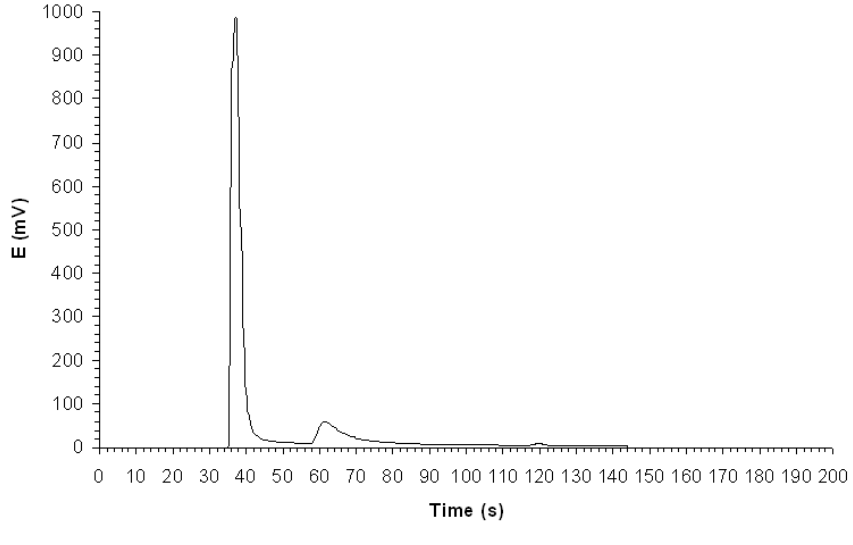

(n) P14 standard

Figure A.2: Chromatograms of the calibration standards (Continued)

As can be seen from the chromatograms, the peaks are not very good. All of them tail and the Propionic Acid peaks tail excessively, having more of a "mound" form than a peak, with the tail sometimes contacting with the next peak. Several strategies were tried to improve peak shape (e.g. replacing the liner, cleaning the injection line, changing temperatures and flowrates, re-installing the column), but none was successful, the chromatograms presented here being the best that were obtained.

A.3 Calibration Curves

Using a Microsoft Excel macro the area of each peak for each of the chromatograms was integrated. Those values were then plotted against composition (molar and mass fraction) and it was found immediately that the plot of area vs. mass fraction has a more linear aspect than the area vs molar fraction plot. Given this, it was decided to do the calibration in order to mass fractions rather than molar fractions. After this calibration plot was done (Fig. A.3), a second plot of mass fraction vs percentage of total area was also constructed (Fig. A.4) in order to address a problem that was observed during the experimental runs, the occasional variation of peak size. This problem, which occured unfrequently, probably resulted from obstructions in the feed line and caused some samples to be injected with a volume lower than the capacity of the injection loop.

Since the peak area is directly related to the amount of liquid injected - and thus, to the composition, because it is expected that the exact same amount is injected in all runs -, a smaller injection resulted in overall smaller peaks. But since the composition was the same, independently of injection size, the diminishing of the peak size was proportional for all components, meaning that the percentage of total peak area for each of the components was always constant, despite variations in the total amount of sample injected.

The use of the percentage of total peak area instead of just peak area is, thus, more advantageous and less vulnerable to injection errors. Furthermore, and looking at the regressions, the value of the squared correlation coefficient is also slightly increased, especially in the Propionic Acid fit. Due to all of these factors, the values obtained for the regressions plotted in Fig. A.4 were the ones used.

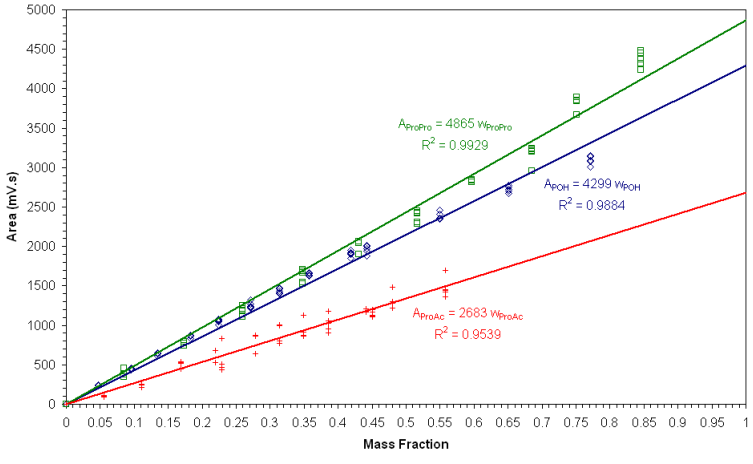

Figure A.3: Plot of mass fraction vs peak area for GC calibration (A- Area [mV.s]- w: Mass fraction; ◊- POH; +- ProAc; □- ProPro; — Regression lines)

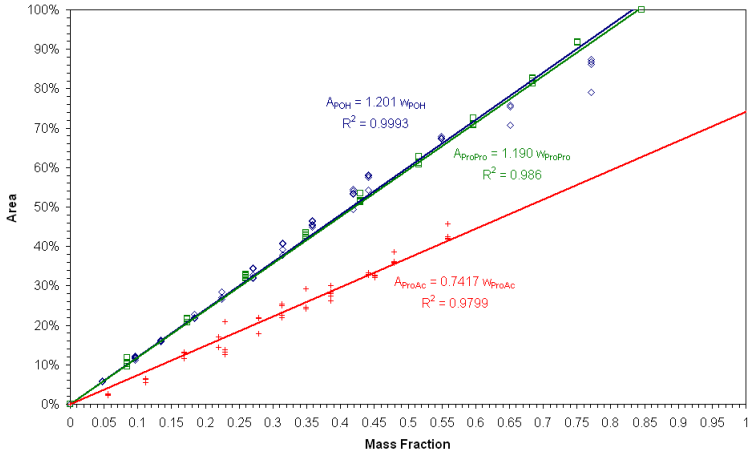

Figure A.4: Plot of mass fraction vs percentage of total peak area for GC calibration (A- Area [mV.s]- w: Mass fraction; ◊- POH; +- ProAc; □- ProPro; — Regression lines)

B PLOTS AND GRAPHICS

B.1 Reaction Kinetics of n-Propyl Propionate

B.1.1 Experimental Results

◊ Propanol
\+ Propionic Acid
□ n-Propyl Propionate
× Water
— Reconciliation run

B.1.1.1 (2005 Results)

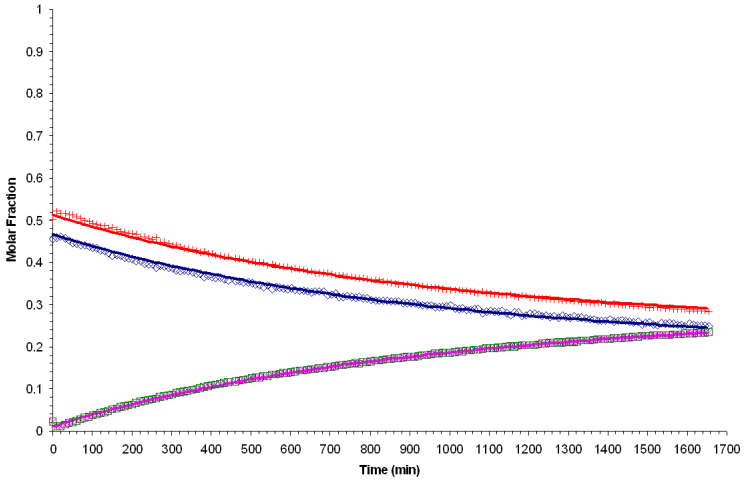

Figure B.1: Experiment 1c (60°C; 1:1 POH:ProAc Molar Ratio)

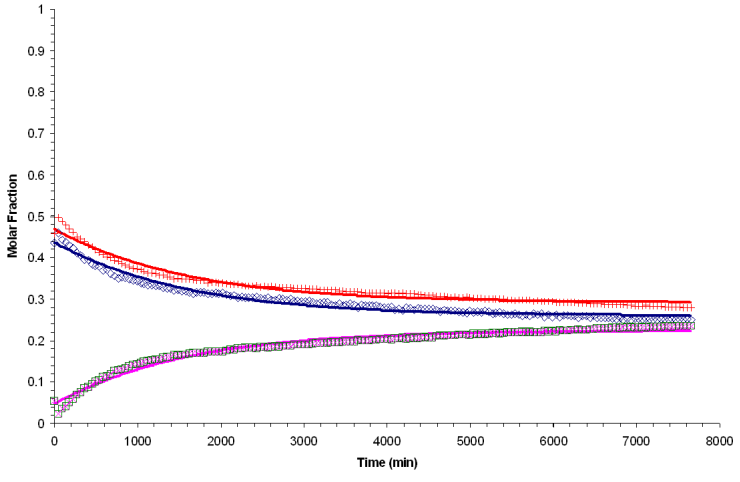

Figure B.2: Experiment 2 (60°C; 1:1 POH:ProAc Molar Ratio)

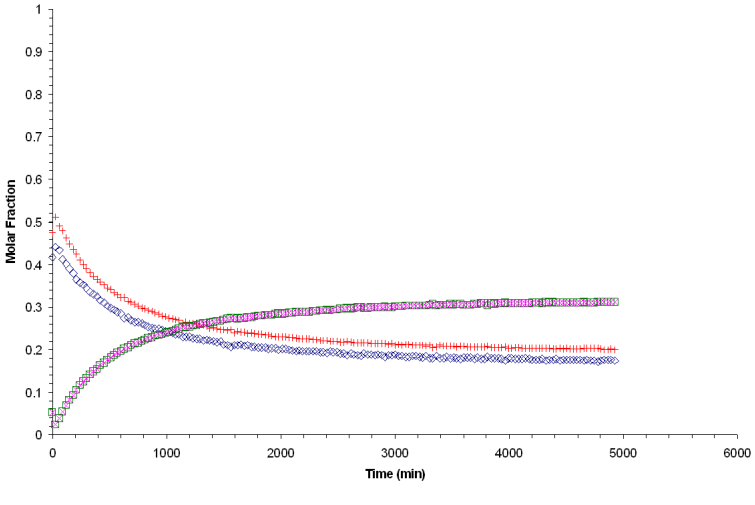

Figure B.3: Experiment 3 (70°C; 1:1 POH:ProAc Molar Ratio)

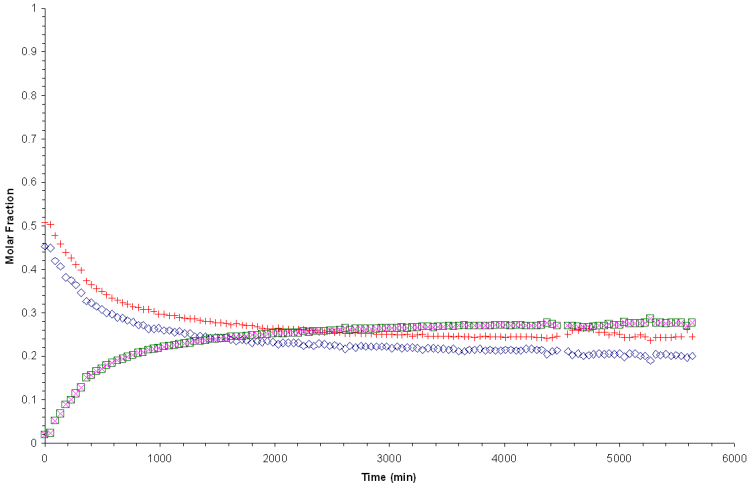

Figure B.4: Experiment 4 (70°C; 1:1 POH:ProAc Molar Ratio)

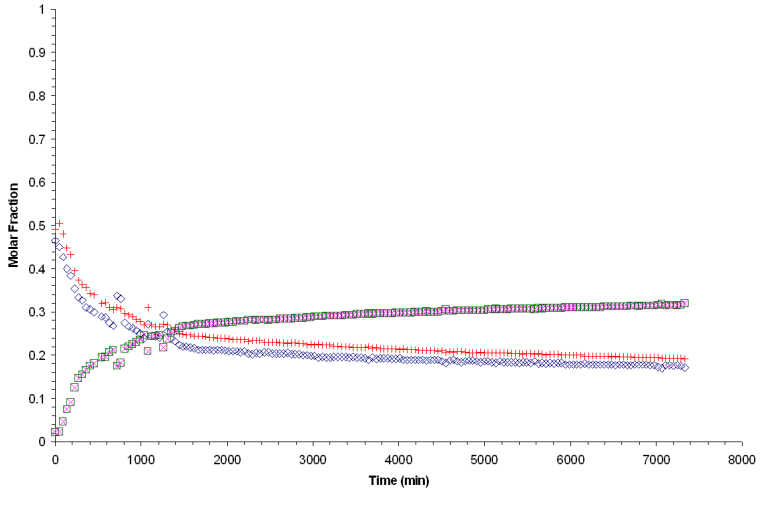

Figure B.5: Experiment 5 (80°C; 1:1 POH:ProAc Molar Ratio)

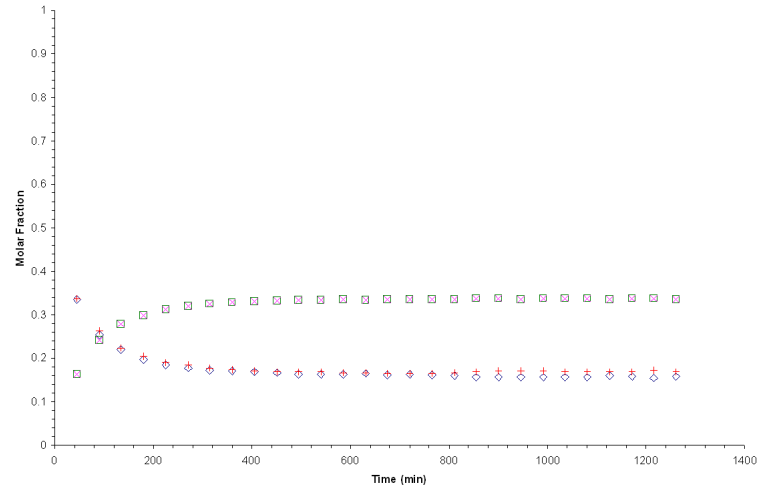

Figure B.6: Experiment 7 (115°C; 1:1 POH:ProAc Molar Ratio)

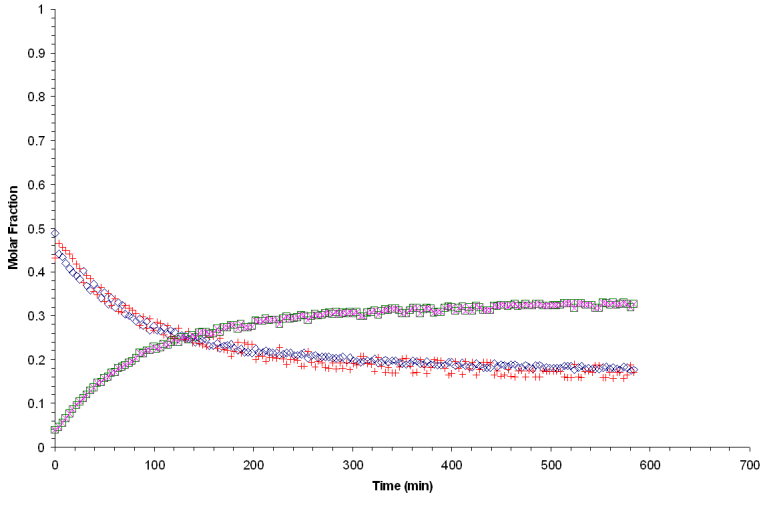

Figure B.7: Experiment 8 (115°C; 1:1 POH:ProAc Molar Ratio)

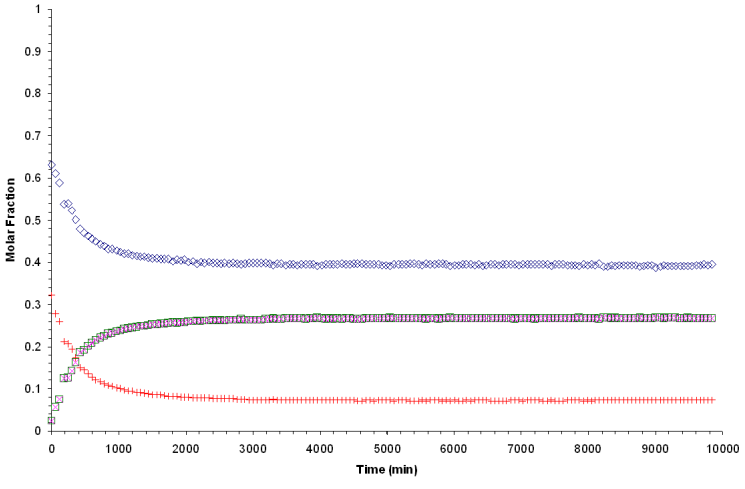

Figure B.8: Experiment 9 (80°C; 2:1 POH:ProAc Molar Ratio)

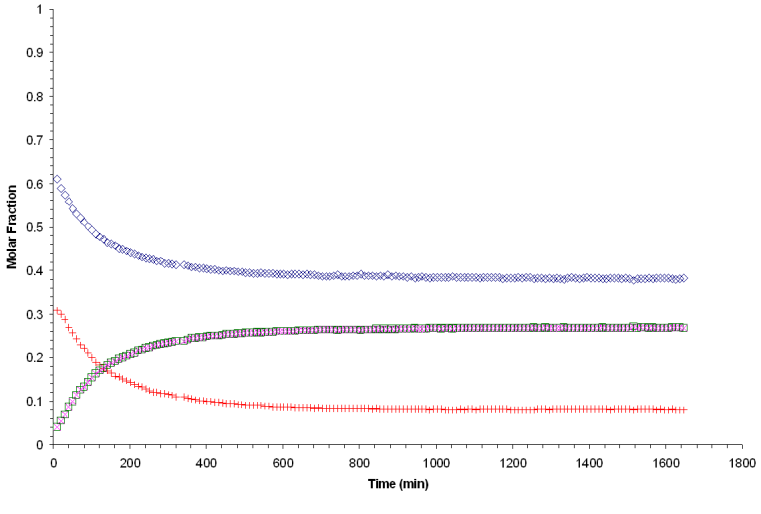

Figure B.9: Experiment 10 (100°C; 2:1 POH:ProAc Molar Ratio)

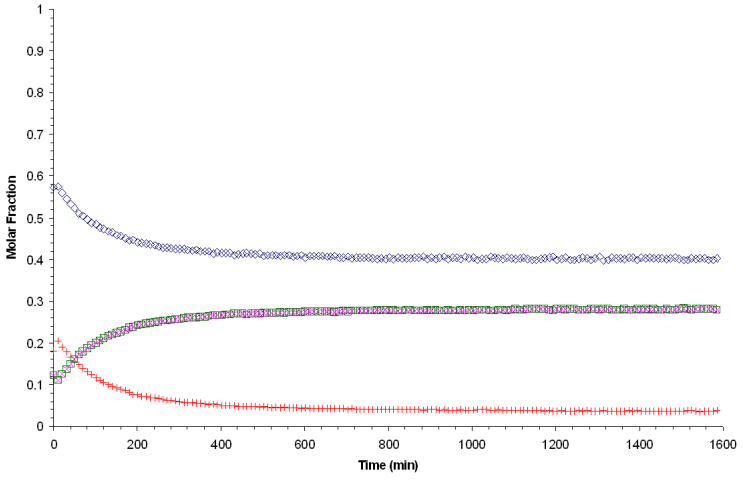

Figure B.10: Experiment 11 (115°C; 2:1 POH:ProAc Molar Ratio)

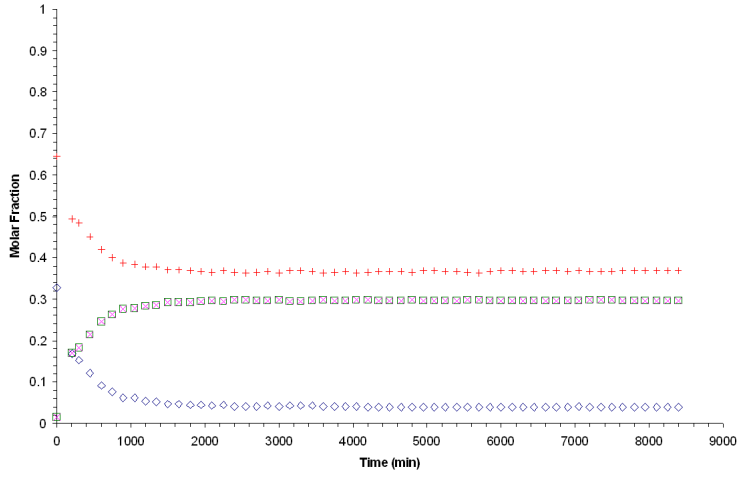

Figure B.11: Experiment 12 (80°C; 1:2 POH:ProAc Molar Ratio)

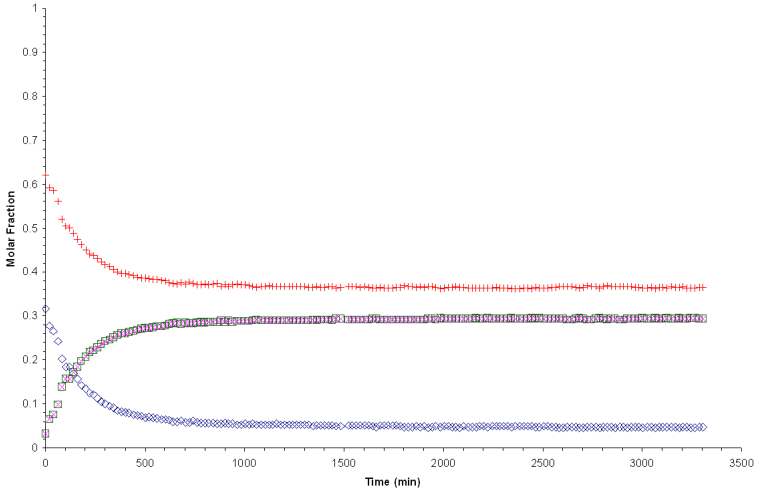

Figure B.12: Experiment 13 (100°C; 1:2 POH:ProAc Molar Ratio)

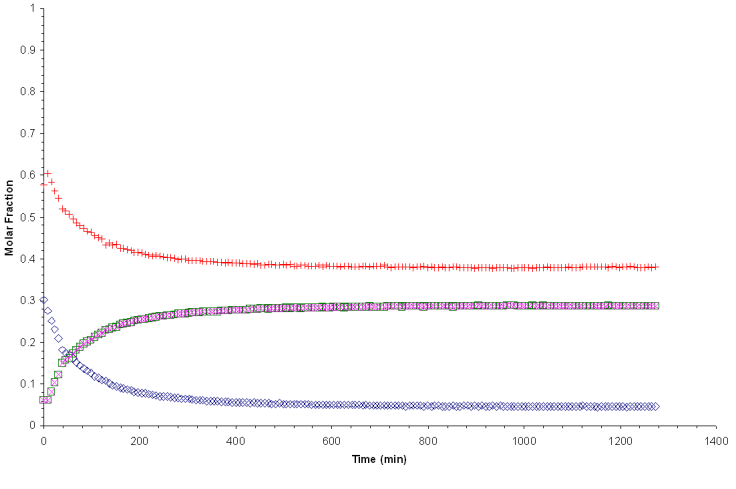

Figure B.13: Experiment 14 (115°C; 1:2 POH:ProAc Molar Ratio)

B.1.1.2 2004 Results: Catalytic

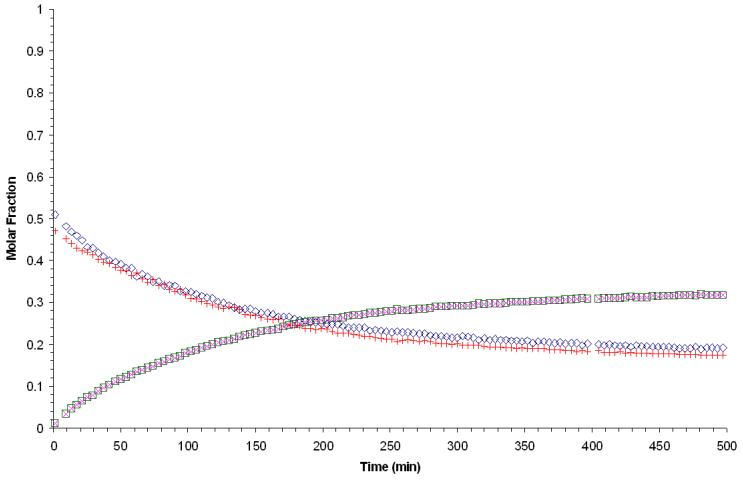

Figure B.14: Experiment 1 (100°C; 1:1 POH:ProAc Molar Ratio)

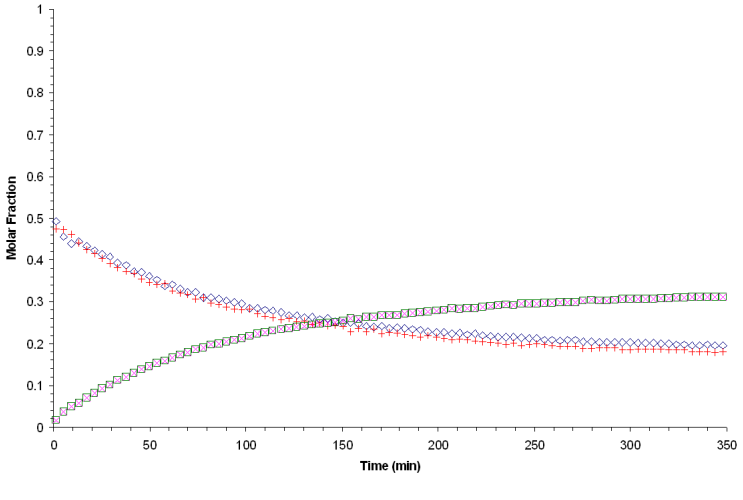

Figure B.15: Experiment 2 (100°C; 1:1 POH:ProAc Molar Ratio)

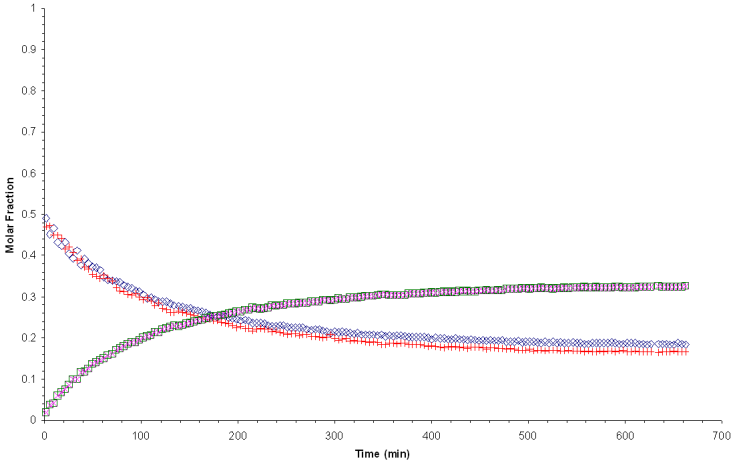

Figure B.16: Experiment 3 (100°C; 1:1 POH:ProAc Molar Ratio)

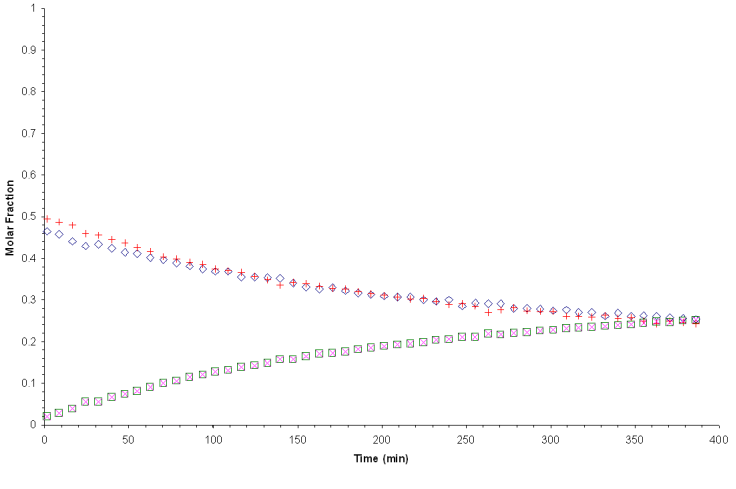

Figure B.17: Experiment 4 (90°C; 1:1 POH:ProAc Molar Ratio)

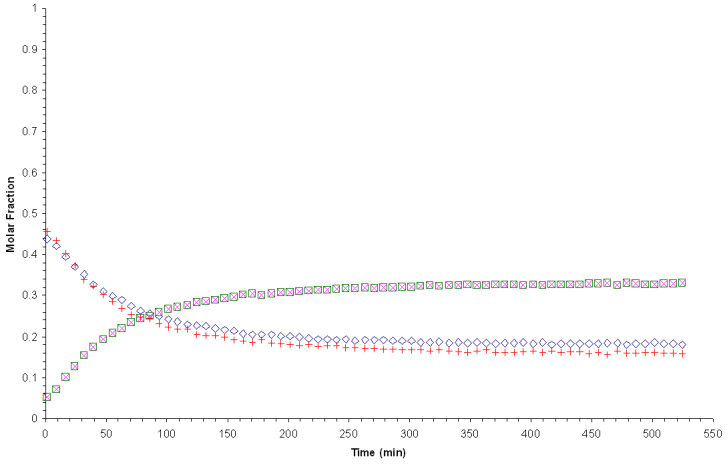

Figure B.18: Experiment 5 (110°C; 1:1 POH:ProAc Molar Ratio)

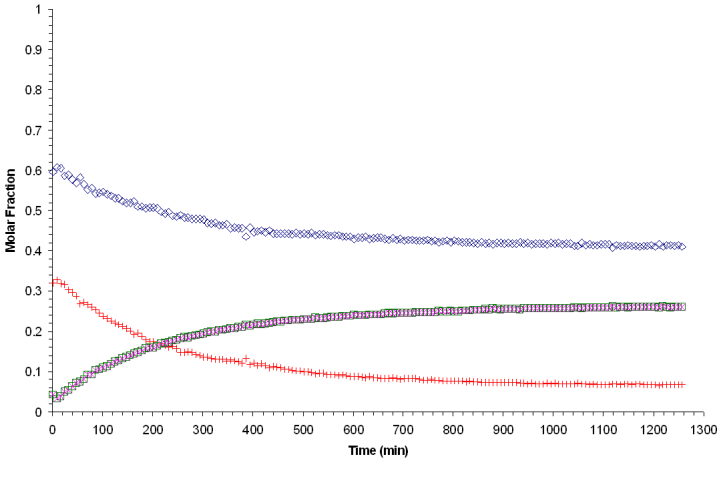

Figure B.19: Experiment 6 (90°C; 2:1 POH:ProAc Molar Ratio)

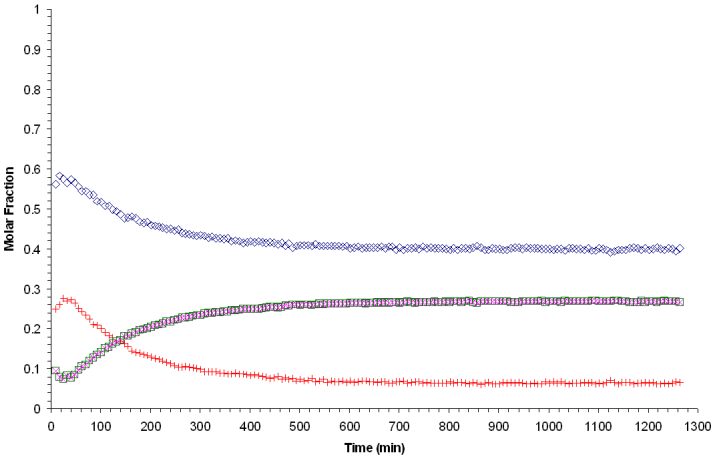

Figure B.20: Experiment 7 (100°C; 1:1 POH:ProAc Molar Ratio)

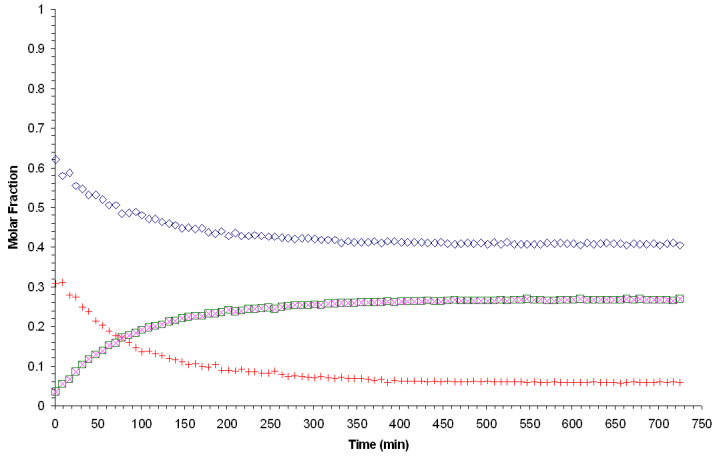

Figure B.21: Experiment 8 (110°C; 2:1 POH:ProAc Molar Ratio)

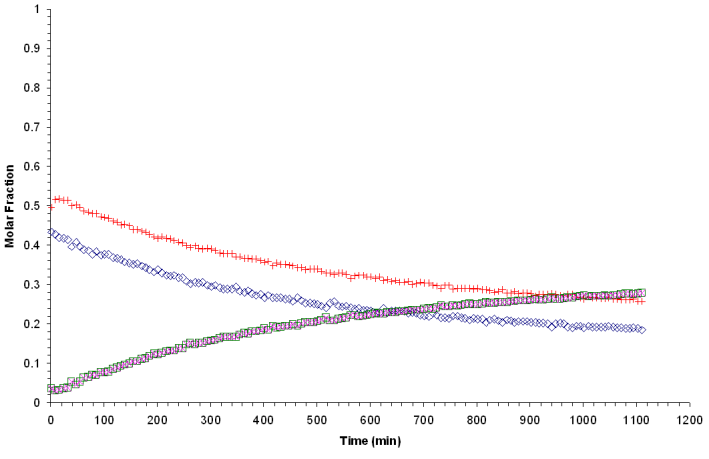

Figure B.22: Experiment 9 (70°C; 2:1 POH:ProAc Molar Ratio)

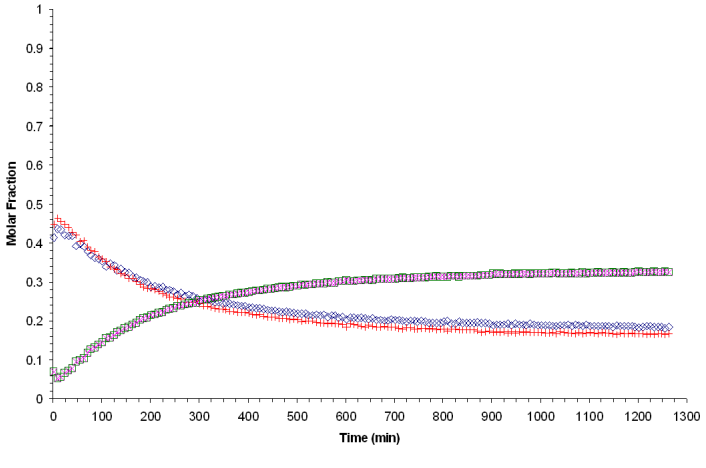

Figure B.23: Experiment 10 (90°C; 2:1 POH:ProAc Molar Ratio)

B.1.1.3 2004 Results: Non-catalytic

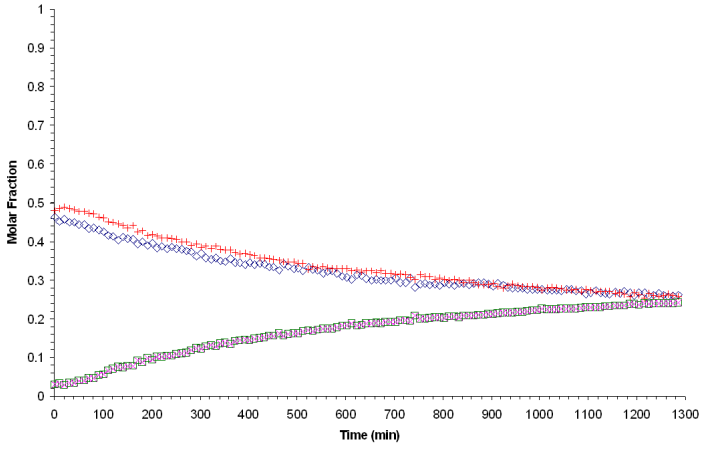

Figure B.24: Experiment nc1 (100°C; 1:1 POH:ProAc Molar Ratio)

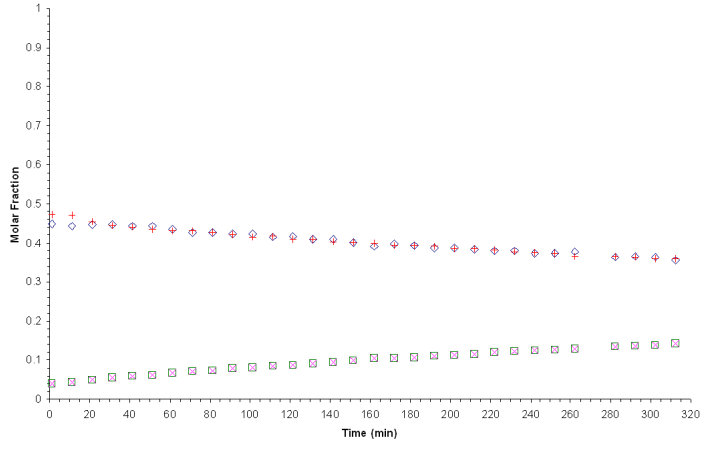

Figure B.25: Experiment nc2 (100°C; 1:1 POH:ProAc Molar Ratio)

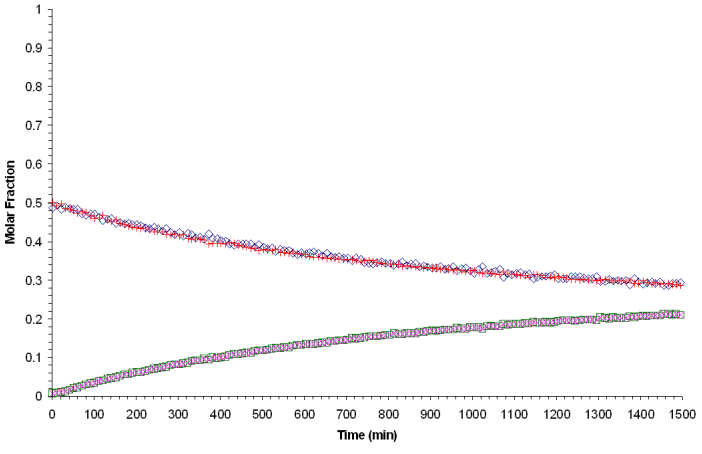

Figure B.26: Experiment nc3 (90°C; 1:1 POH:ProAc Molar Ratio)

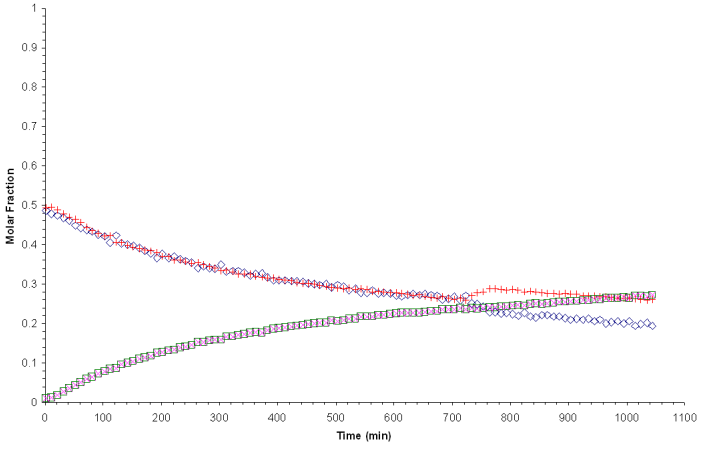

Figure B.27: Experiment nc4 (110°C; 1:1 POH:ProAc Molar Ratio)

B.1.2 Experimental Results with Individual Curve Fitting

B.1.2.1 2005 Results

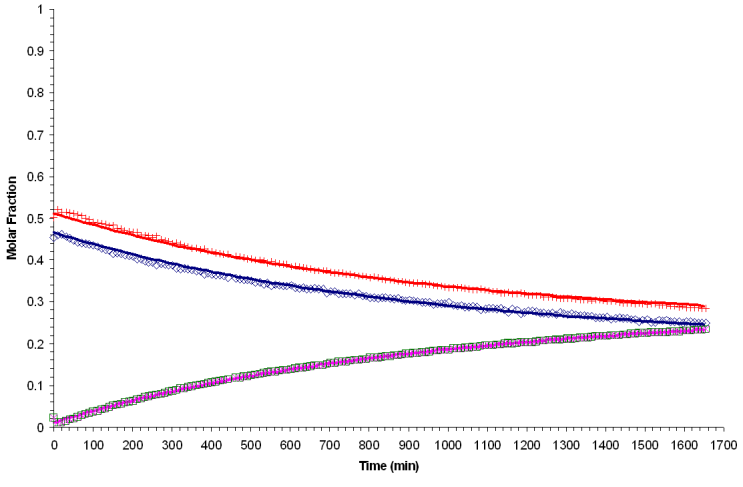

Figure B.28: Experiment 1c (60°C; 1:1 POH:ProAc Molar Ratio)

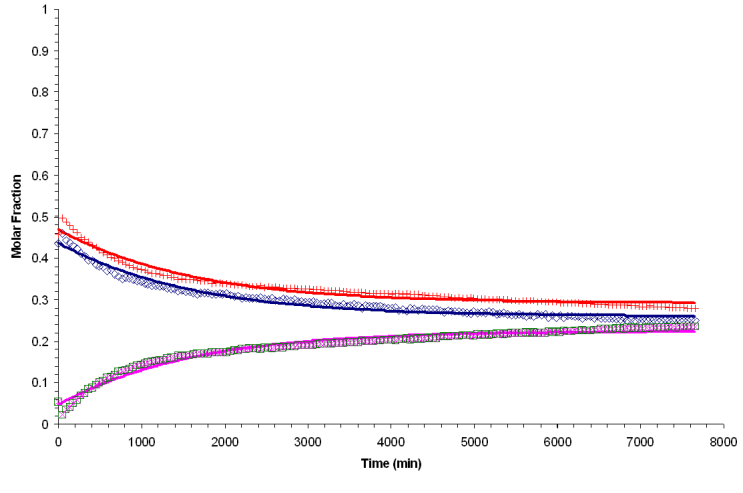

Figure B.29: Experiment 2 (60°C; 1:1 POH:ProAc Molar Ratio)

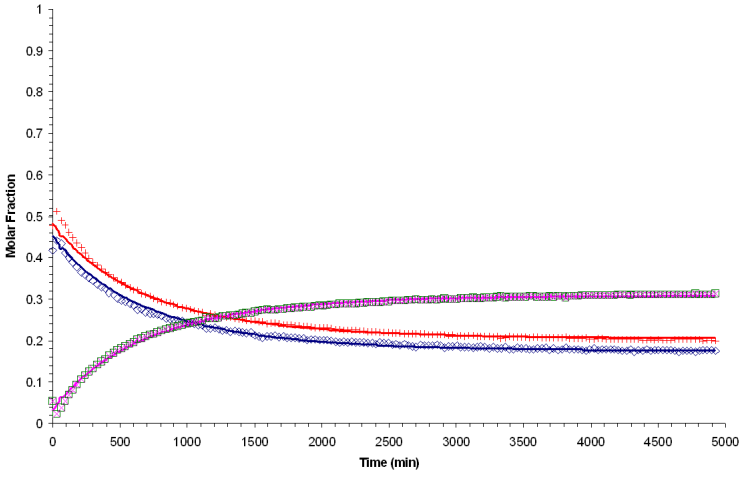

Figure B.30: Experiment 3 (70°C; 1:1 POH:ProAc Molar Ratio)

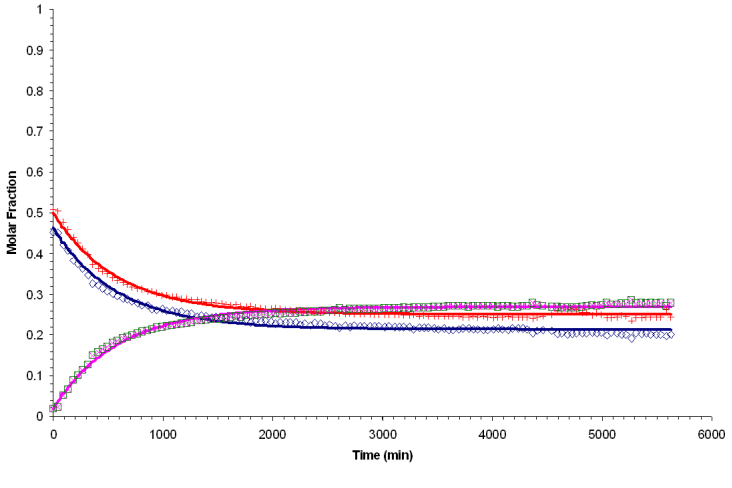

Figure B.31: Experiment 4 (70°C; 1:1 POH:ProAc Molar Ratio)

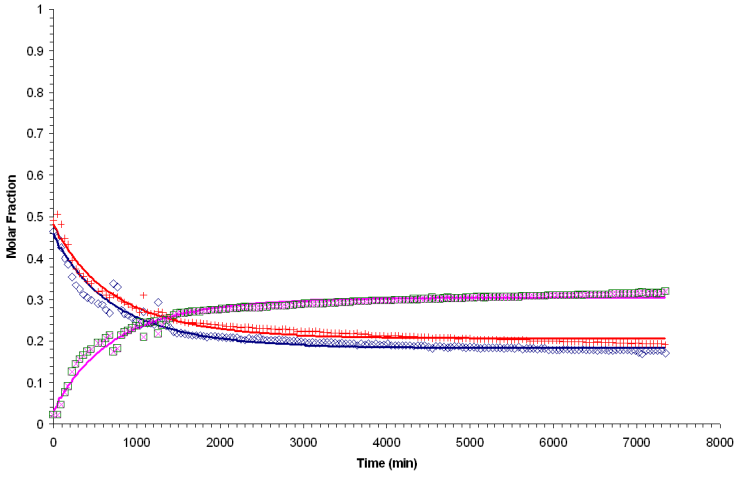

Figure B.32: Experiment 5 (80°C; 1:1 POH:ProAc Molar Ratio)

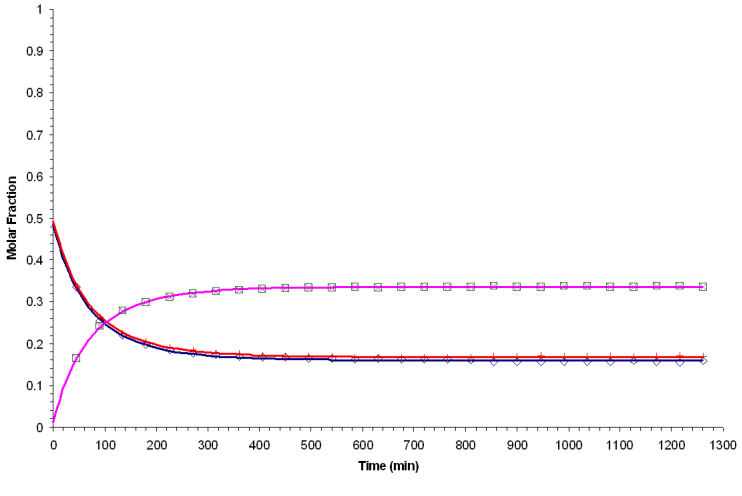

Figure B.33: Experiment 7 (115°C; 1:1 POH:ProAc Molar Ratio)

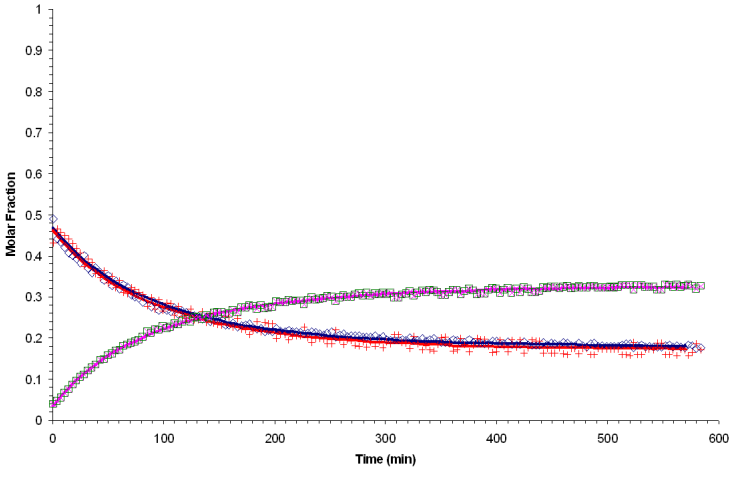

Figure B.34: Experiment 8 (115°C; 1:1 POH:ProAc Molar Ratio)

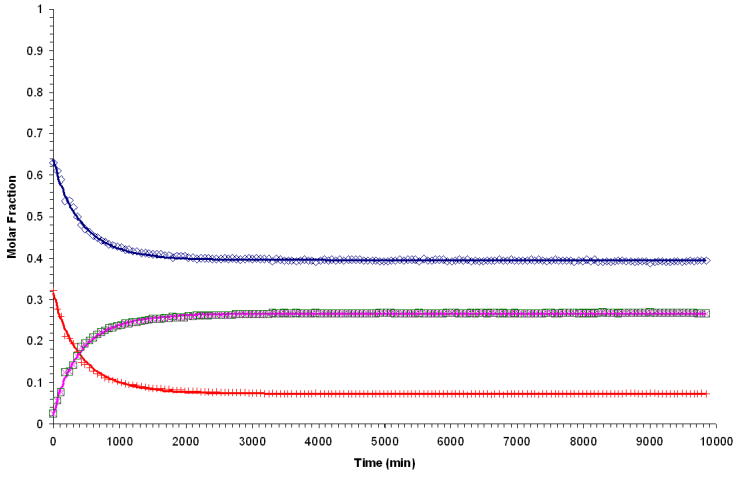

Figure B.35: Experiment 9 (80°C; 2:1 POH:ProAc Molar Ratio)

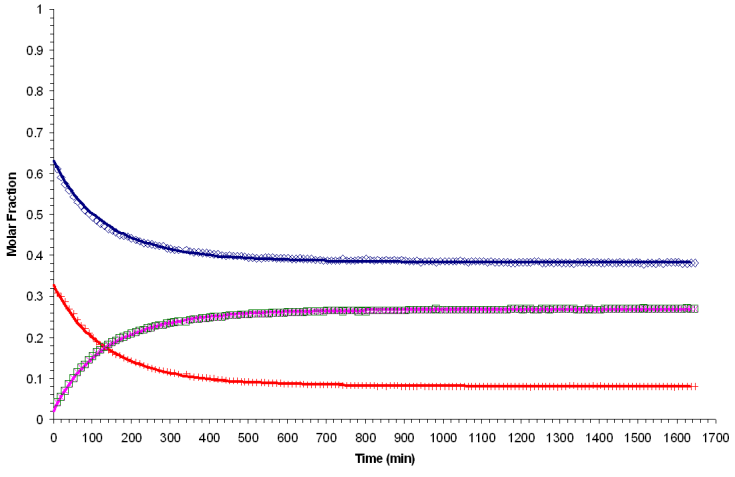

Figure B.36: Experiment 10 (100°C; 2:1 POH:ProAc Molar Ratio)

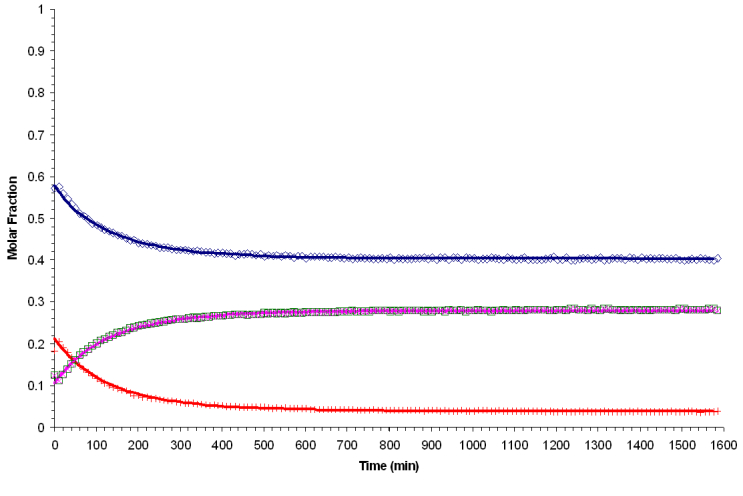

Figure B.37: Experiment 11 (115°C; 2:1 POH:ProAc Molar Ratio)

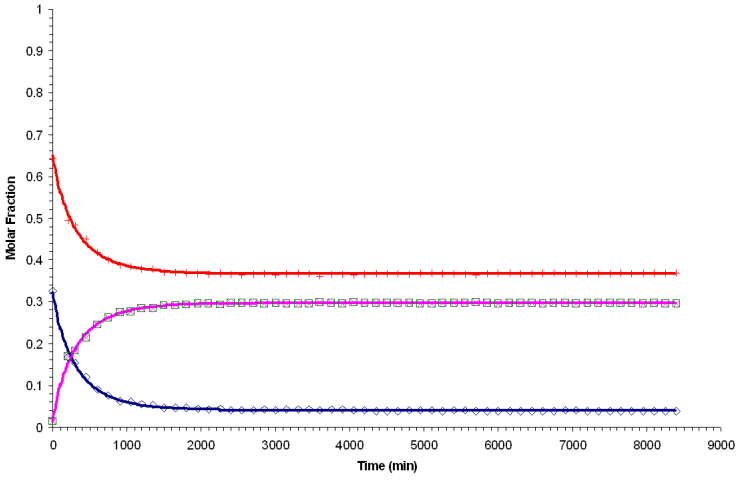

Figure B.38: Experiment 12 (80°C; 1:2 POH:ProAc Molar Ratio)

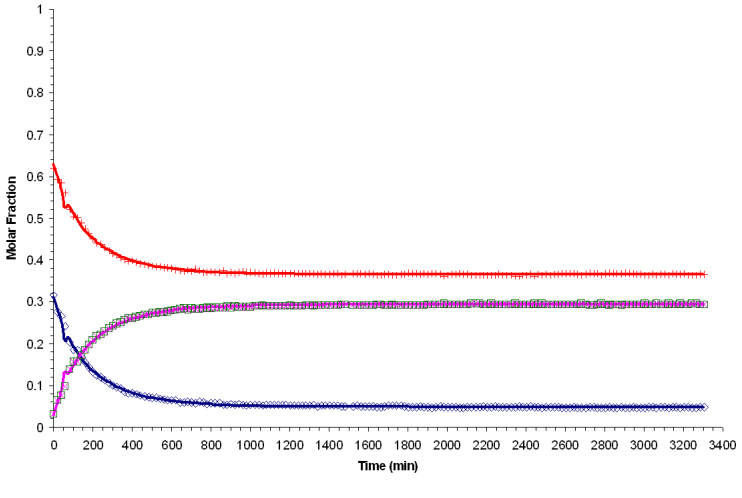

Figure B.39: Experiment 13 (100°C; 1:2 POH:ProAc Molar Ratio)

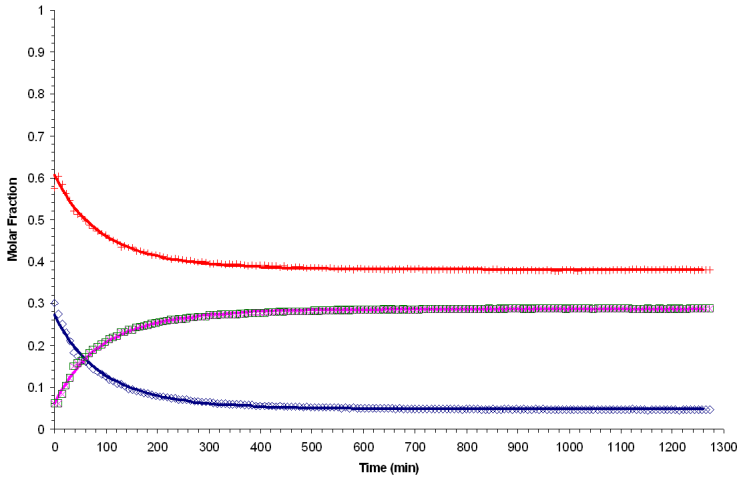

Figure B.40: Experiment 14 (115°C; 1:2 POH:ProAc Molar Ratio)

B.1.2.2 2004 Results: Catalytic

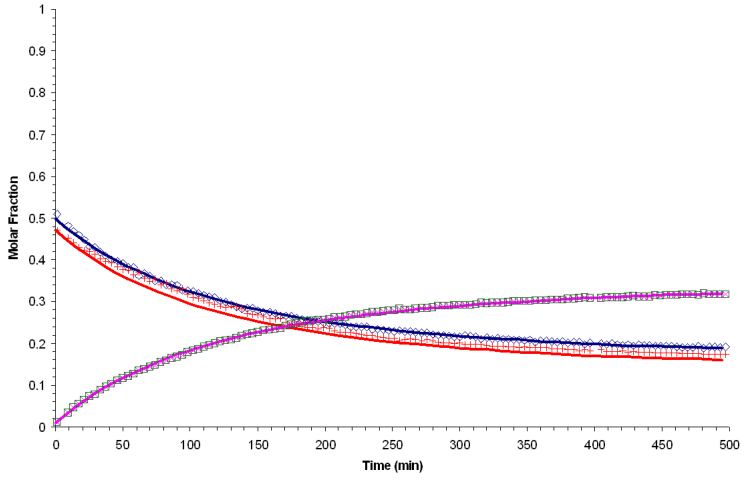

Figure B.41: Experiment 1 (100°C; 1:1 POH:ProAc Molar Ratio)

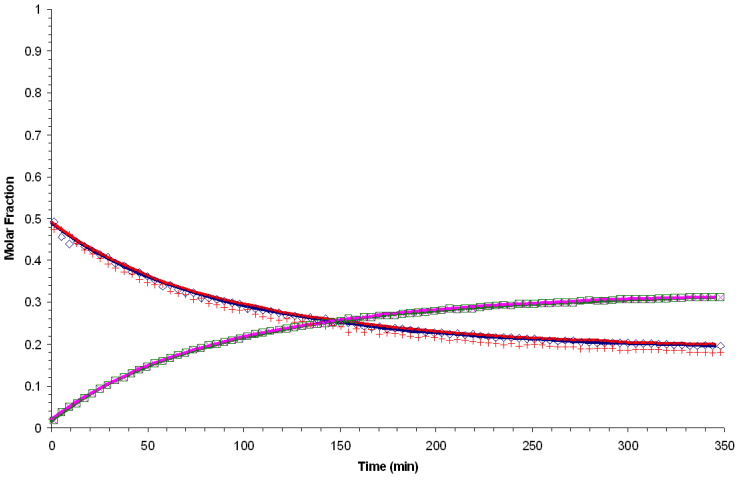

Figure B.42: Experiment 2 (100°C; 1:1 POH:ProAc Molar Ratio)

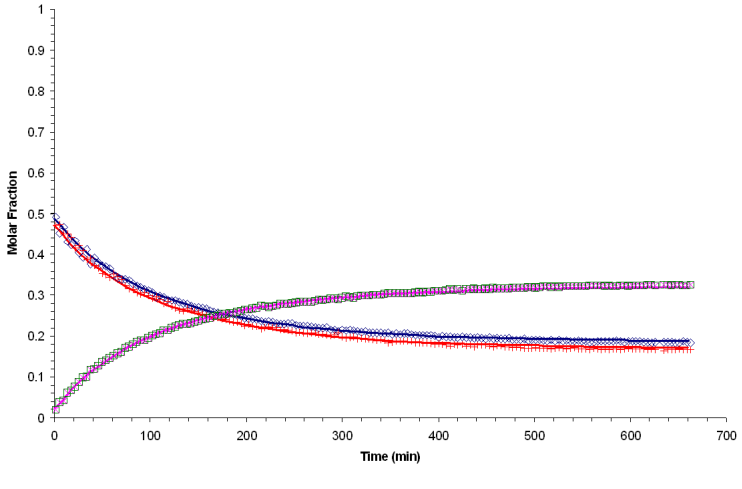

Figure B.43: Experiment 3 (100°C; 1:1 POH:ProAc Molar Ratio)

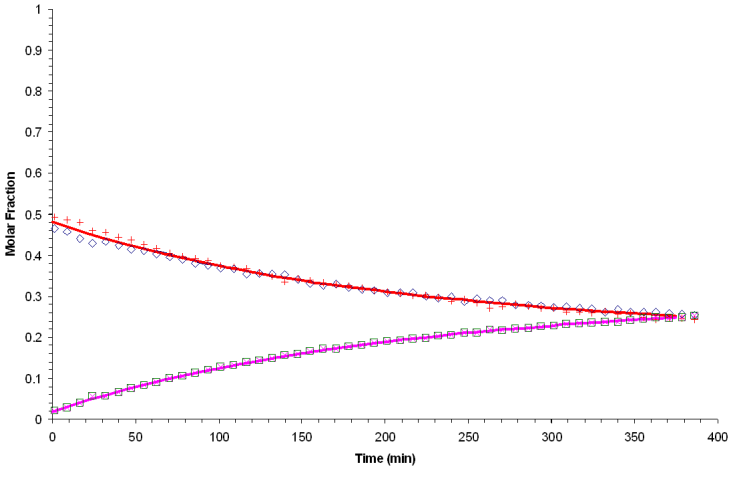

Figure B.44: Experiment 4 (90°C; 1:1 POH:ProAc Molar Ratio)

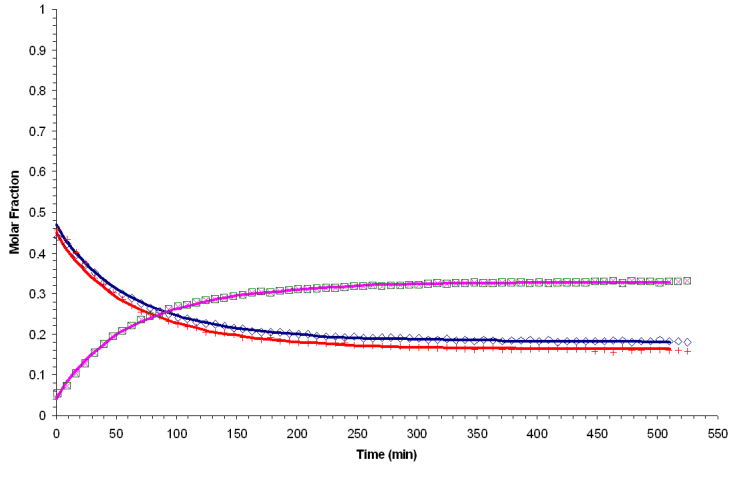

Figure B.45: Experiment 5 (110°C; 1:1 POH:ProAc Molar Ratio)

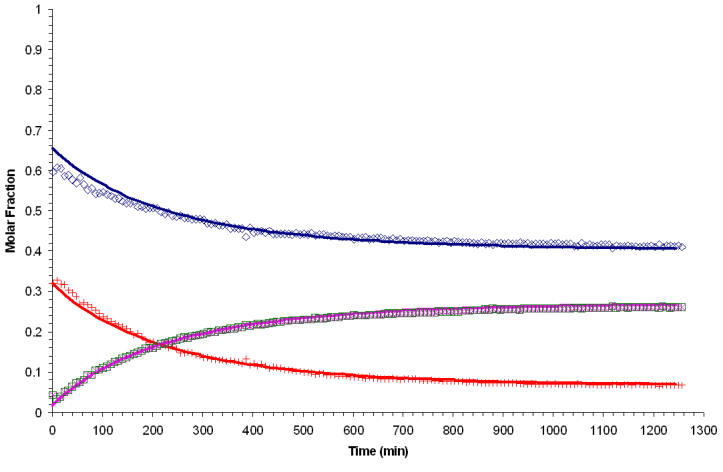

Figure B.46: Experiment 6 (90°C; 2:1 POH:ProAc Molar Ratio)

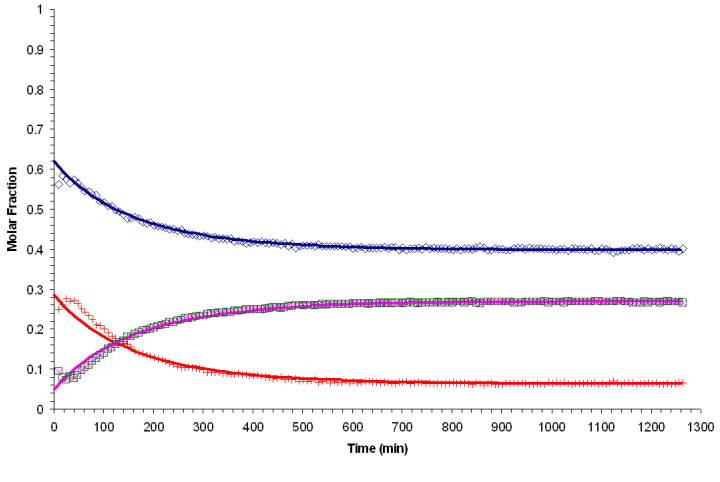

Figure B.47: Experiment 7 (100°C; 1:1 POH:ProAc Molar Ratio)

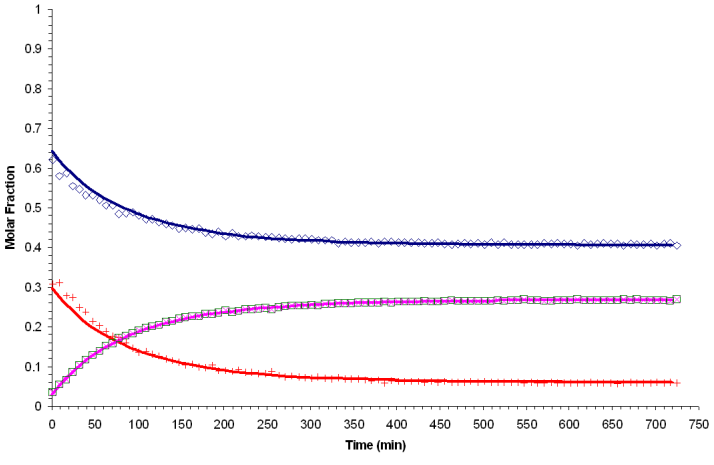

Figure B.48: Experiment 8 (110°C; 2:1 POH:ProAc Molar Ratio)

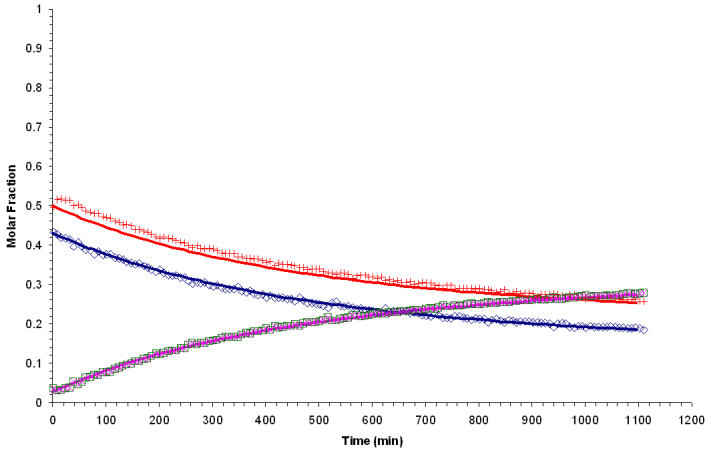

Figure B.49: Experiment 9 (70°C; 2:1 POH:ProAc Molar Ratio)

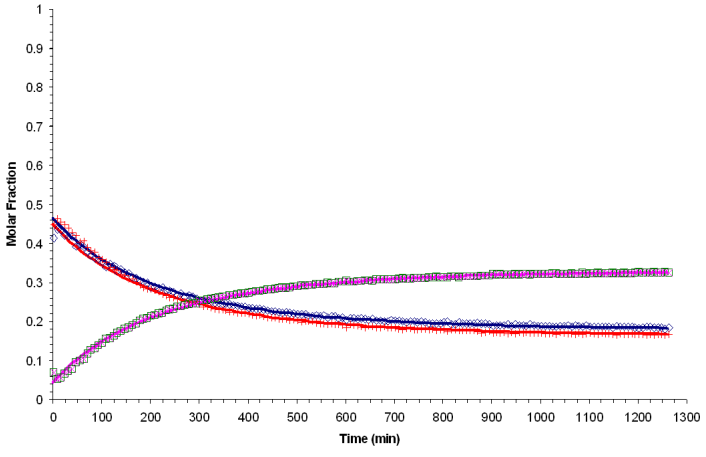

Figure B.50: Experiment 10 (90°C; 2:1 POH:ProAc Molar Ratio)

B.1.2.3 2004 Results: Non-catalytic

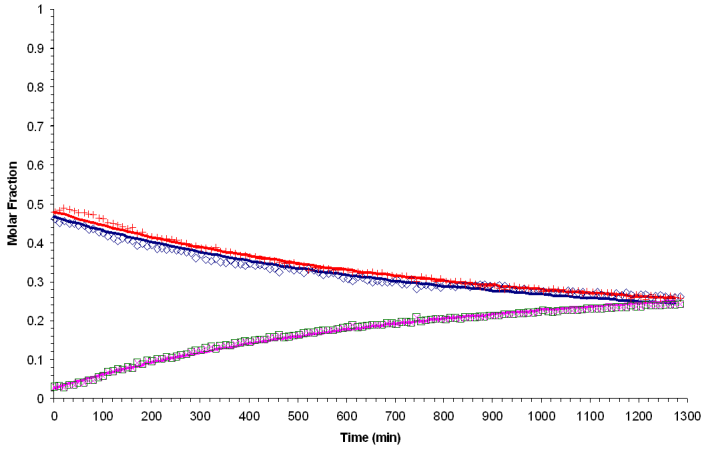

Figure B.51: Experiment nc1 (100°C; 1:1 POH:ProAc Molar Ratio)

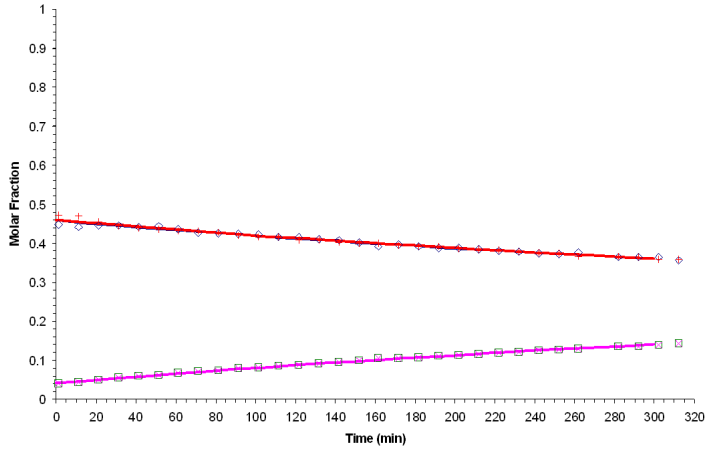

Figure B.52: Experiment nc2 (100°C; 1:1 POH:ProAc Molar Ratio)

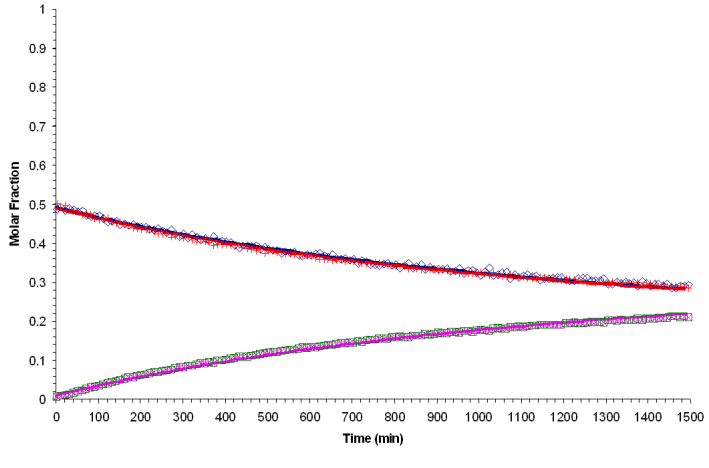

Figure B.53: Experiment nc3 (90°C; 1:1 POH:ProAc Molar Ratio)

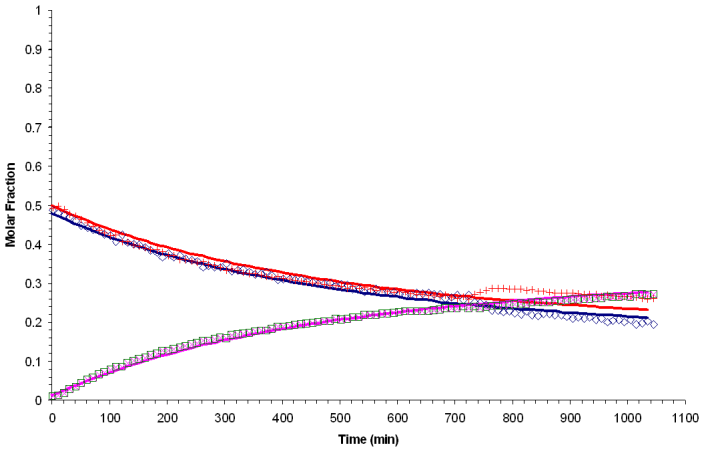

Figure B.54: Experiment nc4 (110°C; 1:1 POH:ProAc Molar Ratio)

B.1.3 Experimental Results with Model reconciliation

B.1.3.1 2005 Results

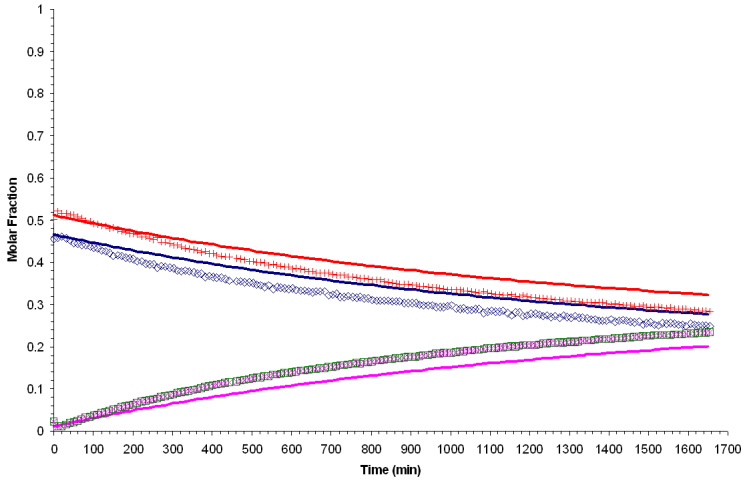

Figure B.55: Experiment 1c (60°C; 1:1 POH:ProAc Molar Ratio)

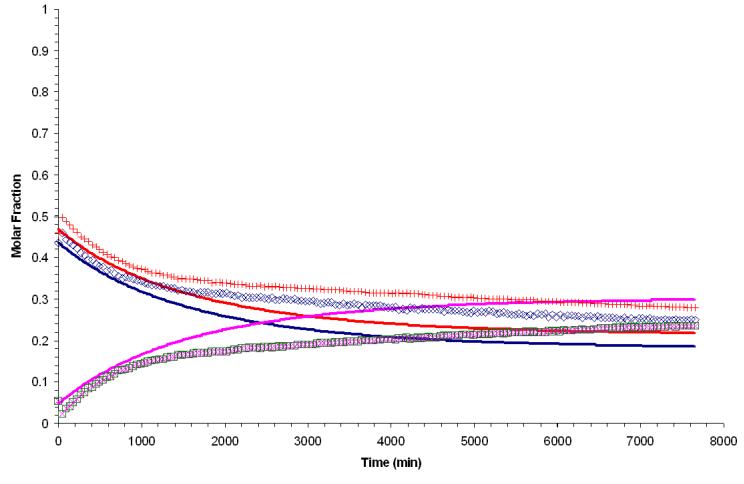

Figure B.56: Experiment 2 (60°C; 1:1 POH:ProAc Molar Ratio)

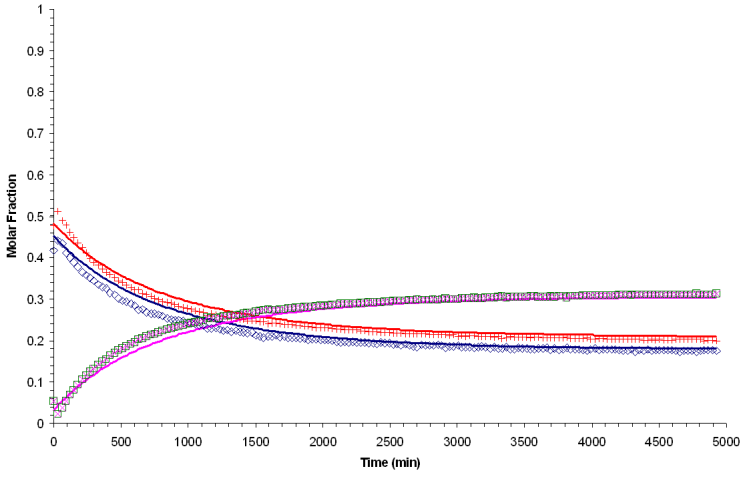

Figure B.57: Experiment 3 (70°C; 1:1 POH:ProAc Molar Ratio)

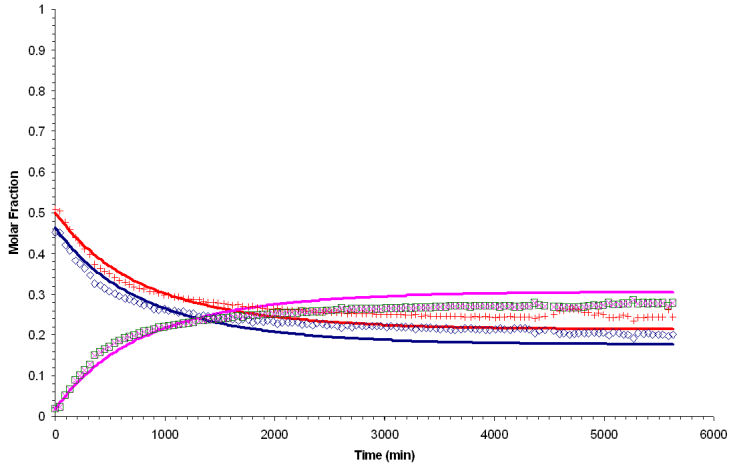

Figure B.58: Experiment 4 (70°C; 1:1 POH:ProAc Molar Ratio)

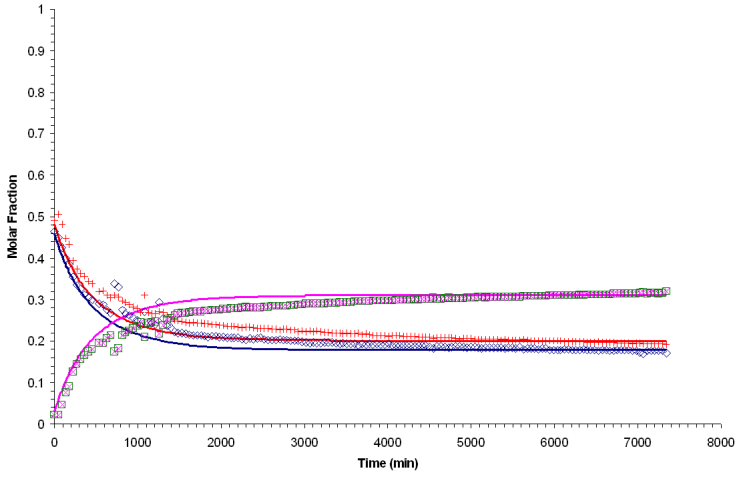

Figure B.59: Experiment 5 (80°C; 1:1 POH:ProAc Molar Ratio)

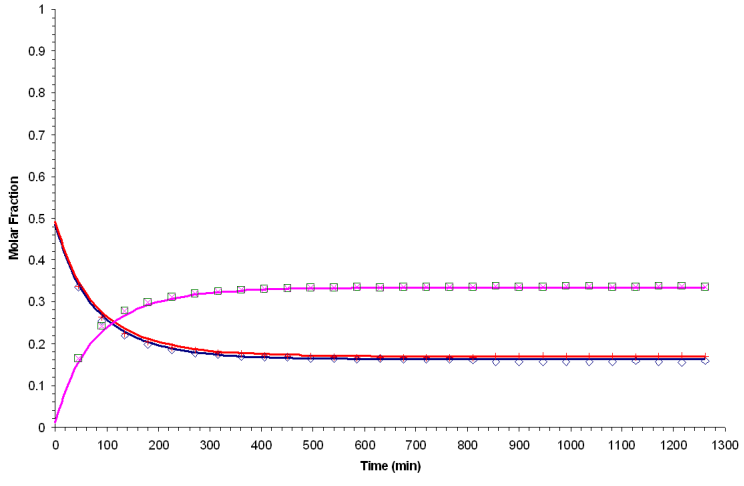

Figure B.60: Experiment 7 (115°C; 1:1 POH:ProAc Molar Ratio)

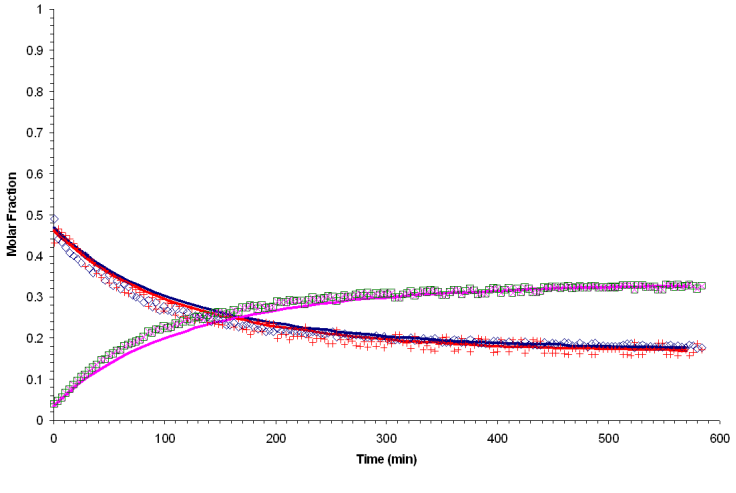

Figure B.61: Experiment 8 (115°C; 1:1 POH:ProAc Molar Ratio)

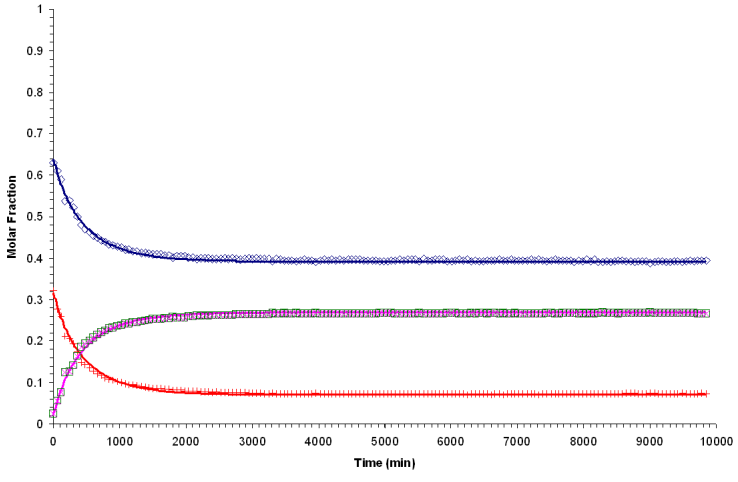

Figure B.62: Experiment 9 (80°C; 2:1 POH:ProAc Molar Ratio)

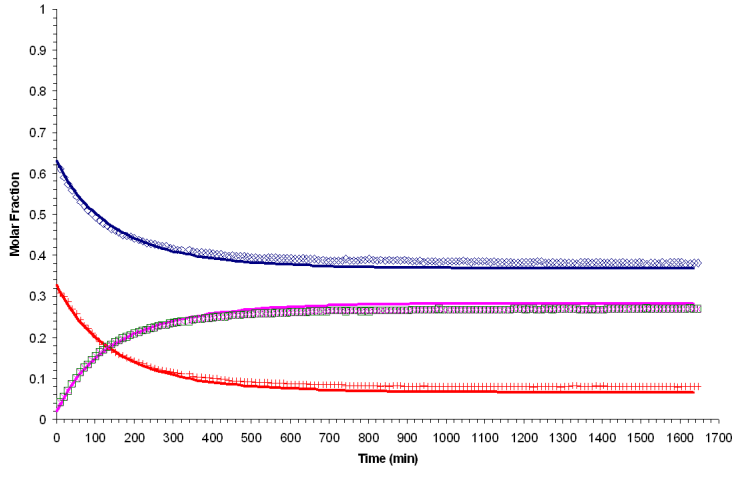

Figure B.63: Experiment 10 (100°C; 2:1 POH:ProAc Molar Ratio)

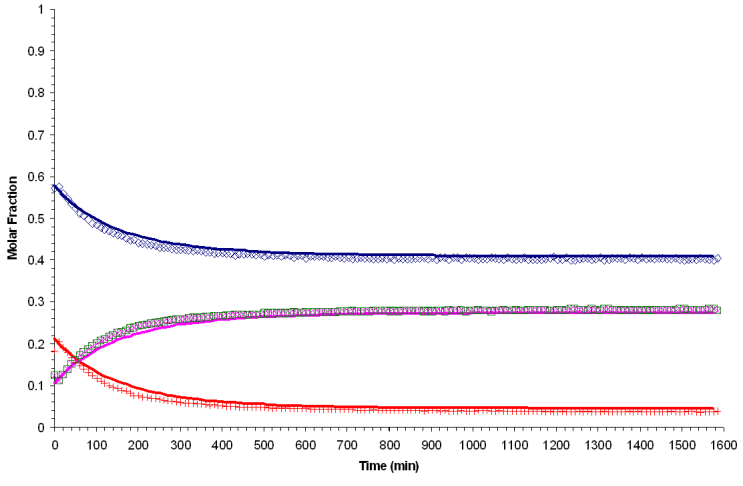

Figure B.64: Experiment 11 (115°C; 2:1 POH:ProAc Molar Ratio)

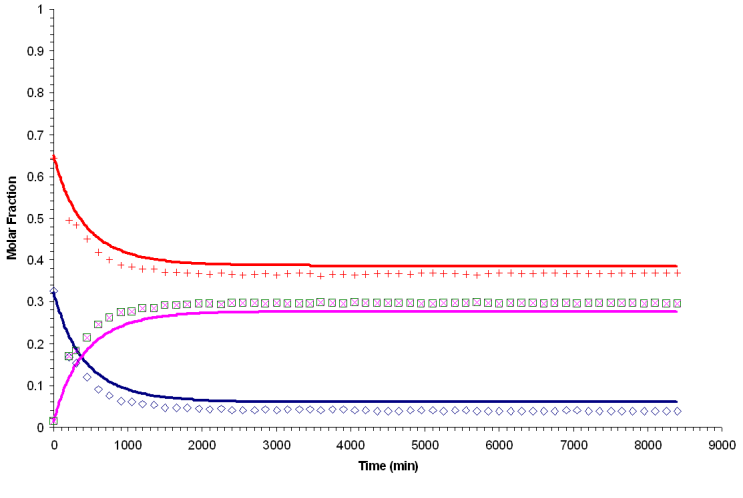

Figure B.65: Experiment 12 (80°C; 1:2 POH:ProAc Molar Ratio)

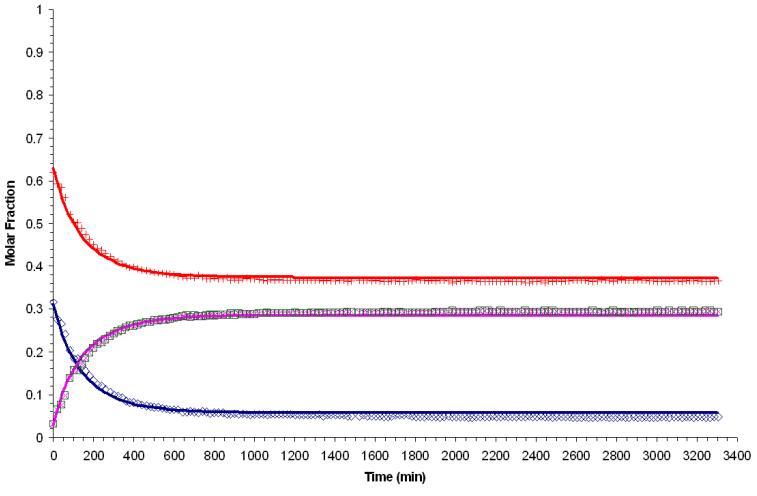

Figure B.66: Experiment 13 (100°C; 1:2 POH:ProAc Molar Ratio)

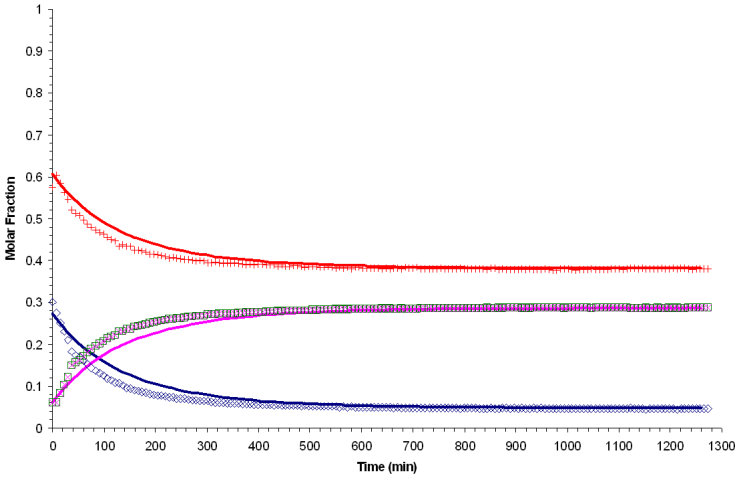

Figure B.67: Experiment 14 (115°C; 1:2 POH:ProAc Molar Ratio)

B.1.3.2 2004 Results: Catalytic

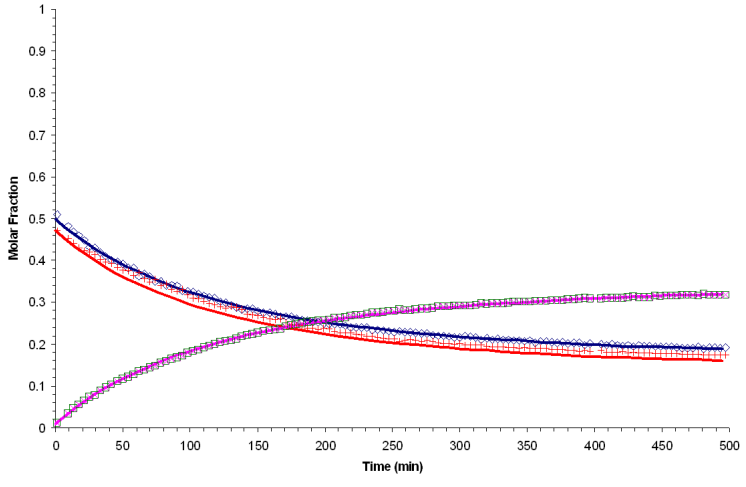

Figure B.68: Experiment 1 (100°C; 1:1 POH:ProAc Molar Ratio)

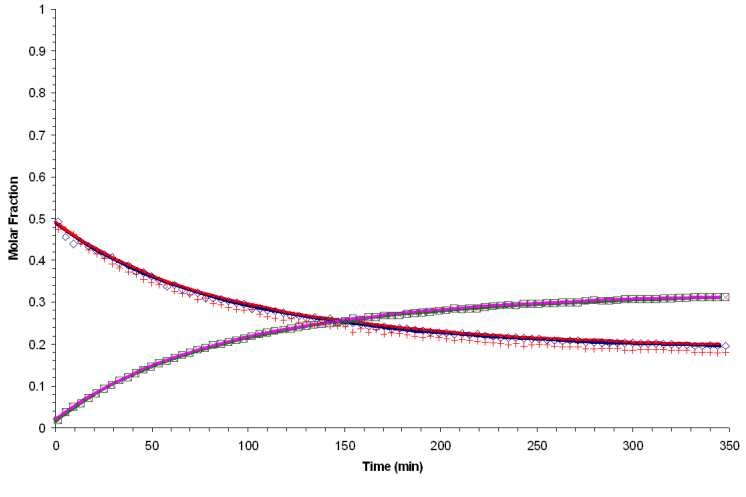

Figure B.69: Experiment 2 (100°C; 1:1 POH:ProAc Molar Ratio)

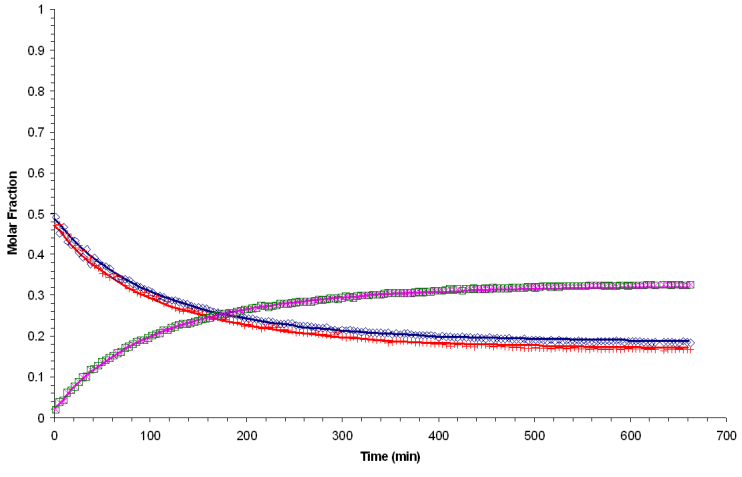

Figure B.70: Experiment 3 (100°C; 1:1 POH:ProAc Molar Ratio)

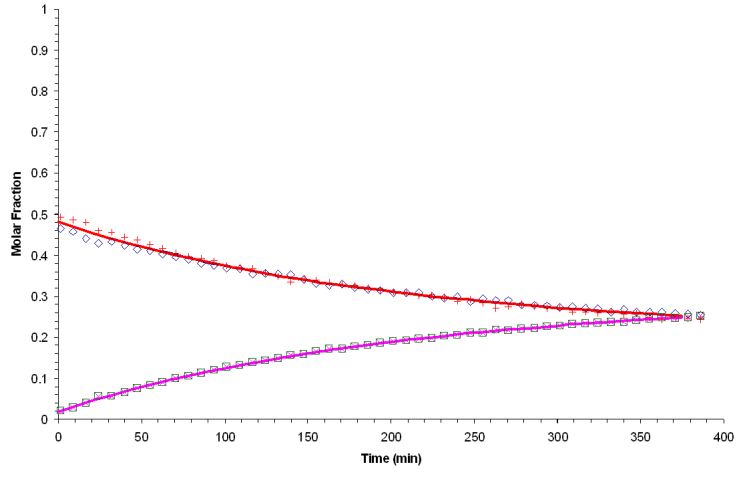

Figure B.71: Experiment 4 (90°C; 1:1 POH:ProAc Molar Ratio)

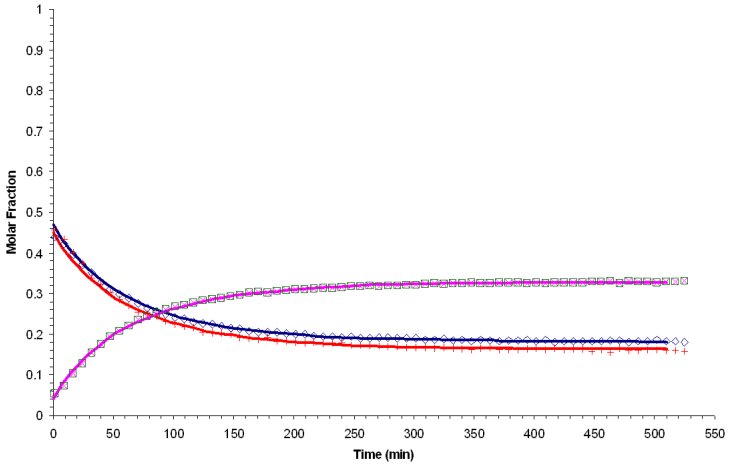

Figure B.72: Experiment 5 (110°C; 1:1 POH:ProAc Molar Ratio)

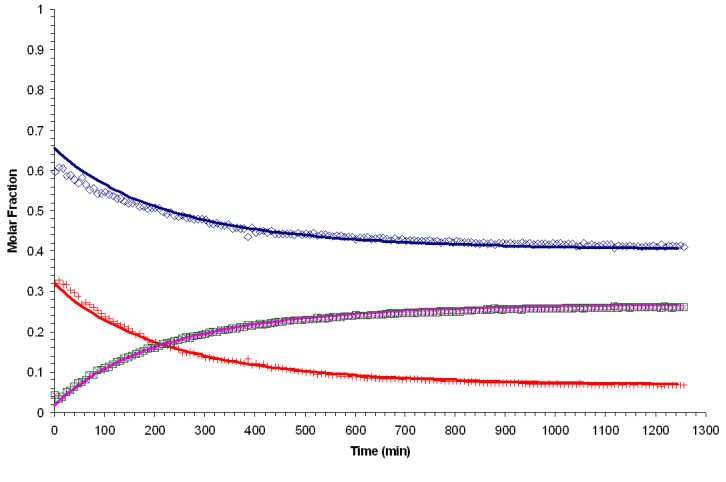

Figure B.73: Experiment 6 (90°C; 2:1 POH:ProAc Molar Ratio)

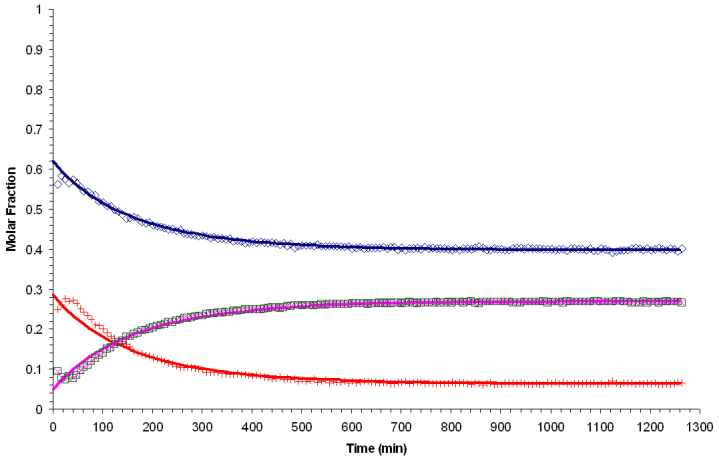

Figure B.74: Experiment 7 (100°C; 1:1 POH:ProAc Molar Ratio)

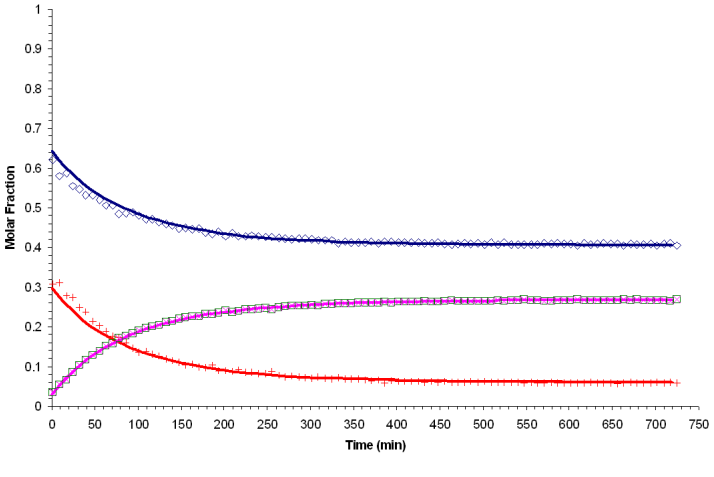

Figure B.75: Experiment 8 (110°C; 2:1 POH:ProAc Molar Ratio)

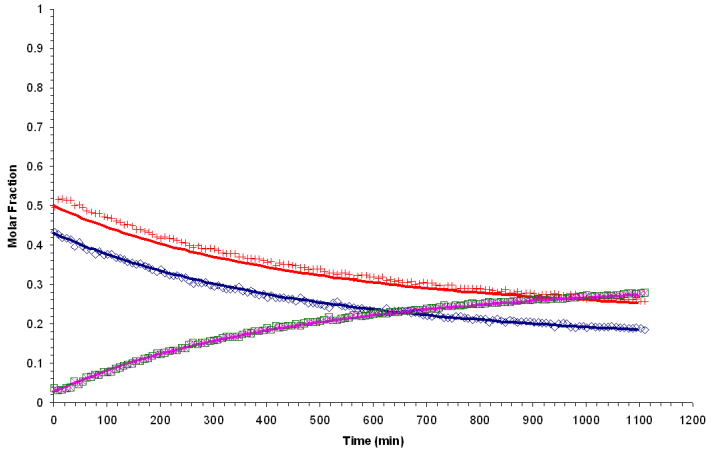

Figure B.76: Experiment 9 (70°C; 2:1 POH:ProAc Molar Ratio)

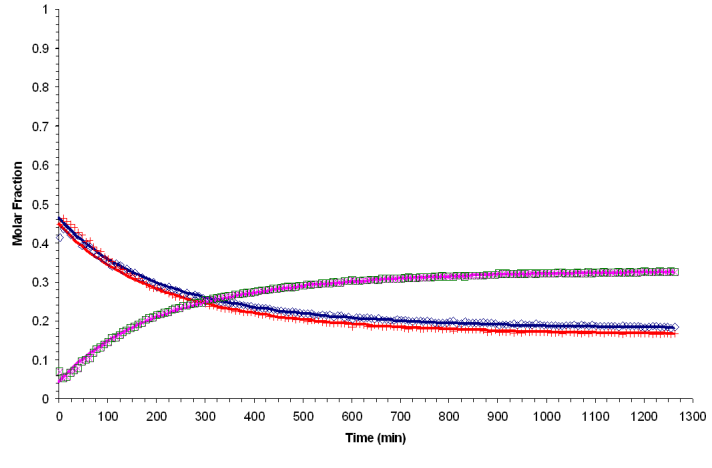

Figure B.77: Experiment 10 (90°C; 2:1 POH:ProAc Molar Ratio)

B.1.3.3 2004 Results: Non-catalytic

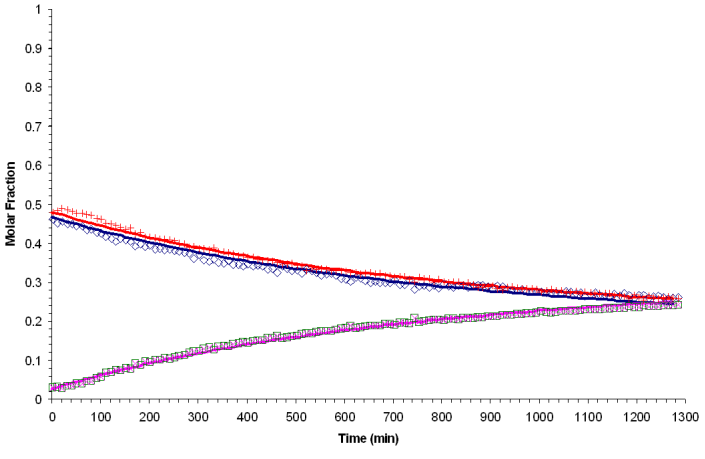

Figure B.78: Experiment nc1 (100°C; 1:1 POH:ProAc Molar Ratio)

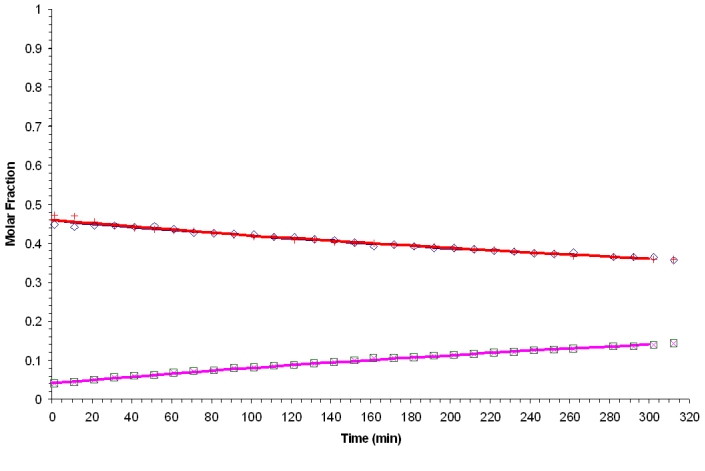

Figure B.79: Experiment nc2 (100°C; 1:1 POH:ProAc Molar Ratio)

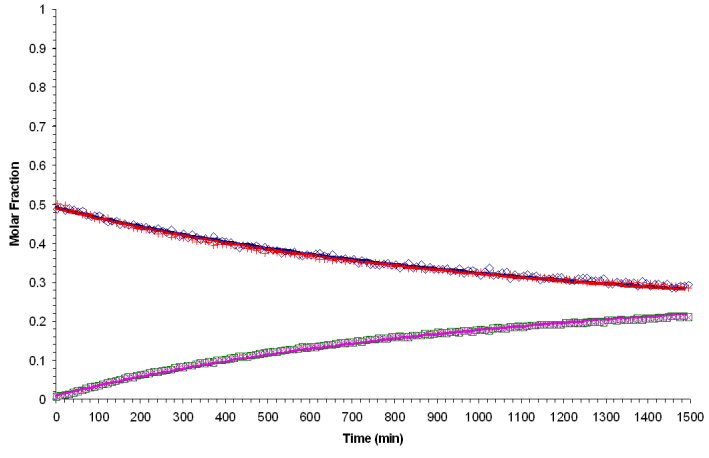

Figure B.80: Experiment nc3 (90°C; 1:1 POH:ProAc Molar Ratio)

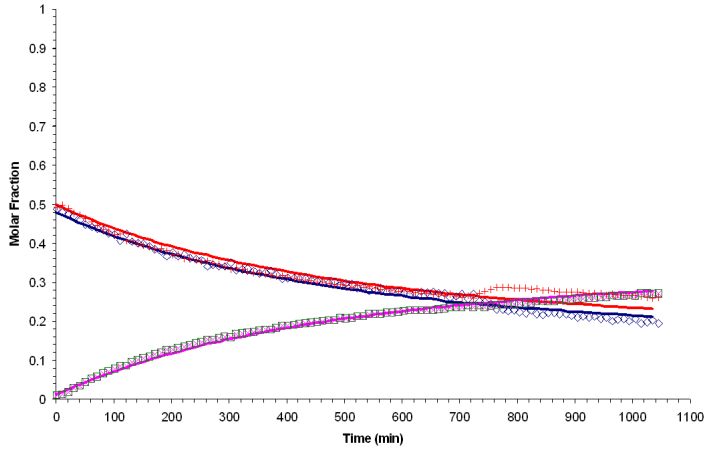

Figure B.81: Experiment nc4 (110°C; 1:1 POH:ProAc Molar Ratio)

C TABLES

Table C.1: Operating Conditions for the Column Parameters' Evaluation

		1A	2A	3A	4A	5A	6A	7A	8A	9A	10A
Pressure [bar]		5.00	5.00	5.00	5.00	5.00	5.00	5.00	5.00	5.00	5.00
Reflux Ratio		1.00	1.00	1.00	1.00	1.00	1.00	1.00	1.50	2.00	2.50
Feed 1	T [°C]	90.00	90.00	90.00	90.00	90.00	90.00	90.00	90.00	90.00	90.00
	x_{2M1B}	0.000	0.000	0.000	0.000	0.000	0.000	0.000	0.000	0.000	0.000
	x_{2M2B}	0.000	0.000	0.000	0.000	0.000	0.000	0.000	0.000	0.000	0.000
	x_{MeOH}	1.000	1.000	1.000	1.000	1.000	1.000	1.000	1.000	1.000	1.000
	x_{TAME}	0.000	0.000	0.000	0.000	0.000	0.000	0.000	0.000	0.000	0.000
	Flowrate	1.000	1.000	1.000	1.000	1.000	1.000	1.000	1.000	1.000	1.000
Feed 2	T [°C]	90.00	90.00	90.00	90.00	90.00	90.00	90.00	90.00	90.00	90.00
	x_{2M1B}	0.500	0.500	0.500	0.500	0.500	0.500	0.500	0.500	0.500	0.500
	x_{2M2B}	0.500	0.500	0.500	0.500	0.500	0.500	0.500	0.500	0.500	0.500
	x_{MeOH}	0.000	0.000	0.000	0.000	0.000	0.000	0.000	0.000	0.000	0.000
	x_{TAME}	0.000	0.000	0.000	0.000	0.000	0.000	0.000	0.000	0.000	0.000
	Flowrate	1.000	1.000	1.000	1.000	1.000	1.000	1.000	1.000	1.000	1.000
Top Flowrate		1.000	1.100	1.200	1.300	0.900	0.800	0.700	1.000	1.000	1.000
Feed1 Stage		3	3	3	3	3	3	3	3	3	3
Feed2 Stage		5	5	5	5	5	5	5	5	5	5
Packing	Stage 1	SZ-BX	SZ-BX	SZ-BX	SZ-BX	SZ-BX	SZ-BX	SZ-BX	SZ-BX	SZ-BX	SZ-BX
	Stage 2	SZ-BX	SZ-BX	SZ-BX	SZ-BX	SZ-BX	SZ-BX	SZ-BX	SZ-BX	SZ-BX	SZ-BX
	Stage 3	MP-II	MP-II	MP-II	MP-II	MP-II	MP-II	MP-II	MP-II	MP-II	MP-II
	Stage 4	MP-II	MP-II	MP-II	MP-II	MP-II	MP-II	MP-II	MP-II	MP-II	MP-II
	Stage 5	SZ-BX	SZ-BX	SZ-BX	SZ-BX	SZ-BX	SZ-BX	SZ-BX	SZ-BX	SZ-BX	SZ-BX
	Stage 6	SZ-BX	SZ-BX	SZ-BX	SZ-BX	SZ-BX	SZ-BX	SZ-BX	SZ-BX	SZ-BX	SZ-BX

Flowrates in $[kg.h^{-1}]$; SZ-BX - Sulzer BX; MP-II - Multipak II

Table C.1: Operating Conditions for the Column Parameters' Evaluation (Continued)

		11A	12A	13A	14A	15A	16A	17A	18A	19A	20A
Pressure [bar]		5.00	5.00	5.00	5.00	5.00	5.00	5.00	5.00	5.00	5.00
Reflux Ratio		3.00	0.85	0.70	0.55	1.00	1.00	1.00	1.00	1.00	1.00
Feed 1	T [°C]	90.00	90.00	90.00	90.00	90.00	90.00	90.00	90.00	90.00	90.00
	x_{2M1B}	0.000	0.000	0.000	0.000	0.000	0.000	0.000	0.000	0.000	0.000
	x_{2M2B}	0.000	0.000	0.000	0.000	0.000	0.000	0.000	0.000	0.000	0.000
	x_{MeOH}	1.000	1.000	1.000	1.000	1.000	1.000	1.000	1.000	1.000	1.000
	x_{TAME}	0.000	0.000	0.000	0.000	0.000	0.000	0.000	0.000	0.000	0.000
	Flowrate	1.000	1.000	1.000	1.000	0.900	0.800	0.700	1.100	1.200	1.300
Feed 2	T [°C]	90.00	90.00	90.00	90.00	90.00	90.00	90.00	90.00	90.00	90.00
	x_{2M1B}	0.500	0.500	0.500	0.500	0.500	0.500	0.500	0.500	0.500	0.500
	x_{2M2B}	0.500	0.500	0.500	0.500	0.500	0.500	0.500	0.500	0.500	0.500
	x_{MeOH}	0.000	0.000	0.000	0.000	0.000	0.000	0.000	0.000	0.000	0.000
	x_{TAME}	0.000	0.000	0.000	0.000	0.000	0.000	0.000	0.000	0.000	0.000
	Flowrate	1.000	1.000	1.000	1.000	1.100	1.200	1.300	0.900	0.800	0.700
Top Flowrate		1.000	1.000	1.000	1.000	1.000	1.000	1.000	1.000	1.000	1.000
Feed2 Stage		3	3	3	3	3	3	3	3	3	3
Feed2 Stage		5	5	5	5	5	5	5	5	5	5
Packing	Stage 1	SZ-BX	SZ-BX	SZ-BX	SZ-BX	SZ-BX	SZ-BX	SZ-BX	SZ-BX	SZ-BX	SZ-BX
	Stage 2	SZ-BX	SZ-BX	SZ-BX	SZ-BX	SZ-BX	SZ-BX	SZ-BX	SZ-BX	SZ-BX	SZ-BX
	Stage 3	MP-II	MP-II	MP-II	MP-II	MP-II	MP-II	MP-II	MP-II	MP-II	MP-II
	Stage 4	MP-II	MP-II	MP-II	MP-II	MP-II	MP-II	MP-II	MP-II	MP-II	MP-II
	Stage 5	SZ-BX	SZ-BX	SZ-BX	SZ-BX	SZ-BX	SZ-BX	SZ-BX	SZ-BX	SZ-BX	SZ-BX
	Stage 6	SZ-BX	SZ-BX	SZ-BX	SZ-BX	SZ-BX	SZ-BX	SZ-BX	SZ-BX	SZ-BX	SZ-BX

Flowrates in $[kg.h^{-1}]$; SZ-BX - Sulzer BX; MP-II - Multipak II

Table C.1: Operating Conditions for the Column Parameters' Evaluation (Continued)

		21A	22A	23A	24A	25A	26A	27A	28A	29A
Pressure [bar]		7.00	9.00	3.00	1.00	5.00	5.00	5.00	5.00	5.00
Reflux Ratio		1.00	1.00	1.00	1.00	1.00	1.00	1.00	1.00	1.00
Feed 1	T [°C]	90.00	90.00	90.00	90.00	90.00	90.00	90.00	90.00	90.00
	x_{2M1B}	0.000	0.000	0.000	0.000	0.000	0.000	0.000	0.000	0.000
	x_{2M2B}	0.000	0.000	0.000	0.000	0.000	0.000	0.000	0.000	0.000
	x_{MeOH}	1.000	1.000	1.000	1.000	1.000	1.000	0.000	1.000	1.000
	x_{TAME}	0.000	0.000	0.000	0.000	0.000	0.000	0.000	0.000	0.000
	Flowrate	1.000	1.000	1.000	1.000	1.000	1.000	0.000	1.000	1.000
Feed 2	T [°C]	90.00	90.00	90.00	90.00	90.00	90.00	90.00	90.00	90.00
	x_{2M1B}	0.500	0.500	0.500	0.500	0.500	0.500	0.157	0.500	0.500
	x_{2M2B}	0.500	0.500	0.500	0.500	0.500	0.500	0.157	0.500	0.500
	x_{MeOH}	0.000	0.000	0.000	0.000	0.000	0.000	0.686	0.000	0.000
	x_{TAME}	0.000	0.000	0.000	0.000	0.000	0.000	0.000	0.000	0.000
	Flowrate	1.000	1.000	1.000	1.000	1.000	1.000	2.000	1.000	1.000
Top Flowrate		1.000	1.000	1.000	1.000	1.000	1.000	1.000	1.000	1.000
Feed1 Stage		3	3	3	3	4	3	3	3	3
Feed2 Stage		5	5	5	5	5	4	4	5	5
Packing	Stage 1	SZ-BX	SZ-BX	SZ-BX	SZ-BX	SZ-BX	SZ-BX	SZ-BX	SZ-BX	SZ-BX
	Stage 2	SZ-BX	SZ-BX	SZ-BX	SZ-BX	SZ-BX	SZ-BX	SZ-BX	SZ-BX	MP-II
	Stage 3	MP-II	MP-II	MP-II	MP-II	MP-II	MP-II	MP-II	MP-II	MP-II
	Stage 4	MP-II	MP-II	MP-II	MP-II	MP-II	MP-II	MP-II	MP-II	MP-II
	Stage 5	SZ-BX	SZ-BX	SZ-BX	SZ-BX	SZ-BX	SZ-BX	SZ-BX	MP-II	MP-II
	Stage 6	SZ-BX	SZ-BX	SZ-BX	SZ-BX	SZ-BX	SZ-BX	SZ-BX	SZ-BX	SZ-BX

Flowrates in $[kg.h^{-1}]$; SZ-BX - Sulzer BX; MP-II - Multipak II

Table C.2: Main Results for the Column Parameters' Evaluation

		1A	2A	3A	4A	5A	6A	7A	8A	9A	10A
Heat Duty		278.0	313.4	349.2	385.3	245.8	219.2	193.1	335.4	385.4	434.9
Top	T [°C]	85.09	85.00	84.94	84.89	85.20	85.37	85.58	84.34	83.81	82.95
	x_{2M1B}	0.0340	0.0349	0.0356	0.0362	0.0328	0.0313	0.0295	0.0416	0.0488	0.0566
	x_{2M2B}	0.2907	0.2986	0.3049	0.3095	0.2801	0.2665	0.2509	0.3548	0.4150	0.4799
	x_{MeOH}	0.6223	0.6126	0.6049	0.5993	0.6354	0.6522	0.6717	0.5486	0.4818	0.4227
	x_{TAME}	0.0530	0.0539	0.0545	0.0550	0.0518	0.0501	0.0479	0.0550	0.0544	0.0407
	Flowrate	1.00	1.10	1.20	1.30	0.90	0.80	0.70	1.00	1.00	1.00
Bottoms	T [°C]	111.33	111.04	110.75	110.49	109.05	103.65	99.38	110.59	110.27	110.16
	x_{2M1B}	0.0000	0.0000	0.0000	0.0000	0.0030	0.0148	0.0320	0.0000	0.0000	0.0000
	x_{2M2B}	0.0000	0.0000	0.0000	0.0000	0.0231	0.0699	0.1003	0.0000	0.0000	0.0000
	x_{MeOH}	0.6268	0.6599	0.6967	0.7375	0.6063	0.6037	0.6033	0.7209	0.7840	0.8324
	x_{TAME}	0.3732	0.3401	0.3033	0.2625	0.3676	0.3116	0.2643	0.2791	0.2160	0.1676
	Flowrate	1.000	0.900	0.800	0.700	1.100	1.200	1.300	1.000	1.000	1.000
Conv.	2M1B	90.10	88.91	87.73	86.56	90.52	88.16	83.22	88.56	87.22	85.65
	2M2B	15.28	05.04	-05.09	-15.03	19.65	15.65	13.65	02.42	-08.74	-21.65
	MeOH	24.07	21.46	18.88	16.34	25.17	23.71	22.13	20.78	17.93	14.62
TAME	Yield	85.33	81.76	77.25	71.43	87.53	88.46	89.46	83.36	81.82	83.87
	Mol. P.	37.32	34.01	30.33	26.25	36.76	31.16	26.43	27.91	21.60	16.76
	Mass P.	65.50	62.17	58.12	53.16	63.86	55.74	48.56	55.25	46.77	39.10
ΔConv.	2M1B	00.00	-01.19	-02.37	-03.54	00.43	-01.93	-06.88	-01.53	-02.88	-04.45
	2M2B	00.00	-10.24	-20.37	-30.31	04.37	00.37	-01.63	-12.86	-24.02	-36.93
	MeOH	00.00	-02.61	-05.19	-07.73	01.10	-00.36	-01.94	-03.29	-06.15	-09.45
ΔTAME	Yield	00.00	-03.57	-08.08	-13.90	02.20	03.12	04.13	-01.97	-03.51	-01.46
	Mol. P.	00.00	-03.31	-06.99	-11.07	-00.56	-06.16	-10.89	-09.41	-15.72	-20.56
	Mass P.	00.00	-03.33	-07.37	-12.34	-01.64	-09.76	-16.94	-10.25	-18.73	-26.40
ΔHeat Duty		00.00	12.77	25.62	38.62	-11.57	-21.15	-30.53	20.65	38.67	56.46

Conv. - Conversion; Mol. P. - Molar-based Purity; Mass P. - Mass-based Purity; Flowrates in $[kg.h^{-1}]$; Conv., TAME, ΔConv., ΔTAME, ΔHeat Duty in [%]

Table C.2: Main Results for the Column Parameters' Evaluation (Continued)

		11A	12A	13A	14A	15A	16A	17A	18A	19A	20A
Heat Duty		480.9	258.7	241.6	224.9	261.9	252.7	245.5	298.1	318.9	340.5
Top	T [°C]	82.21	85.40	85.79	86.27	84.96	84.85	84.73	85.22	85.38	85.57
	x_{2M1B}	0.0641	0.0316	0.0290	0.0264	0.0354	0.0368	0.0383	0.0325	0.0310	0.0293
	x_{2M2B}	0.5410	0.2702	0.2486	0.2263	0.3031	0.3152	0.3288	0.2776	0.2642	0.2494
	x_{MeOH}	0.3699	0.6460	0.6712	0.6974	0.6070	0.5921	0.5758	0.6386	0.6555	0.6741
	x_{TAME}	0.0251	0.0522	0.0512	0.0500	0.0546	0.0559	0.0572	0.0513	0.0494	0.0471
	Flowrate	1.00	1.00	1.00	1.00	1.00	1.00	1.00	1.00	1.00	1.00
Bottoms	T [°C]	110.16	111.72	109.49	106.33	110.19	106.49	105.98	110.50	110.17	110.19
	x_{2M1B}	0.0000	0.0000	0.0034	0.0108	0.0040	0.0227	0.0559	0.0000	0.0000	0.0000
	x_{2M2B}	0.0000	0.0001	0.0266	0.0643	0.0308	0.1136	0.2052	0.0000	0.0000	0.0000
	x_{MeOH}	0.8692	0.5884	0.5552	0.5233	0.4933	0.3547	0.1918	0.7365	0.8196	0.8838
	x_{TAME}	0.1308	0.4114	0.4148	0.4015	0.4719	0.5090	0.5472	0.2635	0.1804	0.1162
	Flowrate	1.000	1.000	1.000	1.000	1.000	1.000	1.000	1.000	1.000	1.000
Conv. TAME	2M1B	84.19	90.62	90.42	89.39	89.97	87.66	84.24	89.32	88.38	87.21
	2M2B	-33.48	19.66	18.54	15.43	14.84	07.15	01.55	08.82	00.92	-08.73
	MeOH	11.58	25.19	24.89	23.94	29.26	32.49	36.40	18.34	13.60	09.65
	Yield	87.80	85.93	85.74	85.20	86.39	86.04	85.63	82.83	79.26	73.82
	Mol. P.	13.08	41.14	41.48	40.15	47.19	50.90	54.72	26.35	18.04	11.62
	Mass P.	32.43	69.02	68.05	65.05	72.54	71.30	69.57	53.29	41.24	29.54
ΔConv.	2M1B	-05.91	00.52	00.33	-00.71	-00.13	-02.44	-05.86	-00.77	-01.72	-02.89
	2M2B	-48.76	04.38	03.26	00.15	-00.44	-08.13	-13.73	-06.46	-14.36	-24.01
	MeOH	-12.49	01.12	00.82	-00.13	05.19	08.41	12.32	-05.73	-10.47	-14.42
ΔTAME	Yield	02.46	00.59	00.40	-00.13	01.05	00.71	00.30	-02.50	-06.07	-11.51
	Mol. P.	-24.24	03.82	04.15	02.83	09.87	13.58	17.40	-10.97	-19.28	-25.70
	Mass P.	-33.07	03.52	02.55	-00.45	07.05	05.80	04.07	-12.20	-24.26	-35.96
ΔHeat Duty		73.01	-06.91	-13.08	-19.08	-05.79	-09.09	-11.67	07.26	14.71	22.51

Conv. - Conversion; Flowrates in [$kg.h^{-1}$]; Conv., TAME, ΔConv., ΔTAME, ΔHeat Duty in [%]

Table C.2: Main Results for the Column Parameters' Evaluation (Continued)

		21A	22A	23A	24A	25A	26A	27A	28A	29A
Heat Duty		286.6	293.3	262.9	174.7	260.8	265.0	220.3	279.9	279.3
Top	T [°C]	96.87	106.14	68.25	30.65	84.72	84.69	82.82	85.14	85.25
	x_{2M1B}	0.0376	0.0404	0.0314	0.3071	0.0395	0.0388	0.0567	0.0332	0.0333
	x_{2M2B}	0.3002	0.3065	0.2842	0.4253	0.3359	0.3270	0.4876	0.2859	0.2839
	x_{MeOH}	0.6173	0.6140	0.6209	0.2555	0.5656	0.5781	0.4181	0.6284	0.6287
	x_{TAME}	0.0450	0.0392	0.0636	0.0120	0.0590	0.0561	0.0376	0.0525	0.0542
	Flowrate	1.00	1.00	1.00	1.00	1.00	1.00	1.00	1.00	1.00
Bottoms	T [°C]	123.51	132.78	94.18	54.99	110.73	110.83	110.15	111.40	111.41
	x_{2M1B}	0.0000	0.0005	0.0000	0.0026	0.0000	0.0000	0.0000	0.0000	0.0000
	x_{2M2B}	0.0001	0.0034	0.0000	0.0214	0.0000	0.0000	0.0000	0.0002	0.0002
	x_{MeOH}	0.6389	0.6482	0.6232	0.9268	0.6999	0.6863	0.8357	0.6177	0.6163
	x_{TAME}	0.3611	0.3479	0.3768	0.0492	0.3001	0.3137	0.1643	0.3821	0.3835
	Flowrate	1.000	1.000	1.000	1.000	1.000	1.000	1.000	1.000	1.000
Conv.	2M1B	89.02	88.09	90.94	28.12	89.03	89.10	85.67	90.27	90.26
	2M2B	12.38	09.61	17.86	-06.38	06.67	08.10	-23.30	16.17	16.85
	MeOH	23.16	22.32	24.85	04.97	21.86	22.20	14.27	24.32	24.47
TAME	Yield	87.06	88.27	83.10	87.22	82.86	83.77	84.74	85.55	85.20
	Mol. P.	36.11	34.79	37.68	04.92	30.01	31.37	16.43	38.21	38.35
	Mass P.	64.31	62.81	65.85	13.81	57.76	59.31	38.53	66.34	66.47
ΔConv.	2M1B	-01.08	-02.01	00.84	-61.97	-01.07	-00.99	-04.43	00.18	00.16
	2M2B	-02.90	-05.67	02.58	-21.66	-08.61	-07.18	-38.58	00.89	01.57
	MeOH	-00.91	-01.75	00.78	-19.10	-02.21	-01.87	-09.80	00.24	00.39
ΔTAME	Yield	01.73	02.94	-02.24	01.89	-02.47	-01.56	-00.60	00.22	-00.13
	Mol. P.	-01.21	-02.53	00.36	-32.40	-07.31	-05.95	-20.89	00.89	01.03
	Mass P.	-01.19	-02.68	00.35	-51.68	-07.74	-06.19	-26.97	00.84	00.97
ΔHeat Duty		03.12	05.52	-05.43	-37.16	-06.17	-04.65	-20.73	00.69	00.48

Conv. - Conversion; Flowrates in $[kg.h^{-1}]$; Conv., TAME, ΔConv., ΔTAME, ΔHeat Duty in [%]